2015

Design and Application of Task-Specific Organic Salts for Chemical and Biochemical Sensing

Waduge Indika Subodha Galpothdeniya
Louisiana State University and Agricultural and Mechanical College, indikagalpothdeniya@gmail.com

DESIGN AND APPLICATION OF TASK-SPECIFIC ORGANIC SALTS FOR CHEMICAL AND BIOCHEMICAL SENSING

A Dissertation

Submitted to the Graduate Faculty of the
Louisiana State University and
Agricultural and Mechanical College
in partial fulfillment of the
requirements for the degree of
Doctor of Philosophy

in

The Department of Chemistry

by
Waduge Indika Subodha Galpothdeniya
BSc, University of Colombo, 2009
August 2015

To my parents Kanthi Hapuarachchi and Ananda Galpothdeniya,

To my wife Dinushi Hansika,

To my brother Buddhika Galpothdeniya,

To my daughter Liana Sehansi

For their endless love, support, encouragement, and patience

ACKNOWLEDGEMENTS

I am truly grateful to the following people for their support in making my "PhD dream" a reality;

- Thesis Advisor: *Prof. Isiah M. Warner* for giving me the opportunity to contribute to his excellent research, for guidance, and financial support
- PhD Committee Members: *Prof. Kermit K. Murray*, *Prof. Samuel D. Gilman*, and *Prof. Aravamudhan Raman* for their time, insightful questions, and helpful discussions
- Graduate Student Mentor: *Dr. Sergio de Rooy* for guiding me in the right direction
- Postdocs: *Dr. Susmita Das*, *Dr. Farhana Hasan*, and *Dr. Noureen Siraj* for continuous support throughout my graduate studies
- Collaborators: *Prof. Kevin S. McCarter*, *Dr. Bishnu P. Regmi*, *Dr. Suzana Hamdan*, *Mingyan Cong*, and *Nimisha Bhattarai* for their invaluable contribution to my thesis research
- Warner Research Group members for their useful suggestions, and discussions
- Last but not least, *my parents*, *my loving wife*, *my brother*, and my *"little cutie"* for their endless love, support, encouragement, and patience throughout my whole life.

TABLE OF CONTENTS

ACKNOWLEDGEMENTS iii

LIST OF TABLES vii

LIST OF FIGURES viii

LIST OF SCHEMES xiv

ABSTRACT xv

CHAPTER 1: INTRODUCTION 1
- 1.1. Ionic Liquids and GUMBOS 1
- 1.2. Chemical Sensors 5
  - 1.2.1. Chemical Sensor: Definition and Principle 5
  - 1.2.2. Recognition 6
  - 1.2.3. Transduction 8
- 1.3. Photometric Sensors 9
  - 1.3.1. UV-Vis Spectroscopy 10
  - 1.3.2. Fluorescence Spectroscopy 13
- 1.4. Chemical Sensor Arrays 16
  - 1.4.1. General Definition 16
  - 1.4.2. Why Chemical Sensor Arrays? 17
  - 1.4.3. General Operating Principal of Chemical Sensor Arrays 19
- 1.5. Scope of the Dissertation 21
- 1.6. References 22

CHAPTER 2: IONIC LIQUID-BASED OPTOELECTRONIC SENSOR ARRAYS FOR CHEMICAL DETECTION 35
- 2.1. Introduction 35
- 2.2. Experimental Section 38
  - 2.2.1. Materials 38
  - 2.2.2. Synthesis and Characterization of ILs 39
  - 2.2.3. Preparation of IL Sensor Arrays Using TLC and Filter Paper Matrices 40
  - 2.2.4. Preparation of an IL Sensor Array Using Cotton Thread Matrix 40
  - 2.2.5. Preparation and Analyses of Aqueous Solutions of Cigarette Smoke 41
  - 2.2.6. Development of Predictive Models for Identification of Chemical Substance 43
- 2.3. Results and Discussion 46
  - 2.3.1. Choice of Matrix 51
  - 2.3.2. Digital Image Maps and Difference Maps 52
  - 2.3.3. Estimation of pH Values 53
  - 2.3.4. Aqueous-Phase Sensing 54
  - 2.3.5. Vapor-Phase Sensing 58
  - 2.3.6. Statistical Discrimination for Identification of pH Values and Acidic/Basic Vapors 61

2.3.7. Identification of Cigarette Smoke 66
2.3.8. Statistical Discrimination of Smoke from Three Brands of Cigarettes 66
2.4. Conclusions 68
2.5. References 69

CHAPTER 3: FLUORESCEIN-BASED IONIC LIQUID SENSOR FOR LABEL-FREE DETECTION OF SERUM ALBUMINS 74
3.1. Introduction 74
3.2. Experimental Section 77
3.2.1. Materials 77
3.2.2. Synthesis and Characterization of ILs 77
3.2.3. Preparation of Protein Solutions 77
3.2.4. Preparation of IL Nanodroplets 78
3.2.5. Characterization of Dispersions by Use of Dynamic Light Scattering (DLS) 78
3.2.6. Absorption and Fluorescence Studies 78
3.2.7. CD Studies 79
3.3. Results and Discussion 79
3.3.1. Preparation and Characterization of FL-Based Nanomaterials 79
3.3.2. Absorption and Fluorescence of FL-Based Nanodroplets 80
3.3.3. Fluorescence Sensing of Proteins Using FL-Based Nanodroplets 86
3.4. Conclusions 98
3.5. References 98

CHAPTER 4: VIRTUAL COLORIMETRIC SENSOR ARRAY: SINGLE IONIC LIQUID FOR SOLVENT DISCRIMINATION 103
4.1. Introduction 103
4.2. Experimental Section 106
4.2.1. Materials 106
4.2.2. Synthesis and Characterization of IL 107
4.2.3. Preparation of IL Solutions 107
4.2.4. Absorption Studies 107
4.2.5. Development of Predictive Models 108
4.3. Results and Discussion 109
4.3.1. Characterization of Spectral Properties of $[P_{66614}]_2[BTB]$ 109
4.3.2. Discrimination of an Extended Set of Closely Related Pure Alcohols 115
4.3.3. Discrimination of Binary Mixtures of Ethanol and Methanol 130
4.4. Conclusion 131
4.5. References 132

CHAPTER 5: TUNABLE, GUMBOS-BASED SENSOR ARRAY FOR LABEL-FREE DETECTION AND DISCRIMINATION OF PROTEINS 140
5.1. Introduction 140
5.2. Materials and Methods 142
5.2.1. Materials 142
5.2.2. Synthesis and Characterization of Functional GUMBOS 143
5.2.3. Single-Crystal X-ray Crystallographic Studies 143

5.2.4. Preparation of Protein Solutions 144
5.2.5. Preparation of TNS-Based Sensor-Protein Solution 144
5.2.6. Absorption and Fluorescence Studies 144
5.2.7. Absolute Quantum Yield Measurements 145
5.2.8. Octanol-Water Partition Coefficient ($K_{o/w}$) 145
5.2.9. Development of Predictive Models 146
5.3. Results and Discussion 146
5.3.1. TNS-Based Sensors 146
5.3.2. Spectral Properties of TNS-based GUMBOS 153
5.3.3. Detection and Discrimination of Proteins using TNS-Based GUMBOS 156
5.4. Conclusion 168
5.5. References 172

CHAPTER 6: CONCLUSIONS AND FUTURE WORK 177
6.1. Conclusions 177
6.2. Future Work 178

APPENDIX A SUPPORTING INFORMATION FOR CHAPTER 2 180

APPENDIX B SUPPORTING INFORMATION FOR CHAPTER 3 187

APPENDIX C SUPPORTING INFORMATION FOR CHAPTER 5 197

APPENDIX D LETTERS OF PERMISSION 209

VITA 211

LIST OF TABLES

Table 3.1 Aggregate to monomer peak ratio $A_{ag(530)}/A_{m(490)}$ derived from absorbance spectra 85

Table 3.2 Aggregate to monomer absorbance peak ratio ($A_{ag(530)}/_{Am(490)}$) at increasing BSA concentrations (final concentration of $[P_{66614}]_2$[FL] is 24 μM) 95

Table 4.1 Variation of absorption peak ratio of 200 μM $[P_{66614}]_2$[BTB] in eight alcohols 115

Table 5.1 Molecular weight (MW), yield (%), melting point (°C), log $K_{o/w}$, and appearances of TNS-based GUMBOS 144

Table 5.2 Absorption maximum for π – π* transition (λ_{abs}), molar extinction coefficient at 355 nm (ε_{355}), emission maximum (λ_{em}), and quantum yield (φ_{fl}) of TNS-based GUMBOS 154

Table A1 List of misclassifications by discriminant model based on three principal component, under cross-classification 180

Table C1 Crystal Data and Structure Refinement for [TPP][TNS], [BTP][TNS] and $[P_{4444}]$[TNS] 203

Table C2 Selected Bond Distances (Å) and Angles (deg) for [TPP][TNS], [BTP][TNS] and $[P_{4444}]$[TNS] 204

LIST OF FIGURES

Figure 1.1. Diagram illustrating the change in ion packing between NaCl and MImCl. 1

Figure 1.2. Some of the commonly used cations and anions to synthesize ILs 3

Figure 1.3. Graphical representation of a chemical sensor. Partially selective sensor response of the sensor is increased form left to right.....6

Figure 1.4. Attenuation of a beam of light in presence of an analyte solution.....10

Figure 1.5. Schematic representation of a UV-visible spectrophotometer.....12

Figure 1.6. Perrin-Jablonski diagram, and characteristic times for various electronic transitions.....13

Figure 1.7. Schematic representation of a spectrofluorometer.....15

Figure 1.8. Graphical representation of a sensor which employs (A) lock-and-key method vs (B) non-specific bonding.....18

Figure 1.9. Schematic representation of the operation of a chemical sensor array. 20

Figure 2.1. Photonic IL sensor arrays (A) fabricated on (i) silica (ii) alumina and (iii) filter paper and their respective (B) digital images. (C) Cotton thread spools stained with chemosensory ILs (P refers to $[P_{66614}]$ ion). (D) Sensor array fabricated from IL-stained threads (i) by using a sewing machine and a (ii) hand-stitched 'warner research' logo 46

Figure 2.2. Image of colorimetric sensor array before exposure (left) and after exposure to ammonia (middle). A subtraction of the two images yields a difference vector in 36 dimensions. This vector is usefully visualized using a difference map (right), which shows the absolute values of the color changes 53

Figure 2.3. (A) Schematic of the experimental setup used to detect pH. The same setup was used to analyze the aqueous solution of cigarette smoke. The difference between (B) the IL-based sensor array and (C) regular indicator dye-based sensor array.....55

Figure 2.4. The difference maps for pH sensing studies by using (A) alumina TLC, (B) filter paper, and (C) cotton thread matrices.....56

Figure 2.5. Difference maps of chemosensory IL sensor array. (A) on exposure to acidic vapors by using alumina TLC matrix, and (B) on exposure to basic vapors by using silica TLC matrix.....59

Figure 2.6. Difference maps for the thread based IL sensor array. (A) after exposing to CF_3COOH acid followed by (B) ammonia, and (C) difference map obtained after alternate exposure to CF_3COOH and ammonia for three cycles, and finally to CF_3COOH. (D) Difference map between (A) and (C) 60

Figure 2.7. (A) Scree plot and (B) cumulative proportion of variability accounted for by the principal components obtained from the color change profile of pH, acidic and basic vapor numerical data 62

Figure 2.8. Plot of the scores for the first three principal components based on the data for the analysis of pH, acidic and basic vapor 63

Figure 2.9. PCA score plot for the identification of cigarette smoke of Marlboro® red, Crowns® and Camel® Turkish domestic blend by using filter paper based ionic liquid sensor arrays 68

Figure 3.1. (a) Absorption and fluorescence emission spectra (λ_{ex} = 490 nm) of $[P_{66614}]_2[FL]$ nanodroplets dispersed in pH 7.4 buffer (final concentration of $[P_{66614}]_2[FL]$ in buffer is 40 µM); (b) absorbance spectra, and (c) fluorescence emission spectra (λ_{ex} = 490 nm) of $[P_{66614}]_2[FL]$ nanodroplets at five different concentrations (8, 16, 24, 32 and 40 µM) 82

Figure 3.2. Integrated fluorescence intensity over the spectral range of 500 to 700 nm (λ_{ex} – 490 nm) of 40 µM $[P_{66614}]_2[FL]$ in the presence of same concentration (1.5 µM) of different albumins and non-albumins. (Error bars represent the standard deviations of three replicate samples) 87

Figure 3.3. CD spectra of (a) $[P_{66614}]_2[FL]$–BSA, (b) $[P_{66614}]_2[FL]$–HSA and (c) $[P_{66614}]_2[FL]$–Cyt–C obtained in a phosphate buffer (pH 7.4/10 mM). The concentrations of nanodroplets and proteins are indicated in the legend 89

Figure 3.4. (a) Fluorescence emission spectra (λ_{ex} = 490 nm) of $[P_{66614}]_2[FL]$ nanoparticles dispersed in different concentrations of BSA, and (b) linear relationship between BSA concentration and relative fluorescence intensity at 512 nm (Errors bars represent the standard deviations for three replicate samples. Note some error bars are too small to be seen over the data points). Absorbance spectra (c) normalized at 490 nm and (d) normalized at 530 nm at different BSA concentrations (final concentration of $[P_{66614}]_2[FL]$ is 24 µM). The concentrations of BSA are indicated in the legend 92

Figure 3.5. Fluorescence emission spectra of 24 µM $[P_{66614}]_2[FL]$ nanodroplets dispersed in different concentrations of HSA solution. The concentrations of HSA are indicated in the legend. (b) Polynomial relationship between

relative fluorescence intensity at 512 nm and HSA concentration. Error bars represent the standard deviations of three replicate samples. Note some error bars are too small to be seen over the data points.....96

Figure 4.1. (A) Normalized absorption spectra of 200 μM $[P_{66614}]_2$[BTB], and (B) 200 μM free BTB in methanol in methanol (red) and 2-butanol (blue). Inset shows the visual appearance of 200 μM $[P_{66614}]_2$[BTB] in methanol and 2-butanol. Alcohol dependent color changes for (C) 200 μM $[P_{66614}]_2$[BTB] and (D) 200 μM free BTB in methanol, and 2-butanol. (I – Methanol, II – 2-butanol).....111

Figure 4.2. (A) Photograph showing alcohol dependent color changes for 200 μM $[P_{66614}]_2$[BTB] and (B) 200 μM free BTB in eight alcohols (M – methanol, E – ethanol, 1P – 1-propanol, 1B – 1-butanol, IBA – isobutanol, 2P – 2-propanol O – 1-octanol, and 2B – 2-butanol). (C) Absorption peak ratio ($^{630}/_{410}$) vs normalized $E_T(30)$ solvent polarity parameter (E_T^N). This provides the relationship between absorption signal and solvent polarity. 116

Figure 4.3. UV-Vis absorption spectra of four different concentrations of $[P_{66614}]_2$[BTB] in seven alcohols (A: methanol, B: ethanol, C: 1-propanol, D: 1-butanol, E: isobutanol, F: 2-propanol, G: 2-butanol H: 1-octanol). Legend: concentration of $[P_{66614}]_2$[BTB] in alcohol (*i.e.* purple– 500 μM; green– 300 μM; red– 200 μM; blue– 100 μM) (Spectra were smoothened using Savitzky-Golay Principle).....120

Figure 4.4. Absorption peak ratio ($^{630}/_{410}$) of various concentrations $[P_{66614}]_2$[BTB] in eight different alcohols (Errors bars represent the standard deviations for seven replicate samples).....125

Figure 4.5. PCA score plot using the first two principal components based on the $^{630}/_{410}$ absorbance ratio of $[P_{66614}]_2$[BTB] in eight different alcohols 126

Figure 4.6. Absorption peak ratio ($^{\lambda_{1\,max}}/_{\lambda_{2\,max}}$) vs normalized $E_T(30)$ solvent polarity parameter (E_T^N). This provides the relationship between absorption signal and solvent polarity 127

Figure 4.7. Absorption peak ratio ($^{\lambda_{1\,max}}/_{\lambda_{2\,max}}$) of various concentrations $[P_{66614}]_2$[BTB] in eight different alcohols (Errors bars represent the standard deviations for seven replicate samples).....128

Figure 4.8. PCA score plot using the first two principal components based on the $\lambda_{1\,max}/\lambda_{2\,max}$ absorbance ratio of $[P_{66614}]_2$[BTB] in eight different alcohols 128

Figure 4.9. PCA score plot using the first two principal components based on the $630/410$ of $[P_{66614}]_2$[BTB] in seven different binary mixtures of ethanol and methanol (E 100 M 0 – ethanol 100%-methanol 0%; E 98 M 2 – ethanol 98%-methanol 2%; E 90 M 10 – ethanol 90%-methanol 10%; E 50 M 50 – ethanol 50%-methanol 50%; E10 M 90 – ethanol 10%-methanol 90%; E 2 M 98 – ethanol 2%-methanol 98%; and E 0 M 100 – ethanol 0%-methanol 100%) 131

Figure 5.1. The solid state structures for (A) $[P_{4444}]$[TNS], (B) [BTP][TNS], and (C) [TPP][TNS] obtained from single-crystal X-ray diffraction. Solvent molecules were removed for clarity. For comparison purposes, TNS moiety was given the same numbering pattern in all three structures 151

Figure 5.2. Normalized absorption and fluorescence emission spectra (λ_{ex}- 355 nm) of 10 μM [4NB][TPP] in ethanol. Absorption spectrum has been normalized to 1.0 at maximum of the longest wavelength absorbance band, and emission spectrum has been normalized to 1.0 at its maximum. A stoke shift of 66 nm was observed 155

Figure 5.3. Relative fluorescence emission intensity (λ_{ex} – 355 nm) of 5 μM TNS-based GUMBOS at 435 nm in presence of different serum and non-serum proteins. Protein concentrations were fixed at 100 nM in pH 7.4 buffer. Error bars represent standard deviations of five replicate samples.....157

Figure 5.4. Relative emission intensity (λ_{ex} – 355 nm) of TNS-based GUMBOS at 435 nm in presence of different concentrations of HSA (H), α-antitrypsin (A) and β-lac (B). Error bars represent the standard deviations of five replicate samples 159

Figure 5.5. PCA score plot using the first two principal components based on the sensor-response patterns obtained from TNS-based sensors in 21 protein concentrations. Protein concentrations are listed in the legend 160

Figure 5.6. PCA score plot using the first two principal components based on the sensor-response patterns obtained from TNS-based sensors. In this experiments, HSA (red) and α-antitrypsin (black) concentrations were not defined during PCA 163

Figure 5.7. PCA score plot using three principal components based on the normalized sensor-response patterns obtained from TNS-based sensors; PC – principal component. In this experiment, HSA (red) and α-antitrypsin (blue) concentrations were not defined during PCA 165

Figure 5.8. PCA score plot using the first two principal components based on the sensor-response patterns obtained from TNS-based sensors. Protein and protein mixture concentrations are listed in the legend. H – HSA; A – α-antitrypsin 167

Figure 5.9. Plot of relative fluorescence emission intensity *versus* the concentration of HSA (red), or α-antitrypsin (black) for (A) [4NB][TNS], (B) $[P_{4444}][TNS]$, (C) [BTP][TNS], and (D) [TPP][TNS]. Error bars represent the standard deviations of five replicate measurements 169

Figure A1. Appearance of ILs 181

Figure A2. (A)Scree plot and (B) cumulative proportion of variability accounted for by the principal components obtained from the color change profile for the identification of cigarette smoke of Marlboro® red, Crowns® and Camel® by using filter paper based ionic liquid sensor arrays 186

Figure B1. Fluorescence emission spectra (λ_{ex} – 490 nm) of 40 µM $[P_{66614}]_2[FL]$ nanodroplets in the presence of same concentration (1.5 µM) of different albumins and non-albumins 187

Figure B2. Fluorescence emission spectra (λ_{ex} = 490 nm) of 40 µM (A) Na_2FL, (B) $[TPP]_2[FL]$ and (C) $[4NB]_2[FL]$ with eight different proteins at the concentration of 1.5 µM.....188

Figure B3. Fluorescence emission spectra (λ_{ex} = 490 nm) of (a) Eosin B, (b) Eosin Y, (c) Phloxine B (d) Erythrosin B and, (e) Rose Bengal nanoparticles dispersed in different concentrations of BSA 191

Figure B4. Relationship between relative fluorescence intensity at 512 nm and HSA concentration in human serum. Human serum samples were diluted for 1000 times before analysis.....195

Figure B5. The fluorescence emission spectra (λ_{ex} – 490 nm) of 24 µM dispersions of $[P_{66614}]_2[FL]$ at 0 and 120 minutes 196

Figure C1. Electrospray ionization mass spectra for TNS based GUMBOS.....198

Figure C2. Absorption and fluorescence emission spectra (λ_{ex}- 355 nm) of 10 µM TNS GUMBOS in ethanol. Emission spectrum has been normalized to 1.0 at its maximum.....203

Figure C3. (A) PCA score plot using the first two principal components based on the sensor-response patterns obtained from TNS-based sensors. HSA and α-antitrypsin were labeled as given in the legend (B) PCA score plot using three principal components based on the normalized sensor-response

patterns obtained from TNS-based sensors. Different proteins concentrations are given in the legend from top to bottom are 10 nM HSA, 20 nM HSA, 30 nM HSA, 50 nM HSA, 70 nM HSA, 100 nM HSA, 10 Antitrypsin, 20 Antitrypsin, 30 Antitrypsin, 50 Antitrypsin, 70 Antitrypsin, 100 Antitrypsin, 200 Antitrypsin, and 500 Antitrypsin. (C) PCA score plot using three principal components based on the normalized sensor-response patterns obtained from TNS-based sensors: Ellipsoids cover 95% of each cluster; HSA – blue ellipsoid, α-antitrypsin – red ellipsoid.....205

LIST OF SCHEMES

Scheme 2.1. Schematic representation of the preparation of IL sensor array on TLC and filer paper-based matrices 40

Scheme 2.2. Schematic representation for the staining procedure of the cotton threads with ILs. A 10 mM solution of IL in DCM was used to stain the natural white cotton threads. Slow constant wounding of the cotton threads yields an evenly coated stained cotton thread spool 41

Scheme 2.3. Schematic representation of the experimental setup used to prepare aqueous solution of cigarette smoke. This technique applies the same suction to all the cigarettes tested. Cigarette was completely burned out before water level reached 350 mL mark 42

Scheme 3.1. Chemical structures of different anions and cations used in this study (I) Fluorescein, (II) Eosin B, (III) Eosin Y, (IV) Phloxine B (V) Erythrosin B and, (VI) Rose Bengal (VII) [P_{66614}], (VIII) [TPP] and (IX) [4NB] 81

Scheme 4.1. The dissociation of BTB 109

Scheme 4.2. Chemical structure of $[P_{66614}]_2$[BTB] used in this study.....110

Scheme 5.1. Chemical structures of TNS-based compounds synthesized in this study.....149

ABSTRACT

There is an increasing demand for development of new sensors and sensor strategies for accurate detection and discrimination of various analytes. In this regard, colorimetric and fluorometric sensor approaches have attracted considerable attention, primarily because they represent facile and inexpensive analytical tools. In this dissertation, I discuss the design and application of sensors and sensor arrays using task-specific organic salts: ionic liquids (ILs) and a ***g***roup of ***u***niform ***m***aterials ***b***ased on ***o***rganic ***s***alts (GUMBOS). As compared to typical ionic compounds, these two classes of organic salts exhibit relatively lower melting points due to bulky organic cations and/or anions. Interestingly, the physicochemical properties of these compounds can be easily tuned by altering either the cation or the anion. Furthermore, the respective ions of ILs and GUMBOS can be independently tailored in order to obtain specific functionalities. The first part of this dissertation provides a general discussion on ILs and GUMBOS. In addition, the principle and application of sensors and sensor arrays are discussed. The second part of this dissertation is primarily focused on four different studies, which involve design and application of task-specific organic salts for chemical and biochemical sensing. All four of these studies, which appear in Chapters 2-5, report on novel sensor or sensor array approaches with distinct advantages for analytical measurements.

CHAPTER 1: INTRODUCTION

1.1. Ionic Liquids and GUMBOS

Ionic compounds are a group of neural chemicals composed of ions with negative and positive charges. Typically, these compounds exhibit high melting points due to the formation of a stable three-dimensional lattice structure between the ions, which results from strong electrostatic interactions. As an example, NaCl has a melting point of ~800 °C. When the cations of NaCl are replaced with a bulky cation such as *N*-Methylimidazolium (MIm) ion, the melting point of MImCl decreases to 72 °C.[1] The observed melting point of MImCl can be attributed to the 'frustrated molecular packing' of the ions.[2] Compared to Na^+, MIm^+ ions are bulky and asymmetric, and therefore, they lack the ability to arrange themselves into a crystalline lattice with Cl^- ions, resulting in a drastic reduction in the melting point. A schematic representation of the change in ionic packing between NaCl and MImCl is given in Figure 1.1.

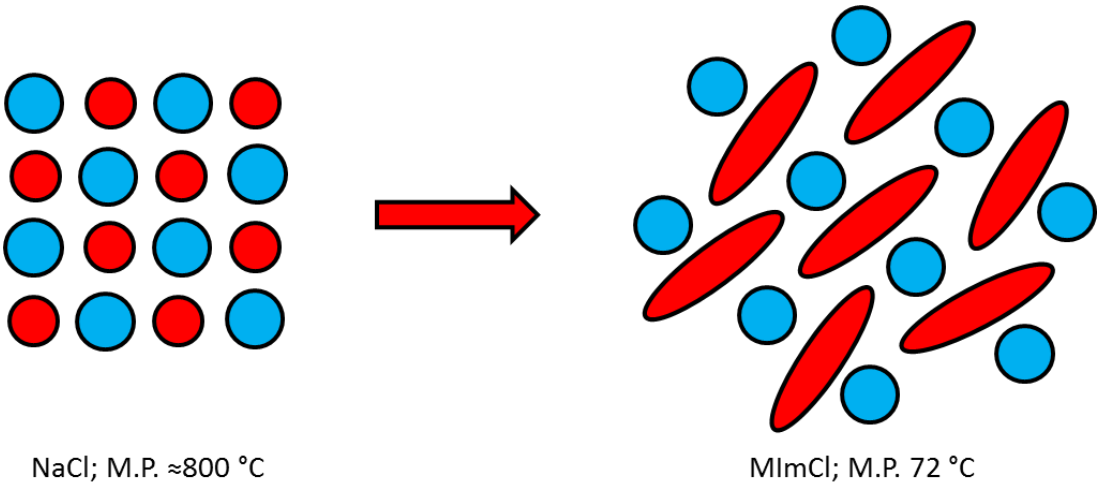

Figure 1.1. A schematic illustrating the change in ion packing between NaCl and MImCl

This dissertation is primarily focused on two categories of low melting point organic salts found in the literature, i.e., ionic liquids (ILs) and a ***g***roup of ***u***niform ***m***aterials ***b***ased on ***o***rganic ***s***alts (GUMBOS). ILs are organic salts with melting points below 100 °C. These ILs can also be separated into two groups according to their melting points. ILs which are liquid under ambient conditions are known as room-temperature ionic liquids (RTILs).[3,4] The remainder of ILs are classified as frozen ionic liquids (FILs) since they are solids at room temperature. A large number of cations and anions can be used to generate more than 10^{18} ILs.[5,6] Some of the commonly used cations and anions to synthesize ILs are given in Figure 1.2.

The history of ILs dates back to the 1800s. In 1888, the first ionic liquid (IL), i.e., ethanolammonium nitrate (melting point 52-55 °C), was discovered by Gabriel and Weiner.[7] Then, in 1914 Walden discovered ethylammonium nitrate (melting point 12 °C), which was credited as the "first IL" for a long period of time.[8] Although there were few reports on ILs in the 1900s, little attention was paid to their chemistry primarily as a result of their low stability.[9] In 1992, after Wilkes and Zaworotko developed an air- and water-stable imidazolium-based IL, there was a huge upsurge of interest in the synthesis and application of ILs.[10]

Presently, ILs have been widely explored as novel materials primarily as a result of their exciting chemical and physical properties such as infinitesimal vapor pressure, broad electrochemical window, wide solubility and miscibility range, and most importantly the ability to tune their physicochemical properties by simply altering either the cation or the anion.[11-15] Furthermore, due to these properties, ILs have shown promising applications in catalysis,[16-18] synthesis,[19-21] extraction,[22-24] electrochemistry,[25-27] mass spectrometry,[28-30] separation science,[31-33] spectroscopy,[34-36] and chemical sensing.[37-40]

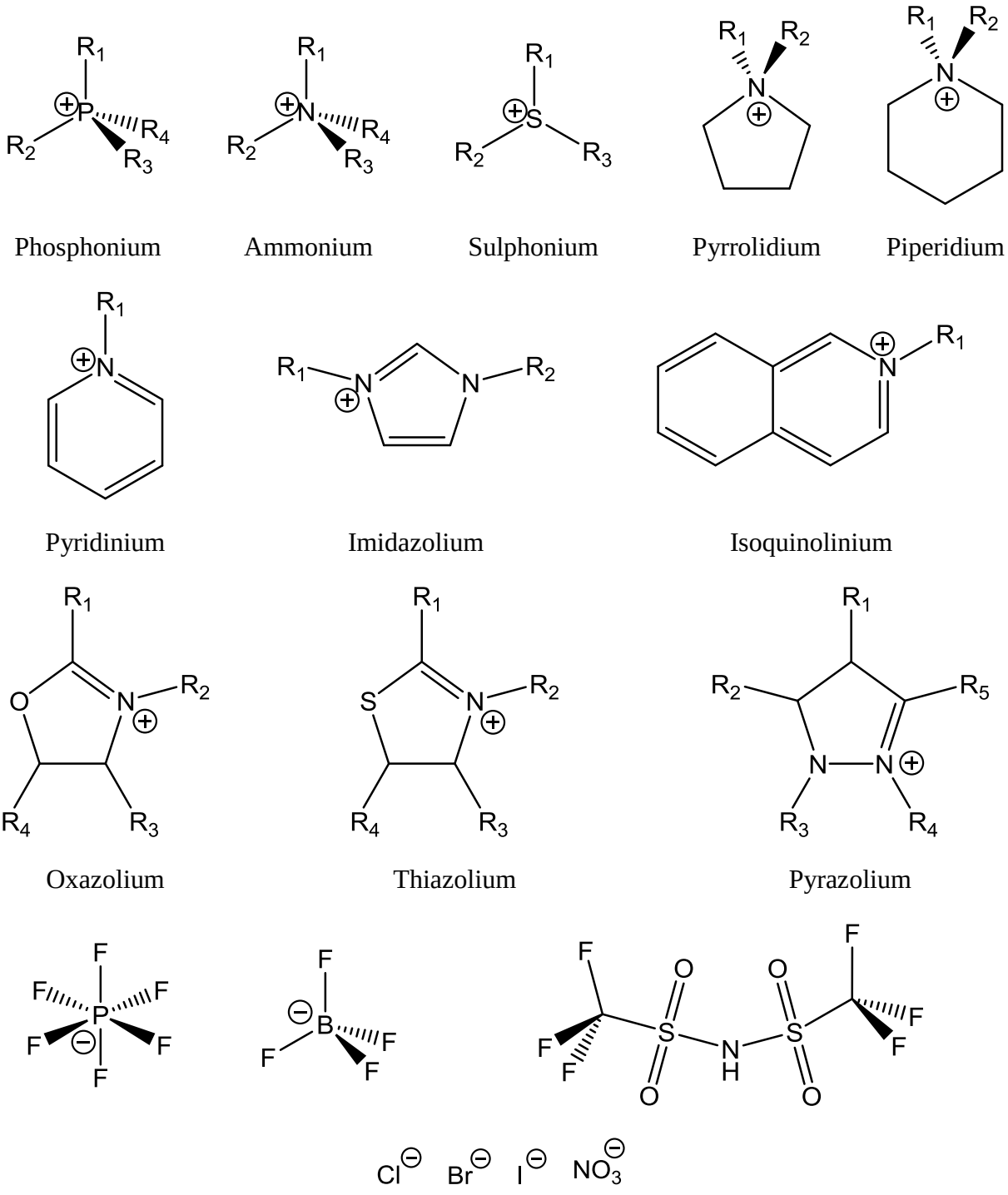

Figure 1.2. A list of commonly used cations and anions to synthesize ILs

As mentioned above, the physicochemical properties of ILs can be tuned by simply varying either the cation or the anion. Moreover, the respective ions in ILs can be independently modified in order to obtain two different functionalities from both the cation and the anion. Over the last two decades, we have observed an increase in ILs, which contain unique functionalities based on their applications. The ILs that are engineered to serve a specific task, are often termed as "task-specific ionic liquids"[41] (TSILs), which have been designed as magnetic,[42-44] chiral,[45-47] luminescent,[48-50] and catalytic[51-53] properties.

GUMBOS or a '***g***roup of ***u***niform ***m***aterials ***b***ased on ***o***rganic ***s***alts[54] are a deviated group of ILs with melting points between 25 °C and 250 °C. Currently, the Warner research group is involved in the design and application of these materials. The properties of these materials are quite similar to ILs, and can also be tuned by changing their respective ions. The ions that are commonly used to synthesize GUMBOS are also used to design ILs. GUMBOS are always solids at ambient conditions, and therefore, can be converted into nanomaterials very easily.[55-59] These nanomaterials, also known as nanoGUMBOS, have been designed for various applications such as biomedical imaging,[60] chemotherapy,[61] dye sensitized solar cells,[62] organic light emitting diodes,[63] and photothermal therapy.[64] Overall, it is important to note that GUMBOS inherit similar traits from ILs, and applications of GUMBOS in various fields of science are still in their early stages. However, the use of GUMBOS has shown exceptional potential for expanding the limits of ionic-material applications for industrial and academic research.

1.2. Chemical Sensors

1.2.1. Chemical Sensor: Definition and Principle

A chemical sensor is a "self-contained device"[65], which is engineered to provide insights into the analytical parameters of a test sample in real time.[66,67] In a chemical sensor, these analytical parameters are often used to gather information about the chemical composition of an analyte. Chemical sensors are usually designed to respond selectively or partially selectively to a desired analyte or a group of analytes through chemical interactions.

There are two functional steps in chemical sensing: recognition and transduction.[65] In the recognition step, analytes interact with sensor elements in a (partially) selective manner. Usually, these sensor elements are tailor-made based on the type of analyte and the information required from the analyte. In the transduction step, chemical (or physical) changes that occur due to the interaction between sensor elements and analytes are converted into a measurable signal. In general, this signal is proportional to the concentration of the targeted analyte. A graphical representation of the chemical sensor's function is given in Figure 1.3. In this figure, chemical change from the interaction between analytes and sensor elements are converted into light. The sensor element used in this figure is shown to be partially selective to the three analytes. Therefore, in the presence of multiple analytes, the signal intensity is altered. The blue analyte provides the highest sensitivity, whereas the sensor is not sensitive to the green analyte. Furthermore, the signal from the orange analyte may be considered interference.

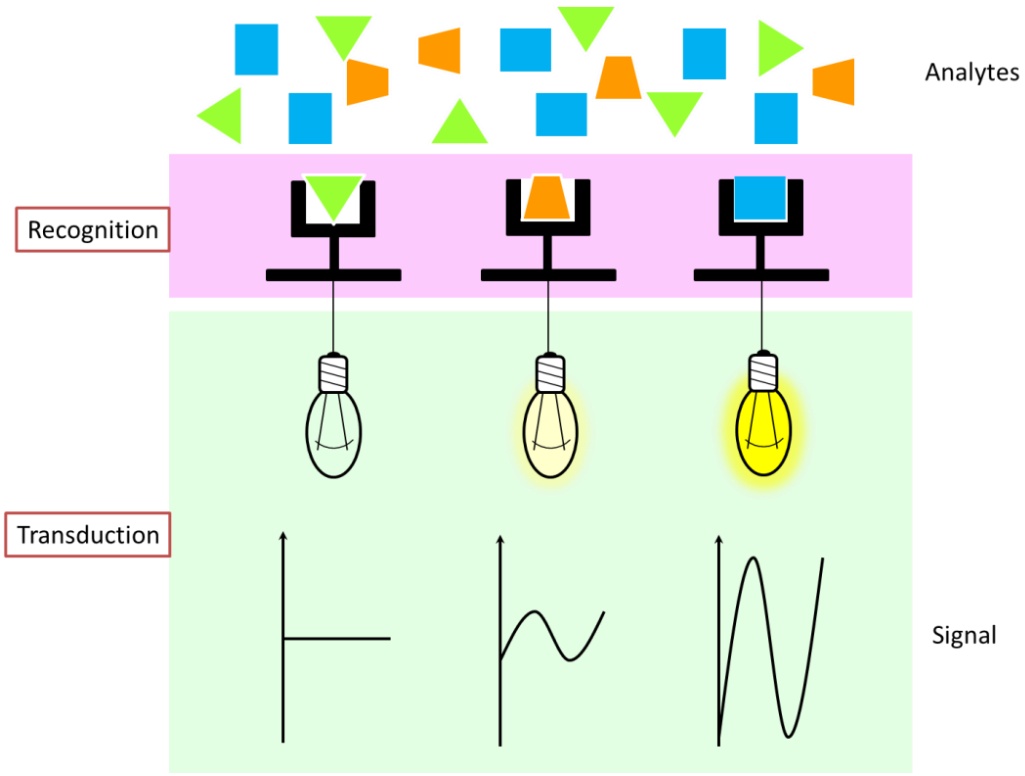

Figure 1.3. A graphical representation of a partially selective chemical sensor. The sensor response is increased from left to right

1.2.2. Recognition

In a chemical sensor, two primary factors determine the efficiency of a sensing process: affinity and selectivity. As an example, consider a reversible-recognition process between two analytes and a sensor element. The two analytes (A_1 and A_2) and sensing element (S) interact to form two analyte-sensor complexes (P_1 and P_2).

$A_1 + S \longleftrightarrow P_1$; K_{a1} – equilibrium constant

$A_2 + S \longleftrightarrow P_2$; K_{a2} – equilibrium constant

Affinity of the sensor element towards each analyte can be estimated by quantifying the two equilibrium constants using the equation: $K_a = {[P]}/{[A][S]}$

If the affinity of a sensor element towards an analyte is high, K_a is high, and *vice versa*. Also, the selectivity of the sensor element towards each analyte can be quantified using the ratio of the two equilibrium constants. When the equilibrium ratio, K_{a1}/K_{a2}, is >> 1, then the sensor element display good selectivity towards analyte A_1, and *vice versa*.

There are multiple types of chemical sensors that depend on various recognition techniques. As mentioned earlier, recognition is based on types of interactions, and types of sensor elements used. The first type of recognition-based chemical sensors is known as ion sensors that are capable of detecting various ions based on their charge and type. The glass pH electrode, developed by Haber and Klemensiewicz, is credited as one of the first ion sensors.[68] Usually, ion recognition is achieved using a wide range of ionic materials with an opposite charge to analyte ions. Overall, the development of ion-selective sensors is an area of intense research.[69]

Over the last few decades, a category of chemical sensors based on non-covalent interactions have attracted much interest among researches. These sensors achieve analyte recognition via multiple intermolecular interactions such as hydrogen bonds, van der Waals, dipole-dipole and ionic interactions between sensor and analyte. These interactions are often weak, and therefore, sensor-analyte interactions are reversible. Various chemical sensors based on organic,[70] organometallic,[71] metal-organic[72], and polymeric[73] materials have been designed using this principle.

The third category of chemical sensors, termed biosensors, utilizes a biological or biochemical mechanism as the recognition system.[66] Compared to the previous two categories, biosensors display extremely high selectivity and sensitivity toward analytes, and hence, have been a subject of intense research. Different types of materials, i.e. bioligands, have been used in biosensors. Some of the most common bioligands that have been reported to date include antibodies/antigens,[74-76] enzymes,[77-79] oligonucleotides,[80-82] and aptamers.[83-85]

The final group of recognition-based sensors is the sorption-based sensors. Sorption-based sensors are often used to sense gas and vapor. Usually, a chemically (partially) selective sensing material is coated on a transducer, which converts the physical interactions between analytes and the sensor material into an electrical signal. The sorption-based sensors can be further categorized into different groups based on transducers used. Few of the most commonly used transducers include chemicapacitors, chemiresistors, and acoustic wave devices.[86] The quartz crystal microbalance is an example of one of the most commonly used acoustic wave devices.[87-89]

1.2.3. Transduction

Transduction is the primary step used by sensors to generate a quantifiable signal as a result of chemical or physical changes that have occurred due to interactions between sensor elements and analytes. There are two types of transduction methods: chemical transduction and physical transduction.[65,67] In chemical transduction, chemical changes that occur in the recognition step are monitored, whereas changes observed in a physical property, such as refractive index or mass of analyte, is monitored in the recognition process of physical transduction. In certain instances, however, none of the components involved in the sensing process generate a measurable

response upon interaction, and therefore, require labeling of either the analyte or the sensor.[65] These labels generate a measurable signal upon interaction of analytes with the sensor elements. It is notable that the physical transduction methods do not require any labeling techniques for sensing.[65]

Similar to the sensor categories observed based on sensor recognition, chemical sensors are also categorized according to the ransduction methods employed in the sensing process. Among these categories electrochemical sensors,[90-93] mass sensors,[94] thermometric sensors,[95,96] and photometric sensors[97-99] have attracted the most interest among researches. The work described in this document primarily focuses on the development of photometric sensors based on ILs and GUMBOS.

1.3. Photometric Sensors

Photometric or optical sensors involve the measurement of interaction between electromagnetic radiation and matter. Common analytical methods that use this principle are known as spectroscopic techniques. Currently, various spectroscopic methods are employed, which use a wide range of wavelengths, to gather information about matter ranging from atomic levels to complex molecular structures.

Occasionally, the analyte itself is able to interacts with the light, primarily because of its unique optical properties, which can be used to gather information about its chemical composition. However, on many occasions, information regarding analytes cannot be collected using only their optical properties. Therefore, chemically selective sensor materials are often employed to convert analytes into optically active sensor-analyte complexes. In a photometric sensor, the resulting sensor-analyte complexes are measured using a beam of light, which is

absorbed and/or emitted during analysis. In this document, two optical sensing strategies, UV-vis spectroscopy and fluorescence spectroscopy, are employed. A brief overview of the two spectroscopic techniques is given below.

1.3.1. UV-Vis Spectroscopy

The ultraviolet-visible (UV-vis) spectroscopy is an analytical technique which measures the molecular absorption of a chemical species in the UV-vis spectral region. When a beam of light passes through a sample, the intensity of light is decreased due to absorption. An absorbing analyte uses the energy of light to move from the ground state to an excited state of energy. The law that quantifies this attenuation of light is called Beer-Lambert's law (Beer's law). According to Beer's law, the attenuation of a light beam (I/I_0) is proportional to two factors: the concentration of the analyte (c) and the distance traveled by the light through the sample (path length– l). The graphical representation of attenuation of light in the presence of an absorbing analyte solution is given in Figure 1.4.

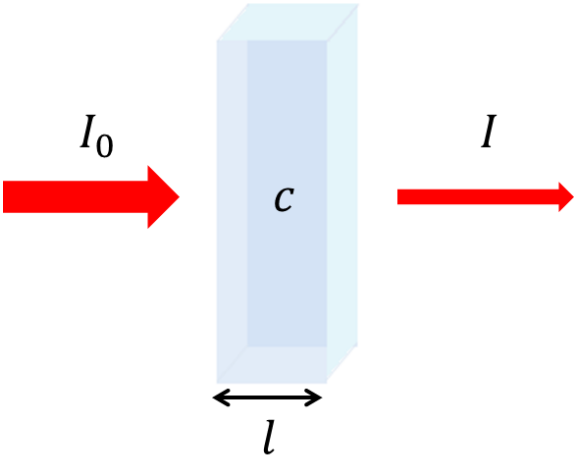

Figure 1.4. The attenuation of a light beam in the presence of an analyte solution

Furthermore, attenuation of a light beam can also be given as transmittance (T), which is the fraction of incident radiation transmitted through the sample analyte (Equation 1.1). The absorbance (A) of an analyte is equal to the negative value of the logarithmic transmittance, which is provided in the Equation 1.2. Consequently, the absorbance of an analyte is also proportional to its concentration and path length.

$$I/I_0 = T \tag{1.1}$$

$I_0 -$ Intensity of incident light

$I -$ Intensity of transmitted beam

$$A = -\log T \tag{1.2}$$

$$A \propto c \quad ; \quad A \propto l \tag{1.3}$$

According to the Equation 1.3, absorbance decreases with increasing concentration of analyte and/or path length. Therefore, the two parts of the Equation 1.3 can be combined to obtain the Equation 1.4.

$$A = kcl \tag{1.4}$$

In the Equation 1.4, k is the proportionality constant called absorptivity. Since, absorbance is unit-less, k is given in mol^{-1} L cm^{-1}, if c is in mol L^{-1} and l is in cm, and therefore, k is known as molar absorptivity (ε). Then, Equation 1.4 can be rewritten as Equation 1.5. Molar absorptivity is dependent on the analyte and the wavelength.

$$A = \varepsilon cl \tag{1.5}$$

According to Equation 1.5 (Beer-Lambert's law), the absorbance of an analyte can be quantified if the three terms of the equation are known. Using a UV-vis spectrophotometer, the intensity of absorbance with respect to wavelength, also known as the absorption spectrum, is measured in the UV-vis region. UV-vis spectrophotometer is often used as a quantitative tool to calculate the concentration of an analyte or a group of analytes using a calibration curve. In UV-vis spectrophotometry, a beam of polarized light is used to measure absorbance. Usually, a beam of polarized light is obtained using a monochromator. A schematic representation of a UV-vis spectrophotometer is given in Figure 1.5.

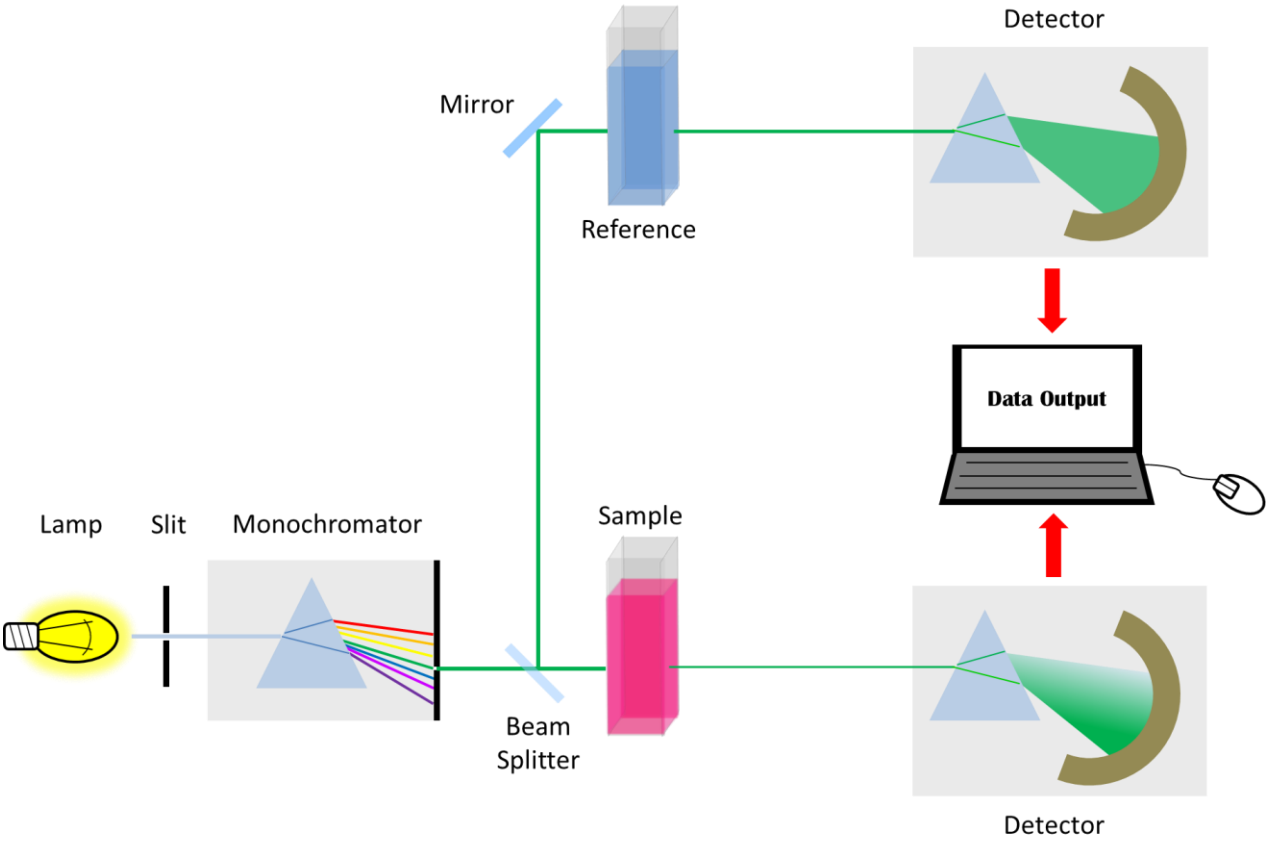

Figure 1.5. A schematic representation of a UV-vis spectrophotometer

1.3.2. Fluorescence Spectroscopy

Fluorescence spectroscopy is an analytical technique that measures the fluorescence of a chemical species, typically, in the visible spectral region. Fluorescence is categorized as one of the two forms of luminescence, also known as a process which involves the emission of photons from an electronically excited state.[100] In fluorescence, the emission of photons occurs due to relaxation between the $S_1 \rightarrow S_0$ energy states. Radiative and non-radiative transitions between electronic states that are accompanied with fluorescence are illustrated using a Jablonski diagram in Figure 1.6. In this diagram, singlet electronic states are denoted as S, whereas the triplet states are denoted as T. The characteristic times for those transitions are also given in Figure 1.6.

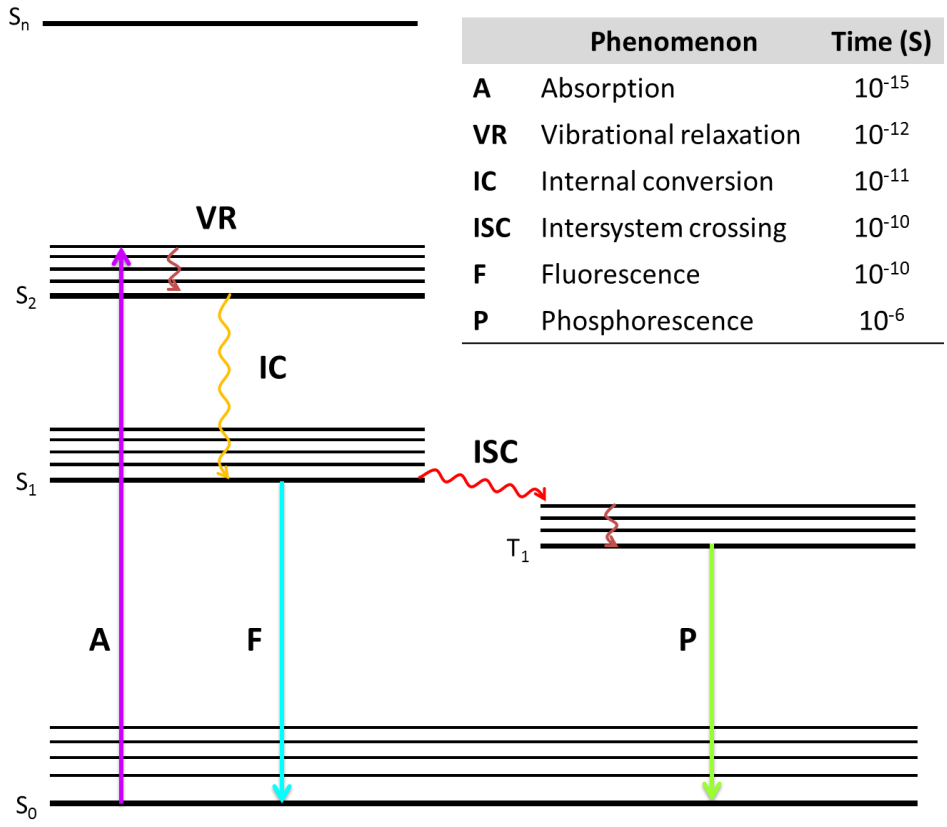

	Phenomenon	Time (S)
A	Absorption	10^{-15}
VR	Vibrational relaxation	10^{-12}
IC	Internal conversion	10^{-11}
ISC	Intersystem crossing	10^{-10}
F	Fluorescence	10^{-10}
P	Phosphorescence	10^{-6}

Figure 1.6. Perrin-Jablonski diagram, and characteristic times for various electronic transitions

The two modes of luminescence, fluorescence and phosphorescence, are initiated through the electronic excitation of a fluorophore by absorption of light. At room temperature, a majority of molecules are at the lowest vibrational energy level of S_0. Therefore, absorption of photons typically promotes those molecules from S_0 to higher vibrational energy levels of either S_1 or S_2. According to the Frank-Condon principle, time of absorption is too short for significant changes in the positions of nuclei.[101] Following absorption, the molecules are rapidly relaxed to the lowest (or to a lower) vibrational level of S_1 via non-radiative processes such as internal conversion and vibrational relaxation. The radiative transition of molecules from $S_1 \rightarrow S_0$ is called fluorescence.

Another possible non-radiative transition occurs from $S_1 \rightarrow T_1$, which is known as intersystem crossing. It should be noted that intersystem crossing happens between two isoenergetic vibrational levels of different multiplicities (e.g. between a singlet state and a triplet state).[101] The radiative emission taking place from $T_1 \rightarrow S_0$ is termed as phosphorescence. Intersystem crossing as well as phosphorescence is spin-forbidden, and therefore, rate of phosphorescence is much lower compared to fluorescence. However, due to spin-orbit coupling, these transitions are often possible.

The instrument that is used to measure fluorescence changes is known as spectrofluorometer (Figure 1.7). A Spectrofluorometer consists of a light source (e.g. xenon lamp), monochromators for excitation and emission wavelengths, and a detector (e.g. photomultiplier tubes or photodiode). The first monochromator is used to select the excitation wavelengths ranging from 200 – 900 nm. Photons emitted from the sample are collected at a right angle to the excitation light beam, and passed to a detector through a second monochromator.

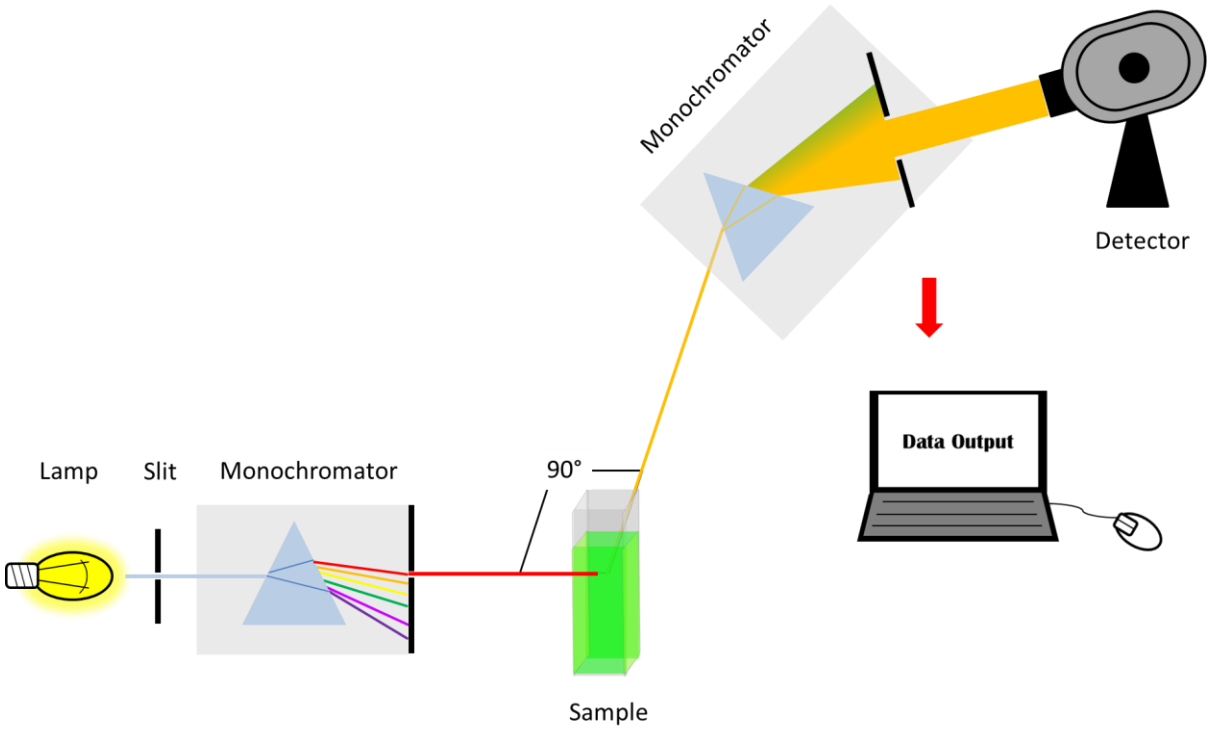

Figure 1.7. A schematic representation of a spectrofluorometer

Usually, fluorescence emission is sensitive to the microenvironment of the fluorophore. Moreover, fluorophores that display fluorescence changes due to specific changes in their microenvironment are used as probes in various applications. Small variations in the parameters such as polarity,[102] viscosity,[103] pH,[104] temperature,[105] surrounding ions,[106] and quenchers[107] of the microenvironment can cause significant spectral changes of a fluorescence probe. The spectral changes, which include absorption /emission peak(s) and their patterns, stoke shift, quantum yield, and fluorescence lifetime are used to study the structure and dynamics of various chemical and biological systems. Fluorescence probes are categorized into two primary groups: intrinsic probes, and extrinsic probes.[101] The extrinsic probes can be further categorized into two groups: covalently bound probes, and associating probes.[101] Each of these categories exhibits advantages and disadvantages, and therefore, should be selected based on application.

1.4. Chemical Sensor Arrays

1.4.1. General Definition

In the past, sensor arrays were recognized as assemblies of sensors that are used to obtain analytical information of a test sample in real time. Usually, the sensors in a sensor array are exposed to a sample of interest and the collective response of these sensors is treated as the sensor array response. The collective response of a sensor array is often termed as a "sensor response pattern". Ideally, different analytes should provide distinct response patterns, which enable the detection and discrimination of those analytes.

Over the last few decades, chemical sensor arrays have been widely explored as analytical tools for aqueous- and gas-phase analytes.[108-117] Sensor arrays that are designed for gas-phase sensing applications are known as electronic noses, whereas sensor arrays that are used in aqueous-phase sensing applications are termed electronic tongues.[118] In 1994, Gardner and Bartlett proposed a definition for the term electronic nose. According to their definition an electronic nose is: "an instrument which comprises an array of electronic chemical sensors with partial specificity and an appropriate pattern recognition system, capable of recognizing simple or complex orders".[119] This definition can be slightly adapted to create a general definition for chemical sensor arrays as given below.

A chemical sensor array is an analytical device, containing an assembly of cross-reactive sensor elements coupled to a pattern recognition tool, which is designed to detect and discriminates simple and complex analyte mixtures

1.4.2. Why Chemical Sensor Arrays?

Chemical selectivity is the most important parameter in the designing step of a chemical sensor. Biosensors such as enzymes and antibodies, which are found in nature, often display excellent selectivity and sensitivity toward a particular analyte. These sensors typically employ a "lock-and-key" approach in molecular recognition which requires specific binding interactions.[117,120] Therefore, design of highly selective sensors often involves imitation of such sensors. Over the years, researchers have made huge strides in designing selective sensors. However, despite considerable success in designing selective sensors, the fabrication of extremely selective sensors is practically a very challenging task.[117]

Researchers have proposed an alternate nature-inspired non-specific binding approach to bypass the design difficulties that arise during fabrication of selective sensors. Mammalian sensory processes such as olfaction and gustation employ differential receptors in nose and tongue respectively.[121] In mammalian olfaction, upon binding of an odorant molecule to an olfactory receptor, an electrical signal is passed from the receptor to brain through a neuron. Then, this electrical signal is transduced into a sense of smell and identified by the brain. As mentioned previously, chemical sensor arrays are also designed to mimic mammalian olfactory and gustatory processes. Therefore, chemical sensor arrays also contain an array of partially-selective sensors, which are also known as differential sensors primarily due to their non-specific binding with analytes.[120] Furthermore, these senor arrays are usually coupled to a pattern recognition system that acts as a brain in analyte recognition. Due to functional similarities between noses or tongues and intelligent sensor arrays, these devices are termed as electronic noses or tongues respectively.[118,121]

A graphical representation of lock-and-key sensors verses differential/non-selective sensors is provided in Figure 1.8. In this figure, both types of sensors are represented as colorimetric sensors. As shown in the figure, the sensor which employs the lock-and-key principal to bind with the analyte is very selective towards its analyte, and hence, there is only one possible outcome. By contrast, the second sensor uses a non-selective binding approach, and therefore, the sensor responses are dependent on the analyte. Sensor arrays typically employ sensors with non-selective binding interactions. Usually, these sensors are capable of binding to various types of analytes via multiple intermolecular interactions, generating differential sensor responses.

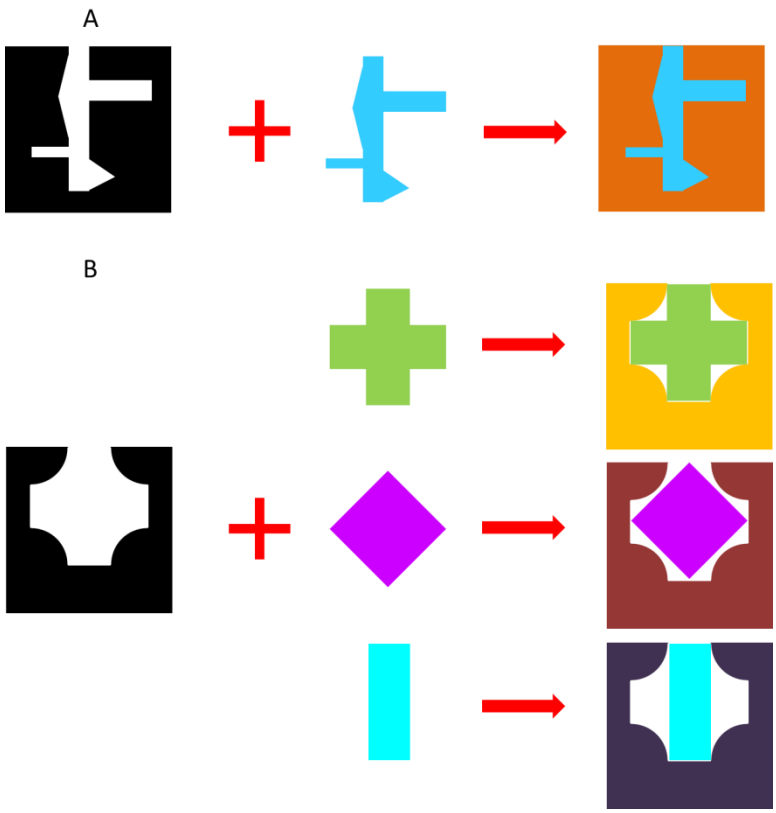

Figure 1.8. A graphical representation of a sensor which employs (A) lock-and-key method vs (B) non-specific bonding

1.4.3. General Operating Principal of Chemical Sensor Arrays

The general operating principle of sensor arrays is described using Figure 1.9. In this figure, a sensor array is used to detect and discriminate three different analyte samples. Each sample contains multiple analytes, and certain analytes are common in multiple samples. The sensor array is composed of four individual sensor elements, which display non-specific binding toward analytes.

After the exposure to different samples, the sensor elements in the array bind with various types of analytes depending on their affinity towards those analytes. As an example, the first two sensors in the sensor array are capable of binding to more than one analyte present in Sample 2. However, those two sensors display higher affinities towards the red analyte compared to the other two. Therefore, the red analyte is bound to the first two sensors in the senor array-analyte complex. As given in Figure 1.9, each sensor array-analyte complex is responsible for a unique sensor response patterns. These response patterns may contain both qualitative and quantitative information about each sample. The response patterns act as a fingerprint signal for each analyte sample, and therefore, can be used for sample discrimination.

The pattern recognition step that is involved in sensor arrays is often achieved by statistical techniques. As an example, sensor array responses are often discriminated using statistical tools such as multivariate data analysis (e.g. principal component analysis and linear discriminant analysis) or artificial neural network. As mentioned earlier, the recognition step in mammalian sensors is done by brain. Consequently, the pattern recognition tools that are used in sensor array applications are often termed artificial brains.

Overall, we observe an ever-increasing demand in design and application of various types of chemical sensor arrays for different applications. Chemical sensor arrays have shown promising qualities and advantages as compared to traditional analytical methods over a wide range of applications. A few of these advantages and applications are discussed in more detail in Chapters 2, 4, and 5.

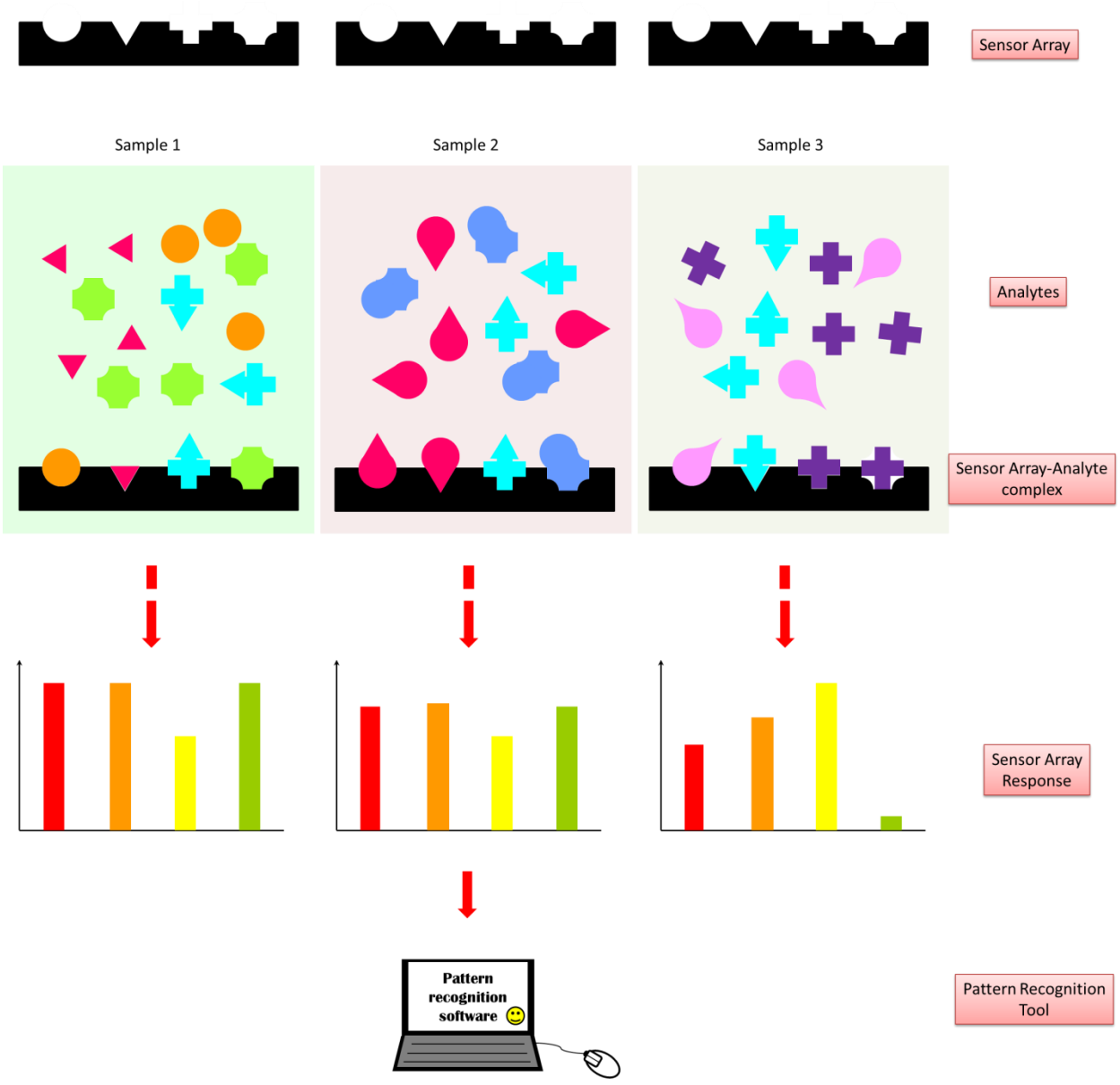

Figure 1.9. A schematic representation of the operation of a chemical sensor array

1.5. Scope of the Dissertation

The overall objective of this thesis research was to develop task-specific organic salts for chemical and biochemical sensing. These functional materials can be classified into two categories: (i) room temperature ionic liquids (RTILs) which remain in liquid state at room temperature and (ii) a ***g***roup of ***u***niform ***m***aterials ***b***ased on ***o***rganic ***s***alts (GUMBOS) with melting points between 25 to 250 °C. This dissertation consists of four different research studies, with distinct advantages for analytical measurements.

In Chapter 2, ionic liquid (IL)-based colorimetric sensor arrays were developed using a series of 12 different indicator dye-based hydrophobic ILs for detection of chemicals in both aqueous and vapor phases. The use of ILs in such sensor arrays overcomes certain limitations that are associated with the current colorimetric sensor arrays, which is the primary advantage of this approach. A total of four matrices including filter papers, cotton threads, silica thin layer chromatography (TLC) plates, and alumina TLC plates were used in fabricating the sensor arrays. Furthermore, this chapter describes fabrication of a wearable personal sensor arrays by using cotton threads as matrices without requiring any expensive pretreatments of the threads. These wearable arrays may be incorporated into bandages, sweatbands, diapers, and similar systems.

Third Chapter involves fabrication of an IL-based sensor for highly selective and sensitive detection of serum albumin. In this project, fluorescein-based IL nanodroplets were used as a label-free fluorescent probe. The IL molecules in these nanodroplets were found to coexist as a mixture of strongly fluorescent monomers and weakly fluorescent molecular aggregates. The relative abundance of these two species (i.e. monomers and aggregates) was

found to be dependent on the type and concentration of proteins. In the presence of HSA, the fluorescence signal increased due to the predominance of the monomeric forms, and an excellent correlation between fluorescence intensity and protein concentration was obtained.

The forth chapter of this dissertation demonstrates fabrication of a virtual colorimetric sensor array using a single IL. In this study, four different concentrations of an indicator dye-based IL sensor were used for accurate discrimination of similar organic solvents and solvent mixtures. The examination of UV-visible spectra of the IL sensor in different alcohols display two absorption bands, and the absorbance ratio of these two bands were found to be extremely sensitive to solvent polarity.

In Chapter 5, a GUMBOS-based fluorometric sensor array approach was developed using a series of four different 6-(p-toluidino)-2-naphthalenesulfonate (TNS)-based organic salts for detection and discrimination of proteins. The physicochemical properties of these GUMBOS were tuned by varying the counter cation of these sensors, and therefore, exhibited a differential fluorescence response depending on the protein composition of the analyte sample. Furthermore, this sensor approach was used to discriminate protein mixtures at different concentration levels. Overall, these four studies demonstrate that ILs and GUMBOS are promising materials, which enable the development of advanced sensor strategies, for both gas- and liquid-phase sensing applications.

1.6. References

(1) Ohno, H.; Yoshizawa, M.: Ion conductive characteristics of ionic liquids prepared by neutralization of alkylimidazoles. *Solid State Ionics* **2002**, *154–155*, 303-309.

(2) Del Pópolo, M. G.; Voth, G. A.: On the structure and dynamics of ionic liquids. *The Journal of Physical Chemistry B* **2004**, *108*, 1744-1752.

(3) Hallett, J. P.; Welton, T.: Room-temperature ionic liquids: solvents for synthesis and catalysis. 2. *Chemical Reviews* **2011**, *111*, 3508-3576.

(4) Welton, T.: Room-temperature ionic liquids. Solvents for synthesis and catalysis. *Chemical reviews* **1999**, *99*, 2071-2084.

(5) Gorman, J.: Faster, better, cleaner?: New liquids take aim at old-fashioned chemistry. *Science News* **2001**, *160*, 156-158.

(6) Holbrey, J.; Seddon, K.: Ionic liquids. *Clean Products and Processes* **1999**, *1*, 223-236.

(7) Gabriel, S.; Weiner, J.: On some derivatives of propylamine. *Deutsche Chemische Gesellschaft* **1888**, *21*, 2669-2679.

(8) Walden, P.: Über die Molekulargröße und elektrische Leitfähigkeit einiger geschmolzener Salze. *Bulletin de l'Académie Impériale des Sciences de Saint-Pétersbourg. St. Petersburg* **1914**, *8*, 405-422.

(9) Soukup-Hein, R. J.; Warnke, M. M.; Armstrong, D. W.: Ionic liquids in analytical chemistry. *Annual Review of Analytical Chemistry* **2009**, *2*, 145-168.

(10) Wilkins, J.; Zawowtko, M.: Air and water stable 1. ethy1. 3. methy1. imidazolium based ionic liquid. *Journal of the Chemical Society, Chemical Communications* **1992**, *13*, 965-967.

(11) MacFarlane, D. R.; Tachikawa, N.; Forsyth, M.; Pringle, J. M.; Howlett, P. C.; Elliott, G. D.; Davis, J. H.; Watanabe, M.; Simon, P.; Angell, C. A.: Energy applications of ionic liquids. *Energy & Environmental Science* **2014**, *7*, 232-250.

(12) Liu, J.; Wang, F.; Zhang, L.; Fang, X.; Zhang, Z.: Thermodynamic properties and thermal stability of ionic liquid-based nanofluids containing graphene as advanced heat transfer fluids for medium-to-high-temperature applications. *Renewable Energy* **2014**, *63*, 519-523.

(13) Miran, M. S.; Yasuda, T.; Susan, M. A. B. H.; Dokko, K.; Watanabe, M.: Binary Protic Ionic Liquid Mixtures as a Proton Conductor: High Fuel Cell Reaction Activity and Facile Proton Transport. *The Journal of Physical Chemistry C* **2014**, *118*, 27631-27639.

(14) Frink, L. A.; Weatherly, C. A.; Armstrong, D. W.: Water determination in active pharmaceutical ingredients using ionic liquid headspace gas chromatography and two different detection protocols. *Journal of pharmaceutical and biomedical analysis* **2014**, *94*, 111-117.

(15) Tang, S.; Baker, G. A.; Zhao, H.: Ether-and alcohol-functionalized task-specific ionic liquids: attractive properties and applications. *Chemical Society Reviews* **2012**, *41*, 4030-4066.

(16) Steinrück, H.-P.; Wasserscheid, P.: Ionic Liquids in Catalysis. *Catalysis Letters* **2015**, *145*, 380-397.

(17) Nowicki, J.; Muszyński, M.; Gryglewicz, S.: Novel basic ionic liquids from cyclic guanidines and amidines–new catalysts for transesterification of oleochemicals. *Journal of Chemical Technology and Biotechnology* **2014**, *89*, 48-55.

(18) Han, X.; Yan, W.; Chen, K.; Hung, C.-T.; Liu, L.-L.; Wu, P.-H.; Huang, S.-J.; Liu, S.-B.: Heteropolyacid-based ionic liquids as effective catalysts for the synthesis of benzaldehyde glycol acetal. *Applied Catalysis A: General* **2014**, *485*, 149-156.

(19) Duan, X.; Ma, J.; Lian, J.; Zheng, W.: The art of using ionic liquids in the synthesis of inorganic nanomaterials. *CrystEngComm* **2014**, *16*, 2550-2559.

(20) Page, Z. A.; Liu, F.; Russell, T. P.; Emrick, T.: Rapid, facile synthesis of conjugated polymer zwitterions in ionic liquids. *Chem. Sci.* **2014**, *5*, 2368-2373.

(21) Schütte, K.; Meyer, H.; Gemel, C.; Barthel, J.; Fischer, R. A.; Janiak, C.: Synthesis of Cu, Zn and Cu/Zn brass alloy nanoparticles from metal amidinate precursors in ionic liquids or propylene carbonate with relevance to methanol synthesis. *Nanoscale* **2014**, *6*, 3116-3126.

(22) Sun, X.; Luo, H.; Dai, S.: Ionic liquids-based extraction: a promising strategy for the advanced nuclear fuel cycle. *Chemical reviews* **2011**, *112*, 2100-2128.

(23) Fischer, L.; Falta, T.; Koellensperger, G.; Stojanovic, A.; Kogelnig, D.; Galanski, M.; Krachler, R.; Keppler, B. K.; Hann, S.: Ionic liquids for extraction of metals and metal containing compounds from communal and industrial waste water. *water research* **2011**, *45*, 4601-4614.

(24) Billard, I.; Ouadi, A.; Gaillard, C.: Liquid–liquid extraction of actinides, lanthanides, and fission products by use of ionic liquids: from discovery to understanding. *Anal Bioanalytical Chemistry* **2011**, *400*, 1555-1566.

(25) Menne, S.; Pires, J.; Anouti, M.; Balducci, A.: Protic ionic liquids as electrolytes for lithium-ion batteries. *Electrochemistry Communications* **2013**, *31*, 39-41.

(26) Lynden-Bell, R. M.; Frolov, A.; Fedorov, M. V.: Electrode screening by ionic liquids. *Physical Chemistry Chemical Physics* **2012**, *14*, 2693-2701.

(27) Zhao, Y.; Gao, Y.; Zhan, D.; Liu, H.; Zhao, Q.; Kou, Y.; Shao, Y.; Li, M.; Zhuang, Q.; Zhu, Z.: Selective detection of dopamine in the presence of ascorbic acid and uric acid by a carbon nanotubes-ionic liquid gel modified electrode. *Talanta* **2005**, *66*, 51-57.

(28) Armstrong, D. W.; Zhang, L.-K.; He, L.; Gross, M. L.: Ionic liquids as matrixes for matrix-assisted laser desorption/ionization mass spectrometry. *Analytical chemistry* **2001**, *73*, 3679-3686.

(29) Carda-Broch, S.; Berthod, A.; Armstrong, D. W.: Ionic matrices for matrix-assisted laser desorption/ionization time-of-flight detection of DNA oligomers. *Rapid communications in mass spectrometry* **2003**, *17*, 553-560.

(30) Fukuyama, Y.; Nakaya, S.; Yamazaki, Y.; Tanaka, K.: Ionic liquid matrixes optimized for MALDI-MS of sulfated/sialylated/neutral oligosaccharides and glycopeptides. *Analytical chemistry* **2008**, *80*, 2171-2179.

(31) Han, X.; Armstrong, D. W.: Ionic liquids in separations. *Accounts of Chemical Research* **2007**, *40*, 1079-1086.

(32) Berthod, A.; Ruiz-Angel, M.; Carda-Broch, S.: Ionic liquids in separation techniques. *Journal of Chromatography A* **2008**, *1184*, 6-18.

(33) Han, D.; Row, K. H.: Recent applications of ionic liquids in separation technology. *Molecules* **2010**, *15*, 2405-2426.

(34) Earle, M. J.; Gordon, C. M.; Plechkova, N. V.; Seddon, K. R.; Welton, T.: Decolorization of ionic liquids for spectroscopy. *Analytical chemistry* **2007**, *79*, 758-764.

(35) Smith, E. F.; Garcia, I. J. V.; Briggs, D.; Licence, P.: Ionic liquids in vacuo; solution-phase X-ray photoelectron spectroscopy. *Chemical communications* **2005**, 5633-5635.

(36) Xia, Z.; Zaijun, L.; Rui, Y.; Huizhen, L.: A novel room temperature ionic liquid extraction spectrophotometric determination of trace germanium in natural water with methybenzeneazosalicylfluorone. *Analytical letters* **2006**, *39*, 863-877.

(37) Shiddiky, M. J.; Torriero, A. A.: Application of ionic liquids in electrochemical sensing systems. *Biosensors and Bioelectronics* **2011**, *26*, 1775-1787.

(38) Galpothdeniya, W. I. S.; McCarter, K. S.; De Rooy, S. L.; Regmi, B. P.; Das, S.; Hasan, F.; Tagge, A.; Warner, I. M.: Ionic liquid-based optoelectronic sensor arrays for chemical detection. *RSC Advances* **2014**, *4*, 7225-7234.

(39) Yung, K. Y.; Schadock-Hewitt, A. J.; Hunter, N. P.; Bright, F. V.; Baker, G. A.: 'Liquid litmus': chemosensory pH-responsive photonic ionic liquids. *Chemical Communications* **2011**, *47*, 4775-4777.

(40) Galpothdeniya, W. I. S.; Das, S.; De Rooy, S. L.; Regmi, B. P.; Hamdan, S.; Warner, I. M.: Fluorescein-based ionic liquid sensor for label-free detection of serum albumins. *Rsc Advances* **2014**, *4*, 17533-17540.

(41) Davis, J. H.: Task-specific ionic liquids. *Chemistry letters* **2004**, *33*, 1072-1077.

(42) Hayashi, S.; Hamaguchi, H.-o.: Discovery of a magnetic ionic liquid [bmim] FeCl4. *Chemistry Letters* **2004**, *33*, 1590-1591.

(43) Okuno, M.; Hamaguchi, H.-o.; Hayashi, S.: Magnetic manipulation of materials in a magnetic ionic liquid. *Applied physics letters* **2006**, *89*, 132506.

(44) Del Sesto, R. E.; McCleskey, T. M.; Burrell, A. K.; Baker, G. A.; Thompson, J. D.; Scott, B. L.; Wilkes, J. S.; Williams, P.: Structure and magnetic behavior of transition metal based ionic liquids. *Chemical Communications* **2008**, 447-449.

(45) Ding, J.; Armstrong, D. W.: Chiral ionic liquids: synthesis and applications. *Chirality* **2005**, *17*, 281-292.

(46) Ding, J.; Welton, T.; Armstrong, D. W.: Chiral ionic liquids as stationary phases in gas chromatography. *Analytical chemistry* **2004**, *76*, 6819-6822.

(47) Luo, S.; Mi, X.; Zhang, L.; Liu, S.; Xu, H.; Cheng, J. P.: Functionalized chiral ionic liquids as highly efficient asymmetric organocatalysts for Michael addition to nitroolefins. *Angewandte Chemie International Edition* **2006**, *45*, 3093-3097.

(48) Tang, S.; Babai, A.; Mudring, A. V.: Europium-Based Ionic Liquids as Luminescent Soft Materials. *Angewandte Chemie International Edition* **2008**, *47*, 7631-7634.

(49) Mallick, B.; Balke, B.; Felser, C.; Mudring, A. V.: Dysprosium Room-Temperature Ionic Liquids with Strong Luminescence and Response to Magnetic Fields. *Angewandte Chemie International Edition* **2008**, *47*, 7635-7638.

(50) Yoshida, Y.; Saito, G.: Design of functional ionic liquids using magneto-and luminescent-active anions. *Physical Chemistry Chemical Physics* **2010**, *12*, 1675-1684.

(51) Sun, H.; Harms, K.; Sundermeyer, J.: Aerobic oxidation of 2, 3, 6-trimethylphenol to trimethyl-1, 4-benzoquinone with copper (II) chloride as catalyst in ionic liquid and structure of the active species. *Journal of the American Chemical Society* **2004**, *126*, 9550-9551.

(52) Sellin, M. F.; Webb, P. B.; Cole-Hamilton, D. J.: Continuous flow homogeneous catalysis: hydroformylation of alkenes in supercritical fluid–ionic liquid biphasic mixtures. *Chemical Communications* **2001**, 781-782.

(53) Wasserscheid, P.; Waffenschmidt, H.; Machnitzki, P.; Kottsieper, K. W.; Stelzer, O.: Cationic phosphine ligands with phenylguanidinium modified xanthene moieties—a successful concept for highly regioselective, biphasic hydroformylation of oct-1-ene in hexafluorophosphate ionic liquids. *Chemical Communications* **2001**, 451-452.

(54) Warner, I. M.; El-Zahab, B.; Siraj, N.: Perspectives on Moving Ionic Liquid Chemistry into the Solid Phase. *Analytical chemistry* **2014**, *86*, 7184-7191.

(55) Wright, A.; Li, M.; Ravula, S.; Cadigan, M.; El-Zahab, B.; Das, S.; Baker, G.; Warner, I.: Soft-and hard-templated organic salt nanoparticles with the Midas touch: gold-shelled nanoGUMBOS. *Journal of Materials Chemistry C* **2014**, *2*, 8996-9003.

(56) Das, S.; de Rooy, S. L.; Jordan, A. N.; Chandler, L.; Negulescu, I. I.; El-Zahab, B.; Warner, I. M.: Tunable Size and Spectral Properties of Fluorescent NanoGUMBOS in Modified Sodium Deoxycholate Hydrogels. *Langmuir* **2011**, *28*, 757-765.

(57) de Rooy, S. L.; Das, S.; Li, M.; El-Zahab, B.; Jordan, A.; Lodes, R.; Weber, A.; Chandler, L.; Baker, G. A.; Warner, I. M.: Ionically Self-Assembled, Multi-Luminophore One-Dimensional Micro-and Nanoscale Aggregates of Thiacarbocyanine GUMBOS. *The Journal of Physical Chemistry C* **2012**, *116*, 8251-8260.

(58) Tesfai, A.; El-Zahab, B.; Kelley, A. T.; Li, M.; Garno, J. C.; Baker, G. A.; Warner, I. M.: Magnetic and nonmagnetic nanoparticles from a group of uniform materials based on organic salts. *Acs Nano* **2009**, *3*, 3244-3250.

(59) Hamdan, S.; Dumke, J. C.; El-Zahab, B.; Das, S.; Boldor, D.; Baker, G. A.; Warner, I. M.: Strategies for Controlled Synthesis of Nanoparticles derived from a Group of Uniform Materials Based on Organic Salts. *Journal of Colloid and Interface Science* **2015**.

(60) Bwambok, D. K.; El-Zahab, B.; Challa, S. K.; Li, M.; Chandler, L.; Baker, G. A.; Warner, I. M.: Near-infrared fluorescent nanoGUMBOS for biomedical imaging. *Acs Nano* **2009**, *3*, 3854-3860.

(61) Magut, P. K.; Das, S.; Fernand, V. E.; Losso, J.; McDonough, K.; Naylor, B. M.; Aggarwal, S.; Warner, I. M.: Tunable cytotoxicity of rhodamine 6G via anion variations. *Journal of the American Chemical Society* **2013**, *135*, 15873-15879.

(62) Jordan, A. N.; Das, S.; Siraj, N.; de Rooy, S. L.; Li, M.; El-Zahab, B.; Chandler, L.; Baker, G. A.; Warner, I. M.: Anion-controlled morphologies and spectral features of cyanine-based nanoGUMBOS–an improved photosensitizer. *Nanoscale* **2012**, *4*, 5031-5038.

(63) Siraj, N.; Hasan, F.; Das, S.; Kiruri, L. W.; Steege Gall, K. E.; Baker, G. A.; Warner, I. M.: Carbazole-derived group of uniform materials based on organic salts: Solid state fluorescent analogues of ionic liquids for potential applications in organic-based blue light-emitting diodes. *The Journal of Physical Chemistry C* **2014**, *118*, 2312-2320.

(64) Dumke, J. C.; Qureshi, A.; Hamdan, S.; El-Zahab, B.; Das, S.; Hayes, D. J.; Boldor, D.; Rupnik, K.; Warner, I. M.: Photothermal Response of Near-Infrared-Absorbing NanoGUMBOS. *Applied spectroscopy* **2014**, *68*, 340-352.

(65) Banica, F.-G.: *Chemical sensors and biosensors: fundamentals and applications*; John Wiley & Sons, 2012.

(66) Thévenot, D. R.; Toth, K.; Durst, R. A.; Wilson, G. S.: Electrochemical biosensors: recommended definitions and classification. *Biosensors and Bioelectronics* **2001**, *16*, 121-131.

(67) Eggins, B. R.: *Chemical sensors and biosensors*; John Wiley & Sons, 2008; Vol. 28.

(68) Scholz, F.: From the Leiden jar to the discovery of the glass electrode by Max Cremer. *Journal of Solid State Electrochemistry* **2011**, *15*, 5-14.

(69) Bakker, E.; Diamond, D.; Lewenstam, A.; Pretsch, E.: Ion sensors: current limits and new trends. *Analytica chimica acta* **1999**, *393*, 11-18.

(70) Janata, J.; Josowicz, M.; Vanýsek, P.; DeVaney, D. M.: Chemical sensors. *Analytical Chemistry* **1998**, *70*, 179-208.

(71) Wenger, O. S.: Vapochromism in organometallic and coordination complexes: chemical sensors for volatile organic compounds. *Chemical reviews* **2013**, *113*, 3686-3733.

(72) Kreno, L. E.; Leong, K.; Farha, O. K.; Allendorf, M.; Van Duyne, R. P.; Hupp, J. T.: Metal–organic framework materials as chemical sensors. *Chemical Reviews* **2011**, *112*, 1105-1125.

(73) Thomas, S. W.; Joly, G. D.; Swager, T. M.: Chemical sensors based on amplifying fluorescent conjugated polymers. *Chemical Reviews* **2007**, *107*, 1339-1386.

(74) Luppa, P. B.; Sokoll, L. J.; Chan, D. W.: Immunosensors—principles and applications to clinical chemistry. *Clinica Chimica Acta* **2001**, *314*, 1-26.

(75) Ghindilis, A. L.; Atanasov, P.; Wilkins, M.; Wilkins, E.: Immunosensors: electrochemical sensing and other engineering approaches. *Biosensors and Bioelectronics* **1998**, *13*, 113-131.

(76) Mani, V.; Chikkaveeraiah, B. V.; Patel, V.; Gutkind, J. S.; Rusling, J. F.: Ultrasensitive immunosensor for cancer biomarker proteins using gold nanoparticle film electrodes and multienzyme-particle amplification. *ACS nano* **2009**, *3*, 585-594.

(77) Karube, I.; Matsuoka, H.; Suzuki, S.; Watanabe, E.; Toyama, K.: Determination of fish freshness with an enzyme sensor system. *Journal of Agricultural and Food Chemistry* **1984**, *32*, 314-319.

(78) Lange, J.; Wittmann, C.: Enzyme sensor array for the determination of biogenic amines in food samples. *Analytical and Bioanalytical Chemistry* **2002**, *372*, 276-283.

(79) Endo, H.; Yonemori, Y.; Hibi, K.; Ren, H.; Hayashi, T.; Tsugawa, W.; Sode, K.: Wireless enzyme sensor system for real-time monitoring of blood glucose levels in fish. *Biosensors and Bioelectronics* **2009**, *24*, 1417-1423.

(80) Cheng, X.; Bing, T.; Liu, X.; Shangguan, D.: A label-free fluorescence sensor for probing the interaction of oligonucleotides with target molecules. *Analytica chimica acta* **2009**, *633*, 97-102.

(81) Tang, L.; Zeng, G.; Shen, G.; Li, Y.; Liu, C.; Li, Z.; Luo, J.; Fan, C.; Yang, C.: Sensitive detection of lip genes by electrochemical DNA sensor and its application in polymerase chain reaction amplicons from Phanerochaete chrysosporium. *Biosensors and Bioelectronics* **2009**, *24*, 1474-1479.

(82) Bürckstümmer, T.; Baumann, C.; Blüml, S.; Dixit, E.; Dürnberger, G.; Jahn, H.; Planyavsky, M.; Bilban, M.; Colinge, J.; Bennett, K. L.: An orthogonal proteomic-genomic

screen identifies AIM2 as a cytoplasmic DNA sensor for the inflammasome. *Nature immunology* **2009**, *10*, 266-272.

(83) Xiao, Y.; Lubin, A. A.; Heeger, A. J.; Plaxco, K. W.: Label-free electronic detection of thrombin in blood serum by using an aptamer-based sensor. *Angewandte Chemie* **2005**, *117*, 5592-5595.

(84) Xiao, Y.; Piorek, B. D.; Plaxco, K. W.; Heeger, A. J.: A reagentless signal-on architecture for electronic, aptamer-based sensors via target-induced strand displacement. *Journal of the American Chemical Society* **2005**, *127*, 17990-17991.

(85) Iliuk, A. B.; Hu, L.; Tao, W. A.: Aptamer in bioanalytical applications. *Analytical chemistry* **2011**, *83*, 4440-4452.

(86) Haick, H.; Broza, Y. Y.; Mochalski, P.; Ruzsanyi, V.; Amann, A.: Assessment, origin, and implementation of breath volatile cancer markers. *Chemical Society Reviews* **2014**, *43*, 1423-1449.

(87) Regmi, B. P.; Galpothdeniya, W. I. S.; Siraj, N.; Webb, M. H.; Speller, N. C.; Warner, I. M.: Phthalocyanine- and porphyrin-based GUMBOS for rapid and sensitive detection of organic vapors. *Sensors and Actuators B: Chemical* **2015**, *209*, 172-179.

(88) Uludag, Y.; Tothill, I. E.: Cancer biomarker detection in serum samples using surface plasmon resonance and quartz crystal microbalance sensors with nanoparticle signal amplification. *Analytical chemistry* **2012**, *84*, 5898-5904.

(89) Toniolo, R.; Pizzariello, A.; Dossi, N.; Lorenzon, S.; Abollino, O.; Bontempelli, G.: Room temperature ionic liquids as useful overlayers for estimating food quality from their odor analysis by quartz crystal microbalance measurements. *Analytical chemistry* **2013**, *85*, 7241-7247.

(90) Bratov, A.; Abramova, N.; Ipatov, A.: Recent trends in potentiometric sensor arrays—A review. *Analytica chimica acta* **2010**, *678*, 149-159.

(91) Bobacka, J.; Ivaska, A.; Lewenstam, A.: Potentiometric ion sensors. *Chemical reviews* **2008**, *108*, 329-351.

(92) Bakker, E.: Electrochemical sensors. *Analytical chemistry* **2004**, *76*, 3285-3298.

(93) Bahrami, A.; Besharati-Seidani, A.; Abbaspour, A.; Shamsipur, M.: A highly selective voltammetric sensor for sub-nanomolar detection of lead ions using a carbon paste electrode impregnated with novel ion imprinted polymeric nanobeads. *Electrochimica Acta* **2014**, *118*, 92-99.

(94) Lu, C.; Czanderna, A. W.: *Applications of piezoelectric quartz crystal microbalances*; Elsevier, 2012.

(95) Najib, F. M.; Zewar, S.; Abdulla, A. M.: A new sensor for thermometric titrations. *Talanta* **2007**, *71*, 141-148.

(96) Ramanathan, K.; Danielsson, B.: Principles and applications of thermal biosensors. *Biosensors and Bioelectronics* **2001**, *16*, 417-423.

(97) Tremblay, N.; Wang, Z.; Cerovic, Z. G.: Sensing crop nitrogen status with fluorescence indicators. A review. *Agronomy for sustainable development* **2012**, *32*, 451-464.

(98) Wang, F.; Wang, L.; Chen, X.; Yoon, J.: Recent progress in the development of fluorometric and colorimetric chemosensors for detection of cyanide ions. *Chemical Society Reviews* **2014**, *43*, 4312-4324.

(99) Galpothdeniya, W. I.; Regmi, B. P.; McCarter, K. S.; de Rooy, S. L.; Siraj, N.; Warner, I. M.: Virtual Colorimetric Sensor Array: Single Ionic Liquid for Solvent Discrimination. *Analytical Chemistry*, **2015,** *87*, 4464–4471.

(100) Lakowicz, J. R.: *Principles of fluorescence spectroscopy*; Springer Science & Business Media, 2007.

(101) Valeur, B.; Berberan-Santos, M. N.: *Molecular fluorescence: principles and applications*; John Wiley & Sons, 2012.

(102) Higginbotham, H. F.; Cox, R. P.; Sandanayake, S.; Graystone, B. A.; Langford, S. J.; Bell, T. D.: A fluorescent "2 in 1" proton sensor and polarity probe based on core substituted naphthalene diimide. *Chemical Communications* **2013**, *49*, 5061-5063.

(103) Liu, F.; Wu, T.; Cao, J.; Cui, S.; Yang, Z.; Qiang, X.; Sun, S.; Song, F.; Fan, J.; Wang, J.: Ratiometric Detection of Viscosity Using a Two-Photon Fluorescent Sensor. *Chemistry-A European Journal* **2013**, *19*, 1548-1553.

(104) Tian, M.; Peng, X.; Fan, J.; Wang, J.; Sun, S.: A fluorescent sensor for pH based on rhodamine fluorophore. *Dyes and Pigments* **2012**, *95*, 112-115.

(105) Kim, K. B.; Kim, H.; Song, E. J.; Kim, S.; Noh, I.; Kim, C.: A cap-type Schiff base acting as a fluorescence sensor for zinc (II) and a colorimetric sensor for iron (II), copper (II), and zinc (II) in aqueous media. *Dalton Transactions* **2013**, *42*, 16569-16577.

(106) Li, M.; Lu, H.-Y.; Liu, R.-L.; Chen, J.-D.; Chen, C.-F.: Turn-on fluorescent sensor for selective detection of Zn2+, Cd2+, and Hg2+ in water. *The Journal of organic chemistry* **2012**, *77*, 3670-3673.

(107) Dong, H.; Zhang, J.; Ju, H.; Lu, H.; Wang, S.; Jin, S.; Hao, K.; Du, H.; Zhang, X.: Highly sensitive multiple microRNA detection based on fluorescence quenching of graphene oxide and isothermal strand-displacement polymerase reaction. *Analytical chemistry* **2012**, *84*, 4587-4593.

(108) Askim, J. R.; Mahmoudi, M.; Suslick, K. S.: Optical sensor arrays for chemical sensing: the optoelectronic nose. *Chemical Society Reviews* **2013**, *42*, 8649-8682.

(109) Carey, J. R.; Suslick, K. S.; Hulkower, K. I.; Imlay, J. A.; Imlay, K. R. C.; Ingison, C. K.; Ponder, J. B.; Sen, A.; Wittrig, A. E.: Rapid Identification of Bacteria with a Disposable Colorimetric Sensing Array. *Journal of the American Chemical Society* **2011**, *133*, 7571-7576.

(110) Zhang, C.; Suslick, K. S.: A colorimetric sensor array for organics in water. *Journal of the American Chemical Society* **2005**, *127*, 11548-11549.

(111) Feng, L.; Musto, C. J.; Kemling, J. W.; Lim, S. H.; Suslick, K. S.: A colorimetric sensor array for identification of toxic gases below permissible exposure limits. *Chemical Communications* **2010**, *46*, 2037-2039.

(112) Miranda, O. R.; You, C.-C.; Phillips, R.; Kim, I.-B.; Ghosh, P. S.; Bunz, U. H.; Rotello, V. M.: Array-based sensing of proteins using conjugated polymers. *Journal of the American Chemical Society* **2007**, *129*, 9856-9857.

(113) De, M.; Rana, S.; Akpinar, H.; Miranda, O. R.; Arvizo, R. R.; Bunz, U. H.; Rotello, V. M.: Sensing of proteins in human serum using conjugates of nanoparticles and green fluorescent protein. *Nature chemistry* **2009**, *1*, 461-465.

(114) Ariza-Avidad, M.; Salinas-Castillo, A.; Cuéllar, M. P.; Agudo-Acemel, M.; Pegalajar, M. C.; Capitán-Vallvey, L. F.: Printed Disposable Colorimetric Array for Metal Ion Discrimination. *Analytical Chemistry* **2014**, *86*, 8634-8641.

(115) Soga, T.; Jimbo, Y.; Suzuki, K.; Citterio, D.: Inkjet-printed paper-based colorimetric sensor array for the discrimination of volatile primary amines. *Analytical chemistry* **2013**, *85*, 8973-8978.

(116) Wright, A. T.; Edwards, N. Y.; Anslyn, E. V.; McDevitt, J. T.: The discriminatory power of differential receptor arrays is improved by prescreening—a demonstration in the analysis of tachykinins and similar peptides. *Angewandte Chemie International Edition* **2007**, *46*, 8212-8215.

(117) Wright, A. T.; Anslyn, E. V.: Differential receptor arrays and assays for solution-based molecular recognition. *Chemical Society Reviews* **2006**, *35*, 14-28.

(118) Gouma, P.; Sberveglieri, G.: Novel materials and applications of electronic noses and tongues. *MRS bulletin* **2004**, *29*, 697-702.

(119) Gardner, J. W.; Bartlett, P. N.: *Electronic noses: principles and applications*; Oxford University Press New York, 1999; Vol. 233.

(120) Lavigne, J. J.; Anslyn, E. V.: Sensing a paradigm shift in the field of molecular recognition: From selective to differential receptors. *Angewandte Chemie International Edition* **2001**, *40*, 3118-3130.

(121) Collins, B. E.; Anslyn, E. V.: Pattern-Based Peptide Recognition. *Chemistry-a European Journal* **2007**, *13*, 4700-4708.

CHAPTER 2: IONIC LIQUID-BASED OPTOELECTRONIC SENSOR ARRAYS FOR CHEMICAL DETECTION[*]

2.1. Introduction

Over the last several decades, electronic devices that can mimic human olfactory and gustatory processes have attracted considerable attention amongst researchers.[1] These artificial electronic noses and tongues, which are often defined as intelligent chemical array sensor systems,[2] are emerging as rapid, low-cost, and sensitive tools for chemical analysis, as compared to traditional more expensive instrumentation such as gas chromatography/mass spectroscopy (GC/MS).[1,3-5] Among the current electronic nose and tongue technologies, optoelectronic noses and tongues fabricated by use of an array of different dyes, which change colors based on intermolecular interactions (acid-base, dipole-dipole, and π-π), have shown higher chemical selectivity and sensitivity as compared to other types of sensor arrays.[6-9] This advantage has generated intense interest among a number of research groups to develop colorimetric sensor arrays for a wide range of applications.[10-13] Among such studies, work conducted by Suslick and co-workers can be identified as quite inspirational. For example, the studies by these authors include detection and identification of chemically diverse analytes using sensor arrays fabricated by immobilization of hydrophobic water-insoluble dyes onto hydrophobic membranes[7] or incorporating chemically-sensitive dyes into nanoporous silica microspheres.[5,6,14,15] A colorimetric sensor array using reversed phase silica gel plates as a matrix has also been developed by Huang *et al.*[11] for evaluation of freshness of fish. In addition, incorporation of

[*] This Chapter previously appeared as Galpothdeniya, W. I. S.; McCarter, K. S.; De Rooy, S. L.; Regmi, B. P.; Das, S.; Hasan, F.; Tagge, A.; Warner, I. M. Ionic Liquid-Based Optoelectronic Sensor Arrays for Chemical Detection. *RSC Advances* **2014**, *4*, 7225-7234. It is reproduced by permission of the Royal Society of Chemistry.
http://pubs.rsc.org/en/content/articlelanding/2014/ra/c3ra47518b/unauth#!divAbstract

various dyes into inorganic materials such as silica, alumina, and UVM-7 in order to monitor the aging of chicken meat has been reported by Salinas *et al*.[10]

Fabrication of optoelectronic tongues or colorimetric-taste sensor arrays, which are capable of operating in aqueous environments, is inherently challenging due to interferences from water. For aqueous-phase analysis, the sensor arrays should be relatively hydrophobic in order to avoid dissolution of the arrays. Despite considerable success in this field, current colorimetric sensor arrays are limited with regard to their ability to detect compounds in aqueous samples. The primary reason is that dyes which are used for aqueous-phase analysis should be hydrophobic and thus highly insoluble in water. Therefore, the number of dyes which fulfill this criterion are very limited. Moreover, this approach eliminates the ability to use the same dyes in both optoelectronic noses and tongues. In addition, the matrix/substrate on which the dyes are immobilized is required to be highly hydrophobic. Thus, the requirement of a specialized hydrophobic surface adds an additional constraint to the number of applications for a particular sensor array. Therefore, a proper choice of matrix is also important in successful fabrication of such sensor arrays. We note that there has recently been a burgeoning interest in using cotton threads as a matrix to immobilize dyes or other chemically active species. This interest is primarily due to inherent advantages such as facile, low-cost, low-volume, and excellent materials for displaying colorimetric results.[16,17] Natural cotton threads are hydrophobic due to the presence of a surface wax, and hence have low wettability.[16,18] Therefore, an expensive pretreatment such as plasma oxidation is required to allow adequate staining or wicking with aqueous dyes.[17,19] Otherwise, a specialized hydrophilic cotton thread is required for fabrication, which limits the applicability of the matrix.

As low melting organic salts,[20] ionic liquids (ILs), often have virtually no vapor pressure. These compounds are considered excellent alternatives to conventional organic solvents. Favorable properties of these liquid salts include good thermal stability, wide liquid temperature range, considerable ionic conductivity, a broad electrochemical window, and a wide solubility and miscibility range.[21,22] In addition, ILs can be designed or tuned for specific applications by altering either the cation or anion. In addition, ILs have recently been demonstrated to be excellent sensing materials for a number of different applications.[23-30] For example, Zeng and co-workers[23] have utilized a number of room temperature ILs (RTILs) to design a QCM sensor array for detection of organic vapors at high temperature.[24] Recently, a few parallel studies on development of sensor arrays based on ILs have also been reported.[25,26] Baker and co-workers[27] have recently synthesized a class of luminescent ILs using a pyranine anion, and have used these ILs for sensitive detection of alkylamines. Wang and coworkers[28,29] have demonstrated the potential use of ILs as fluorescence probes for highly sensitive detection of proteins. Over the last several years, ILs derived from indicator dyes have also been the focus of many studies. For example, Branco and Pina[30] have reported a series of photochromic ILs derived from methyl orange, and have showed that the photochromic response of these ILs can be tuned by simply changing the cation. In addition, the sensing performance of IL-modified dyes derived from methyl orange and methyl red, toward acids in aqueous and non-aqueous media have been reported by Zhang *et al*.[14]

Despite many of the aforementioned outstanding properties of ILs, their use in colorimetric sensor arrays remains largely unexplored. Herein, we outline the development of an IL-based optoelectronic sensor array, and demonstrate its applicability for prediction of values of pH in aqueous solution, detection of acidic and basic vapors, as well as discrimination of

complex mixtures such as aqueous samples containing dissolved smoke from various brands of cigarettes. A series of 12 different ILs, all employing [P_{66614}] as the counter ion, were synthesized from anionic dyes via a metathesis reaction. The pairing of [P_{66614}] cation with the dye anions imparted considerable hydrophobicity to the resultant ILs. As a result, these ILs were insoluble in aqueous solution, and thus exhibited reduced interferences from humidity. More importantly, it was found that these ILs do not require a specialized hydrophobic matrix as is normally required for analyses of aqueous samples using this approach. These ILs were immobilized on four commonly available matrices including silica and alumina TLC plates, filter papers, and cotton threads, which allowed successful fabrication of sensor arrays. Furthermore, the sensor arrays fabricated by use of cotton threads as matrices did not require expensive pretreatments or specialized cotton threads. The use of cotton threads as a sensor matrix is a promising approach for preparation of inexpensive wearable sensor arrays. In order to accurately identify the analytes, predictive models were developed using principal component analysis (PCA) and discriminant analysis. The resubstitution and cross-validation methods were used to assess the predictive accuracy of the models.

2.2. Experimental Section

2.2.1. Materials

All 12 indicator dyes (Phenol red (PR), Brilliant yellow (BY), Bromocresol green (BCG), *m*-cresol purple (mCP), Methyl Orange (MO), Methyl red (MR), p-Xylanol blue (Xyl), Bromophenol blue (BPB), Thymolphthalein (Thy), phenolphthalein (FFT), Chlorophenol red (ClR) and Bromothymol blue (BTB)), trihexyl-(tetradecyl)phosphonium chloride [P_{66614}] [Cl] (≥95%), ethanol (EtOH), and dichloromethane (DCM) were purchased from Sigma-Aldrich and

used as received. The 12 pH indicator dyes that are used in this study can be considered as very common choices for traditional colorimetric sensor arrays.[10,31,32] Triply deionized water (18.2 MΩ cm) from an Elga model PURELAB ultra water-filtration system was used for preparation of all buffer systems. Three brands of commercially available cigarettes (Marlboro® red, Crowns®, and Camel® Turkish domestic blend) were purchased from a local grocery store and used as received for smoke identification purposes.

2.2.2. Synthesis and Characterization of ILs

The ILs used in these studies were prepared using a previously reported anion exchange procedure.[33,34] Briefly, as an example, a mixture of NaMO and $P_{66614}Cl$ with a 1:1 mole ratio was dissolved in DCM-water (5:1 v/v) mixture, and stirred overnight. Afterwards, the DCM layer was washed with water several times in order to remove the NaCl byproduct. The resultant IL product, $[P_{66614}][MO]$, was obtained after removing DCM and water *in vacuo*. Other ILs were prepared using a similar procedure where the sodium salt of each indicator dye was coupled with the $[P_{66614}]$ cation to obtain the desired products. Finally, all ILs were characterized using nuclear magnetic resonance (NMR), Fourier transform infrared spectroscopy (FTIR) and Ultraviolet–visible spectroscopy (UV–Vis), and electron spray ionization mass spectrometry (ESI-MS). The resulted ILs showed weak or no fluorescence. Examination of results obtained from ESI-MS, when performed in both positive and negative ion modes, indicated exact masses corresponding to the respective cations and anions present in a given IL, thus confirming formation of the product. The presences of $[P_{66614}]$ cation and pH indicator anion in the ILs were further confirmed by ^{1}H NMR and FTIR spectra.

2.2.3. Preparation of IL Sensor Arrays Using TLC and Filter Paper Matrices

The twelve synthesized ILs were individually dissolved into ethanol to obtain twelve different 1.0 mM solutions of each IL. Each of these solutions was then spotted as a single spot onto a 25 mm x 25 mm matrix surface to obtain a 12-spot IL sensor array, and the resulting sensor array was kept in a desiccator for 24-48 hours. A schematic of the preparation of the sensor array is shown in Scheme 2.1.

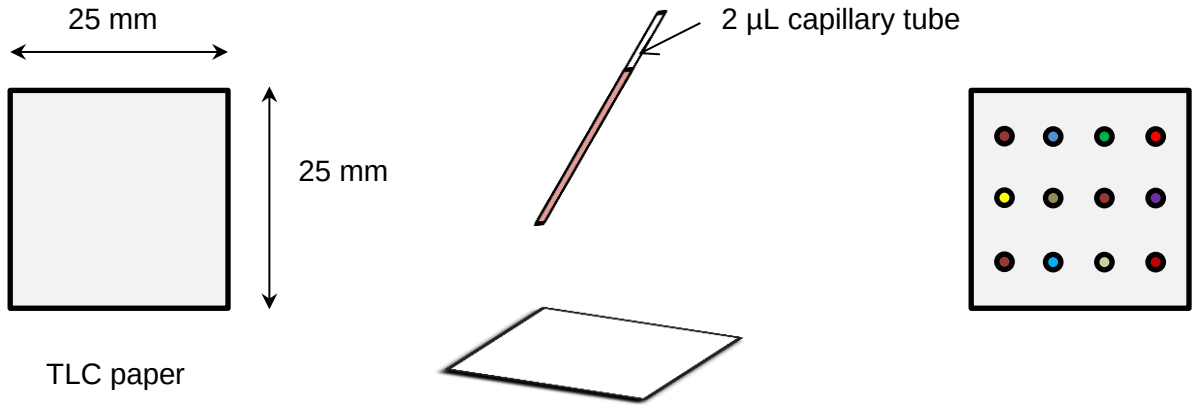

Scheme 2.1. Schematic representation of the preparation of IL sensor array on TLC and filer paper-based matrices

2.2.4. Preparation of an IL Sensor Array Using Cotton Thread Matrix

In order to stain the natural white cotton threads, 10 mM solution of IL was prepared by dissolving pure IL in DCM. Then 10 mL of each solution was placed in a U-tube and the cotton threads were passed through the tube and wound around a different spool. A schematic representation of this staining procedure is shown in Scheme 2.2. Afterwards, the IL-stained threads were sewn onto a cotton fabric template using a Singer (model number-7258) sewing machine.

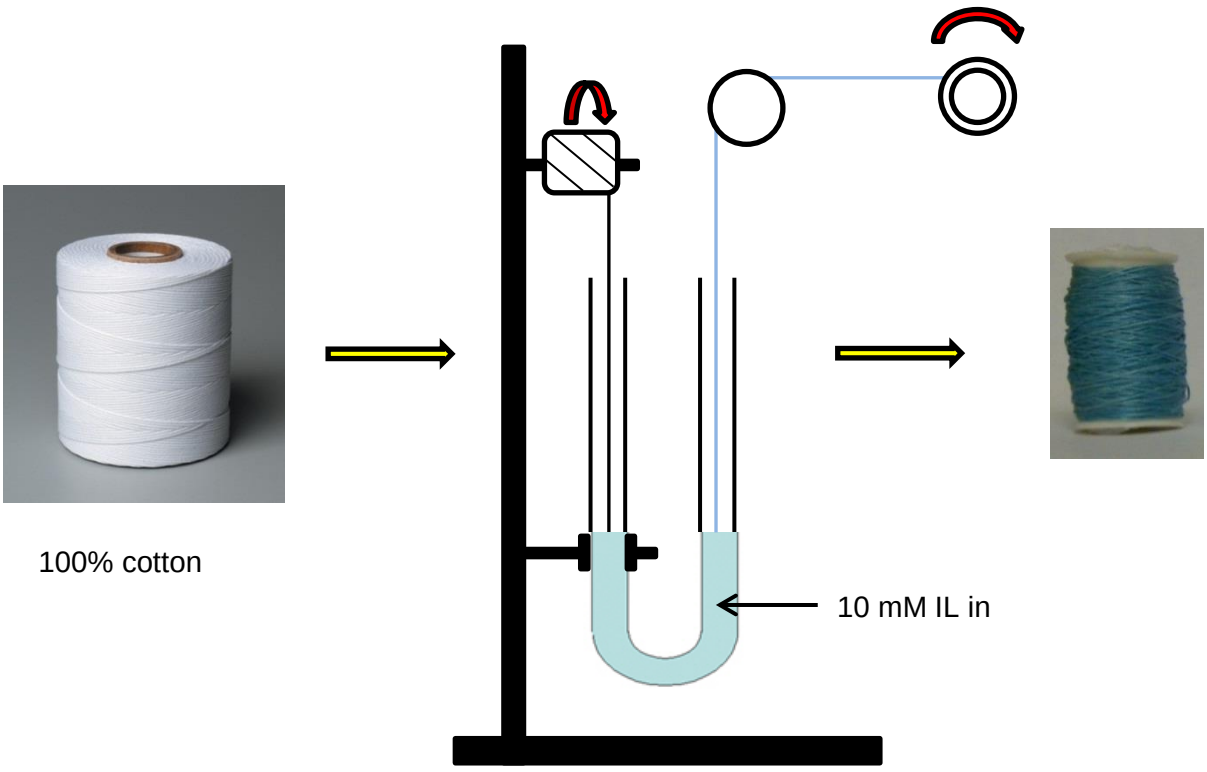

Scheme 2.2. Schematic representation for the staining procedure of the cotton threads with ILs. A 10 mM solution of IL in DCM was used to stain the natural white cotton threads. Slow constant wounding of the cotton threads yields an evenly coated stained cotton thread spool

2.2.5. Preparation and Analyses of Aqueous Solutions of Cigarette Smoke

Aqueous solutions of cigarette smoke were freshly prepared using a custom-made device (Scheme 2.3). This apparatus was fabricated to achieve three main goals: 1) to provide the suction necessary to extract smoke from the cigarette, 2) to collect the cigarette smoke in a closed environment, and 3) to supply an aqueous medium for dissolution of the cigarette smoke. A 1-liter-plastic bottle was drilled from the lid and a side, and a one inch rubber tube with a cap was attached to each hole. The hole on the side of the wall was drilled in such a manner as to retain only 350 mL of aqueous layer in the bottle. The bottle was filled with triply deionized water, and the cigarette to be analyzed was fixed into the hole of the lid and sealed by using

parafilm. Later, the cigarette smoke was collected after lighting the cigarette followed by releasing the cap from the side-wall outlet. The collected cigarette smoke was dissolved into 350 mL of the residual distilled water by vigorously shaking the bottle for five minutes, and the system allowed to equilibrate for 30 minutes. Finally, the sensor array fabricated by using the filter paper matrix was inserted into a 10 mL portion of the aqueous layer for five minutes in order to obtain color changes that correlate with a particular cigarette brand. In these studies, seven cigarettes of each brand were analyzed.

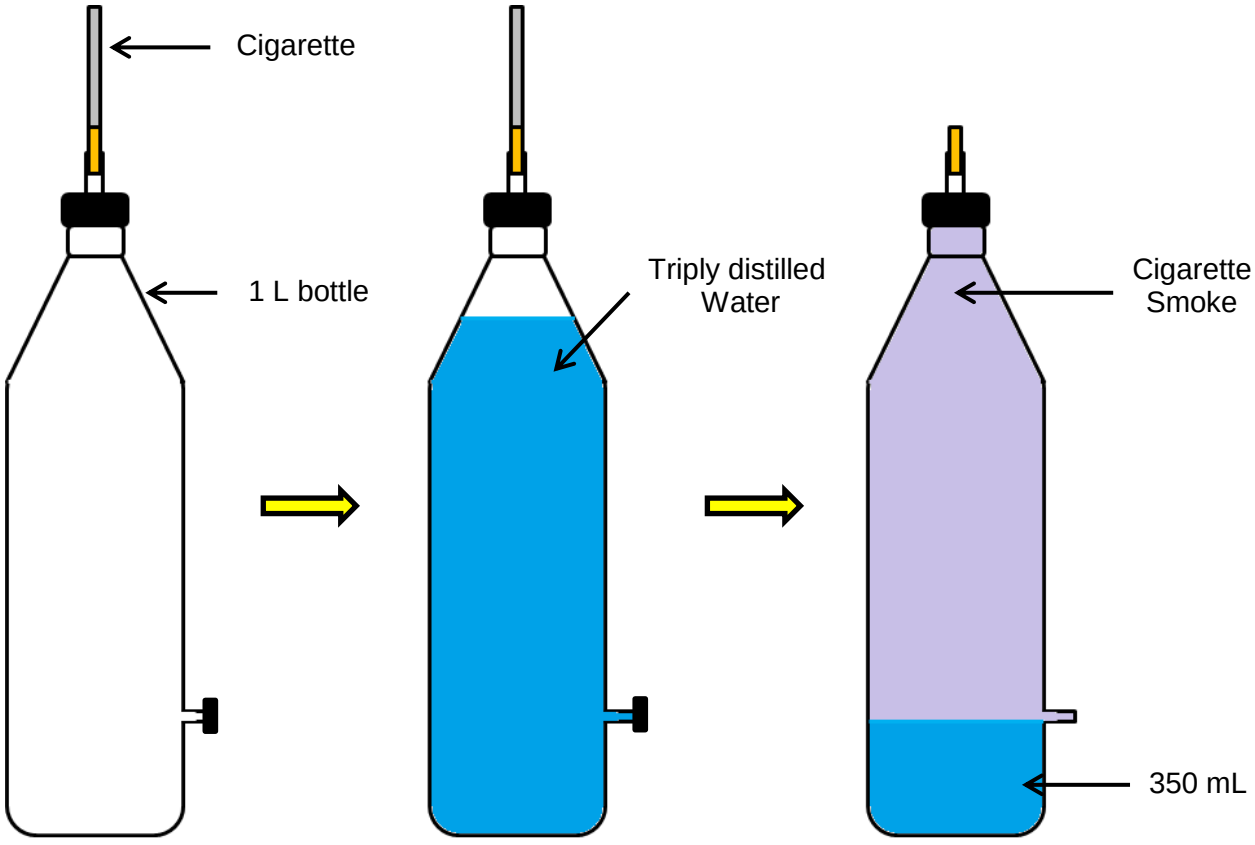

Scheme 2.3. Schematic representation of the experimental setup used to prepare aqueous solution of cigarette smoke. This technique applies the same suction to all the cigarettes tested. Cigarette was completely burned out before water level reached 350 mL mark

2.2.6. Development of Predictive Models for Identification of Chemical Substance

The goal of this study is to use the developed sensor arrays to identify chemical substances accurately and consistently, and as efficiently and as quickly as possible. To accomplish this goal, the information contained on a sensor array can be quantified and processed using a predictive model. Quantitative models can be automated, improving efficiency and timeliness, and their use removes inconsistencies in the prediction process that can result from subjective assessment of qualitative information. In addition, the accuracy of predictive models can be quantified. When more than one potential model is available, such accuracy measures allow for comparisons of models and the selection of the best model from a set of competing models. There are several approaches to quantifying a model's predictive accuracy. One approach is to use the model to classify the observations that were used in constructing the model and calculate the proportions of observations correctly and incorrectly classified. In the SAS documentation and output this is called the resubstitution method, and the resulting estimate of the error rate is called the apparent error rate. This method is easily implemented, but it tends to overstate the predictive ability of the model. That is, the estimated error rates tend to be too low and the estimated accuracy rates too high. This stems from the fact that the data being classified were used to construct the model. The model therefore tends to do a better job of classification for that dataset than it would for other datasets in general. An approach that gets around this problem is the cross-validation method. Using cross-validation, each observation in the dataset is classified using a model that is constructed from a dataset that excludes the observation to be classified. This method is more complicated to implement, but has the advantage of providing more reasonable, less biased estimates of the correct and incorrect classification rates of a model. Finally, predictive models can be updated as more information becomes available. To improve a

model's accuracy and reliability, it can be updated using additional data for chemical substances that are already in the model's substance database. To broaden a sensor array's applicability, the predictive model's chemical substances database can be expanded by updating the model with data for new substances.

To quantify the information contained on a sensor array, the array is optically scanned. The color of each spot on the array is quantified by determining the red, green, and blue (RGB) components comprising that color. Each of these color components is represented by an integer value ranging from 0 to 255. Since a sensor array contains twelve spots, the scanning process generates 36 numeric values each time the array is scanned. Because of potential variation in spot-color intensities from one sensor array to another, an array is scanned twice i.e. before it is exposed to any substance, and then after it has been exposed to a substance to be identified. This results in 72 numeric values for a given array, 36 values taken before exposure and 36 values taken after exposure. The pre-exposure scan provides baseline values by which the post-exposure scan values can be adjusted. Specifically, the pre-exposure RGB component for a given spot is subtracted from the corresponding post-exposure RGB component. This type of adjustment removes the array-to-array variability from the measurement, decreasing the variability in spot intensities for a given analyte and thereby improving the quality and predictive ability of the data. The resulting 36 differences are then used as variables in a predictive model.

The sensor array is the scientifically developed instrument by which measurements are obtained on a chemical substance (i.e. analyte). A predictive model then takes these measurements, and uses them together to generate a prediction about the identity of the analyte. Statistical analysis is used to develop this predictive model, using experimental sensor array data for which the analytes are known. Once the model has been developed, it can be used to identify

analytes for which it has been developed by exposing a sensor to the analyte whose identity is unknown and processing the resulting data using the model, generating a prediction.

Discriminant analysis was used to develop statistical models using the sensor array data obtained from these experiments. Two approaches were used in constructing the discriminant models. The first approach utilized as predictor variables all of the original 36 RGB color differences described above. The second approach utilized a smaller number of new variables, constructed from the original 36 variables via PCA.

The discriminant model uses estimates of certain underlying distributional characteristics in its calculations. The two main categories of parametric discriminant models being used here are linear and quadratic discriminant models. Quadratic discriminant models are more generally appropriate, but require more data to fit. Linear discriminant models require less data to fit, but are appropriate in less general circumstances. The question of whether a linear discriminant model is adequate in a given situation is a statistical question that is answered in the context of the discriminant analysis model-building process. The problem is that if there is not enough data to fit a quadratic discriminant model, there will not be enough data to perform the statistical analysis to answer the question of whether a linear discriminant model is adequate. In some cases, there may not even be enough observations to fit a linear discriminant model. In situations where there is enough data to a linear discriminant model but not enough to fit a quadratic model, one approach is to fit a linear discriminant model, and to issue the disclaimer that there is not enough data to formally test whether a quadratic model would be better. Another way to get through the problem is to reduce the dimensionality of the predictor space, either by using only a subset of the measured predictor variables, or by constructing a small number of new variables based on the original measured variables. When the number of predictor variables is small

enough relative to the number of observations within the each classification group, the process alluded to above for choosing between quadratic and linear discriminant models can be performed. Choosing a subset of variables to use can be problematic. As an example in the current context, some variables may be important for identifying certain analytes, while other variables may be important for identifying other analytes. Alternatively, PCA can be used to reduce the dimensionality of the predictor variable space while at the same time using all of the original variables. If a small number of principal components account for a sufficiently large proportion of the variability in the original variables, and if the various groups are sufficiently separated with respect to those principal components, then they may be effective as predictors in a discriminant model. All statistical analyses for this paper were generated using version 9.3 of the SAS System. All statistical analyses for this study were generated using version 9.3 of the SAS System.[35]

2.3. Results and Discussion

The commercially available indicator dyes were modified by incorporating the counter cation, [P_{66614}], which has often been designated as a 'universal liquifier' within the ionic liquid community.[27] This cation induces hydrophobic properties to the ILs as well as transforms the physical state, of all 12 indicator dyes, from high melting solids to viscous liquids or low melting solids (Figure A1).[27,34] Because of the resultant hydrophobic characteristics, these ILs are very compatible for detection of analytes dissolved in aqueous medium. In addition, these ILs exhibited reduced interferences from humidity, which has been recognized as an important factor in vapor sensing. In aggregate, this approach allows selection of dyes for sensor arrays without considering hydrophobicity as the selection criterion. In principle, liquids serve as better sensory materials than solids mainly due to the rapid diffusion of analytes.[36] Therefore, these IL-based

sensors are expected to show higher sensitivity and faster response than a traditional dye-based sensor, which can be attributed to easy accessibility of all dye molecules to the analytes.

For sensing applications involving chemosensory pigments, there are basically two primary considerations: 1) analytes must be able to easily access the dyes, and 2) the dye must be immobilized onto a porous or permeable host material in order to avoid leaching of the dye.[37] Thus, selecting a host material should not be limited by the pigments of the sensor array. In addition, when designing a facile and inexpensive sensor, the selected host material or matrix should be readily available. The host matrix should also be selected according to the desired application. In this study, we have used $[P_{66614}]$-based ILs, which are reported to possess good permeability towards gases,[38] and are excellent dyes for sensing studies. Additionally, we have used four different matrices including silica and alumina TLC plates, filter papers, and cotton threads depending on the application. Also, these matrices are known to be readily available and relatively inexpensive. Figure 2.1 is a schematic representation of the four IL sensor arrays fabricated using these matrices. Moreover, these four materials were found to be effective in immobilizing the ILs without leaching during aqueous-phase analysis.

Compared to a traditional pH paper, pH meter or a colorimetric sensor (which use just a single dye to identify analytes), the discriminatory power of colorimetric sensor arrays are found to be extremely higher.[3] In this study, our IL sensor arrays were composed of 12 sensor elements, where each element is a three dimensional vector (RGB). Therefore, each analyte is represented as a 36-dimensional vector. Because of the high dimensionality of our sensor arrays, it is expected to display extraordinarily high levels of chemical discrimination which is extremely useful in the discrimination of closely-related analytes or complex sample mixtures. Compared to the traditional techniques, the data obtained by these colorimetric sensor arrays can

Figure 2.1. Photonic IL sensor arrays (A) fabricated on (i) silica (ii) alumina and (iii) filter paper and their respective (B) digital images. (C) Cotton thread spools stained with chemosensory ILs (P refers to $[P_{66614}]$ ion). (D) Sensor array fabricated from IL-stained threads (i) by using a sewing machine and a (ii) hand-stitched 'warner research' logo (continues through pages 48-50)

A

i

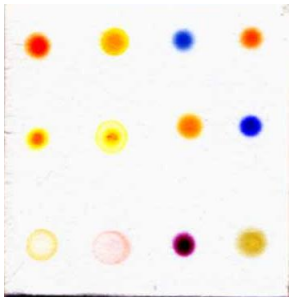

ii

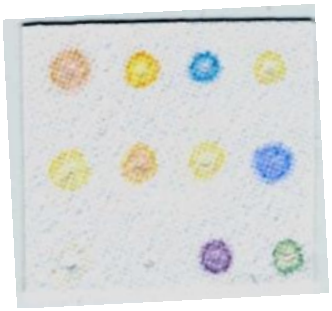

iii

B

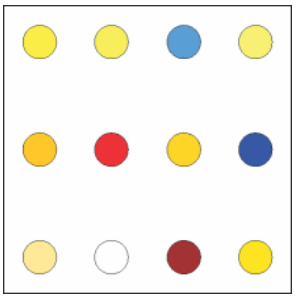

i

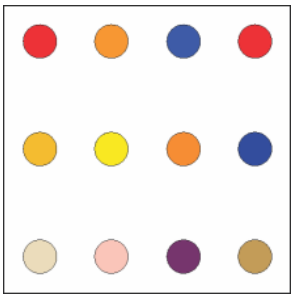

ii

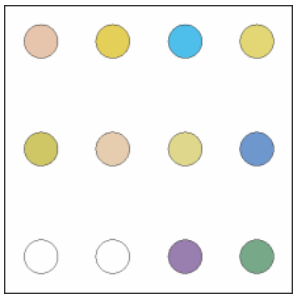

iii

C

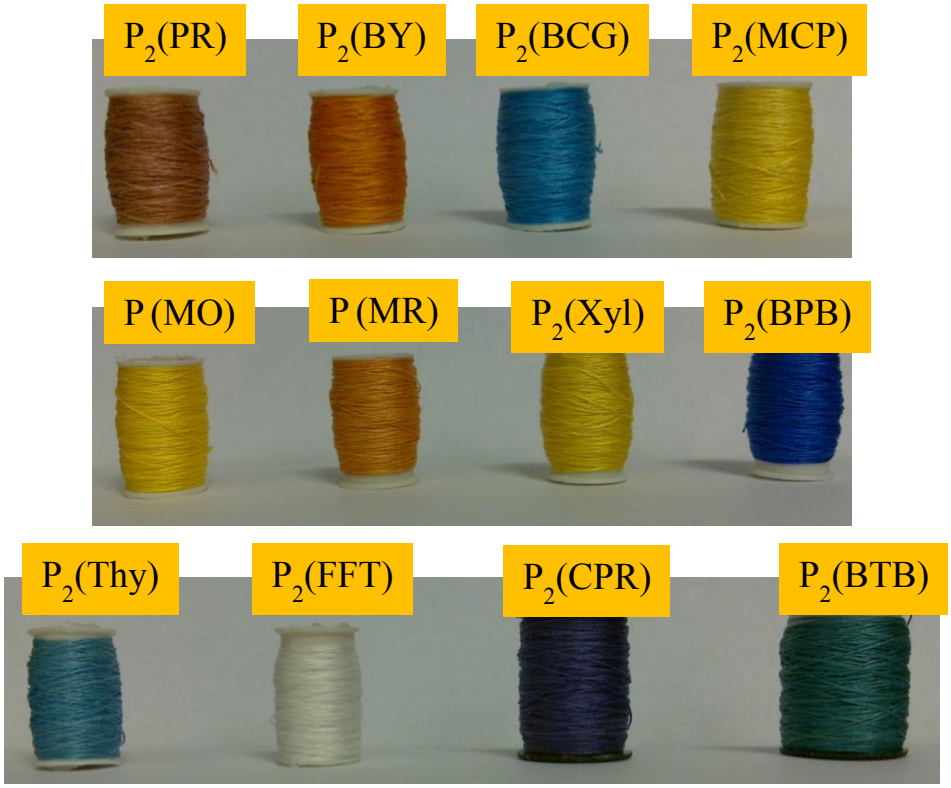

D

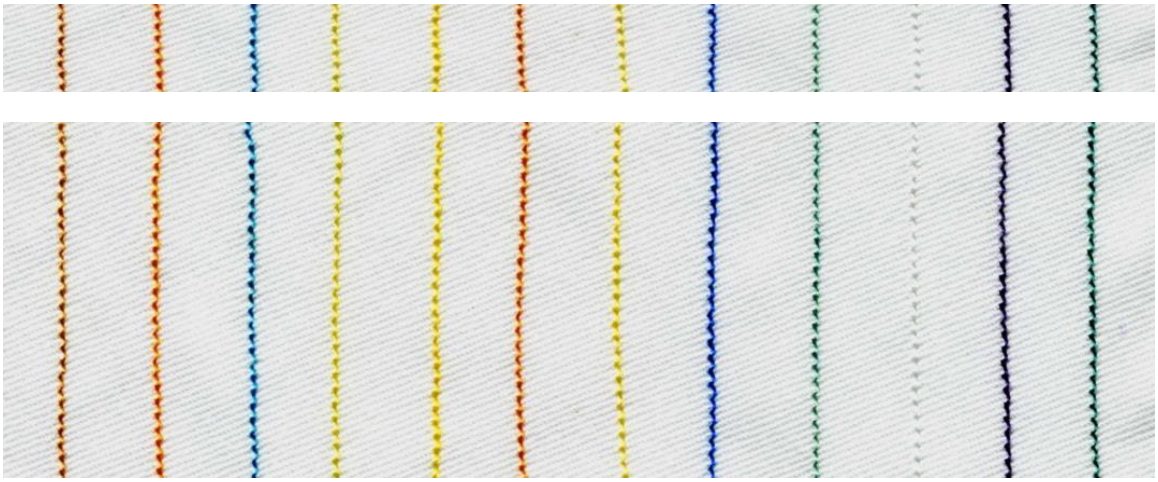

i

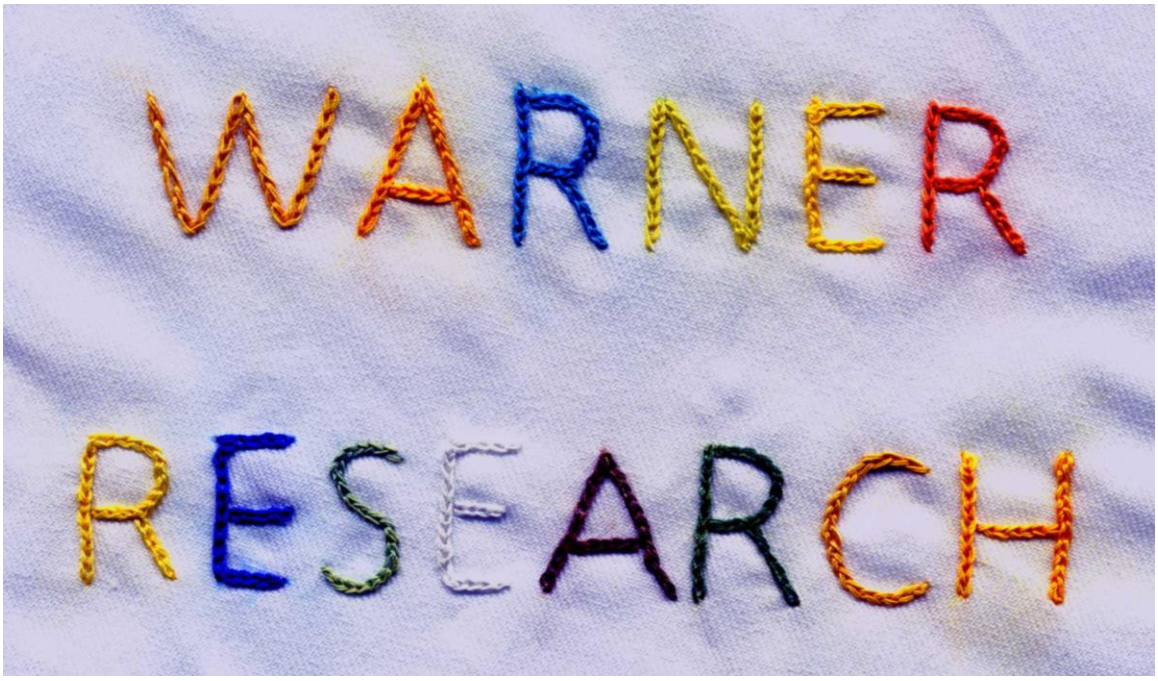

ii

be accurately analyzed by use of predictive models which is tremendously important in real time analysis of analyte mixtures.

2.3.1. Choice of Matrix

Our first choice as a host matrix was silica TLC plates. Due to exposed hydroxyl groups, the surface of silica is slightly acidic. Therefore, some of our chemosensory ILs tended to exhibit acidic colors on this blank sensor. As a result, such a sensor would be excellent for detection of basic vapors. In comparison to a silica surface, an alumina TLC matrix has a neutral pH due to the amphoteric properties of alumina. Therefore, ILs deposited on this surface tend to maintain their neutral color, which should make this matrix a good choice for detection over the entire range of pH values. Our third matrix of choice is a glass microfiber filter paper. A filter paper matrix provides greater flexibility over silica and alumina matrices because it can be folded and twisted without damaging the matrix. In addition, exploration of paper-based matrices such as filter paper would allow printing of sensor arrays. Finally, we employed cotton threads to develop the sensor arrays. We note that the potential for using these cotton threads as matrices in microfluidic devices has been recently reported.[16,17] In general, dewaxing techniques are employed on natural cotton threads in order to produce wettability, and hence to allow staining or wicking of aqueous dyes.[16-18] In this study, dewaxing of cotton threads, by expensive pretreatments such as plasma oxidation, was not required in order to dewax the cotton threads due to hydrophobic characteristic of the ILs. The use of threads as matrices for fabricating sensor arrays has several advantages over many other matrices. First, thread is inexpensive, broadly available, and easy-to-handle. In addition, a sensor array fabricated from cotton thread is flexible, lightweight and has very low volume. These properties allow easy transport and storage. As a result of the low volume of thread, a complex sensor array can be fabricated onto a very

small volume by use of a sewing machine. Thus, chemosensory IL-stained threads should be applicable to developing wearable sensors. Consequently, potential application areas of such sensors include bandages, sweatbands, headbands, diapers, and other similar matters. Moreover, these arrays can be incorporated into a garment similar to applications using radiation badges. Thus, wearable materials with potential military applications are a distinct possibility.

For a successful colorimetric sensor array, the matrix material and dyes should be chemically and physically stable in order to provide reasonable shelf life. The four sensor arrays that we describe in this study have excellent stabilities over a four-week period when covered with aluminum foil and stored in a desiccator. Therefore, due to flexibility in selecting a matrix when using chemosensory ILs, one can select from a variety of very stable matrices with controllable accessibility for a given set of analytes.

2.3.2. Digital Image Maps and Difference Maps

The accumulation of colorimetric sensor array data is usually done by optically scanning the sensor arrays by using a flatbed scanner.[32,39] This helps to minimize the effects of variation in imaging or environmental conditions on experimental data. In this study, each sensor array was scanned using an Epson Perfection 2400 scanner before and after exposure to analytes, and two digital image maps were generated to allow removal of edge artifacts. For each spot in the array, color values of RGB were measured before and after digital image mapping, and a difference map was generated for each spot (Figure 2.2).[40,41] These difference maps have been confirmed to be a convenient methodology to facile and clear representation of a series of color changes which occur after analyte exposure.[40,41]

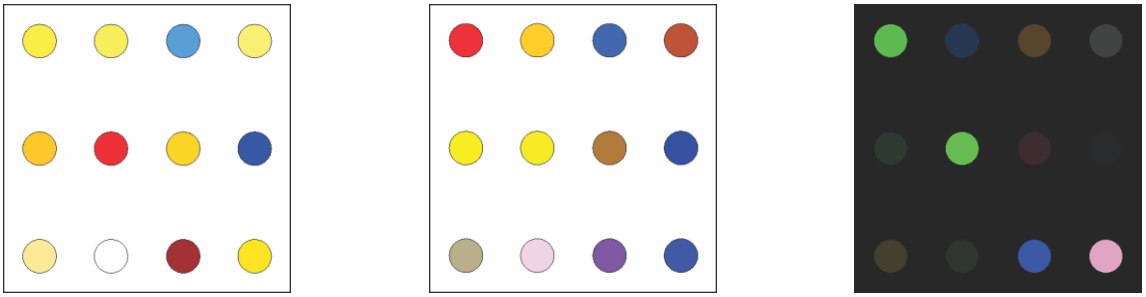

Figure 2.2. Image of colorimetric sensor array before exposure (left) and after exposure to ammonia (middle). A subtraction of the two images yields a difference vector in 36 dimensions. This vector is usefully visualized using a difference map (right), which shows the absolute values of the color changes

2.3.3. Estimation of pH Values

A pH indicator dye is a halochromic chemical compound that changes colors as a result of protonation or deprotonation depending on the pK_a of the dye and the pH value of its surroundings. In other words, it possesses different colors in its protonated and deprotonated forms, and the color at a given pH value depends on the ratio of the two forms. The protonated form of a pH indicator dye can also be defined as a weak acid, while its deprotonated form as a weak base:

$$HIn + H_2O \quad \Leftrightarrow \quad H_3O^+ + In^- \qquad K_a = \frac{[H_3O^+][\boldsymbol{In}^-]}{[\boldsymbol{HIn}]} \qquad (2.1)$$

Thus, the effect of pH on the change in color of an indicator dye is readily explained by use of the Henderson-Hasselbalch equation (Equation 2.2):

$$pH = pK_a + \log \frac{[\boldsymbol{In}^-]}{[\boldsymbol{HIn}]} \qquad (2.2)$$

Examination of Equation 2.2 indicates that the color change of the system at a particular pH value is dependent on the ratio between the protonated and deprotonated forms, and the acid dissociation constant (K_a) of the indicator dye. Therefore, by having different K_a values with different indicator dyes, different color changes over different pH values can be obtained. When selecting a series of indicator dyes for a given sensor array, we have selected dyes with a range of pK_a values and colors in order to obtain different color combinations which cover the entire pH range. By using an increased number of ILs with different pK_a values in the array, one can further increase the resolution of the pH sensor.

2.3.4. Aqueous-Phase Sensing

As noted earlier, the proposed arrays can be used to estimate the pH values of aqueous solutions without the need for specialized hydrophobic matrices. The experimental procedure used for estimating pH, and the differences between the IL-based sensor arrays and the water soluble indicator-based sensor array is displayed in Figure 2.3. Note that the regular indicator dye-based sensor array loses much of its integrity and smears over the TLC stripe, while the IL-based sensor array remains stable throughout the experiment. Five different solutions with pH values of 1, 4, 7, 10, and 13 were used in these analyses. The difference maps for pH sensing obtained by using alumina TLC plate, filter paper, and thread-based matrices are shown in Figure 2.4. Regardless of the unique individual advantages of each matrix over the other, all three matrices allowed to discriminate between the five pH values with higher degree of variation between each difference map. It is very important to have higher degree of variation between two difference maps of adjacent pH values which enables the sensor arrays to be applied in the discrimination of pH values which are very close. In addition, by using three different matrices, it is clear that matrix specific color changes can be exploited.

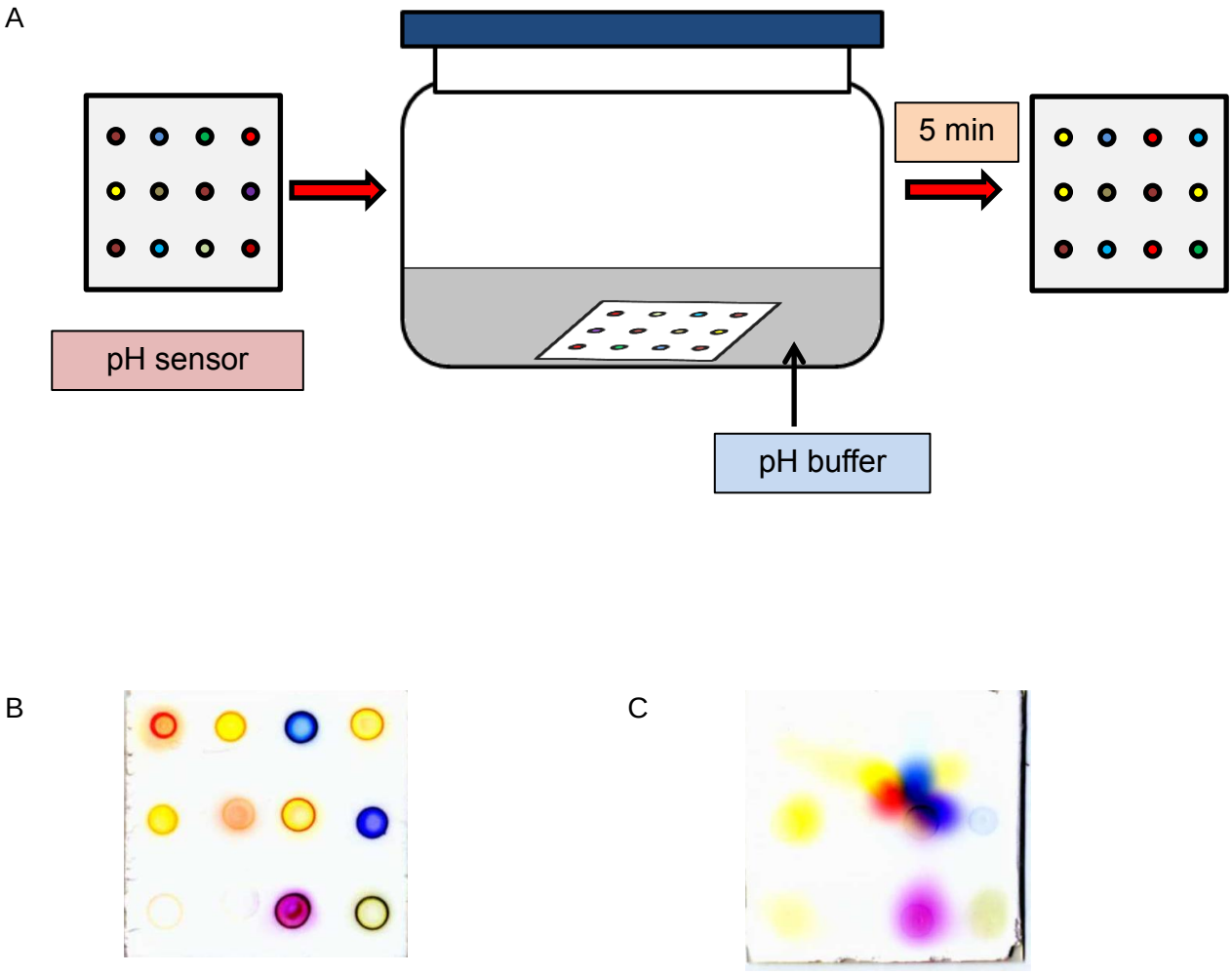

Figure 2.3. (A) Schematic of the experimental setup used to detect pH. The same setup was used to analyze the aqueous solution of cigarette smoke. The difference between (B) the IL-based sensor array and (C) regular indicator dye-based sensor array

Figure 2.4. The difference maps for pH sensing studies by using (A) alumina TLC, (B) filter paper, and (C) cotton thread matrices (continues through pages 56-58)

A

pH 1

pH 4

pH 7

pH 10

pH 13

B

pH 1

pH 4

pH 7

pH 10

pH 13

C

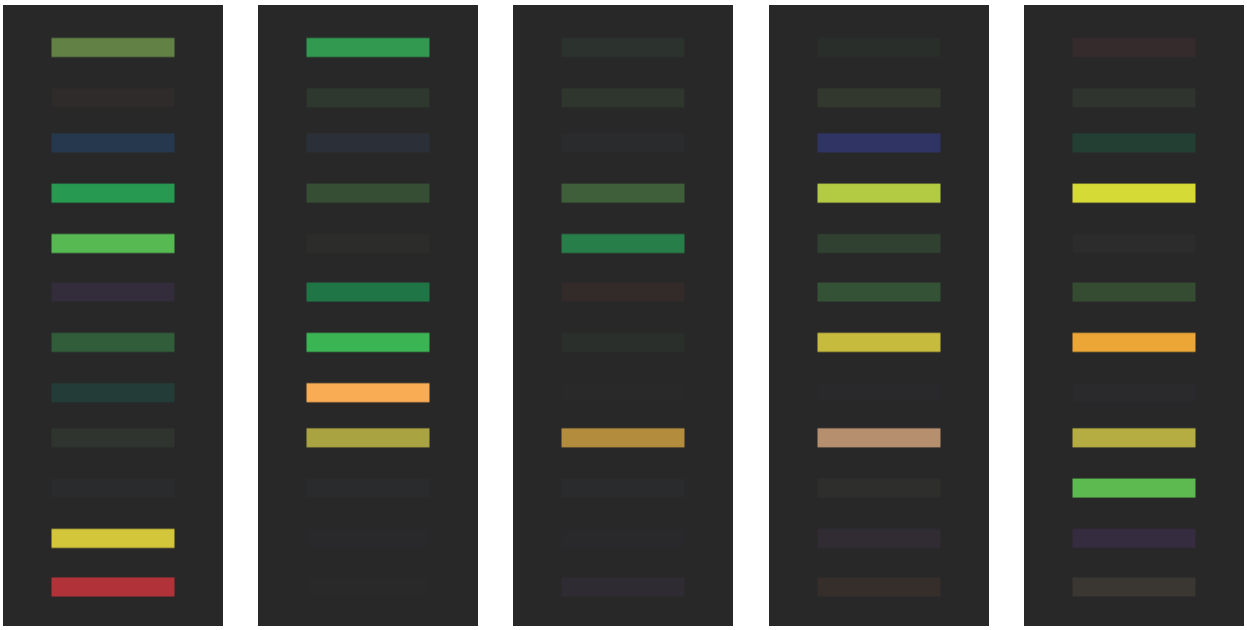

2.3.5. Vapor-Phase Sensing

The vapor sensing experiments were performed by exposing the sensor arrays to saturated vapors of different volatile compounds at room temperature, i.e. 298 K. Acidic vapor sensing studies were conducted by using four vapors of acids including hydrochloric acid (HCl), trifluoroacetic acid (CF_3COOH), formic acid (HCOOH), and acetic acid (CH_3COOH). Basic vapor sensing studies were performed by using six vapors of bases including 1-methylimidazole (1MIm), pyridine, ammonia, diethylamine, triethylamine and dimethylformamide (DMF). Sensor arrays fabricated on alumina and silica TLC plates were used to detect acidic and basic vapors, respectively. These difference maps are shown in Figure 2.5. Color changes obtained from silica and alumina TLC plates clearly provide a higher degree of discrimination between closely related groups of chemical vapors, e.g. (1) ammonia, diethylamine, and triethylamine; (2) HCl,

A

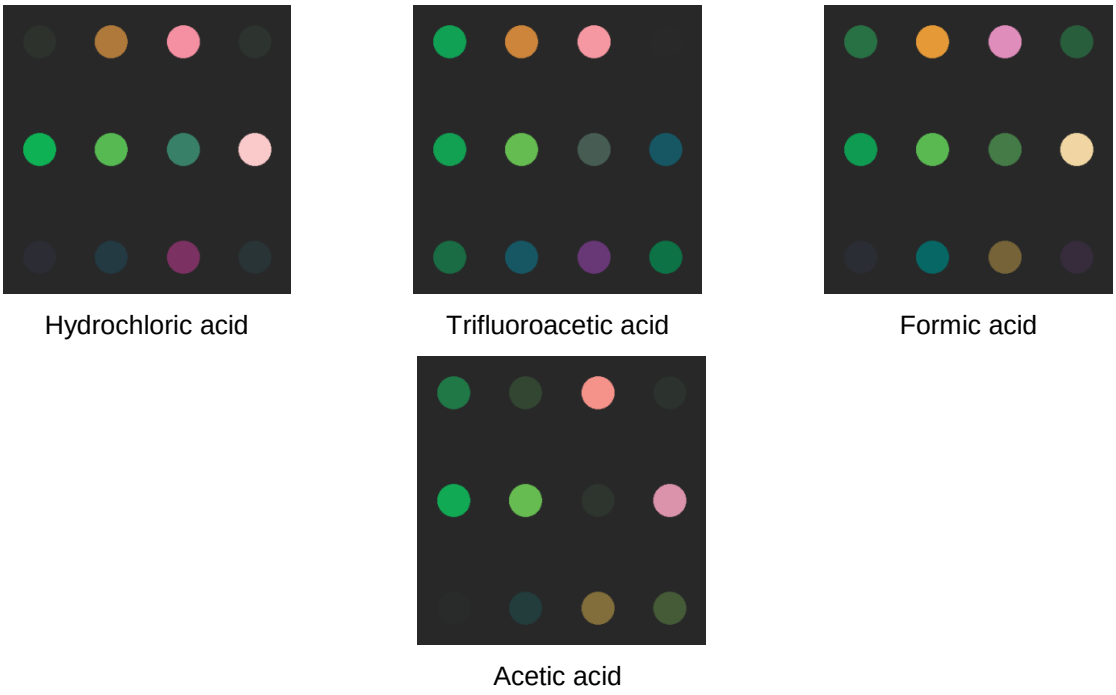

B

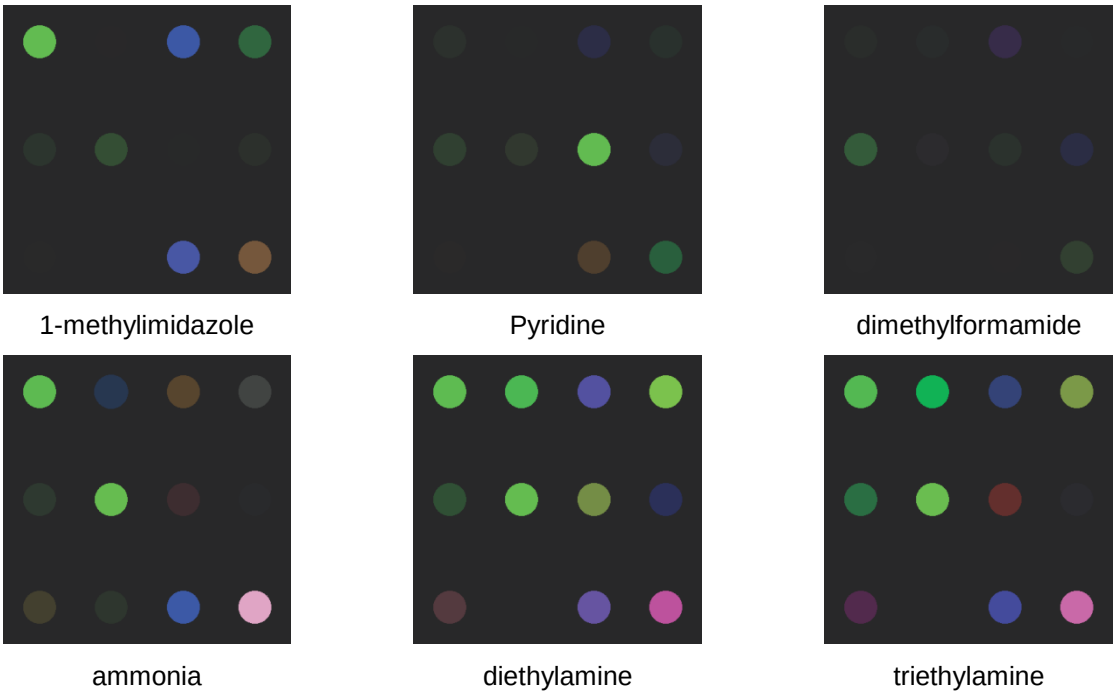

Figure 2.5. Difference maps of chemosensory IL sensor array. (A) on exposure to acidic vapors by using alumina TLC matrix, and (B) on exposure to basic vapors by using silica TLC matrix.

CH_3COOH, and CF_3COOH. Liberty in selecting a matrix, which offers additional number of changes in colors, provides a significant variation in the difference maps, and enables rapid and facile discrimination of vapors. Therefore, this study confirms that the use of alumina matrix for acidic vapor sensing and silica matrix for basic vapor sensing provides better discriminatory power for the IL sensor array. Thread-based sensor arrays were also used to detect CF_3COOH and reusability was also tested for that matrix (Figure 2.6). After exposing the sensor array to CF_3COOH, it was exposed to ammonia, and back again to CF_3COOH. This exposure cycle was repeated three times and the difference maps corresponding to the first and last exposure to CF_3COOH were compared. Examination of Figure 2.6d shows that these two difference maps have very little deviation in RGB levels for most of the IL spots, and this confirms the capability of reusing the thread-based IL sensor arrays. Thus, the thread-based sensor array shows considerable promise for regeneration and reuse.

Figure 2.6. Difference maps for the thread based IL sensor array. (A) after exposing to CF_3COOH acid followed by (B) ammonia, and (C) difference map obtained after alternate exposure to CF_3COOH and ammonia for three cycles, and finally to CF_3COOH. (D) Difference map between (A) and (C)

2.3.6. Statistical Discrimination for Identification of pH Values and Acidic/Basic Vapors

Our first study involved developing a sensor array and corresponding predictive model to identify 15 chemical samples including acidic and basic vapors, and solutions of varying pH values. Five replicate experiments were performed by exposing the sensor array to each of the 15 chemical samples, for a total of 75 observations. Each sensor array was processed as described above. The resulting dataset contained 36 RGB color difference values measured on each of these 75 observations.

Using the first approach described above, a discriminant analysis was performed for the 15 different samples using all 36 variables in the dataset. Because the number of sensor arrays exposed to each substance is small relative to the number of predictor variables used in the model, it was not possible to fit a quadratic discriminant model. The total sample size was large enough to fit a linear discriminant model, however. Using the resubstitution method of assessing the accuracy of the model, the linear discriminant model correctly identified all substances in the dataset. Using the cross-classification method of assessment, the linear discriminant model correctly identified all but one of the substances, for an estimated error rate of 1.33%. In this case, one diethylamine sample was misclassified as triethylamine. The linear discriminant model using all 36 variables does a very good job of utilizing the sensor array data to correctly differentiate among the fifteen substances.

To build a discriminant model using the second approach described above, a PCA was first performed to reduce the dimensionality of the predictor variable space. Figure 2.7 shows that the first three principal components account for approximately 80% of the variability in the original 36 variables. In Figure 2.8, the observations are plotted with respect to their scores on

A

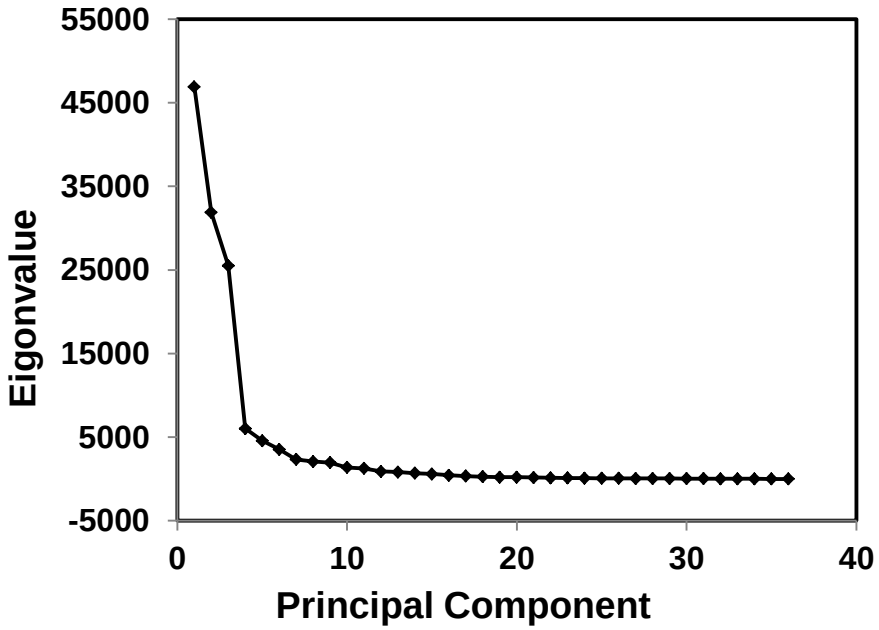

B

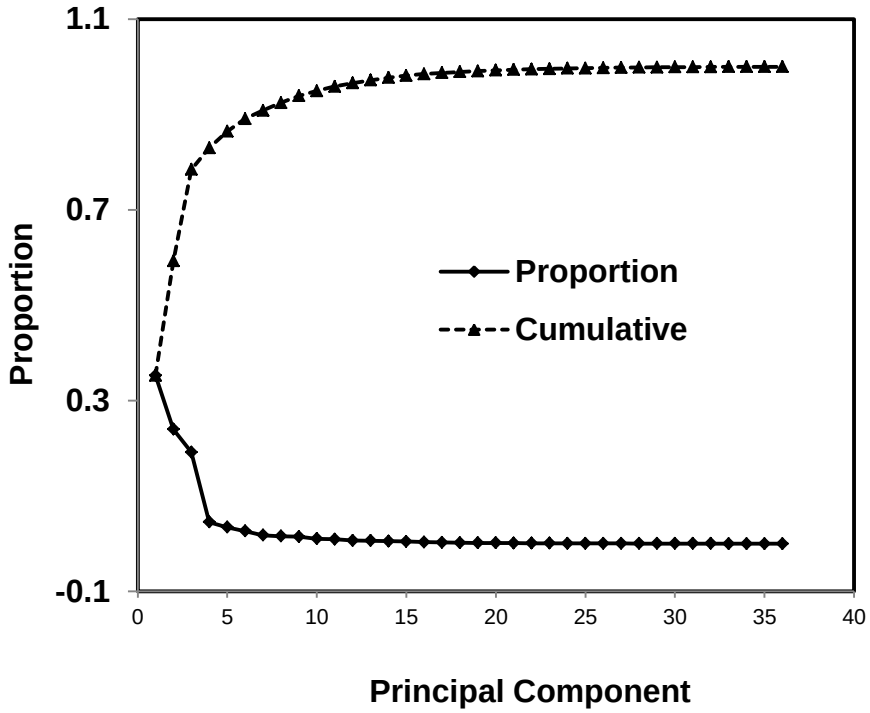

Figure 2.7. (A) Scree plot and (B) cumulative proportion of variability accounted for by the principal components obtained from the color change profile of pH, acidic and basic vapor numerical data

the first three principal components. From the plot, it appears that the three principal components are adequate in separating many of the analytes although some of the analytes are quite close. Based on Figure 2.8, we might expect a discriminant function centered on these principal components would do a good job of distinguishing among most of the fifteen analytes. In an effort to find the simplest model possible, discriminant analysis models were fit using one, two, and three principal components each.

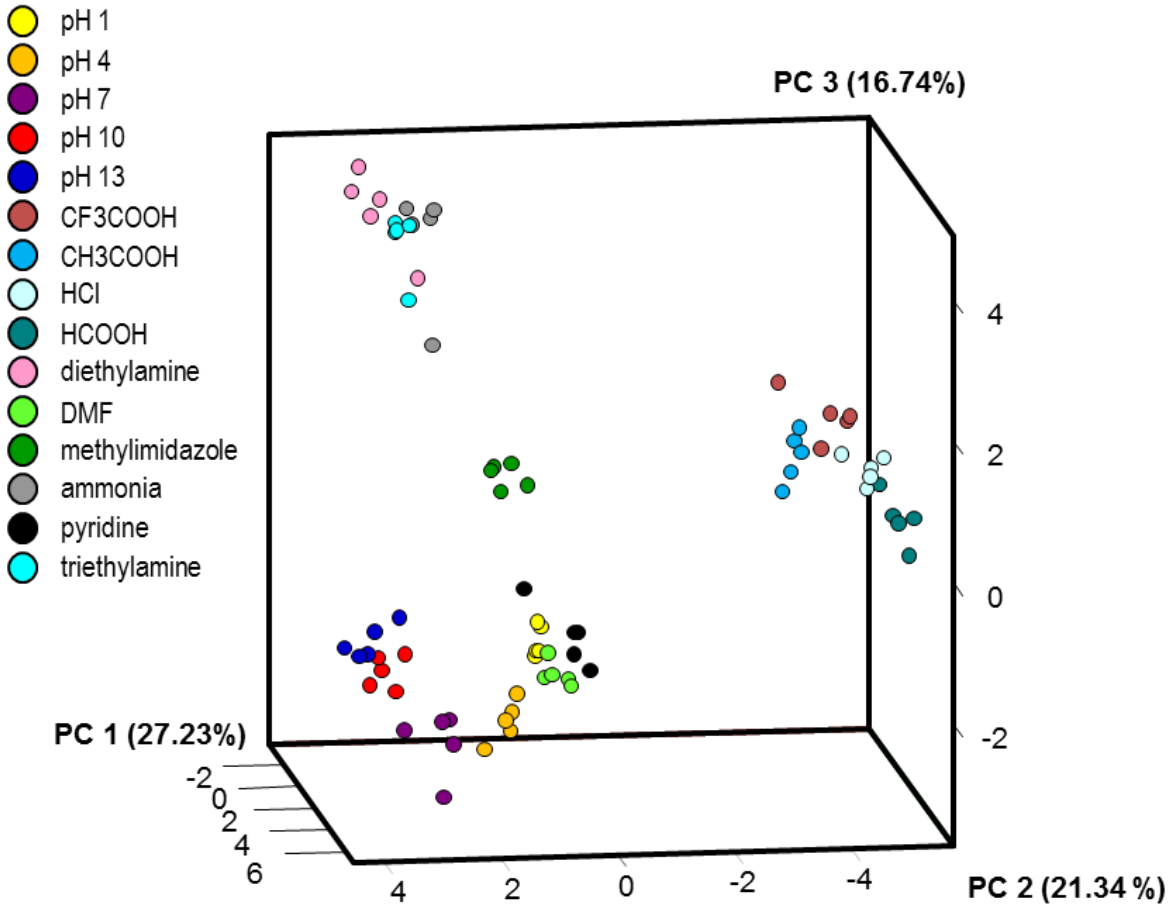

Figure 2.8. Plot of the scores for the first three principal components based on the data for the analysis of pH, acidic and basic vapor

We first fit a model using the first principal component as the only predictor variable in the model. As part of the model-building process, the hypothesis that a linear discriminant model would be adequate was tested. The p-value of the test was less than 0.0001. It was therefore concluded that a linear discriminant model would not adequately fit the data, and a quadratic discriminant model was constructed instead. The accuracy of the model was then assessed. Using the resubstitution method of assessment, the quadratic discriminant model had a resubstitution error rate of 30.7%. Using the cross-classification method, the error rate was 40%.

The next model to be considered used the first two principal components as predictor variables. Again, the hypothesis that a linear discriminant model was adequate was tested. The hypothesis was rejected (p-value < 0.0001), and a quadratic model was constructed. This model had a resubstitution error rate of only 6.7%. However, under cross-classification, the error rate was 34.7%.

The final model for consideration used the first three principal components as predictor variables. A test of the hypothesis that a linear discriminant model was adequate had a p-value of less than 0.0001, and so again a quadratic discriminant model was constructed. For this model, the resubstitution error rate dropped to 0%, but the cross-classification error rate was quite a bit larger at 28%. In order to understand the problem of this model distinguishing between analytes, Table A1 lists the misclassifications under cross-validation by this model. Based on this list, the model appears to have difficulty distinguishing between substances within the following groups: (1) ammonia, diethylamine, and triethylamine; (2) HCl, CH3COOH, and CF3COOH; and (3) DMF and Pyridine. In Figure 2.8, we see that within each of these three groups, the substances are very close together and in some cases overlap. This explains the difficulty of the model distinguishing between analyes within these groups. In contrast, the model does not have a

trouble in distinguishing between the larger groups of substances because of the relatively large amount of separation as seen in the plot. Note that only five training samples for each analyte were available for building the model. If additional training samples were to become available and the model updated, it is possible that we could see an improvement in the model's accuracy. There is no guarantee of that, however. In fact, given the close proximity of some of the groups with respect to these three principal components, it may be that using only three principal components is too great a reduction in the predictor variable space to allow for highly accurate discrimination among these substances.

Based on these results, the first model that uses all 36 of the original predictor variables appears to be the model to use for identifying these 15 analytes. As it stands, the model has very little trouble distinguishing between the substances, even those that were close together in terms of the first three principal components. With the availability of more training samples, the model could be updated and refined, and with the addition of enough training samples a quadratic model could be developed if deemed necessary. Each of these improvements would be expected to improve the accuracy of the model. As a final note on model development for study one, the analyses above demonstrate the importance of evaluating the predictive accuracy of the model. Doing so can illuminate situations where the models may have difficulty. It also provides a basis for comparison and the selection of a best model when more than one is available. What is also critically important is using a method like cross-validation that provides more realistic estimates of the error rates than the resubstitution method.

2.3.7. Identification of Cigarette Smoke

One of the greatest advantages of having a colorimetric sensor array over a traditional pH probe is tremendously improved dimensionality, which was obtained by using 12 ILs. Therefore, these sensor arrays could achieve exceptional discrimination among very similar analytes. To demonstrate that the IL sensor arrays can be used to sense complex analytes, and discriminate between closely-related analytes, aqueous smoke solutions prepared from three commercially available cigarette brands (Marlboro® red, Crowns® and Camel® Turkish domestic blend) were analyzed. Cigarette smoke is a very complex mixture of chemical compounds for which more than 4800 compounds have been identified, and many more remain unidentified.[42] The chemical composition of the smoke varies widely depending on the brand of cigarette primarily due to the amount and type of tobacco present, and the filter. By using an IL sensor array, these identified and unidentified components of cigarette smoke are used to generate a fingerprint signal which corresponds to the brand of cigarette. After obtaining the pixel differences from the color maps before and after exposure of the IL sensor array, those data were analyzed by use of statistical methods. Overall, the cigarette smoke experiment that discussed in the article can be considered as an ideal example for an application such as environmental monitoring. Also, these IL sensor arrays show promise to be used in military applications, medical diagnosis, water quality analysis, and food safety.

2.3.8. Statistical Discrimination of Smoke from Three Brands of Cigarettes

Seven replicate experiments were performed by exposing freshly prepared aqueous solutions of smoke from each of the three brands, giving a total of 21 observations. Each of the sensor arrays

was processed as described above. The analysis dataset therefore contained 36 RGB color difference values measured on each of 21 observations.

The first modeling approach described above, in which the original 36 RGB color difference values are used in the model, could not be applied to this study. This is because the total number of observations is less than the number of predictor variables. As a result, not even a linear discriminant model can be fit. Therefore only the second approach, which uses PCA to reduce the dimensionality of the predictor variable space, was used to develop a discriminant model for this study.

Figure A2 shows that the first two principal components account for more than 90% of the variability in the original 36 variables. In Figure 2.9, the observations are plotted with respect to their scores on the first two principal components. The three different cigarette brands are tightly grouped, and there is a significant separation between them with respect to these two principal components. We therefore expect that a discriminant model based on these principal components will do a good job of distinguishing between cigarette brands.

Discriminant models using one and two principal components were fit. For each of these models, a linear discriminant analysis was determined to be adequate (minimum p-value = 0.4270). The models fit very well. The resubstitution and cross-validation error rates were each 0% for both models. Hence, even the model based on only the first principal component was able to correctly identify the brand for every sample, both under resubstitution and under cross-validation. This is not surprising, given the large amount of separation between brands seen in Figure 2.9.

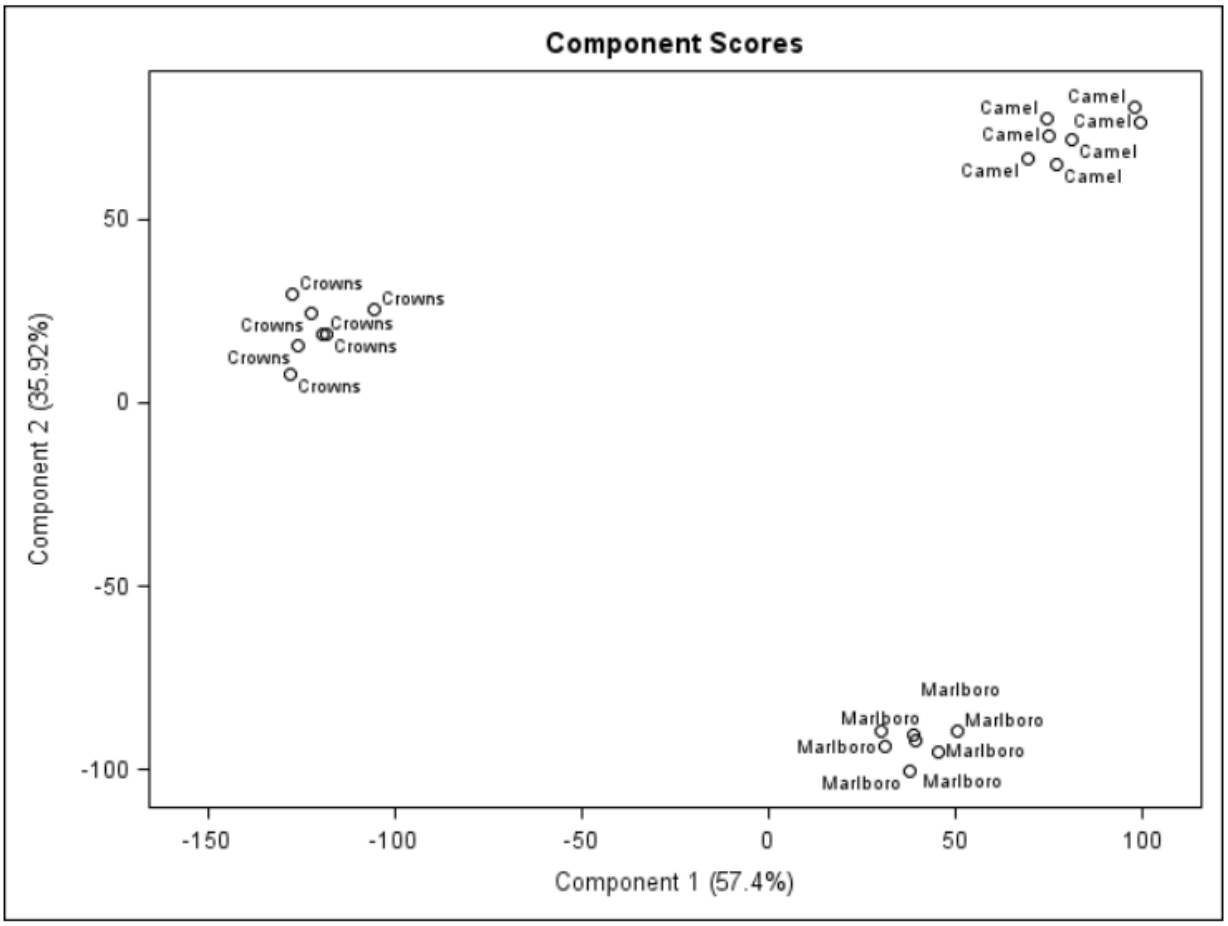

Figure 2.9. PCA score plot for the identification of cigarette smoke of Marlboro® red, Crowns® and Camel® Turkish domestic blend by using filter paper based ionic liquid sensor arrays

2.4. Conclusions

In summary, we have successfully designed facile, inexpensive, and disposable photonic IL-based sensor arrays that are sensitive to pH values, as well as acidic and basic vapors. We have fabricated four different sensor arrays by using four different matrices, all of which are highly compatible for using in aqueous media. We have also demonstrated that this sensor array allows discrimination between closely related complex mixtures in aqueous medium. Predictive models were used for successful discrimination and identification of a range of analytes. By use of a

variety of matrices, we have demonstrated that these chemosensory ILs do not require any specialized hydrophobic matrix for fabrication of a sensor array. Thus, depending on the particular application, a broadly available, low-cost material can be used as a matrix when fabricating a sensor array. We have also successfully demonstrated the fabrication of a wearable personal sensor arrays by using cotton threads. These wearable sensor arrays can be easily fabricated by manipulating IL-stained cotton threads through use of common household tools such as sewing machines. These thread-based IL sensor arrays can be manufactured on a large scale, allowing applications in bandages, sweatbands, diapers, and other similar systems. Although it needs to be fully evaluated, an IL-based sensor is expected to exhibit a higher sensitivity as compared to a traditional dye-based sensor because of easy accessibility of all dye molecules to the analytes. Finally, we believe that by proper choice of ILs and matrices, these arrays can be constructed to sense a wide range of analytes in a variety of applications, e.g. military applications, medical diagnosis, environmental monitoring, water quality analysis, and food safety.

2.5. References

(1) Gouma, P.; Sberveglieri, G.; Dutta, R.; Gardner, J. W.; Hines, E. L.: Novel materials and applications of electronic noses and tongues. *MRS Bulletin* **2004**, *29*, 697-700.

(2) Gardner, J. W.; Bartlett, P. N.: A brief history of electronic noses. *Sensors and Actuators B: Chemical* **1994**, *18*, 210-211.

(3) Gardner, J. W.; Bartlett, P. N.: *Electronic noses : principles and applications*; Oxford University Press: Oxford ; New York, 1999.

(4) Kress-Rogers, E.: *Handbook of biosensors and electronic noses : medicine, food, and the environment*; CRC Press: Boca Raton, 1997.

(5) Marks, R.: *Handbook of biosensors and biochips*; John Wiley & Sons: Chichester ; Hoboken, N.J., 2007.

(6) Zhang, C.; Suslick, K. S.: A Colorimetric Sensor Array for Organics in Water. *Journal of the American Chemical Society* **2005**, *127*, 11548-11549.

(7) Suslick, K. S.: An optoelectronic nose: "Seeing" smells by means of colorimetric sensor arrays. *MRS Bulletin* **2004**, *29*, 720-725.

(8) Feng, L. A.; Musto, C. J.; Kemling, J. W.; Lim, S. H.; Zhong, W. X.; Suslick, K. S.: Colorimetric Sensor Array for Determination and Identification of Toxic Industrial Chemicals. *Analytical Chemistry* **2010**, *82*, 9433-9440.

(9) Suslick, B. A.; Feng, L.; Suslick, K. S.: Discrimination of Complex Mixtures by a Colorimetric Sensor Array: Coffee Aromas. *Analytical Chemistry* **2010**, *82*, 2067-2073.

(10) Salinas, Y.; Ros-Lis, J. V.; Vivancos, J.-L.; Martinez-Manez, R.; Marcos, M. D.; Aucejo, S.; Herranz, N.; Lorente, I.: Monitoring of chicken meat freshness by means of a colorimetric sensor array. *Analyst* **2012**, *137*, 3635-3643.

(11) Huang, X. Y.; Xin, J. W.; Zhao, J. W.: A novel technique for rapid evaluation of fish freshness using colorimetric sensor array. *Journal of Food Sciennce and Engineering* **2011**, *105*, 632-637.

(12) Huo, D. Q.; Zhang, G. P.; Hou, C. J.; Dong, J. L.; Zhang, Y. C.; Liu, Z.; Luo, X. G.; Fa, H. B.; Zhang, S. Y.: A Colorimetric Sensor Array for Identification of Natural Amino Acids. *Chinese Journal of Analytical Chemistry* **2010**, *38*, 1115-1120.

(13) Rakow, N. A.; Suslick, K. S.: A colorimetric sensor array for odour visualization. *Nature* **2000**, *406*, 710-713.

(14) Zhang, Q.; Zhang, S.; Liu, S.; Ma, X.; Lu, L.; Deng, Y.: Ionic liquid-modified dyes and their sensing performance toward acids in aqueous and non-aqueous solutions. *Analyst* **2011**, *136*, 1302-1304.

(15) Feng, L.; Musto, C. J.; Kemling, J. W.; Lim, S. H.; Suslick, K. S.: A colorimetric sensor array for identification of toxic gases below permissible exposure limits. *Chemical Communications* **2010**, *46*, 2037-2039.

(16) Li, X.; Tian, J.; Shen, W.: Thread as a Versatile Material for Low-Cost Microfluidic Diagnostics. *ACS Applied Materials & Interfaces* **2009**, *2*, 1-6.

(17) Reches, M.; Mirica, K. A.; Dasgupta, R.; Dickey, M. D.; Butte, M. J.; Whitesides, G. M.: Thread as a Matrix for Biomedical Assays. *ACS Applied Materials & Interfaces* **2010**, *2*, 1722-1728.

(18) Reniers, G. L. L.; Brebbia, C. A.: *Sustainable chemistry*; WIT Press: Southampton ; Boston, **2011**.

(19) Tomasino, C.; Cuomo, J. J.; Smith, C. B.; Oehrlein, G.: Plasma Treatments of Textiles. *Journal of Industrial Textiles* **1995**, *25*, 115-127.

(20) Hallett, J. P.; Welton, T.: Room-temperature ionic liquids: solvents for synthesis and catalysis. 2. *Chemical Reviews* **2011**, *111*, 3508-3576.

(21) Pandey, S.: Analytical applications of room-temperature ionic liquids: a review of recent efforts. *Analytica chimica acta* **2006**, *556*, 38-45.

(22) Plechkova, N. V.; Seddon, K. R.: Applications of ionic liquids in the chemical industry. *Chemical Society reviews* **2008**, *37*, 123-50.

(23) Jin, X. X.; Yu, L.; Garcia, D.; Ren, R. X.; Zeng, X. Q.: Ionic liquid high-temperature gas sensor array. *Anal. Chem.* **2006**, *78*, 6980-6989.

(24) Yu, L.; Garcia, D.; Ren, R.; Zeng, X.: Ionic liquid high temperature gas sensors. *Chemical communications* **2005**, 2277-2279.

(25) Toniolo, R.; Pizzariello, A.; Dossi, N.; Lorenzon, S.; Abollino, O.; Bontempelli, G.: Room temperature ionic liquids as useful overlayers for estimating food quality from their odor analysis by quartz crystal microbalance measurements. *Analytical Chemistry* **2013**, *85*, 7241-7.

(26) Zhu, W.; Li, W.; Yang, H.; Jiang, Y.; Wang, C.; Chen, Y.; Li, G.: A rapid and efficient way to dynamic creation of cross-reactive sensor arrays based on ionic liquids. *Chemistry* **2013**, *19*, 11603-12.

(27) Yung, K. Y.; Schadock-Hewitt, A. J.; Hunter, N. P.; Bright, F. V.; Baker, G. A.: 'Liquid litmus': chemosensory pH-responsive photonic ionic liquids. *Chemical Communications* **2011**, *47*, 4775-4777.

(28) Chen, X.-W.; Liu, J.-W.; Wang, J.-H.: A highly fluorescent hydrophilic ionic liquid as a potential probe for the sensing of biomacromolecules. *The Journal of Physical Chemistry B* **2011**, *115*, 1524-1530.

(29) Shu, Y.; Liu, M.; Chen, S.; Chen, X.; Wang, J.: New insight into molecular interactions of imidazolium ionic liquids with bovine serum albumin. *The Journal of Physical Chemistry B* **2011**, *115*, 12306-12314.

(30) Branco, L. C.; Pina, F.: Intrinsically photochromic ionic liquids. *Chemical Communications* **2009**, 6204-6206.

(31) Suslick, K. S.: An optoelectronic nose:"seeing" smells by means of colorimetric sensor arrays. *MRS bulletin* **2004**, *29*, 720-725.

(32) Lim, S. H.; Feng, L.; Kemling, J. W.; Musto, C. J.; Suslick, K. S.: An optoelectronic nose for the detection of toxic gases. *Nature Chemistry* **2009**, *1*, 562-567.

(33) Bwambok, D. K.; Marwani, H. M.; Fernand, V. E.; Fakayode, S. O.; Lowry, M.; Negulescu, I.; Strongin, R. M.; Warner, I. M.: Synthesis and characterization of novel chiral ionic liquids and investigation of their enantiomeric recognition properties. *Chirality* **2008**, *20*, 151-158.

(34) Del Sesto, R. E.; McCleskey, T. M.; Burrell, A. K.; Baker, G. A.; Thompson, J. D.; Scott, B. L.; Wilkes, J. S.; Williams, P.: Structure and magnetic behavior of transition metal based ionic liquids. *Chemical Communications* **2008**, 447-449.

(35) Institute, S.: *SAS/STAT 9.3 user's guide*; SAS Institute, 2011.

(36) Liang, C.; Yuan, C.-Y.; Warmack, R. J.; Barnes, C. E.; Dai, S.: Ionic Liquids: A New Class of Sensing Materials for Detection of Organic Vapors Based on the Use of a Quartz Crystal Microbalance. *Analytical Chemistry* **2002**, *74*, 2172-2176.

(37) Bang, J. H.; Lim, S. H.; Park, E.; Suslick, K. S.: Chemically Responsive Nanoporous Pigments: Colorimetric Sensor Arrays and the Identification of Aliphatic Amines. *Langmuir* **2008**, *24*, 13168-13172.

(38) Ferguson, L.; Scovazzo, P.: Solubility, Diffusivity, and Permeability of Gases in Phosphonium-Based Room Temperature Ionic Liquids: Data and Correlations. *Industrial & Engineering Chemistry Research* **2007**, *46*, 1369-1374.

(39) Sen, A.; Albarella, J. D.; Carey, J. R.; Kim, P.; McNamara Iii, W. B.: Low-cost colorimetric sensor for the quantitative detection of gaseous hydrogen sulfide. *Sensors and Actuators B: Chemical* **2008**, *134*, 234-237.

(40) Suslick, K. S.; Rakow, N. A.; Sen, A.: Colorimetric sensor arrays for molecular recognition. *Tetrahedron* **2004**, *60*, 11133-11138.

(41) Janzen, M. C.; Ponder, J. B.; Bailey, D. P.; Ingison, C. K.; Suslick, K. S.: Colorimetric Sensor Arrays for Volatile Organic Compounds. *Analytical Chemistry* **2006**, *78*, 3591-3600.

(42) Torikaiu, K.; Uwano, Y.; Nakamori, T.; Tarora, W.; Takahashi, H.: Study on tobacco components involved in the pyrolytic generation of selected smoke constituents. *Food and Chemical Toxicology* **2005**, *43*, 559-568.

CHAPTER 3: FLUORESCEIN-BASED IONIC LIQUID SENSOR FOR LABEL-FREE DETECTION OF SERUM ALBUMINS[†]

3.1. Introduction

Accurate detection of albumins such as human serum albumin (HSA) is critical to understanding numerous biological processes within the human body. HSA, a 66.5-kDa protein, is the most abundant protein in blood plasma, and is typically present at a concentration of approximately 0.6 mM (40 mg/mL).[1] HSA is an important multifunctional protein since it aids in maintaining the oncotic pressure; binds and transports a range of metabolites and xenobiotics; acts as an antioxidant; and exhibits catalytic activities toward a range of organic compounds.[1-4] A low level of HSA in blood plasma, also known as hypoalbuminemia, is indicative of medical conditions such as cirrhosis of the liver.[5,6] A small amount of HSA is normally found in urine; however, a persistent urinary excretion of HSA in the range of 30-299 mg/24 h is referred to as microalbuminuria, while albumin excretion above this range is known as macroalbuminuria.[7,8] Abnormal levels of albumin in urine indicate a chronic kidney disease which is common in patients with diabetes and hypertension.[7,8] Monitoring albumin levels in serum and urine has therefore been advocated in high-risk patients for early detection of possible medical complications.

A wide range of analytical methods are currently available for detection and quantification of proteins. Among them, immunoassays are commonly employed for analyses of protein mixtures because they provide an outstanding sensitivity and selectivity due to strong

[†] This Chapter previously appeared as Galpothdeniya, W. I. S.; Das, S.; De Rooy, S. L.; Regmi, B. P.; Hamdan, S.; Warner, I. M.: Fluorescein-based ionic liquid sensor for label-free detection of serum albumins. *Rsc Advances* **2014**, *4*, 17533-17540. It is reproduced by permission of the Royal Society of Chemistry.
http://pubs.rsc.org/en/content/articlelanding/2014/ra/c4ra01461h/unauth#!divAbstract

specific interactions between an antibody and an antigen. However, preparation of immunoassays is labor-intensive and time-consuming; and requires expensive reagents and instrumentation. We note that there has been a recent upsurge of interest in the development of fluorescence-based label-free approaches for protein analysis because of the inherent merits of ease of sensor fabrication along with high sensitivity and selectivity. Fluorescence-based methods are particularly noted for their low background noise and wide dynamic range.[9,10] When a fluorescent probe interacts with a target protein, a change in fluorescence intensity and/or a shift in the fluorescence emission spectra may be observed; and monitoring these changes can be very useful for detection of various proteins. Fluorescence-based methods have been widely explored for detection of albumins, and the fluorescent probes employed in such studies are primarily organic dye molecules as well as modified gold nanoparticles.[5,11-18] Despite considerable success in detection of albumins by use of fluorescence-based methods, many fluorescence probes are limited in application due to the need for complex synthetic procedures employing complex chemical reactions which often involve low product yields. In addition, these probes exhibit only partial selectivity towards albumins. Development of alternate fluorescence probes for albumins is therefore highly desirable.

Recently, Chen and coworkers[19,20] have introduced the concept of using ionic liquids (ILs) as potential fluorescence probes for protein detection. ILs are classically defined as organic salts with melting points below 100 °C.[21] ILs have also been demonstrated as useful sensing materials for detection of vapors and estimating values of pH.[22-25] These materials are easy to synthesize, and their physicochemical properties can be easily tuned simply by altering the counter cation or anion. ILs are typically nonvolatile and can often be easily dispersed in water

to form nanomaterials.[26,27] Hence, these materials hold considerable promise for use in biosensing applications.

Despite the significant potential of ILs for developing biosensors, uses of ILs as fluorescence probes for detection of albumins or other biomolecules are still in infancy. In the study reported in this manuscript, we outline a method for the selective and sensitive detection of albumins using aqueous dispersions of nanodroplets from a highly fluorescent ionic liquid prepared by pairing a fluorescein (FL) anion and trihexyl(tetradecyl)phosphonium (P_{66614}) cation. Examination of data from fluorescence and UV-vis spectroscopic studies of these dispersed $[FL]_2[P_{66614}]$ nanodroplets revealed that these molecules coexist as a mixture of strongly fluorescent monomers and weakly fluorescent molecular aggregates. Nanodroplets dispersions were prepared in the presence of eight different proteins, and the spectroscopic behavior was studied. Interestingly, it was observed that the monomeric species tended to dominate in the presence of HSA or bovine serum albumin (BSA), while the aggregate forms dominated in the blank or presence of other proteins. As a result, there is a strong enhancement of fluorescence intensity in the presence of HSA or BSA. Circular dichroism (CD) spectra of the serum albumins in the presence of IL showed considerable changes in secondary structures, thereby inferring strong interactions between these proteins and ILs. The intensity of the monomer fluorescence was found to increase linearly as a function of HSA or BSA concentrations, thereby allowing detection and quantification of these proteins. Therefore, the simple method outlined here should allow for rapid, sensitive, selective, and label-free detection of serum albumins in aqueous medium.

3.2. Experimental Section

3.2.1. Materials

Fluorescein disodium salt (Na_2FL), trihexyl(tetradecyl)phosphonium chloride ($[P_{66614}][Cl]$) (≥95%), tetraphenylphosphonium chloride ([TPP][Cl]), (4-nitrobenzyl)triphenylphosphonium chloride ([4NB][Cl]), ethanol (spectroscopic grade), human serum (heat inactivated), and all proteins were purchased from Sigma-Aldrich, and used as received. Triply deionized water (18.2 MΩ cm) from an Elga model PURELAB ultra water-filtration system was used for preparation of the sodium phosphate buffer (pH 7.4/10 mM).

3.2.2. Synthesis and Characterization of ILs

ILs were synthesized using an ion exchange procedure reported elsewhere.[27-30] Briefly, Na_2FL and $[P_{66614}][Cl]$ at a molar ratio of 1.1:2 were dissolved in a mixture of methylene chloride and water (5:1 v/v). This mixture was stirred for 48 h. The methylene chloride layer was washed with excess water several times in order to remove NaCl byproduct. The product $[P_{66614}]_2[FL]$ was dried by removing the solvent *in vacuo*. The product was obtained as a red viscous liquid (yield 88%). Finally, the IL was characterized by use of nuclear magnetic resonance (NMR) spectroscopy, Fourier transform infrared spectroscopy (FTIR), and electron spray ionization-mass spectrometry (ESI-MS).

3.2.3. Preparation of Protein Solutions

All protein samples were prepared in 10 mM sodium phosphate buffer (pH = 7.4) A stock solution of 2 mg/mL protein was initially prepared, and then diluted to obtain concentrations ranging from 2 to 50 μg/mL.

3.2.4. Preparation of IL Nanodroplets

IL nanodroplets were prepared using a modified reprecipitation method similar to that used for preparation of organic nanoparticles.[31] Briefly, 200 µL of 0.6 mM ethanolic IL solution were rapidly introduced into 5.0 mL of 10 mM sodium phosphate buffer solution (pH = 7.4) containing proteins and ultrasonicated for 5 min. After 10 minutes of equilibration time, the dispersions were characterized using various techniques as described below.

3.2.5. Characterization of Dispersions by Use of Dynamic Light Scattering (DLS)

The average size and size distribution of nanodroplets were determined by use of DLS. DLS data were obtained using a Nano ZS dynamic light scatterer (Malvern Instruments, Malvern, UK). This instrument provides mean hydrodynamic diameter and polydispersity index (PDI) of the nanodroplet population with a PDI range from 0 (monodisperse) to 0.5 (broad distribution). Two different $[P_{66614}]_2[FL]$ (24 µM) samples including a sample without proteins (blank), and the other sample with 20 µg/mL HSA were tested.

3.2.6. Absorption and Fluorescence Studies

Absorbance measurements were acquired using a Shimadzu UV-3101PC spectrophotometer. Fluorescence studies were performed on a Spex Fluorolog-3 spectrofluorimeter (model FL3-22TAU3; Jobin Yvon, Edison, NJ). A 0.4-cm path length quartz cuvette (Starna Cells) was used to collect the fluorescence and absorbance spectra. Absorption spectra were collected against an identical cell filled with sodium phosphate buffer (pH 7.4/10 mM) as the blank. Fluorescence studies were all performed by adapting a synchronous scan protocol with right angle geometry.[32,33]

3.2.7. CD Studies

In order to examine structural changes that occur in proteins due to interactions with our IL sensor, chiroptical analysis was performed using a J-815 CD spectrometer. All protein samples were prepared by using the sodium phosphate buffer solutions mentioned above. A 01-mm path length quartz cuvette (Precision Cells Inc.) was used to reduce interferences from buffer when collecting the CD spectra.

3.3. Results and Discussion

3.3.1. Preparation and Characterization of FL-Based Nanomaterials

Fluorescein (FL) and its derivatives are derived from a class of fluorophores known as xanthenes. Xanthene-based dyes often exhibit high chemical and photochemical stability. In addition, they are ideally suited for various sensing applications as a result of high optical sensitivity (high extinction coefficient and fluorescence quantum yield).[34,35] In this study, $[P_{66614}]$ cation, which has often been labeled a 'universal liquifier' for production of ILs,[23,28] was paired with the FL dianion resulting in a room temperature ionic liquid (RTIL) i.e. $[P_{66614}]_2[FL]$. Hence, this IL displays relatively strong fluorescence as compared to previously reported ILs as protein probes. Authors in a recent study have described the synthesis and spectroscopic behavior of a FL-based RTIL.[36] Recent studies from our laboratory have demonstrated that $[P_{66614}]_2[FL]$ nanodroplets can be used as a colorimetric pH sensor.[27]

The work outlined in this manuscript is an example of detection of proteins by use of $[P_{66614}]_2[FL]$ nanodroplets prepared by employing a simple reprecipitation method.[31,32] DLS studies revealed that these nanodroplets have a mean hydrodynamic diameter of 134.4 ± 1.4 nm, and a PDI of 0.29 ± 0.01 at the IL concentration of 24 μM, while the mean hydrodynamic

diameter and PDI values obtained for the same concentration of IL in the presence of 20 µg/mL HSA are 150.9 ± 3.3 and 0.22 ± 0.01 respectively. In the presence of HSA, the mean hydrodynamic diameter and PDI of the nanodroplets show only slight deviations as compared to the blank sample. These slight changes in the size and dispersion of nanodroplets may be attributed to changes in the environment due to the presence of HSA since all other parameters were held constant during experimentation. In addition to $[P_{66614}]_2[FL]$, two other FL-based salts, i.e. $[TPP]_2[FL]$, and $[4NB]_2[FL]$, were synthesized and characterized using the procedure described above. Both compounds were solids at room temperature, and are highly soluble in ethanol, but insoluble in water. Similarly, five other ILs were synthesized by pairing Eosin B (EoB), Eosin Y (EoY), Phloxine B (Phl), Erythrosin B (ER) or Rose Bengal (RoB) dianions with $[P_{66614}]$ cation, and all products were liquid at room temperature. The chemical structures of all cations and dye anions are given in Scheme 3.1.

3.3.2. Absorption and Fluorescence of FL-Based Nanodroplets

The absorption and fluorescence spectra of 40 µM $[P_{66614}]_2[FL]$ nanodroplets dispersed in a phosphate buffer (pH 7.4/10 mM) are shown in Figure 3.1a. From this figure, it is evident that the absorption spectrum shows an absorption maximum at ~530 nm with a blue-shifted absorption shoulder at ~490 nm. Similarly, the fluorescence spectrum exhibits two peaks, one at ~545 nm and the other at ~512 nm. In order to gain better insight into the spectral properties of $[P_{66614}]_2[FL]$ nanodroplets, absorption and fluorescence spectra at five different IL concentrations i.e. 8, 16, 24, 32, and 40 µM, were measured (Figs. 3.1b-c). Absorption spectra (Figure 3.1b) depict a decrease in absorbance with decreasing concentrations of $[P_{66614}]_2[FL]$. In addition, the ratio of absorbance at 490 and 530 nm is found to increase with decreased concentrations of IL.

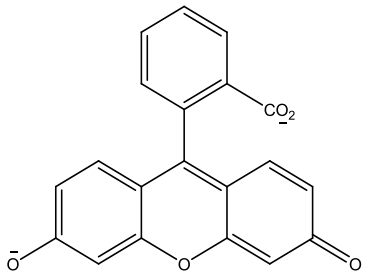

(I)

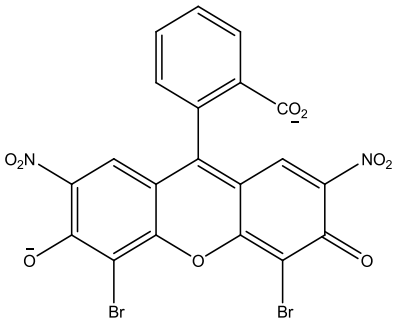

(II)

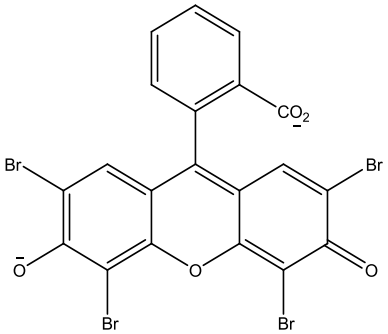

(III)

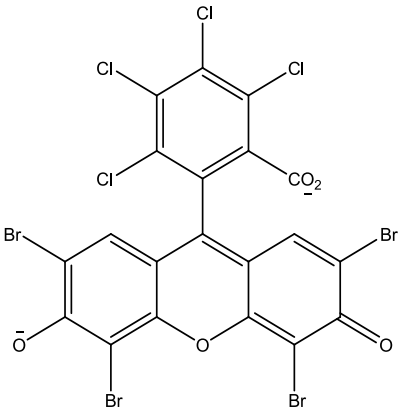

(IV)

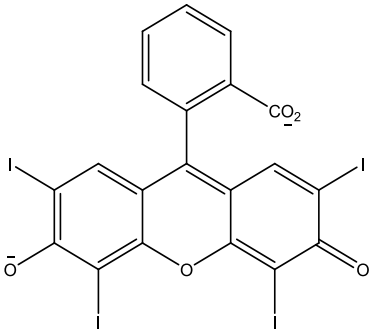

(V)

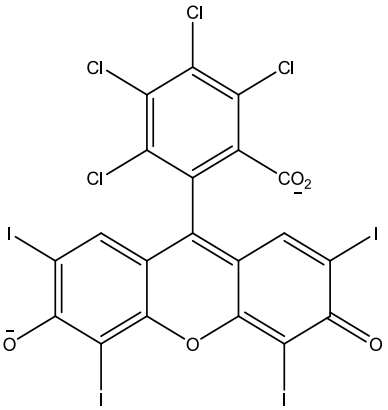

(VI)

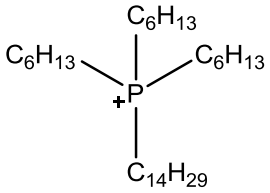

(VII)

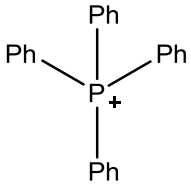

(VIII)

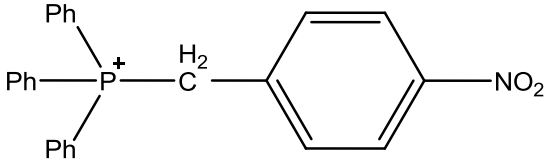

(IX)

Scheme 3.1. Chemical structures of different anions and cations used in this study (I) Fluorescein, (II) Eosin B, (III) Eosin Y, (IV) Phloxine B (V) Erythrosin B and, (VI) Rose Bengal (VII) [P_{66614}], (VIII) [TPP] and (IX) [4NB]

Figure 3.1. (a) Absorption and fluorescence emission spectra (λ_{ex} = 490 nm) of $[P_{66614}]_2[FL]$ nanodroplets dispersed in pH 7.4 buffer (final concentration of $[P_{66614}]_2[FL]$ in buffer is 40 μM); (b) absorbance spectra, and (c) fluorescence emission spectra (λ_{ex} = 490 nm) of $[P_{66614}]_2[FL]$ nanodroplets at five different concentrations (8, 16, 24, 32 and 40 μM) (continues through pages 82-84)

A

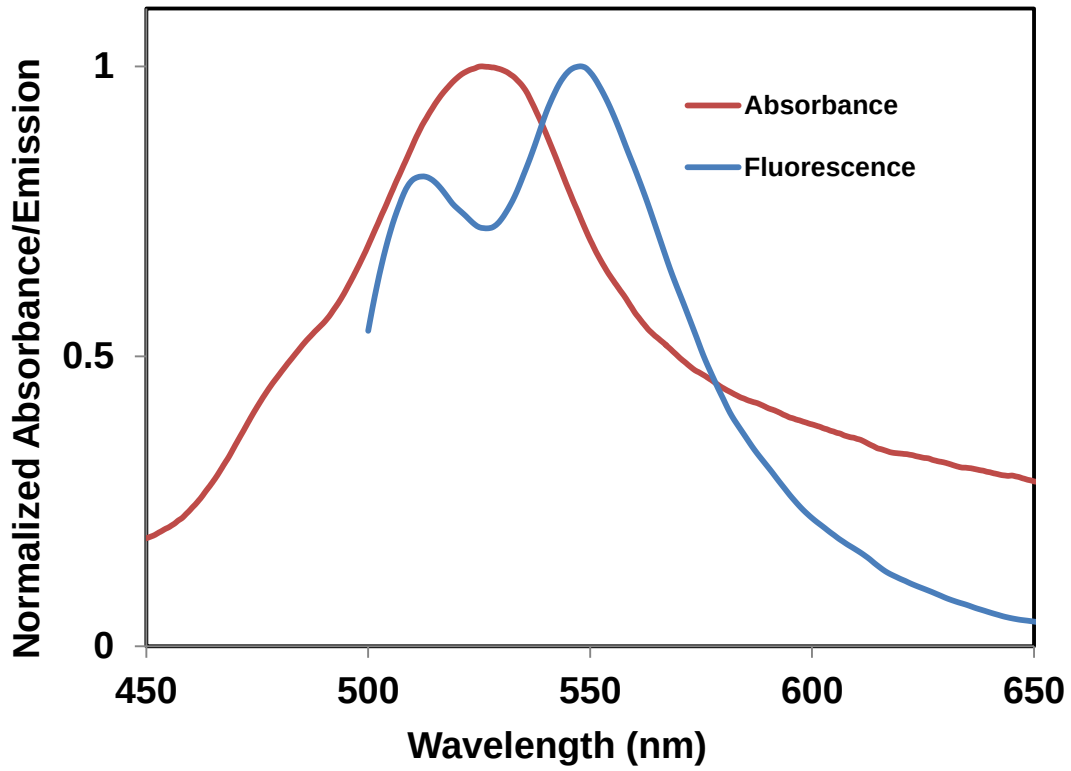
Normalized Absorbance/Emission
1
0.5
0
450
500
550
600
650
Wavelength (nm)
Absorbance
Fluorescence

B

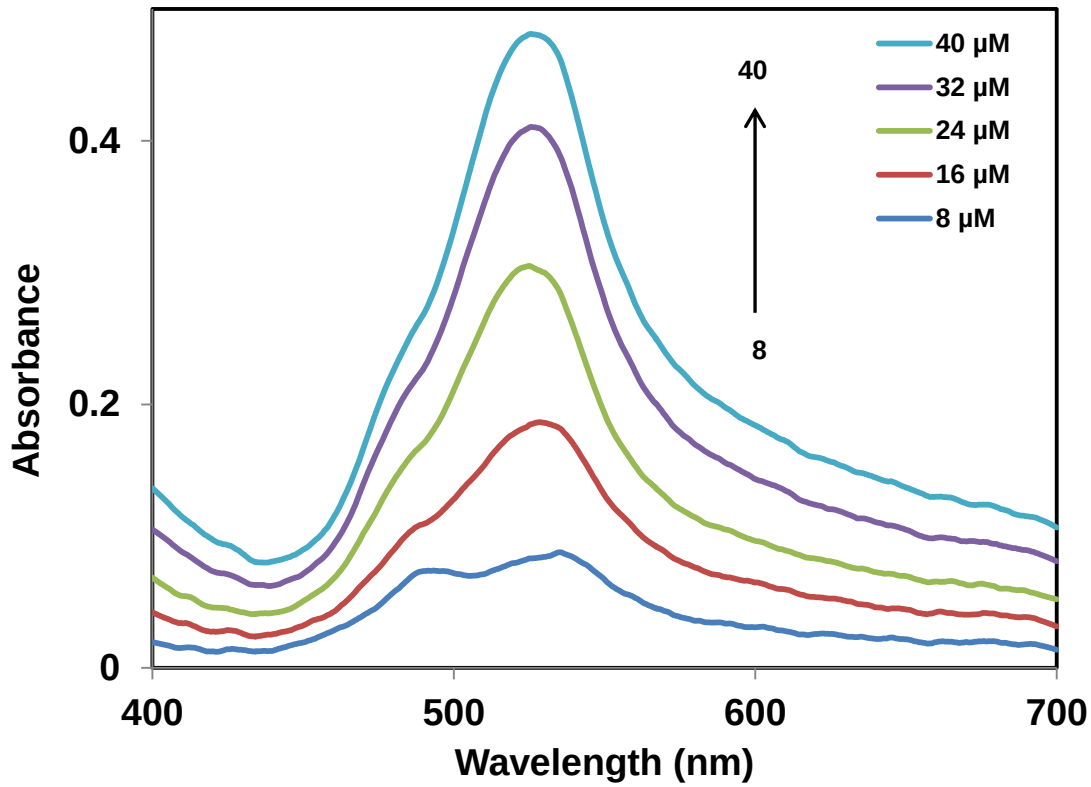
Absorbance
0.4
0.2
0
400
500
600
700
Wavelength (nm)
40 μM
32 μM
24 μM
16 μM
8 μM
40
8

C

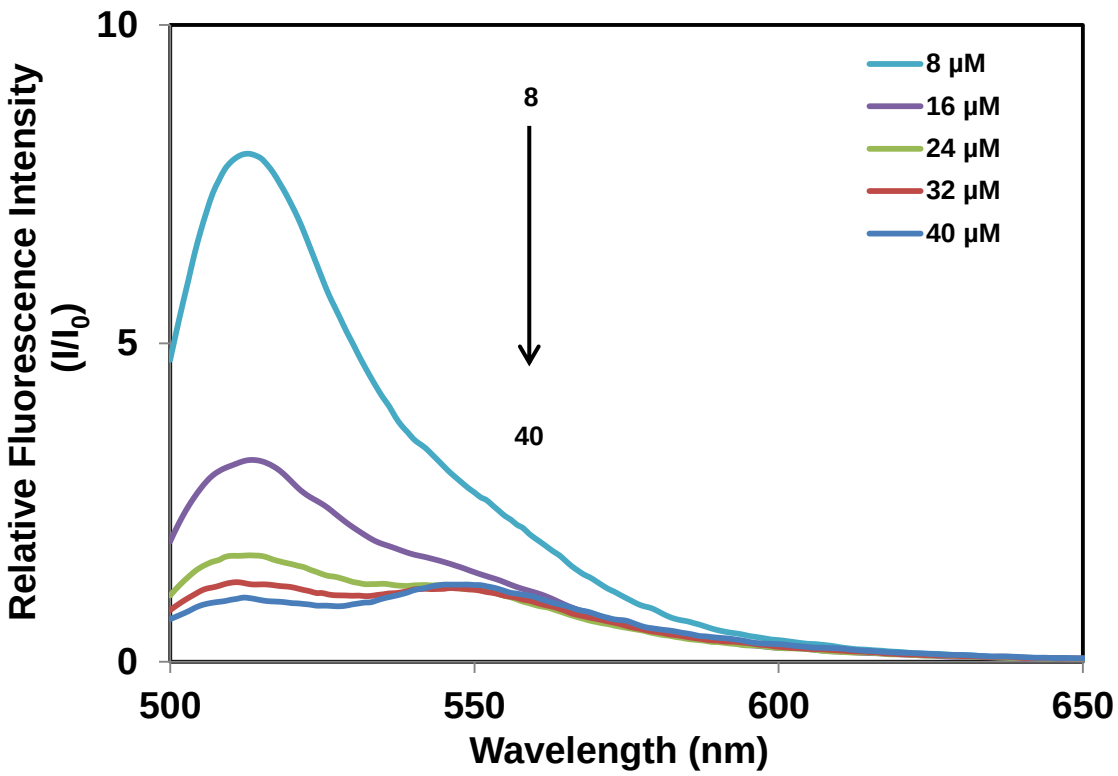

The dye assemblies responsible for production of the 530 nm peak and 490 nm shoulder were identified through examination of previous studies on dye assemblies in solution.[37] Dye aggregations are often characterized by broadening of the absorption spectra[38] or the appearance of either hypsochromically shifted (H aggregates) or bathochromically shifted (J aggregates) bands as compared to the monomer absorption band.[32,39] Therefore, the component absorbing at ~490 nm may be attributed to the monomeric form, while the bathochromically-shifted component absorbing at ~530 nm is possibly due to J-type aggregation, in which the dye transition dipoles are arranged in a staircase manner. As previously noted, a decrease in IL concentration results in a decrease in the ratio of aggregate to monomer absorption peaks. The ratios are given in Table 3.1 for various concentrations of ILs.

Table 3.1 Aggregate to monomer peak ratio $A_{ag(530)}/A_{m(490)}$ derived from absorbance spectra

$[P_{66614}]_2$[FL] Concentration(μM)	$A_{ag(530)}/A_{m(490)}$ ratio
40	1.9
32	1.9
24	1.9
16	1.6
08	1.1

A_{ag} – Absorbance of the aggregate peak, A_m – Absorbance of the monomer peak

The fluorescence emission spectra of the nanodroplets at various concentrations ranging from 8 to 40 μM are shown in Figure 3.1c. It is evident from these spectra that there is a remarkable increase in fluorescence intensity, accompanied by a gradual peak shift from ~545 nm to ~512 nm with decreasing concentrations of $[P_{66614}]_2$[FL]. The fluorescence peak at approximately 512 nm is attributable to monomeric species, and the peak at 545 nm is ascribed to J-type aggregations. Surprisingly, in contrast to absorbance, the fluorescence intensity increases with a decrease in IL concentration.

It is important to note that at higher IL concentrations, J-type aggregates are more pronounced than monomers as evidenced by the higher aggregate to monomer peak ratio ($A_{ag(530)}/A_{m(490)}$) in absorbance. However, the fluorescence intensity of the aggregate peak is not very high as compared to the monomer peak. At lower IL concentrations where the $A_{ag(530)}/A_{m(490)}$ ratio is small, the fluorescence intensity for the monomeric peak increases. Thus, as leaned from the absorption and fluorescence spectra, the monomer form is more fluorescent than the J-type aggregates. However, we note that for classical examples of dye assemblies, J aggregates usually display an intense fluorescence emission, whereas H aggregates are usually

characterized by diminished fluorescence with a typically large Stokes shift.[39,40] The decrease in observed fluorescence intensity of the J aggregates in this work may be attributed to the self-quenching of fluorescence by the dye molecules within the nanodroplets.[41]

3.3.3. Fluorescence Sensing of Proteins Using FL-Based Nanodroplets

In this manuscript, detection of proteins employing FL-based nanodroplets was studied using eight different proteins, i.e. 1) Human serum albumin (HSA), 2) Bovine serum albumin (BSA), 3) α-Lactalbumin from bovine milk (α-lac), 4) Albumin from chicken egg white (CEA), 5) Ribonuclease A from bovine pancreas (Rib-A), 6) α-Chymotrypsin from bovine pancreas (α-CTP), 7) Cytochrome C from bovine heart (Cyt-C), and 8) Lysozyme from chicken egg white (CEL). Figure 3.2 is a comparison of the integrated fluorescence intensity of $[P_{66614}]_2[FL]$ nanodroplets in the presence of each protein at the same molar concentration (fluorescence emission spectra which corresponds to these integrated fluorescence intensities are given in Figure B1). The concentrations of $[P_{66614}]_2[FL]$ and proteins were fixed at 40 and 1.5 μM, respectively. Fluorescence spectra were recorded using 490 nm excitation. Interestingly, BSA and HSA produced more than 19-fold enhancement in the integrated fluorescence emission signal, whereas CEA produced 4.5-fold enhancement. In contrast, the remaining proteins produced essentially no change in fluorescence intensity. Therefore, examination of the acquired data suggests that these nanodroplets are highly selective for detection of albumins. Since HSA is not found together with BSA and CEA in actual samples, it is reasonable to conclude that this method is very promising for selective detection of HSA in real samples. Several reports exist in the literature on fluorescence sensing of proteins. In most of these studies, the fluorescence signal is shown to be quenched due to interactions between the protein and IL.[19] However, in our

case, the fluorescence signal is enhanced upon addition of proteins. From an analytical viewpoint, this observation should be more useful for sensor applications.

In an attempt to understand the sensing properties of related compounds, similar ILs were synthesized by using cations and anions with slightly different structures. The starting material Na_2[FL], and two other ion pairs, $[4NB]_2$[FL] and $[TPP]_2$[FL], showed essentially no difference in fluorescence signal when combined with all proteins at the tested concentration of 1.5 µM (Figure B2a-c).

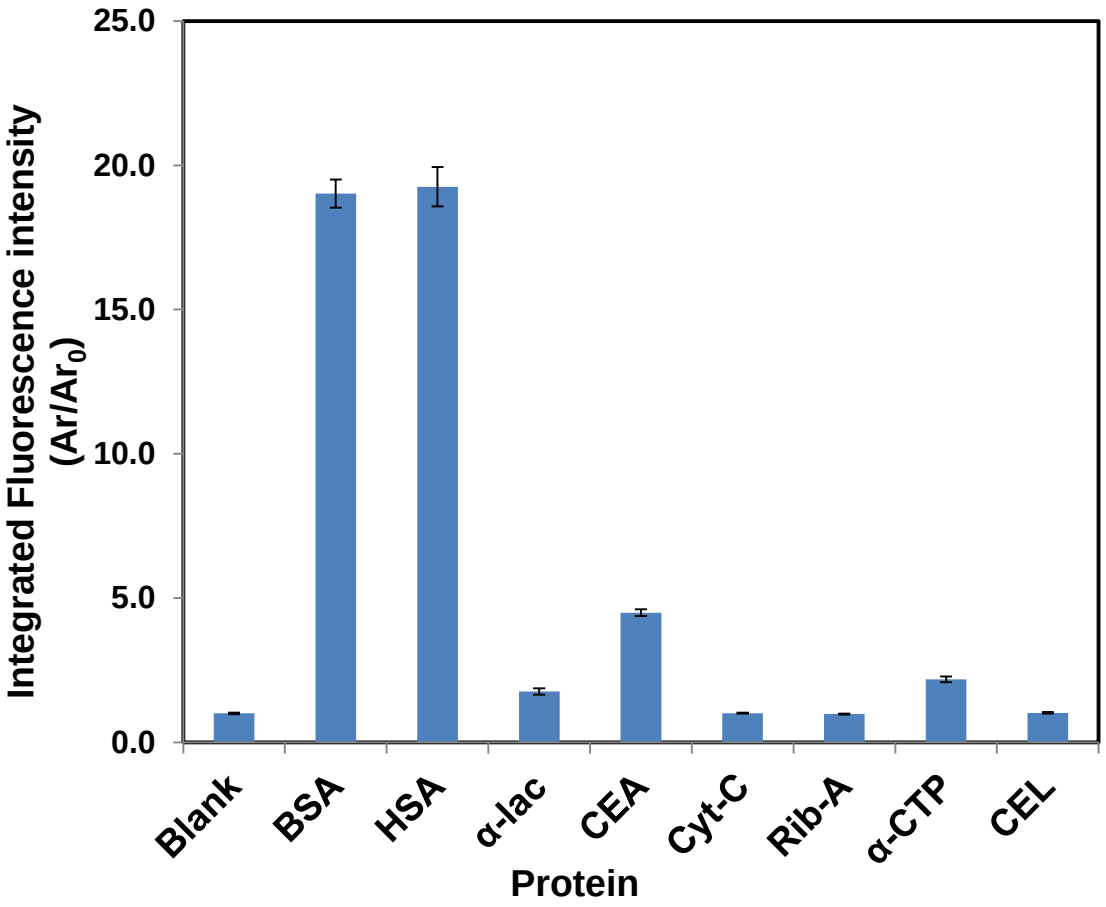

Figure 3.2. Integrated fluorescence intensity over the spectral range of 500 to 700 nm (λ_{ex} – 490 nm) of 40 µM $[P_{66614}]_2$[FL] in the presence of same concentration (1.5 µM) of different albumins and non-albumins. (Error bars represent the standard deviations of three replicate samples).

Similarly, the role of the anion towards the fluorescence sensing of albumins was investigated by use of five previously mentioned ILs containing other xanthene dye dianions instead of FL. Although these molecules are structurally similar to FL, the spectroscopic behaviors of these nanodroplets were found to be very different from $[P_{66614}]_2[FL]$ nanodroplets (data not shown). Specifically, no substantial change in fluorescence signal was observed upon treating these nanodroplets with BSA or HSA over the tested protein concentration range of 10-50 µg/mL (Figure B3a-e)†. We note that these ILs were not tested for other proteins since our focus is on a sensor for HSA. Our studies demonstrate that there are unique interactions between albumins and $[P_{66614}]_2[FL]$ ion pairs, which may allow development of highly selective sensors for albumins.

To further elucidate interactions between proteins and $[P_{66614}]_2[FL]$, we utilized circular dichroism (CD) spectroscopy. The CD spectra of BSA, HSA and Cyt-C in the absence and presence of IL are shown in Figure 3.3 (data not shown for other proteins). These CD studies revealed notable changes in the secondary structure of albumins (Figs. 3.3a-b) in the presence of $[P_{66614}]_2[FL]$ nanodroplets indicating strong interactions between albumins and $[P_{66614}]_2[FL]$. It is further noted that the observed change in secondary structure of BSA and HSA is increased when the concentration ratio of $[P_{66614}]_2[FL]$ to albumin is increased from 8:1 to 40:1. For non-albumins (e.g. Cyt-C), the CD spectra (Figure 3.3c) show little or no changes at various concentration ratios of $[P_{66614}]_2[FL]$ and Cyt-C, suggesting an unaltered secondary structure for Cyt-C. This may be attributed to negligible interactions between Cyt-C and $[P_{66614}]_2[FL]$. Thus, it can be inferred from these CD measurements that albumins interact strongly with our sensor, while other proteins show negligible interactions. This key property of $[P_{66614}]_2[FL]$ makes it a promising material for sensing of albumins.

Figure 3.3. CD spectra of (a) $[P_{66614}]_2$[FL]–BSA, (b) $[P_{66614}]_2$[FL]–HSA and (c) $[P_{66614}]_2$[FL]–Cyt–C obtained in a phosphate buffer (pH 7.4/10 mM). The concentrations of nanodroplets and proteins are indicated in the legend (continues through pages 89-91)

A

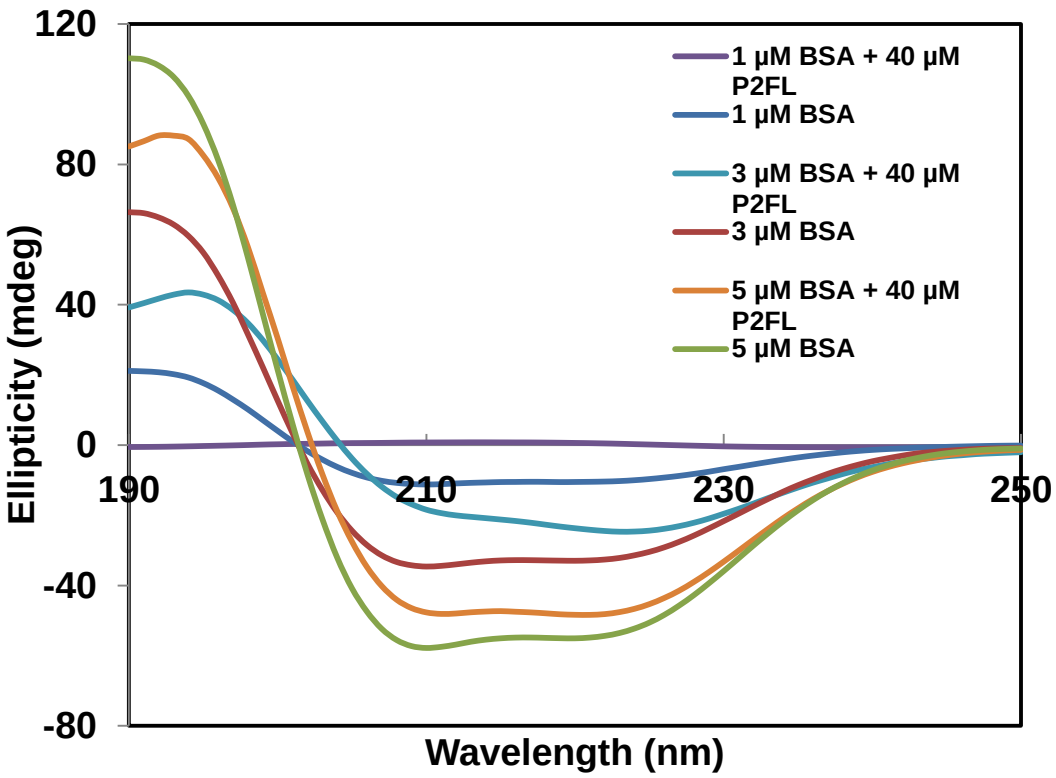
120
80
40
0
-40
-80
190
210
230
250
Ellipticity (mdeg)
Wavelength (nm)
1 μM BSA + 40 μM P2FL
1 μM BSA
3 μM BSA + 40 μM P2FL
3 μM BSA
5 μM BSA + 40 μM P2FL
5 μM BSA

B

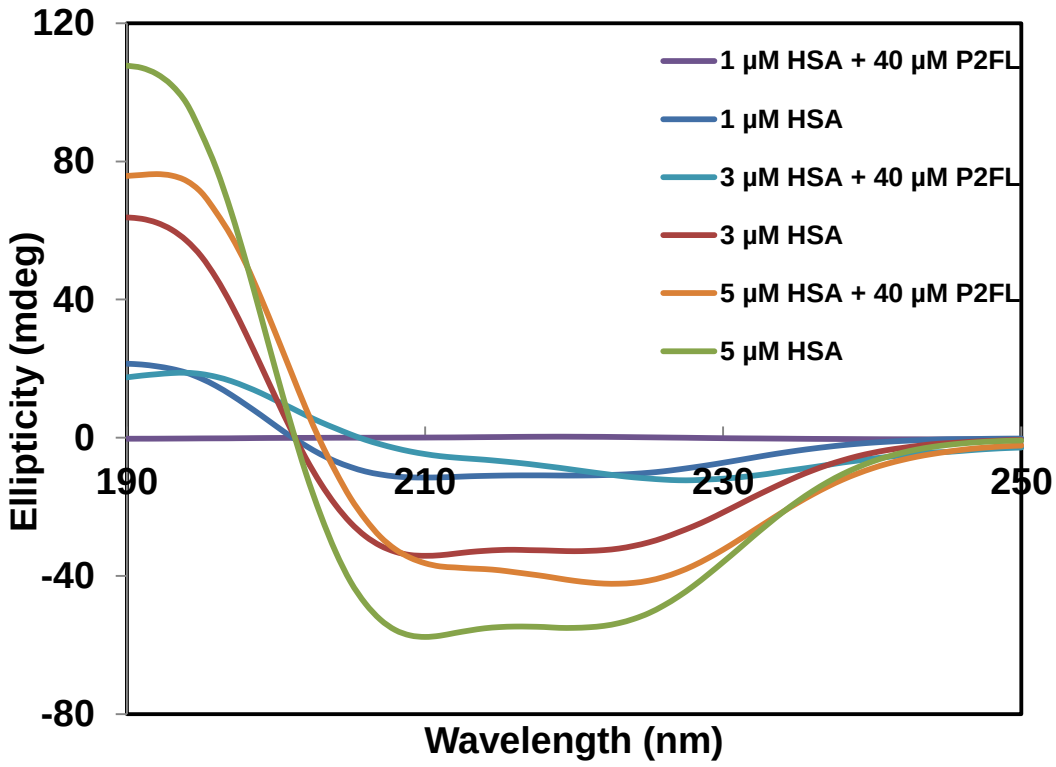
120
80
40
0
-40
-80
190
210
230
250
Ellipticity (mdeg)
Wavelength (nm)
1 μM HSA + 40 μM P2FL
1 μM HSA
3 μM HSA + 40 μM P2FL
3 μM HSA
5 μM HSA + 40 μM P2FL
5 μM HSA

C

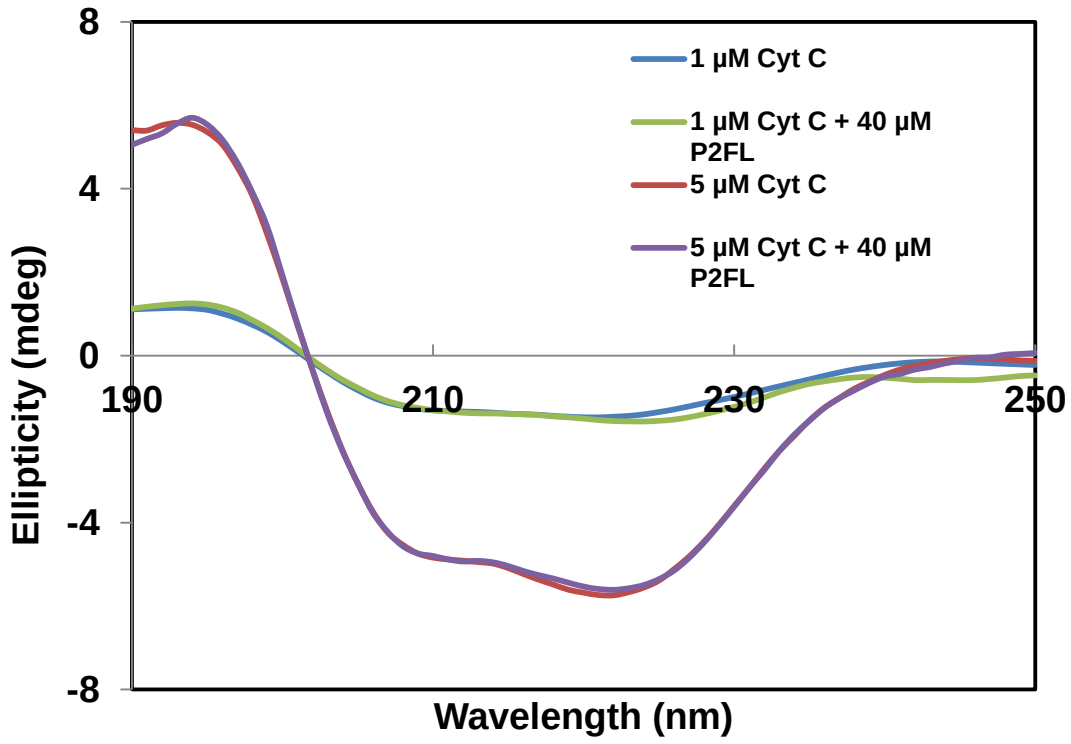

Figure 3.4a is an illustration of the measured fluorescence spectra of $[P_{66614}]_2[FL]$ nanodroplets dispersed in various concentrations of BSA. Examination of Figure 3.4b shows that the fluorescence intensity varies linearly as a function of BSA concentration over the concentration range of 10 to 50 µg/mL. As previously noted, peak at 512 nm is attributable to monomeric species, and the peak at 545 nm is ascribed to J-type aggregations. The intensity of the peak at ~512 nm, increases with respect to the J-aggregate peak with increasing BSA concentrations. This increase in the intensity of the monomer peak indicates formation of monomeric form through deaggregation of J-type aggregates in the presence of BSA molecules. In other words, the presence of BSA minimizes the aggregation of IL molecules. Further studies to understand the interactions at the molecular level are in progress. In order to gain better insight, absorbance studies were also performed for the same samples along with fluorescence studies. Upon normalization of the absorption spectra in the region of the monomer peak, it is

Figure 3.4. (a) Fluorescence emission spectra (λ_{ex} = 490 nm) of $[P_{66614}]_2[FL]$ nanoparticles dispersed in different concentrations of BSA, and (b) linear relationship between BSA concentration and relative fluorescence intensity at 512 nm (Errors bars represent the standard deviations for three replicate samples. Note some error bars are too small to be seen over the data points). Absorbance spectra (c) normalized at 490 nm and (d) normalized at 530 nm at different BSA concentrations (final concentration of $[P_{66614}]_2[FL]$ is 24 μM). The concentrations of BSA are indicated in the legend (continues through pages 92-94)

A

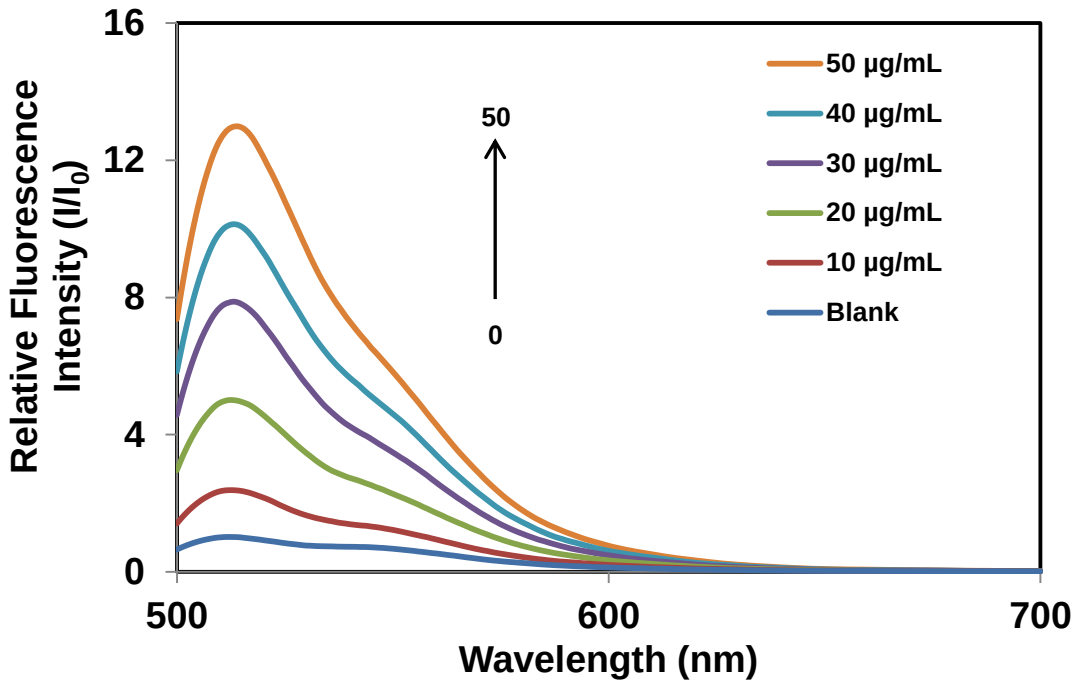
16
12
8
4
0
Relative Fluorescence Intensity (I/I0)
50
0
50 µg/mL
40 µg/mL
30 µg/mL
20 µg/mL
10 µg/mL
Blank
500
600
700
Wavelength (nm)

B

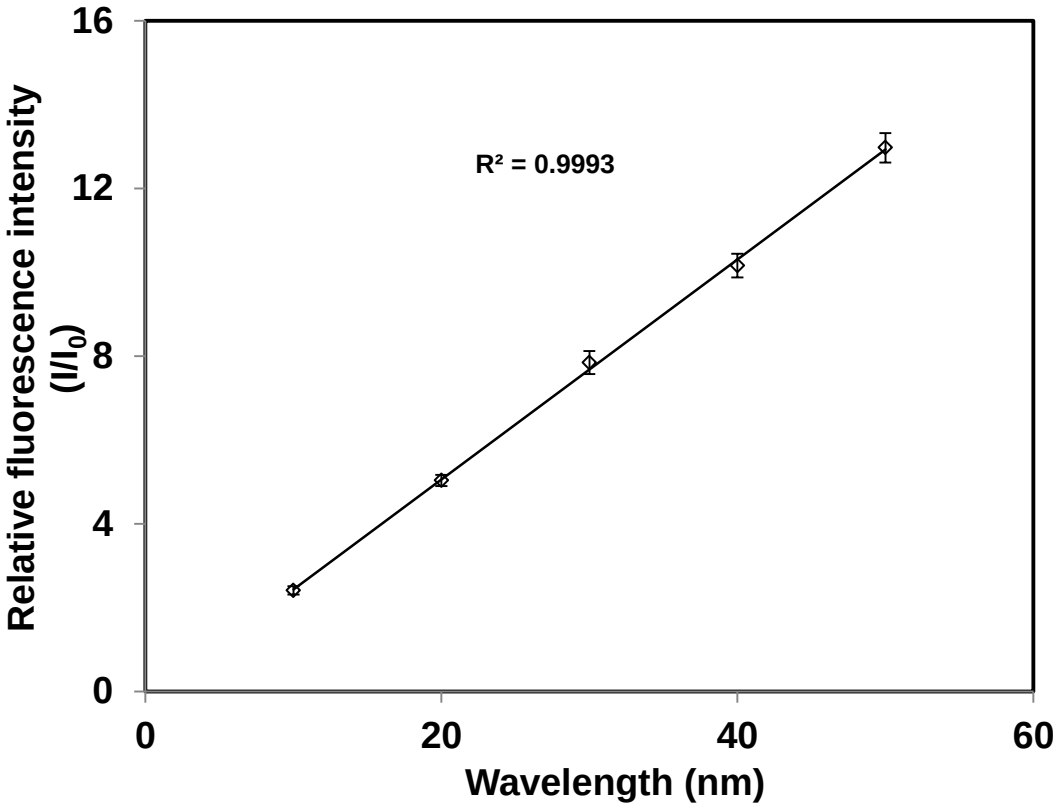
16
12
8
4
0
Relative fluorescence intensity (I/I0)
R² = 0.9993
0
20
40
60
Wavelength (nm)

C

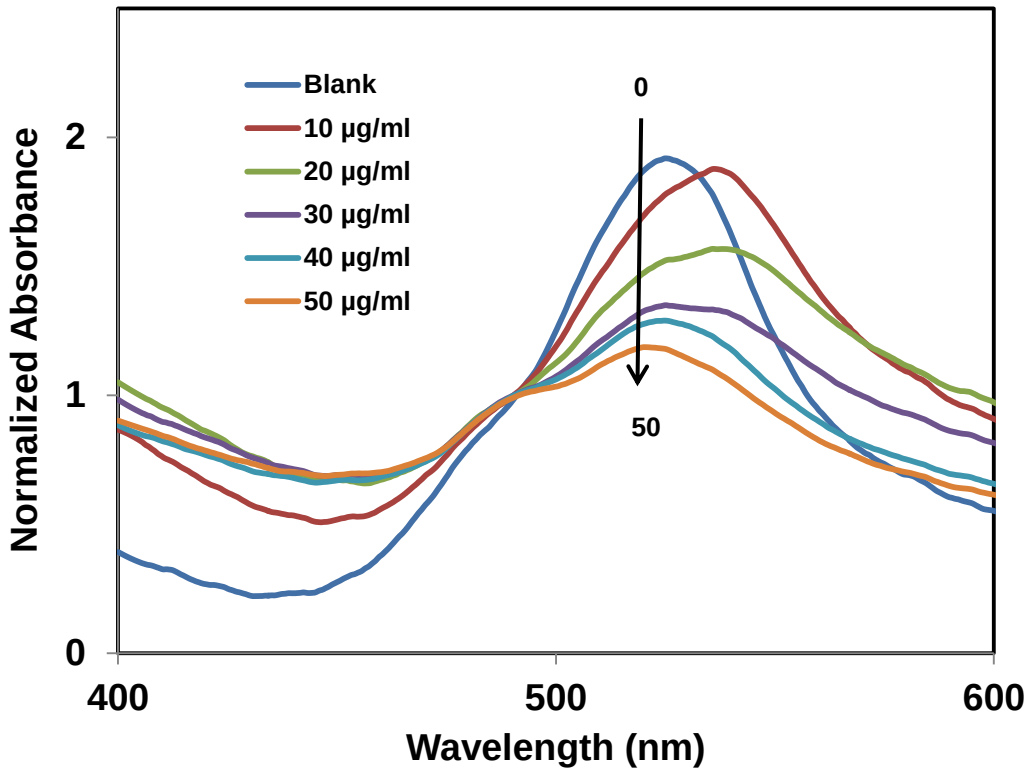
Blank
10 µg/ml
20 µg/ml
30 µg/ml
40 µg/ml
50 µg/ml
0
50
Normalized Absorbance
2
1
0
400
500
600
Wavelength (nm)

D

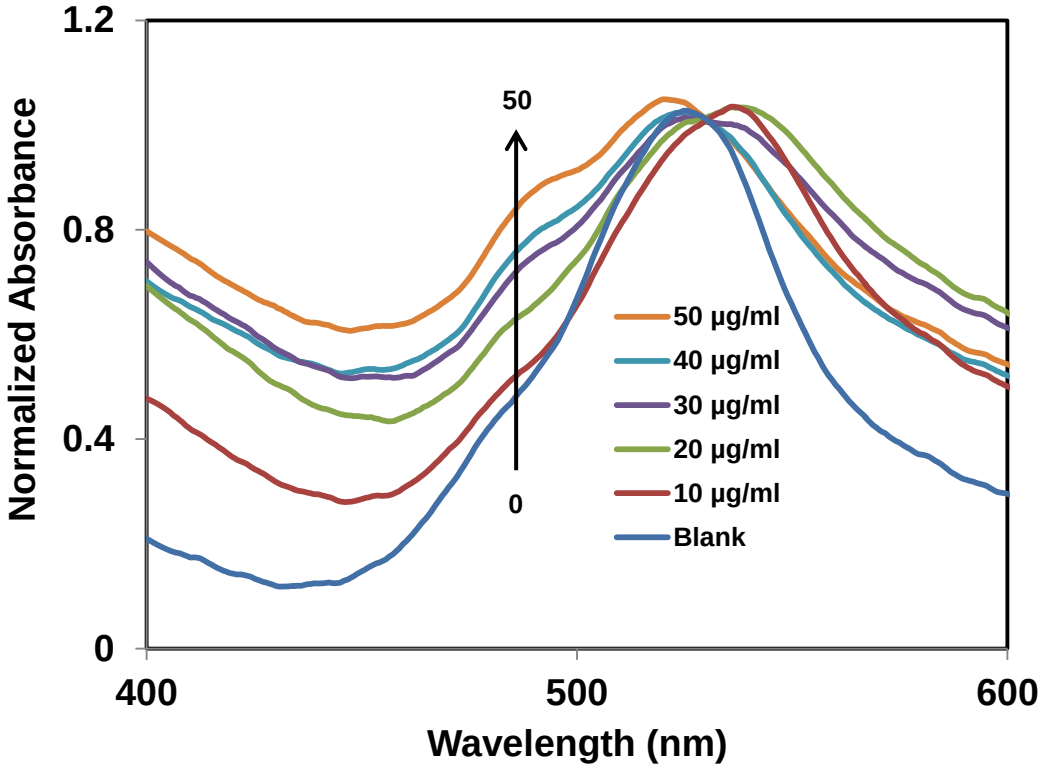
50
0
50 µg/ml
40 µg/ml
30 µg/ml
20 µg/ml
10 µg/ml
Blank
Normalized Absorbance
1.2
0.8
0.4
0
400
500
600
Wavelength (nm)

observed that the absorbance for the aggregate peak decreases with increasing concentrations of BSA (Figure 3.4c). Similarly, upon normalization of the absorption spectra at the aggregate peak, it is observed that the monomer peak increases with increasing concentrations of BSA (Figure 3.4d). It was also observed that the aggregate to monomer peak ratio ($A_{ag(530)}/A_{m(490)}$) decreases with increasing BSA concentration (Table 3.2). These findings are consistent with our assumption that BSA converts weakly fluorescent dye aggregates into strongly fluorescent monomeric forms upon interaction with our IL sensor. Therefore, an increase in fluorescence signal at ~512 nm is observed with increasing concentrations of BSA. Similar arguments apply to HSA since HSA and BSA are structurally homologous proteins which perform similar functions.

Table 3.2 Aggregate to monomer absorbance peak ratio ($A_{ag(530)}/_{Am(490)}$) at increasing BSA concentrations (final concentration of $[P_{66614}]_2$[FL] is 24 µM)

BSA concentration(µg/mL)	$A_{ag(530)}/A_{m(490)}$ ratio
10	1.87
20	1.81
30	1.52
40	1.33
50	1.13

The fluorescence emission spectra of the nanodroplets in the presence of various concentrations of HSA, ranging from 2 µg/mL to 50 µg/mL, were measured (Figure 3.5a). A plot of relative fluorescence intensity versus the concentration of HSA is found to be a second-degree polynomial with r^2 of 0.998 (Figure 3.5b). Hence, the concentration of HSA in an unknown sample can be estimated from these data.

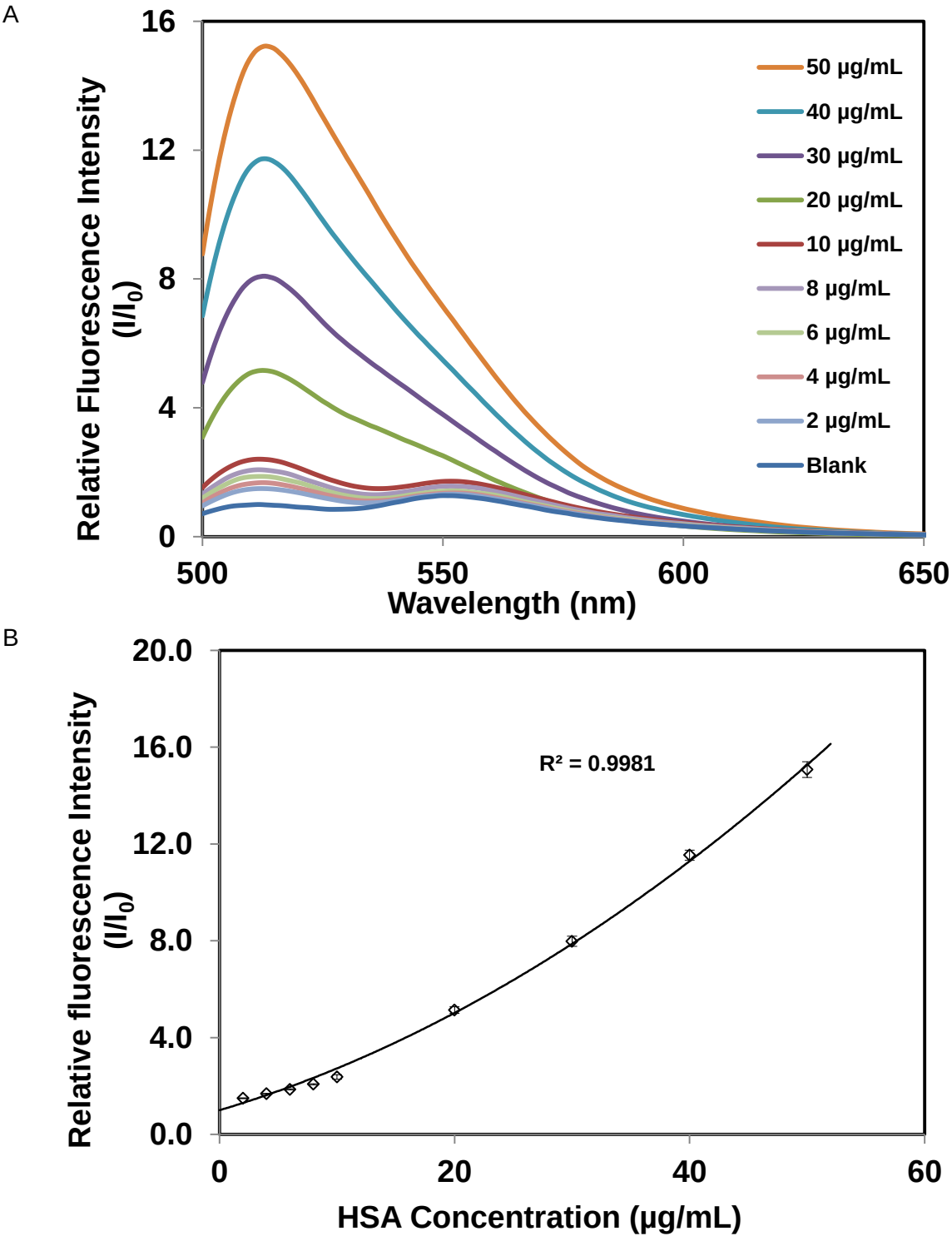

Figure 3.5. Fluorescence emission spectra of 24 µM $[P_{66614}]_2[FL]$ nanodroplets dispersed in different concentrations of HSA solution. The concentrations of HSA are indicated in the legend. (b) Polynomial relationship between relative fluorescence intensity at 512 nm and HSA concentration. Error bars represent the standard deviations of three replicate samples. Note some error bars are too small to be seen over the data points

The detection limit for HSA was estimated by use of the equation $3\sigma/m_{sl}$, where σ the standard deviation of three replicate blank samples, and m_{sl} is the slope of the calibration curve obtained in the region of low HSA concentration. On this basis, the detection limit for HSA was estimated to be ~300 ng/mL (4.5 nM).

Finally, to further demonstrate the sensor performance in real samples, fluorescence emission of spiked HSA in a diluted serum was measured. In general, detection of serum albumins from real samples such as blood serum is inherently challenging mainly due to extreme complexity of the sample matrix. Also, the fluorescence emission may have interference from fluorescence emission of other biological molecules in the sample. However, the concentration of HSA is very high in blood serum (40 mg/mL),[1] and our method can be used to detect HSA concentrations which are much lower than that. Therefore, human serum samples were diluted 1000 times before spiking with HSA. A plot of relative fluorescence intensity versus the concentration of HSA (10-50 µg/mL) in serum is given in Figure B4. Examination of data in Figure B4 suggests that there is good correlation between relative fluorescence intensity and HSA concentration in the human serum. However, there is a notable difference between the calibration plots of HSA in buffer and serum. This can be attributed to the interferences present in serum. One way to get around these interferences is to design a sensor array with sensors that respond in a manner similar to $[P_{66614}]_2[FL]$. Currently, we are investigating other possible IL candidates which can be used with $[P_{66614}]_2[FL]$.

One of the key requirements for a successful sensor is the stability of the signal. The stability of the dispersions of $[P_{66614}]_2[FL]$ nanodroplets were studied by monitoring the fluorescence emission spectra of a blank sample at different times. The fluorescence spectra did not change appreciably (<1%) during the test period of 120 minutes (Figure B5). This illustrates

that the observed dispersions are very stable, i.e. at least over the time period of these measurements. In addition, a relatively high zeta potential (i.e. +36.5 mV) indicates very good stability of these dispersion.[27]

3.4. Conclusions

In this work, the application of a fluorescent ionic liquid sensor, i.e. $[P_{66614}]_2[FL]$, for highly selective and sensitive detection of albumins has been demonstrated. Aqueous dispersions of $[P_{66614}]_2[FL]$ nanodroplets display strongly fluorescent J-type aggregates and weakly fluorescent monomeric forms. Examination of data from CD spectroscopic studies revealed remarkable changes in albumin structures in the presence of $[P_{66614}]_2[FL]$, indicating strong interactions between IL molecules and albumins. Both absorbance and fluorescence data support the conclusion that BSA and HSA convert the aggregate forms of our sensor into monomeric forms, which leads to a proportional increase in fluorescence signal in the presence of albumins. Furthermore, this conversion is dependent on the amount of proteins present in aqueous solution. As a result, this allows label-free detection of albumins aqueous samples. Based on our data, the estimated LOD value for HSA is 300 ng/mL. Thus, $[P_{66614}]_2[FL]$ should be an excellent fluorescent probe for selective measurement of HSA in aqueous samples.

3.5. References

(1) Kragh-Hansen, U.: Molecular and practical aspects of the enzymatic properties of human serum albumin and of albumin–ligand complexes. *Biochimica et Biophysica Acta (BBA) - General Subjects* **2013**, *1830*, 5535-5544.

(2) Kragh-Hansen, U.; Chuang, V. T. G.; Otagiri, M.: Practical aspects of the ligand-binding and enzymatic properties of human serum albumin. *Biological & Pharmaceutical Bulletin* **2002**, *25*, 695-704.

(3) Cordova, J.; Ryan, J. D.; Boonyaratanakornkit, B. B.; Clark, D. S.: Esterase activity of bovine serum albumin up to 160 degrees C: A new benchmark for biocatalysis. *Enzyme and Microbial Technology* **2008**, *42*, 278-283.

(4) Iwao, Y.; Ishima, Y.; Yamada, J.; Noguchi, T.; Kragh-Hansen, U.; Mera, K.; Honda, D.; Suenaga, A.; Maruyama, T.; Otagiri, M.: Quantitative evaluation of the role of cysteine and methionine residues in the antioxidant activity of human serum albumin using recombinant mutants. *Iubmb Life* **2012**, *64*, 450-454.

(5) Chung, C. Y.-S.; Yam, V. W.-W.: Induced Self-Assembly and Förster Resonance Energy Transfer Studies of Alkynylplatinum(II) Terpyridine Complex Through Interaction With Water-Soluble Poly(phenylene ethynylene sulfonate) and the Proof-of-Principle Demonstration of this Two-Component Ensemble for Selective Label-Free Detection of Human Serum Albumin. *Journal of the American Chemical Society* **2011**, *133*, 18775-18784.

(6) Bernardi, M.; Maggioli, C.; Zaccherini, G.: Human albumin in the management of complications of liver cirrhosis. *Critical Care* **2012**, *16*.

(7) Kramer, H.; Molitch, M. E.: Screening for kidney disease in adults with diabetes. *Diabetes Care* **2005**, *28*, 1813-1816.

(8) Levey, A. S.; Coresh, J.: Chronic kidney disease. *The Lancet* **2012**, *379*, 165-180.

(9) Ambrose, W. P.; Goodwin, P. M.; Jett, J. H.; Van Orden, A.; Werner, J. H.; Keller, R. A.: Single molecule fluorescence spectroscopy at ambient temperature. *Chemical reviews* **1999**, *99*, 2929-56.

(10) Patton, W. F.: Making blind robots see: the synergy between fluorescent dyes and imaging devices in automated proteomics. *BioTechniques* **2000**, *28*, 944-8, 950-7.

(11) Sun, Y.; Wei, S.; Zhao, Y.; Hu, X.; Fan, J.: Interactions between 4-(2-dimethylaminoethyloxy)-N-octadecyl-1,8-naphthalimide and serum albumins: Investigation by spectroscopic approach. *Journal of Luminescence* **2012**, *132*, 879-886.

(12) Volkova, K. D.; Kovalska, V. B.; Losytskyy, M. Y.; Reis, L. V.; Santos, P. F.; Almeida, P.; Lynch, D. E.; Yarmoluk, S. M.: Aza-substituted squaraines for the fluorescent detection of albumins. *Dyes and Pigments* **2011**, *90*, 41-47.

(13) Kar, C.; Ojha, B.; Das, G.: A novel amphiphilic thiosemicarbazone derivative for binding and selective sensing of human serum albumin. *Luminescence* **2013**, *28*, 339-344.

(14) Lu, H.; Xu, B.; Dong, Y.; Chen, F.; Li, Y.; Li, Z.; He, J.; Li, H.; Tian, W.: Novel fluorescent pH sensors and a biological probe based on anthracene derivatives with aggregation-induced emission characteristics. *Langmuir* **2010**, *26*, 6838-6844.

(15) Tong, H.; Hong, Y.; Dong, Y.; Häussler, M.; Li, Z.; Lam, J. W. Y.; Dong, Y.; Sung, H. H. Y.; Williams, I. D.; Tang, B. Z.: Protein Detection and Quantitation by Tetraphenylethene-Based Fluorescent Probes with Aggregation-Induced Emission Characteristics. *The Journal of Physical Chemistry B* **2007**, *111*, 11817-11823.

(16) Tong, H.; Hong, Y.; Dong, Y.; Hau; Lam, J. W. Y.; Li, Z.; Guo, Z.; Guo, Z.; Tang, B. Z.: Fluorescent "light-up" bioprobes based on tetraphenylethylene derivatives with aggregation-induced emission characteristics. *Chemical Communications* **2006**, 3705-3707.

(17) Comby, S.; Gunnlaugsson, T.: Luminescent lanthanide-functionalized gold nanoparticles: exploiting the interaction with bovine serum albumin for potential sensing applications. *ACS nano* **2011**, *5*, 7184-7197.

(18) Lacerda, S. H. D. P.; Park, J. J.; Meuse, C.; Pristinski, D.; Becker, M. L.; Karim, A.; Douglas, J. F.: Interaction of Gold Nanoparticles with Common Human Blood Proteins. *ACS Nano* **2009**, *4*, 365-379.

(19) Shu, Y.; Liu, M.; Chen, S.; Chen, X.; Wang, J.: New insight into molecular interactions of imidazolium ionic liquids with bovine serum albumin. *The Journal of Physical Chemistry B* **2011**, *115*, 12306-12314.

(20) Chen, X. W.; Liu, J. W.; Wang, J. H.: A highly fluorescent hydrophilic ionic liquid as a potential probe for the sensing of biomacromolecules. *The journal of physical chemistry. B* **2011**, *115*, 1524-30.

(21) Hallett, J. P.; Welton, T.: Room-temperature ionic liquids: solvents for synthesis and catalysis. 2. *Chemical Reviews* **2011**, *111*, 3508-3576.

(22) Galpothdeniya, W. I. S.; McCarter, K. S.; De Rooy, S. L.; Regmi, B. P.; Das, S.; Hasan, F.; Tagge, A.; Warner, I. M.: Ionic liquid-based optoelectronic sensor arrays for chemical detection. *RSC Advances* **2014**, *4*, 7225-7234.

(23) Yung, K. Y.; Schadock-Hewitt, A. J.; Hunter, N. P.; Bright, F. V.; Baker, G. A.: 'Liquid litmus': chemosensory pH-responsive photonic ionic liquids. *Chemical Communications* **2011**, *47*, 4775-4777.

(24) Yu, L.; Garcia, D.; Ren, R.; Zeng, X.: Ionic liquid high temperature gas sensors. *Chemical communications* **2005**, 2277-2279.

(25) Zhang, Q.; Zhang, S.; Liu, S.; Ma, X.; Lu, L.; Deng, Y.: Ionic liquid-modified dyes and their sensing performance toward acids in aqueous and non-aqueous solutions. *Analyst* **2011**, *136*, 1302-1304.

(26) Bwambok, D. K.; El-Zahab, B.; Challa, S. K.; Li, M.; Chandler, L.; Baker, G. A.; Warner, I. M.: Near-Infrared Fluorescent NanoGUMBOS for Biomedical Imaging. *ACS Nano* **2009**, *3*, 3854-3860.

(27) Das, S.; Magut, P. K. S.; de Rooy, S. L.; Hasan, F.; Warner, I. M.: Ionic liquid-based fluorescein colorimetric pH nanosensors. *RSC Advances* **2013**, *3*, 21054-21061.

(28) Del Sesto, R. E.; McCleskey, T. M.; Burrell, A. K.; Baker, G. A.; Thompson, J. D.; Scott, B. L.; Wilkes, J. S.; Williams, P.: Structure and magnetic behavior of transition metal based ionic liquids. *Chemical Communications* **2008**, 447-449.

(29) Bwambok, D. K.; Marwani, H. M.; Fernand, V. E.; Fakayode, S. O.; Lowry, M.; Negulescu, I.; Strongin, R. M.; Warner, I. M.: Synthesis and characterization of novel chiral ionic liquids and investigation of their enantiomeric recognition properties. *Chirality* **2008**, *20*, 151-158.

(30) Earle, M. J.; Gordon, C. M.; Plechkova, N. V.; Seddon, K. R.; Welton, T.: Decolorization of ionic liquids for spectroscopy. *Analytical chemistry* **2007**, *79*, 758-64.

(31) Kasai, H. K., H.; Okada, S.; Oikawa, H.; Mastuda, H.; Nakanishi, H.: Size-Dependent Colors and Luminescences of Organic Microcrystals. *Jpn. J. Appl. Phys.* **1996**, *35*, L221–223.

(32) Das, S.; Bwambok, D.; El-Zahab, B.; Monk, J.; de Rooy, S. L.; Challa, S.; Li, M.; Hung, F. R.; Baker, G. A.; Warner, I. M.: Nontemplated approach to tuning the spectral properties of cyanine-based fluorescent nanoGUMBOS. *Langmuir : the ACS journal of surfaces and colloids* **2010**, *26*, 12867-76.

(33) Das, S.; de Rooy, S. L.; Jordan, A. N.; Chandler, L.; Negulescu, II; El-Zahab, B.; Warner, I. M.: Tunable Size and Spectral Properties of Fluorescent NanoGUMBOS in Modified Sodium Deoxycholate Hydrogels. *Langmuir* **2012**, *28*, 757-765.

(34) Ishida, H.; Tobita, S.; Hasegawa, Y.; Katoh, R.; Nozaki, K.: Recent advances in instrumentation for absolute emission quantum yield measurements. *Coordination Chemistry Reviews* **2010**, *254*, 2449-2458.

(35) Wang, E.; Zhu, L.; Ma, L.; Patel, H.: Optical sensors for sodium, potassium and ammonium ions based on lipophilic fluorescein anionic dye and neutral carriers. *Analytica Chimica Acta* **1997**, *357*, 85-90.

(36) Sanderson, W. M.; Johnson, R. D.: Spectroscopic behavior of fluorescein as a constituent anion in a phosphonium-based ionic liquid material. *Materials Chemistry and Physics* **2012**, *132*, 239-243.

(37) Kasai, H.; Kamatani, H.; Okada, S.; Oikawa, H.; Matsuda, H.; Nakanishi, H.: Size-Dependent Colors and Luminescences of Organic Microcrystals. *Jpn. J. Appl. Phys.* **1996**, *35*, L221-L223.

(38) Daehne, L.: Self-Organization of Polymethine Dyes in Thin Solid Layers. *Journal of the American Chemical Society* **1995**, *117*, 12855-12860.

(39) Jelley, E. E.: Spectral Absorption and Fluorescence of Dyes in the Molecular State. *Nature (London)* **1936**, *138*, 1009-1010.

(40) Kasha, M. R., H. R.; Ashraf El-Bayoumi: The exciton model in molecular spectroscopy. *Pure Appl. Chem.* **1965**, *11*, 371-392.

(41) Zheng, J. Y.; Zhang, C.; Zhao, Y. S.; Yao, J.: Detection of chemical vapors with tunable emission of binary organic nanobelts. *Physical Chemistry Chemical Physics* **2010**, *12*, 12935-12938.

CHAPTER 4: VIRTUAL COLORIMETRIC SENSOR ARRAY: SINGLE IONIC LIQUID FOR SOLVENT DISCRIMINATION[‡]

4.1. Introduction

Organic solvents have been widely used for both industrial applications and academic research. As a result of such ubiquitous use and the environmental impact of these compounds, detection and identification of organic solvents and their complex mixtures remains an area of intense interest. However, accurate discrimination of chemically and structurally similar solvents and solvent mixtures is inherently challenging. Traditional analytical techniques such as gas chromatography/mass spectrometry (GC/MS) are powerful tools for such applications. However, most of these tools tend to be labor intensive and often require expensive instrumentation. Thus, there has been a recent upsurge of interest towards development of facile and low-cost techniques such as colorimetric sensors for discrimination of organic solvents.[1-7] Many colorimetric sensor elements integrate solvatochromic materials with organic[8-13] or metal-organic[14-17] backbones for discrimination of closely related solvents. These sensors typically provide rapid sensor information with a high degree of sensitivity. However, conventional solvatochromic pigments are designed to display absorption and emission peak shifts primarily as a function of polarity of the chemical environment.[18,19] While these materials are quite promising for accurate discrimination of analytes with reasonable polarity differences, discrimination of a group of closely related solvents, or solvent mixtures with subtle differences in polarities, presents an unresolved challenge in the analytical sciences.[1,19]

[‡] This Chapter previously appeared as Galpothdeniya, W. I.; Regmi, B. P.; McCarter, K. S.; de Rooy, S. L.; Siraj, N.; Warner, I. M.: Virtual Colorimetric Sensor Array: Single Ionic Liquid for Solvent Discrimination. *Analytical Chemistry*, **2015,** *87*, 4464–4471. It is reproduced by permission of the Americal Chemical Society.
http://pubs.acs.org/doi/abs/10.1021/acs.analchem.5b00714

In order to discriminate between closely related analytes, the concept of sensor arrays has been introduced, and in this regard colorimetric sensor arrays have remained at the forefront of measurement science.[20-22] Colorimetric sensor arrays are defined as assemblies of cross-reactive colorimetric sensor elements, which are designed to discriminately respond to different analytes.[23] When such sensor arrays are designed for gas-phase sensing applications, they are defined as electronic noses. In contrast, those designed for liquid-phase sensing are sometimes termed electronic tongues.[24,25] There are two key advantages of employing sensor arrays over individual sensor elements: 1) array-based sensors improve resolving power, which in turn increases with increasing number of sensor elements[26] and 2) multiple measurements by use of several sensors and subsequent analyses of data or data patterns using suitable statistical models vastly improves accuracy and reproducibility of the analytical measurements. In addition, it has been observed that the resolving power of sensor arrays depends on the orthogonality of sensor responses.[26,27] Despite these considerable advantages, there are defined limitations that impede widespread use of sensor arrays for discrimination of analytes. Specifically, traditional colorimetric sensor arrays will typically require a large number of sensor elements that depend on the types and number of analytes to be sensed.[28] Therefore, fabrication of such sensor arrays is often expensive and time consuming. In addition, finding a compatible matrix or substrate for immobilization of dyes can be quite challenging. In liquid-based applications, leaching of dyes into an analyte liquid also poses design difficulties.[29,30]

Herein, we outline the use of a single ionic liquid (IL) for development of a virtual colorimetric sensor array to be used for accurate discrimination of closely related organic solvents and solvent mixtures. To provide a stringent test for this proposed sensor array, a group of chemically and structurally similar alcohols and alcohol mixtures are selected as analytes. In

addition, discrimination of alcohols and alcohol mixtures is tremendously important for numerous applications in chemistry, biology, industry, and medicine.[31,32] For example, ethanol and methanol have increasingly become alternative liquid fuel additives to fossil fuels, primarily due to low cost and reduced environmental effects of these additives.[33]

Ionic liquids (ILs) are classically defined as organic salts with melting points below 100 °C. It has been demonstrated that the properties of these compounds can be easily tuned by simply varying the counter cation or anion.[34] As a result of this ease of synthesis and tunable physicochemical properties, ILs have attracted considerable attention for development of chemical sensors.[35-44] In fact, we have recently introduced one such approach where we employed the concept of indicator dye-based ILs for fabrication of colorimetric sensor arrays for chemical detection.[35]

In the studies outlined here, a unique and efficient virtual colorimetric sensor array system is reported which employs a single IL, *i.e.*, di-trihexyl(tetradecyl)phosphonium bromothymol blue ($[P_{66614}]_2$[BTB]). Traditional solvatochromic pigments often involve multiple complex chemical reactions which ultimately produce low product yields. In contrast, synthesis of $[P_{66614}]_2$[BTB] is an extremely simple, one step ion-exchange reaction with greater than 95% product yield, and a single byproduct of NaCl which can be easily removed by water washing. The UV-visible spectra of $[P_{66614}]_2$[BTB] in different organic solvents reveals two absorption bands that correspond to the monoprotonated and deprotonated forms of bromothymol blue (BTB). It is important to note that these two bands are observed only in the IL form, while the free BTB displays only one band in organic solvents. Interestingly, the ratio of these two absorption bands is found to depend on the concentration of $[P_{66614}]_2$[BTB] and the type of solvent. Therefore, by employing different concentrations of this IL in various solvents and

treating the peak ratios as individual sensor responses, a characteristic pattern can be obtained for each analyte. Thus, by use of four different concentrations of $[P_{66614}]_2[BTB]$, a new concept of fabricating sensor arrays is produced.

In this study, eight closely related alcohols and seven binary mixtures of methanol and ethanol are tested as analytes for evaluating the performance of this sensor array. The peak ratios obtained at different concentrations of $[P_{66614}]_2[BTB]$ are analyzed by use of principal component analysis (PCA) and linear discriminant analysis (LDA). The cross-validated accuracy of the sensor is found to be 96.4% for differentiation of pure alcohols, and 100% for differentiation of various methanol-ethanol mixtures. It is further demonstrated that a single sensor is capable of discriminating between many different analytes. Overall, the present study demonstrates that $[P_{66614}]_2[BTB]$ is a promising material for accurate differentiation of a wide range of closely related organic solvents.

4.2. Experimental Section

4.2.1. Materials

Bromothymol blue, *i.e.*, protonated form (BTB), sodium hydroxide (NaOH) trihexyl(tetradecyl)phosphonium chloride ($[P_{66614}]_2[Cl]$) (≥ 95%), and anhydrous alcohols (ethanol (200 proof, 99.5%), methanol (99.8%), 1-propanol (99.7%), 2-propanol (99.5), 1-butanol (99.8%), 2-butanol (99.5%), and isobutanol (99.5%)) were purchased from Sigma-Aldrich, and used as received.

4.2.2. Synthesis and Characterization of IL

The synthesis and characterization of pH indicator based ILs including $[P_{66614}]_2$[BTB] has been recently reported by our group.[35] First, BTB was dissolved in water (Triply deionized, 18.2 MΩ cm) and neutralized using an excess of NaOH to produce the disodium salt of BTB. [P66614]2[Cl] was dissolved in methylene chloride (DCM). Afterwards, the disodium salt of BTB and [P66614]2[Cl] were mixed in water-DCM (5: 1 v/v) mixture at a molar ratio of 1.5: 2, and stirred for 48 h (After stirring both layers should be dark blue). Then, the DCM layer was separated from the water layer and washed repeatedly with water in order to remove excess NaOH and NaCl byproduct. The product [P66614]2[BTB] was dried by removing the solvents in vacuo. The final product appeared to be a blue viscous liquid (yield 95%). Finally, the resultant IL was characterized by use of nuclear magnetic resonance (NMR), electron spray ionization mass spectroscopy (ESI-MS), and Fourier transform infrared spectroscopy (FTIR).

4.2.3. Preparation of IL Solutions

Stock solutions of 1 mM $[P_{66614}]_2$[BTB] were prepared by dissolving the IL in each alcohol or alcohol mixture. Then, four solutions of different concentrations (100, 200, 300, and 400 μM) of $[P_{66614}]_2$[BTB] were prepared by diluting the stock solution in the same alcohol or alcohol mixture, and UV-visible absorption was monitored. All solutions were handled in anhydrous conditions under a constant flow of N_2 gas.

4.2.4. Absorption Studies

Absorbance measurements were obtained using a Shimadzu UV-3101PC spectrophotometer. A 0.1 cm (1 mm) path length quartz cuvette (Precision Cells) was used to collect absorption spectra.

4.2.5. Development of Predictive Models

Two experiments were employed in this study, both involving the development of predictive models to distinguish among a set of analytes. The experiments were similar in design and execution, and therefore, the same approach was used for data analyses in each experiment. Our first experiment involved eight analytes, while the second experiment involved examination of seven analytes. For each analyte, seven replicate samples were analyzed, producing a total sample size of 56 and 49 observations for the first and second experiment. A multivariate response consisting of four peak ratios was measured for each sample, one peak ratio response variable for each of the four concentrations used in the sensor array. Principal component analysis (PCA) was used to reduce the dimensionality of the predictor space prior to development of a predictive model. In each experiment, the first principal component accounted for a large proportion of the variability in the four peak ratio responses ($\geq$ 95%), and two principal components accounted for approximately 99%. Hence, a useful reduction in the dimensionality of the predictor space was accomplished for each experiment by use of PCA.

The computed principal components were used as input variables in developing the predictive models to distinguish analytes. Linear discriminant analysis was used in developing the predictive models. Data were evaluated separately for each experiment, and in each case formal tests indicated the necessity of linear discriminant analysis. After development of predictive models, each model was evaluated for predictive accuracy. The cross-validation method was used to assess predictive accuracy.

4.3. Results and Discussion

4.3.1. Characterization of Spectral Properties of $[P_{66614}]_2$[BTB]

To provide a more efficient colorimetric sensor array system for accurate discrimination of chemically and structurally similar solvents, we have created a virtual sensor array employing a single IL, *i.e.*, $[P_{66614}]_2$[BTB]. This IL was synthesized by modifying a commercially available pH indicator dye, bromothymol blue (BTB), which is also known as 3′,3″-dibromothymolsulfonephthalein. The dissociation of BTB can be described as shown in Scheme 4.1. The biprotonated (H_2R) form of BTB is neutral and successively dissociates in two steps to give the monoprotonated (HR^-) form and deprotonated (R^{2-}) form. HR^- is yellow, whereas R^{2-} is blue. The pK_1 is reported to be less than 2, while the reported value of pK_2 is approximately 7.[45-49] In the present study, it is the second ionization that is critical for solvent discrimination. In the IL $[P_{66614}]_2$[BTB], the $[P_{66614}]^+$ ion, which has often been termed a 'universal liquifier', was used as the counter cation.[37,50] This cation has been shown to convert high melting solids into viscous liquids or low melting solids. The chemical structure of the IL synthesized for this study is given in Scheme 4.2.

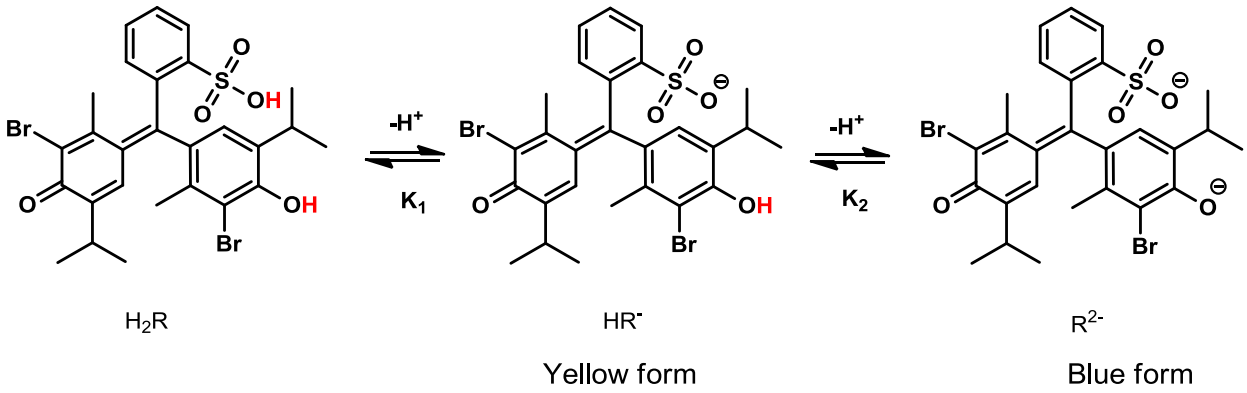

Scheme 4.1. The dissociation of BTB

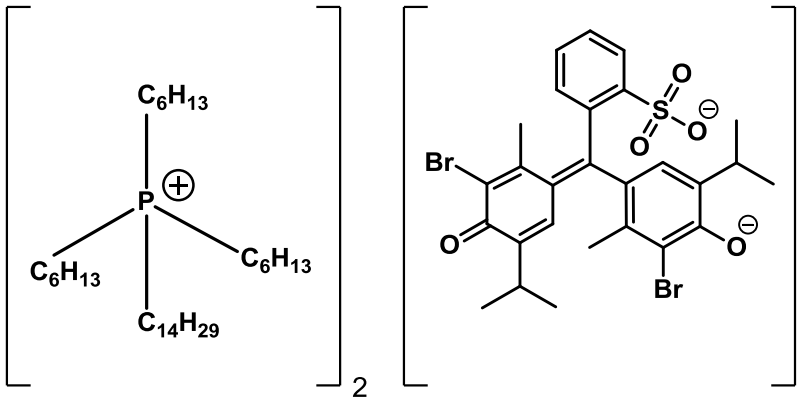

Scheme 4.2 Chemical structure of $[P_{66614}]_2$[BTB] used in this study

The majority of colorimetric sensors used for solvent detection are based on solvatochromic dyes. Solvatochromic dyes change colors as a function of the polarity of the chemical environment. Solvents, depending on polarity, tend to change the energy gap between the ground and excited states of a dye molecule due to differential stabilization. A change in energy gap results in a spectral shift, which typically results in a color change. There are two primary types of spectral shifts: 1) a hypsochromic shift (blue shift) with increasing solvent polarity also known as negative solvatochromism and 2) a bathochromic shift (red shift) with increasing solvent polarity commonly known as positive solvatochromism. From an analytical point of view, pigments that achieve large spectral shifts due to small polarity changes are more desirable for solvent discrimination.

The normalized absorption spectra of 200 µM $[P_{66614}]_2$[BTB] in two different solvents, (methanol and 2-butanol), are provided in Figure 4.1a. It is evident from this figure that the absorption spectrum of the IL is characterized by two absorption bands. These two absorptions bands, with absorption maxima at ~630 and ~410 nm, are characteristics of BTB.[51] The component absorbing at ~630 nm is attributed to the deprotonated (R^{2-}) form, which is blue in

Figure 4.1. (A) Normalized absorption spectra of 200 μM $[P_{66614}]_2$[BTB], and (B) 200 μM free BTB in methanol in methanol (red) and 2-butanol (blue). Inset shows the visual appearance of 200 μM $[P_{66614}]_2$[BTB] in methanol and 2-butanol. Alcohol dependent color changes for (C) 200 μM $[P_{66614}]_2$[BTB] and (D) 200 μM free BTB in methanol, and 2-butanol. (I – Methanol, II – 2-butanol) (continues through pages 111-113)

(A)

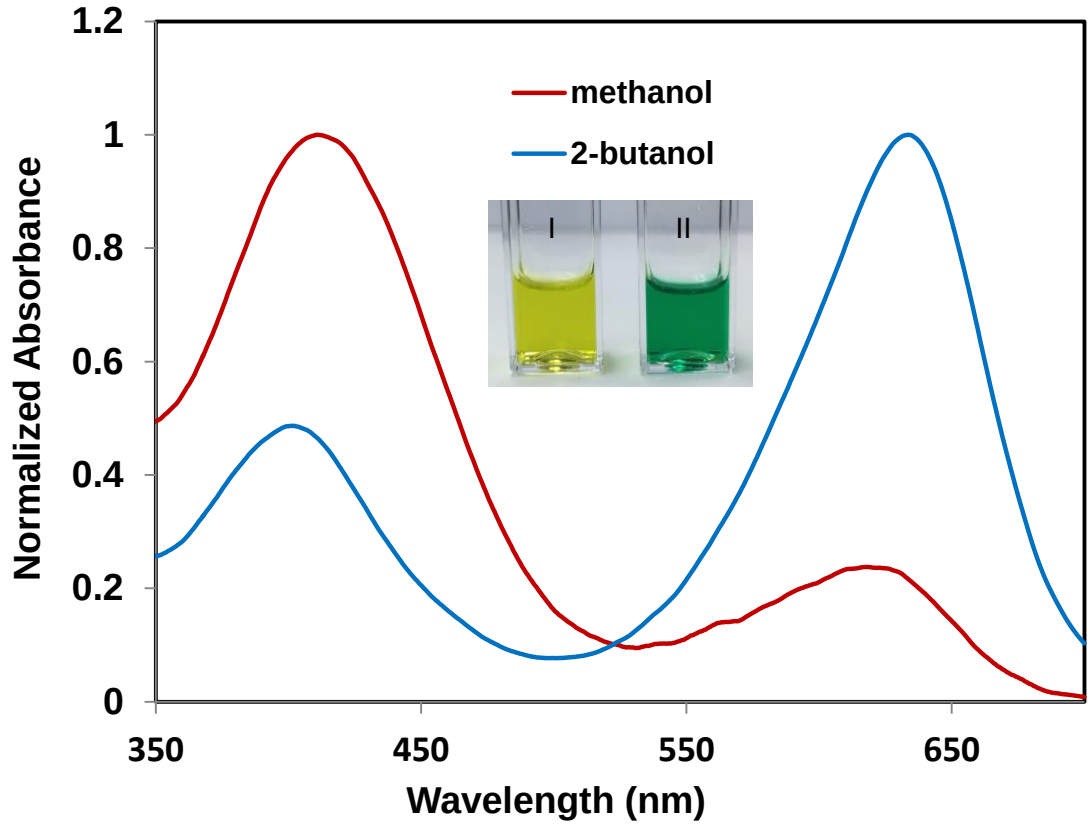
1.2
1
0.8
0.6
0.4
0.2
0
Normalized Absorbance
methanol
2-butanol
I
II
350
450
550
650
Wavelength (nm)

(B)

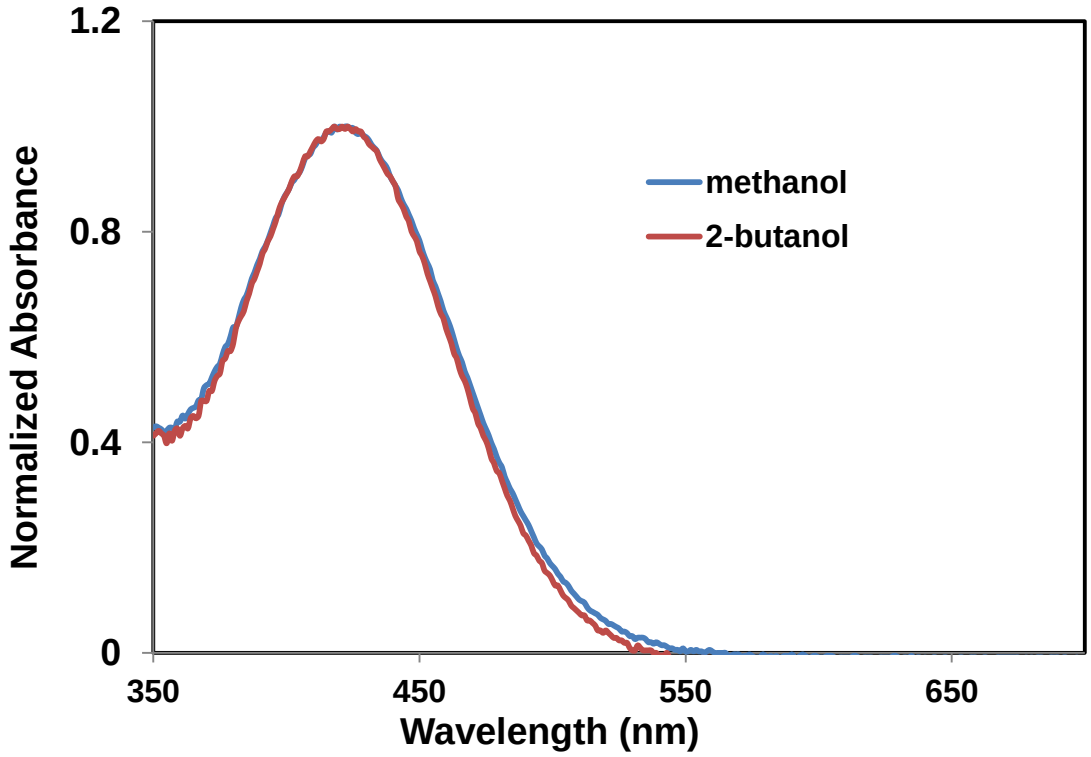
1.2
0.8
0.4
0
Normalized Absorbance
methanol
2-butanol
350
450
550
650
Wavelength (nm)

(C)

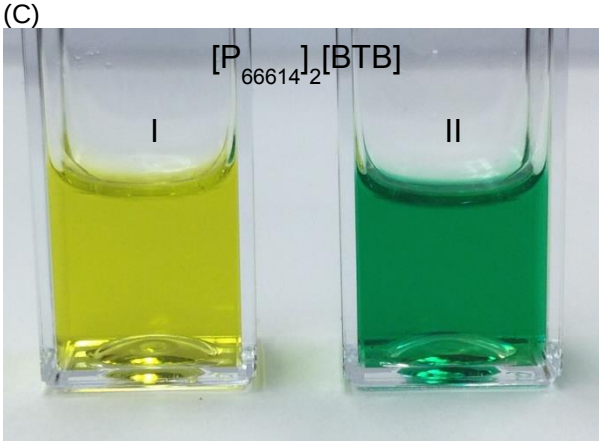

(D)

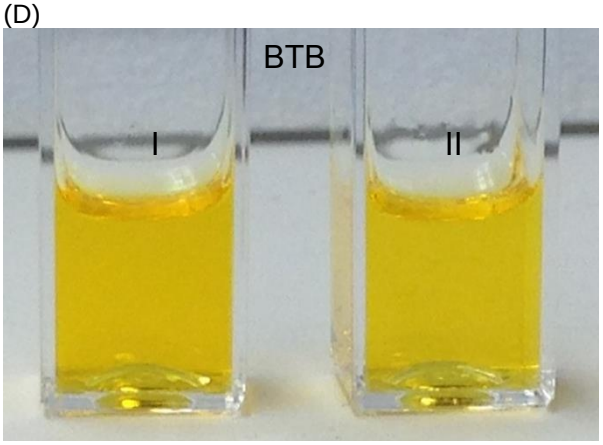

color, while the hypsochromically shifted component absorbing at ~410 nm is attributed to the monoprotonated (HR^-) form, which is yellow in color. In other words, the absorption maxima at ~630 and ~410 nm are attributed to the basic and acidic forms of the second ionization of BTB, respectively. In methanol, the first absorption band has a maximum ($\lambda_{1\,max}$) at 618 nm, whereas the second absorption band maximum ($\lambda_{2\,max}$) is at 410 nm. However, compared to methanol, the two absorption bands of $[P_{66614}]_2$[BTB] show a shift in 2-butanol. In 2-butanol, $\lambda_{1\,max}$ is at 633 nm, whereas $\lambda_{2\,max}$ is at 401 nm. Therefore, $\lambda_{1\,max}$ is bathochromically shifted by 15 nm (negative solvatochromism) and $\lambda_{2\,max}$ is hypsochromically shifted by 9 nm (positive solvatochromism) in 2-butanol as compared to methanol. These wavelength shifts observed for $\lambda_{1\,max}$ and $\lambda_{2\,max}$ are quite typical for a traditional solvatochromic dye. Therefore, discrimination of a group of similar alcohols by use of only these wavelength shifts is challenging. However, we have also observed a very interesting scenario upon close examination of Figure 4.1a, and this observation appears to also be very useful for solvent discrimination. There is a substantial difference in peak ratios ($\lambda_{1\,max}/\lambda_{2\,max}$) between these two alcohols. It is clear that, the relative intensities of the two peaks are inverted for the two alcohols. In other

words, the concentration ratio of $^{R^{2-}}/_{HR^-}$ is lower in methanol as compared to 2-butanol as the solvent. The $^{\lambda_{1\,max}}/_{\lambda_{2\,max}}$ peak ratio in methanol was found to be 0.24 ± 0.01, and the ratio was observed to be 2.04 ± 0.04 in 2-butanol. The absorption peak ratio in 2-butanol is approximately nine times greater than that in methanol. This vast difference in peak ratios qualifies $[P_{66614}]_2$[BTB] as an excellent colorimetric probe for discrimination of closely related alcohols and alcohol mixtures.

Alcohol dependent color changes of 200 μM $[P_{66614}]_2$[BTB] and free BTB are given in Figures 4.1b and c respectively. In the following discussions, the words 'free BTB' are used to designate the biprotonated from of BTB. There is a considerable difference in color of the IL in methanol as compared to that in 2-butanol. In the presence of the IL, methanol is greenish-yellow in color, whereas 2-butanol is a bluish-green in color (Figure 4.1c). This substantial difference in colors is sufficient for unaided eye discrimination between methanol and 2-butanol. However, in the presence of the starting material, namely free BTB, the alcohol solutions showed essentially no difference in color (Figure 4.1d). In addition, the normalized absorption spectra of 200 μM free BTB in methanol, as well as in 2-butanol show only a single absorption band with an absorption maximum at ~410 nm (Figure 4.1b). Furthermore, there is a minimal shift in the absorption maximum of free BTB in the presence of these two solvents. Therefore, it is evident that free BTB is not a suitable sensing material for discrimination of alcohols such as methanol and 2-butanol. From an analytical viewpoint, the unique ratiometric absorption signal ($^{\lambda_{1\,max}}/_{\lambda_{2\,max}}$) observed for $[P_{66614}]_2$[BTB] as compared to that of free BTB, makes the IL an ideal material for discrimination of organic solvents.

4.3.2. Discrimination of an Extended Set of Closely Related Pure Alcohols

After demonstrating that our IL can easily discriminate between methanol and 2-butanol, we examined possible discrimination of an extended set of alcohols. For this purpose, we have selected eight closely related alcohols, all of which are listed in the order of increasing polarity in Table 4.1. The solvent polarities in this table are produced by use of Reichardt's normalized $E_T(30)$ solvent polarity parameter (E_T^N).[18,19] It is noted that the higher the E_T^N value, the higher will be the polarity and *vice versa*. These eight alcohols are chemically and structurally very similar, and include two pairs of skeletal isomers and two pairs of positional isomers. Preliminary studies on discrimination of these eight alcohols were performed by using 200 µM $[P_{66614}]_2$[BTB] (Figures 4.2a and c). Figure 4.2a is a photograph of the IL dissolved in eight different alcohols. As noted in the figure, there is a gradual change in the color of the IL solutions from bluish-green to greenish-yellow with increasing alcohol polarity. In contrast to the IL solutions, in the presence of starting material, i.e. free BTB, eight alcohol solutions showed essentially no difference in color (Figure 4.2b).

Table 4.1 Variation of absorption peak ratio of 200 µM $[P_{66614}]_2$[BTB] in eight alcohols

Alcohol	E_T^{N*}	$^{630}/_{410}$
2-butanol	0.506	2.08 ± 0.03
1-octanol	0.537	1.57 ± 0.03
2-propanol	0.546	1.82 ± 0.01
Isobutanol	0.552	1.53 ± 0.04
1-butanol	0.586	1.08 ± 0.03
1-propanol	0.617	0.78 ± 0.01
Ethanol	0.654	0.54 ± 0.01
Methanol	0.762	0.23 ± 0.01

* E_T^N refers to normalized $E_T(30)$ solvent polarity parameter (Reichardt's) (see refs 18 and 19)

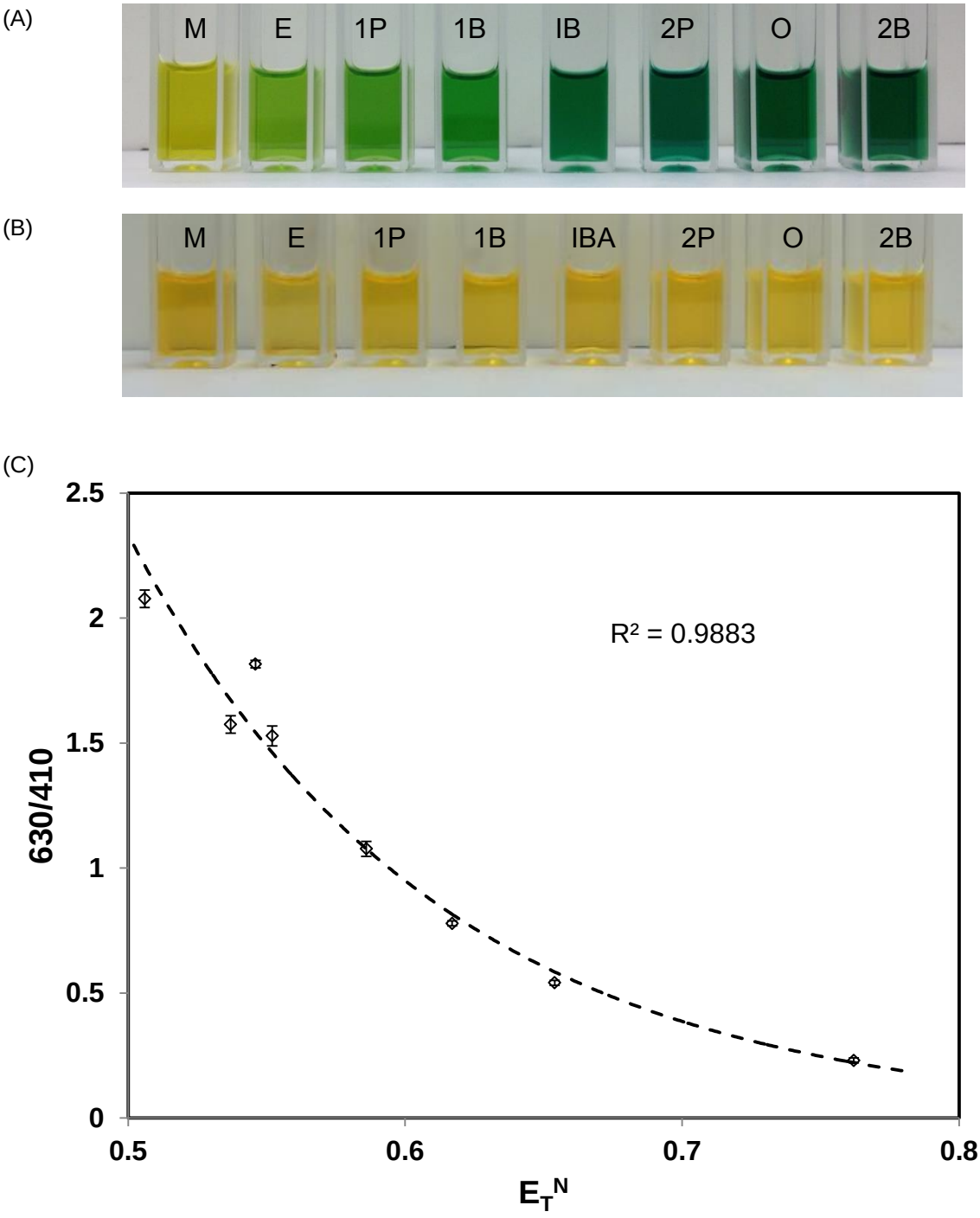

Figure 4.2. (A) Photograph showing alcohol dependent color changes for 200 µM $[P_{66614}]_2$[BTB] and (B) 200 µM free BTB in eight alcohols (M – methanol, E – ethanol, 1P – 1-propanol, 1B – 1-butanol, IBA – isobutanol, 2P – 2-propanol O – 1-octanol, and 2B – 2-butanol). (C) Absorption peak ratio ($^{630}/_{410}$) vs normalized $E_T(30)$ solvent polarity parameter (E_T^N). This provides the relationship between absorption signal and solvent polarity

It should be noted that the shifts in peak positions are small. Specifically, the largest shifts in $\lambda_{1\,max}$ and $\lambda_{2\,max}$ were observed in 2-butanol as compared to methanol. Given the fact that these shifts are even smaller in other alcohols, we simplified our approach by taking the absorption ratio $^{630}/_{410}$ to discriminate the analytes by assuming that the error occurred by taking this ratio rather than the exact absorption peak ratio ($^{\lambda_{1\,max}}/_{\lambda_{2\,max}}$) is insignificant.

The $^{630}/_{410}$ absorption ratio for $[P_{66614}]_2[BTB]$ in different alcohols are listed also in Table 4.1. Moreover, a plot of $^{630}/_{410}$ versus E_T^N of the alcohols is found to have an exponential relationship with r^2 of 0.988 (Figure 4.2c). From Table 4.1 and Figure 4.2c, it is evident that there is a substantial decrease in the $^{630}/_{410}$ absorption ratio with increasing solvent polarity. Therefore, the concentration ratio of $^{R^{2-}}/_{HR^-}$ is increased in the presence of less-polar alcohols. In other words, the concentration ratio of $^{R^{2-}}/_{HR^-}$ is decreased in more polar alcohols. From the foregoing discussions, we conclude that $[P_{66614}]_2[BTB]$ exhibits a polarity-dependent protonation and deprotonation in the presence of alcohols. In fact, solvent polarity-dependent protonation and deprotonation behavior has been previously described in the literature.[52-54]

A possible explanation for the above noted polarity-induced protonation-deprotonation process can be described as follows. The R^{2-} form (*i.e.* $[P_{66614}]_2[BTB]$) is more stable in less-polar alcohols than in more-polar alcohols possibly due to imparted hydrophobicity from the $[P_{66614}]^+$ cation. Alternatively, the HR^- form is more stable in highly polar alcohols. Therefore, the equilibrium constant (K_2) increases with decreased polarity of the solvent (K_2 in less-polar

alcohols > K_2 in highly polar alcohols). This results in a decrease in the $^{630}/_{410}$ absorption ratio with increasing solvent polarity. However, due to the very limited solubility of the R^{2-} in organic solvents, the observation of similar spectroscopic behavior is non-existent if the pH indicator dye, free BTB, is not paired with the [P_{66614}] ion.

Examination of the UV-Vis spectroscopic data reveals that the absorbance ratio at a fixed concentration of IL is sufficient to differentiate most of the analytes. In order to further differentiate more closely related analytes, the concept of sensor arrays was utilized. When compared to a single sensor, sensor arrays provide higher resolution which has proven to be extremely useful for discrimination of very similar compounds. In addition, sensor arrays allow a fingerprint signal for each analyte, which can be accurately identified by use of pattern recognition tools.

Fabrication of traditional colorimetric sensor arrays often involves immobilization of chemically responsive sensor elements onto a solid matrix. Immobilization techniques that are used to fabricate sensor arrays may decrease the discriminatory power of such sensor arrays primarily due to lack of homogeneity in the resulting sensor arrays.[55] Therefore, fabrication of highly reproducible colorimetric sensor arrays could be expensive due to high cost of printing techniques. Furthermore, typical colorimetric sensor array systems may require a large number of sensor elements that depend on the type of analysis and the number of analytes to be sensed.[28] For example, sensor arrays with as many as 36 sensor elements have been reported in the literature.[56] In addition to chemically responsive dyes, the performance of traditional colorimetric sensor arrays is influenced by the immobilization matrix employed or its morphology.[57] It has been demonstrated that colorimetric sensor arrays are typically affected by many environmental factors such as humidity, and a proper selection of solid support is critical

in this regard.[25,58,59] Therefore, finding a suitable matrix for immobilization of colorimetric pigments could be quite challenging. In addition, fabrication of optoelectronic tongues or colorimetric taster sensor arrays is inherently challenging primarily due to leaching of the dyes into analyte liquids.[29,30] From the foregoing discussions, it is evident that the development of colorimetric sensor array systems can be complicated, expensive, and time consuming in addition to requiring a large number of cross-reactive dyes.

In this study, this virtual sensor array was fabricated by use of four different concentrations of $[P_{66614}]_2$[BTB] (*i.e.* 100, 200, 300, and 500 µM) as individual sensor elements. In order to use different concentrations of a single IL as multiple sensor elements, each concentration must provide distinct peak patterns relative to each other. The appearance of discrete peak patterns mimics the presence of chemically different sensor elements. The UV-Vis absorption spectra for $[P_{66614}]_2$[BTB] in the presence of different alcohols are given in Figure 4.3 a-h. Examination of absorption spectra suggests that there is a decrease in absorbance with decreasing concentrations of $[P_{66614}]_2$[BTB]. In addition, the two absorption bands are present in each absorption spectrum with $\lambda_{1\,max}$ at ~630 nm and $\lambda_{2\,max}$ at ~410 nm. Moreover, the relative intensity of the two absorption peaks is dependent on the concentration of IL. A comparison of $^{630}/_{410}$ at different concentrations of the IL in various alcohols is given in Figure 4.4.

The error bars in Figure 4.4 represent the standard deviations of seven replicate measurements. At higher concentrations of $[P_{66614}]_2$[BTB], the $^{630}/_{410}$ ratio is higher and *vice versa*. Therefore, at higher concentrations of IL, the ratio of $^{R^{2-}}/_{HR^-}$ is increased, whereas the ration of $^{R^{2-}}/_{HR^-}$ is decreased at lower concentrations of IL. This phenomenon is very similar

Figure 4.3. UV-Vis absorption spectra of four different concentrations of $[P_{66614}]_2$[BTB] in seven alcohols (A: methanol, B: ethanol, C: 1-propanol, D: 1-butanol, E: isobutanol, F: 2-propanol, G: 2-butanol H: 1-octanol). Legend: concentration of $[P_{66614}]_2$[BTB] in alcohol (*i.e.* purple– 500 µM; green– 300 µM; red– 200 µM; blue– 100 µM) (Spectra were smoothened using Savitzky-Golay Principle) (continues through pages 120-124)

A

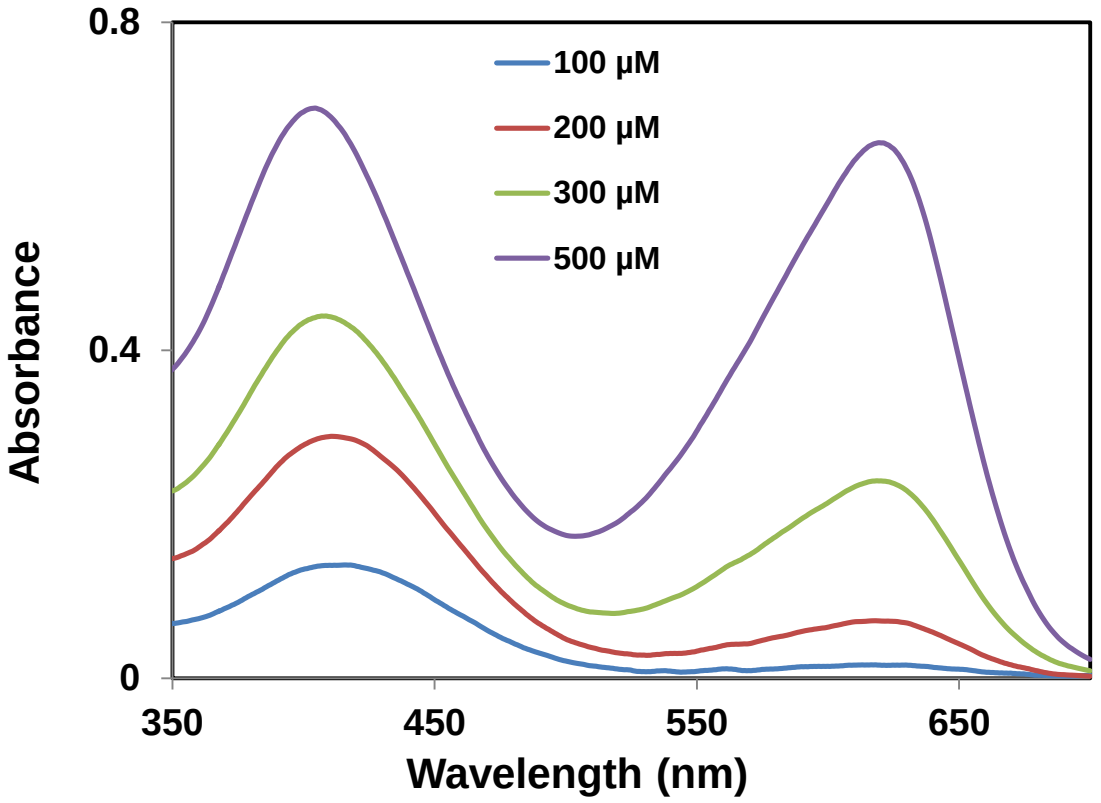
0.8
0.4
0
Absorbance
100 µM
200 µM
300 µM
500 µM
350
450
550
650
Wavelength (nm)

B

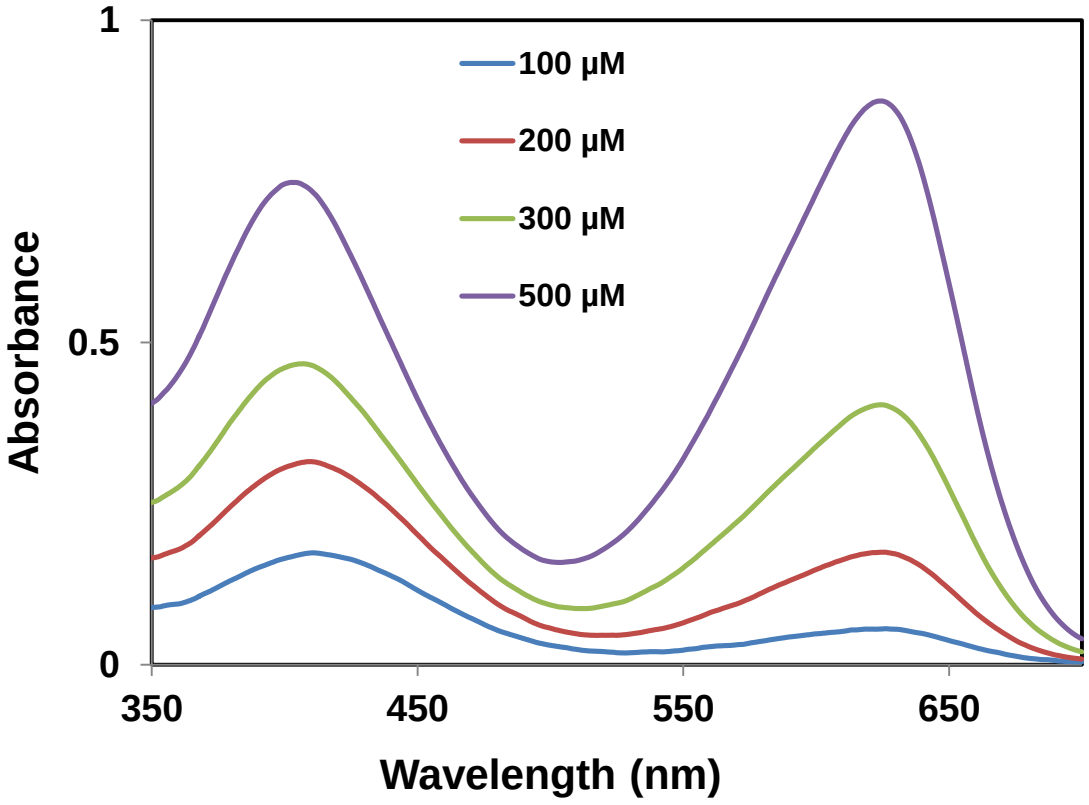
1
0.5
0
Absorbance
100 µM
200 µM
300 µM
500 µM
350
450
550
650
Wavelength (nm)

C

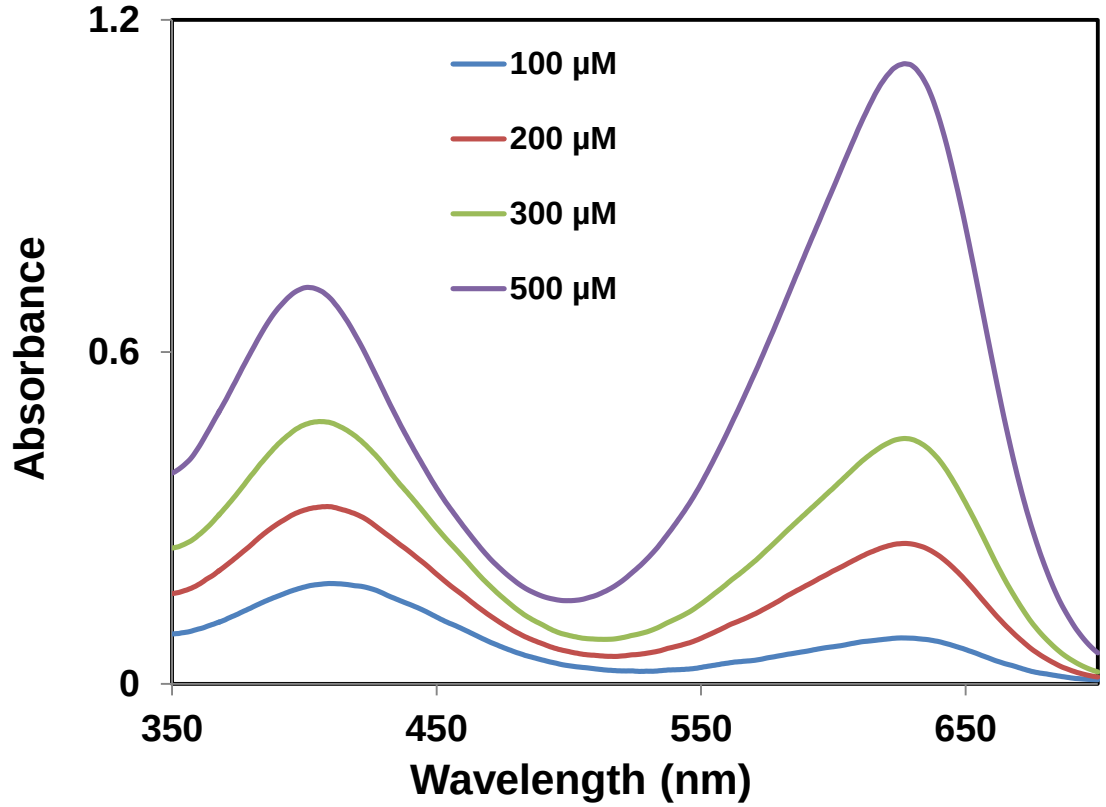
1.2
0.6
0
Absorbance
100 µM
200 µM
300 µM
500 µM
350
450
550
650
Wavelength (nm)

D

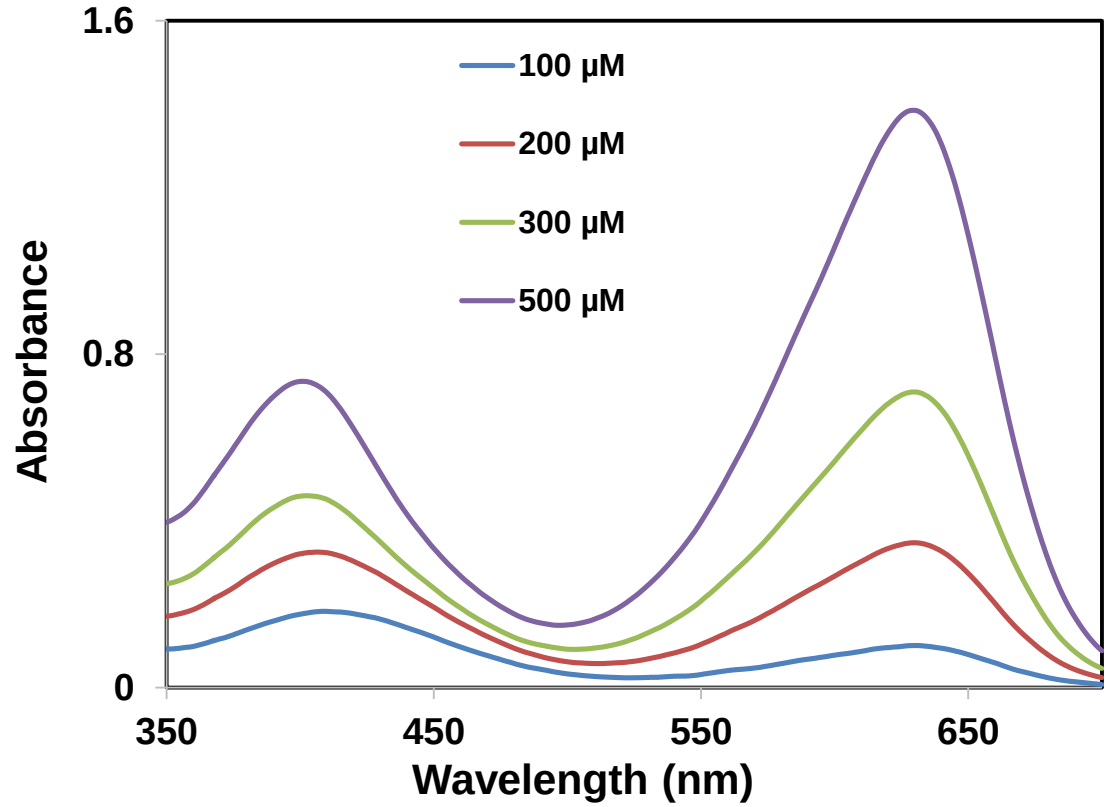
1.6
0.8
0
Absorbance
100 µM
200 µM
300 µM
500 µM
350
450
550
650
Wavelength (nm)

E

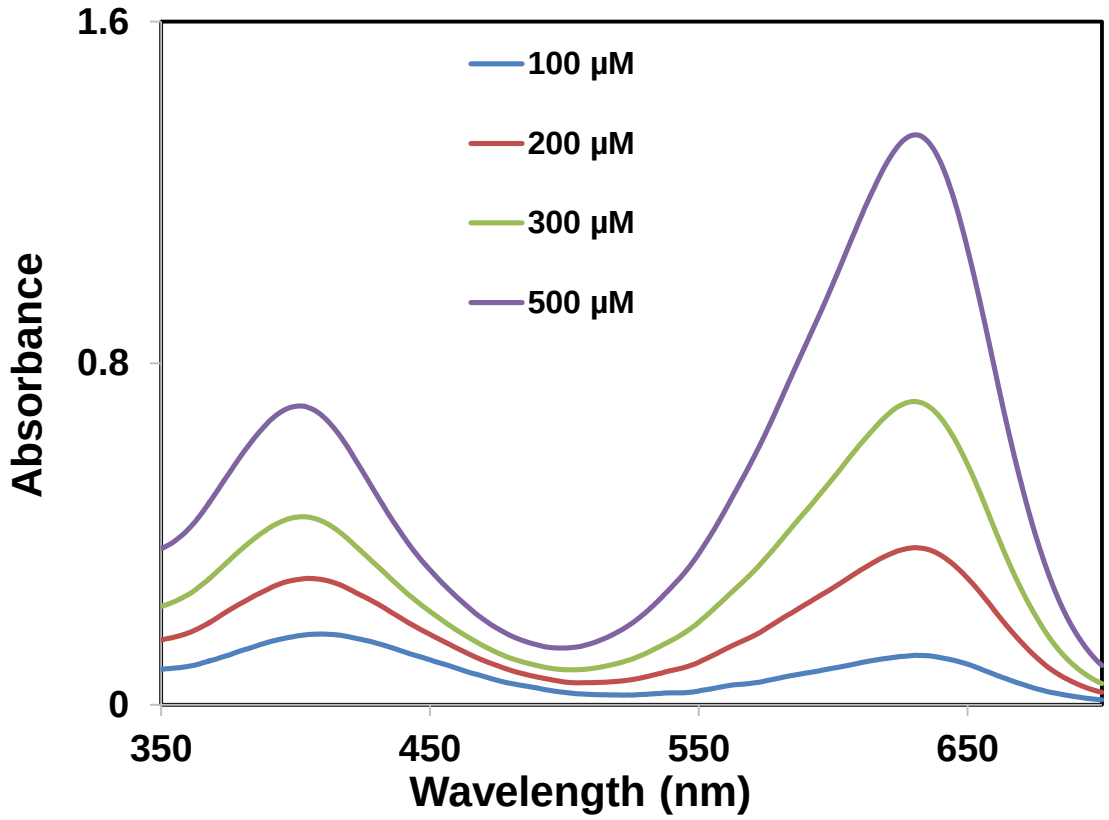
1.6
0.8
0
Absorbance
100 µM
200 µM
300 µM
500 µM
350
450
550
650
Wavelength (nm)

F

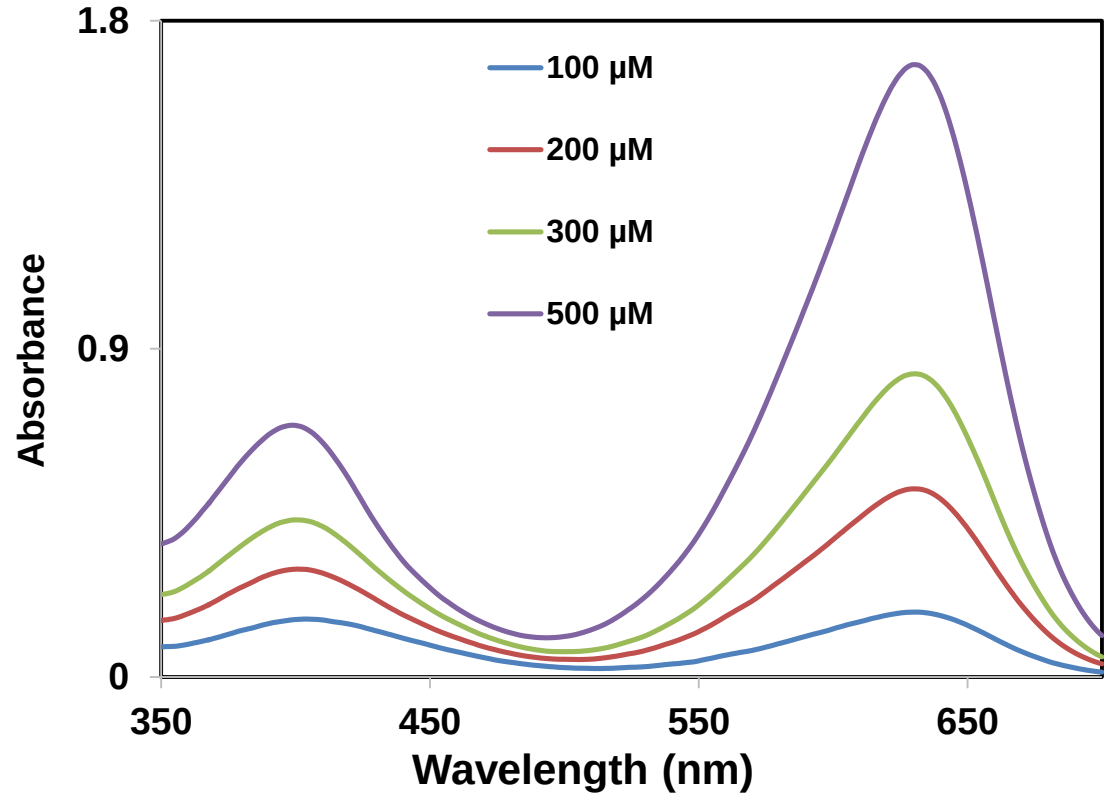
1.8
0.9
0
Absorbance
100 µM
200 µM
300 µM
500 µM
350
450
550
650
Wavelength (nm)

G

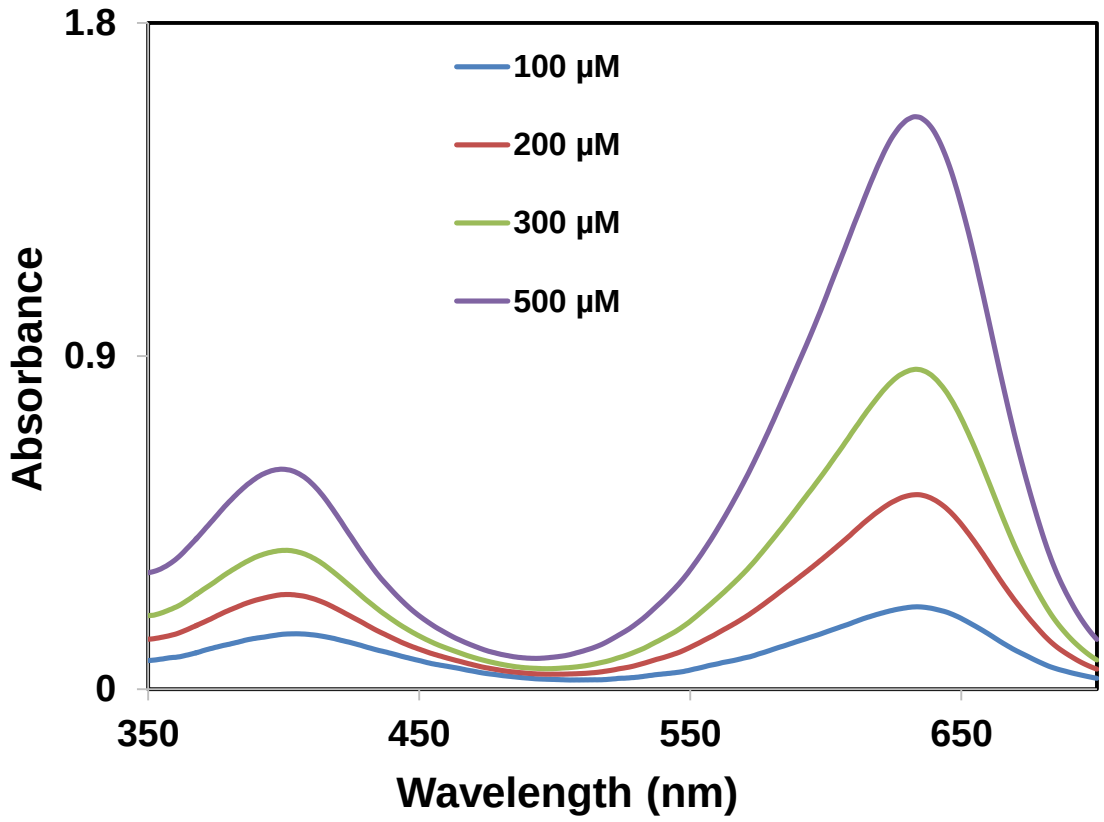
1.8
0.9
0
Absorbance
100 µM
200 µM
300 µM
500 µM
350
450
550
650
Wavelength (nm)

H

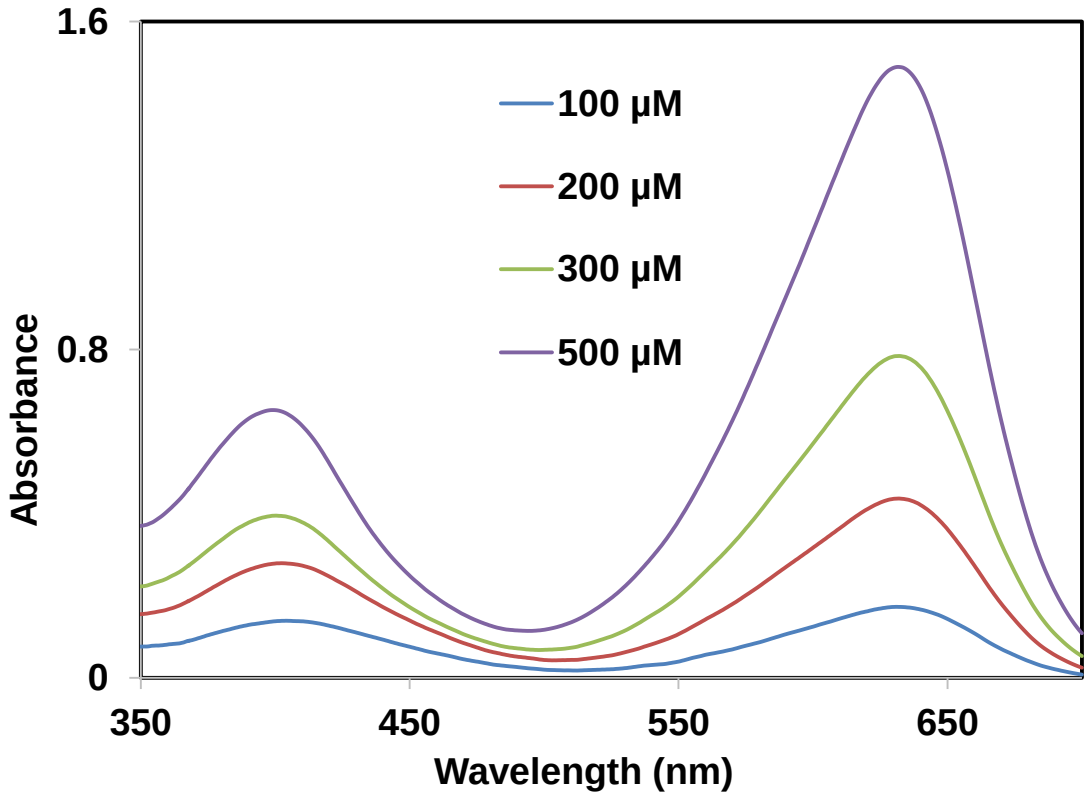
1.6
0.8
0
Absorbance
100 µM
200 µM
300 µM
500 µM
350
450
550
650
Wavelength (nm)

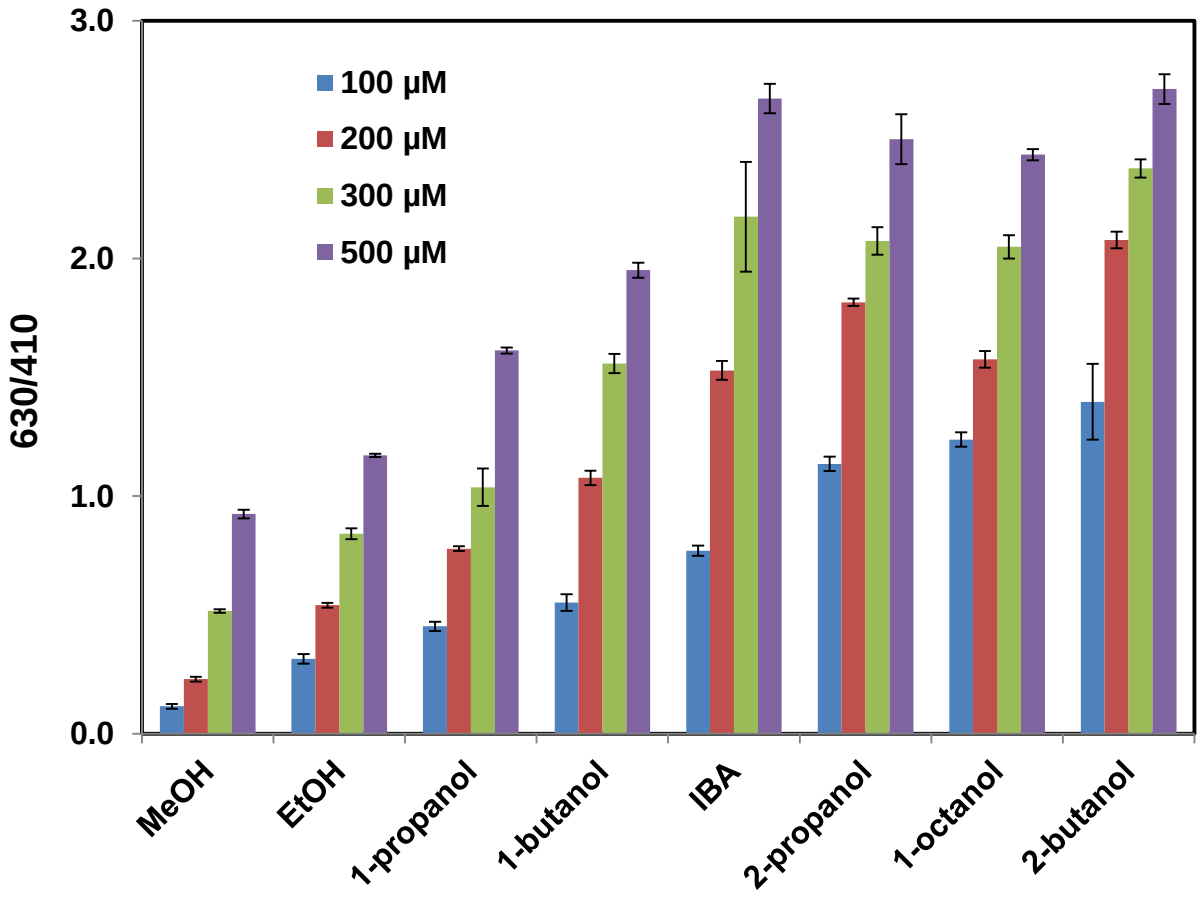

Figure 4.4. Absorption peak ratio ($^{630}/_{410}$) of various concentrations $[P_{66614}]_2[BTB]$ in eight different alcohols (Errors bars represent the standard deviations for seven replicate samples).

to polarity induced protonation with respect to alcohol polarity, and can be explained in a similar manner. Upon dilution of the IL with alcohol, the microenvironment of the IL becomes more-polar, creating a more favorable environment for HR^-, resulting in a decrease in the $^{630}/_{410}$ absorption ratio.

The $^{630}/_{410}$ ratios obtained from four concentrations of $[P_{66614}]_2[BTB]$ in the presence of eight alcohols were used in the development of predictive models. In Figure 4.5, the output data from PCA analysis of the eight alcohols (*i.e.* eight alcohols × seven replicates) are plotted

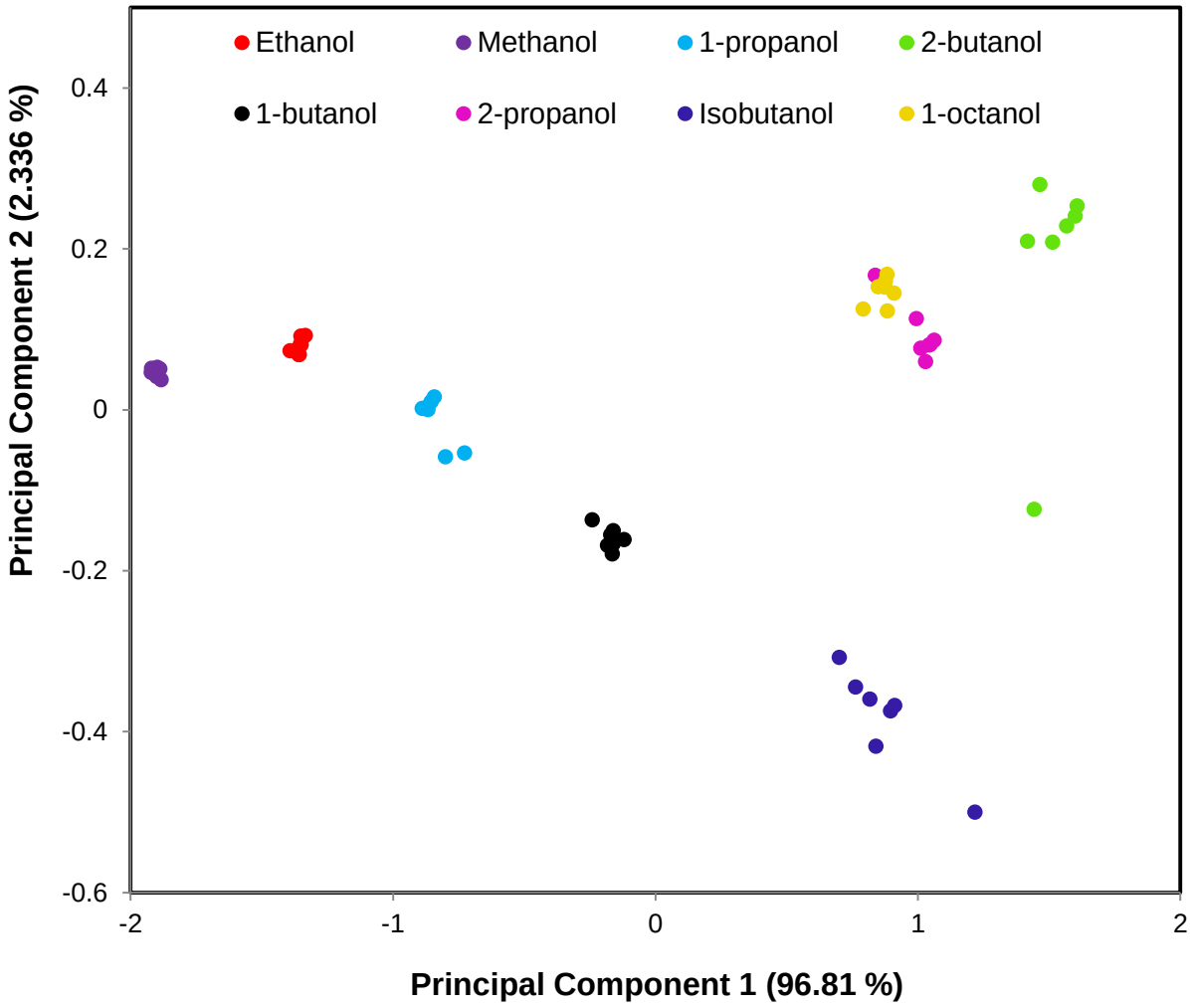

Figure 4.5. PCA score plot using the first two principal components based on the $^{630}/_{410}$ absorbance ratio of $[P_{66614}]_2$[BTB] in eight different alcohols.

with respect to their first two principal components. Each alcohol is found to form tight clusters with a substantial separation between each other. It is clear from Figure 4.5 that the first principal component provides very good visual separation between most of the groups with the exception of isobutanol, 1-octanol, and 2-propanol, which overlap along this dimension. However, these analytes show a clear separation along the second principal component. Therefore, two principal components were used in developing the predictive model to distinguish among the various

alcohols. The predictive accuracy of the resultant model was calculated by using LDA, and the cross-validation identification accuracy was found to be 96.4%. During this analysis, one 2-propanol measurement was misclassified as 1-octanol and one 2-butanol measurement was misclassified as 2-propanol. As mentioned before, in order to simplify the data analysis step, we used $^{630}/_{410}$ ratio instead of $^{\lambda_{1\,max}}/_{\lambda_{2\,max}}$. For comparison purposes, the Figure 4.2c, Figure 4.4 and Figure 4.5 were redone by use of exact peak ratios ($^{\lambda_{1\,max}}/_{\lambda_{2\,max}}$) and given in the Figures 4.6-4.8.

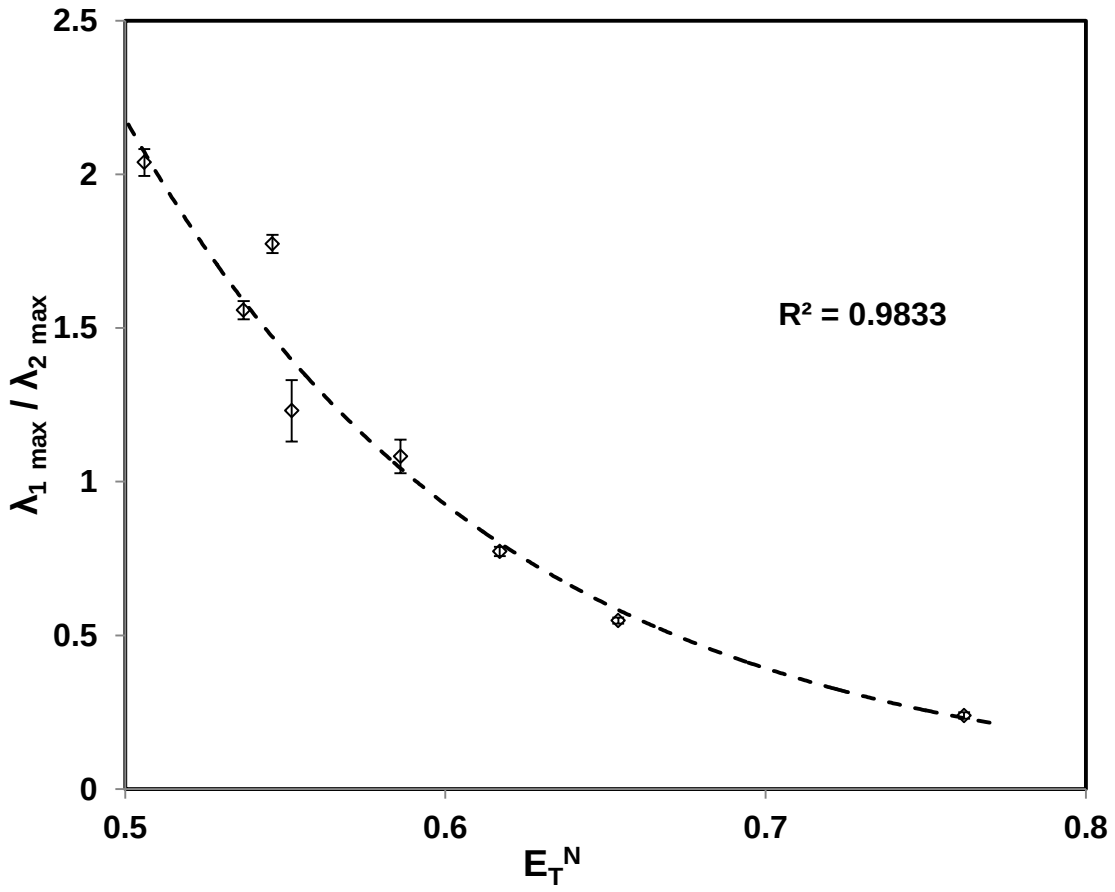

Figure 4.6. Absorption peak ratio ($^{\lambda_{1\,max}}/_{\lambda_{2\,max}}$) vs normalized $E_{\mathrm{T}}(30)$ solvent polarity parameter ($E_{\mathrm{T}}^{\mathrm{N}}$). This provides the relationship between absorption signal and solvent polarity

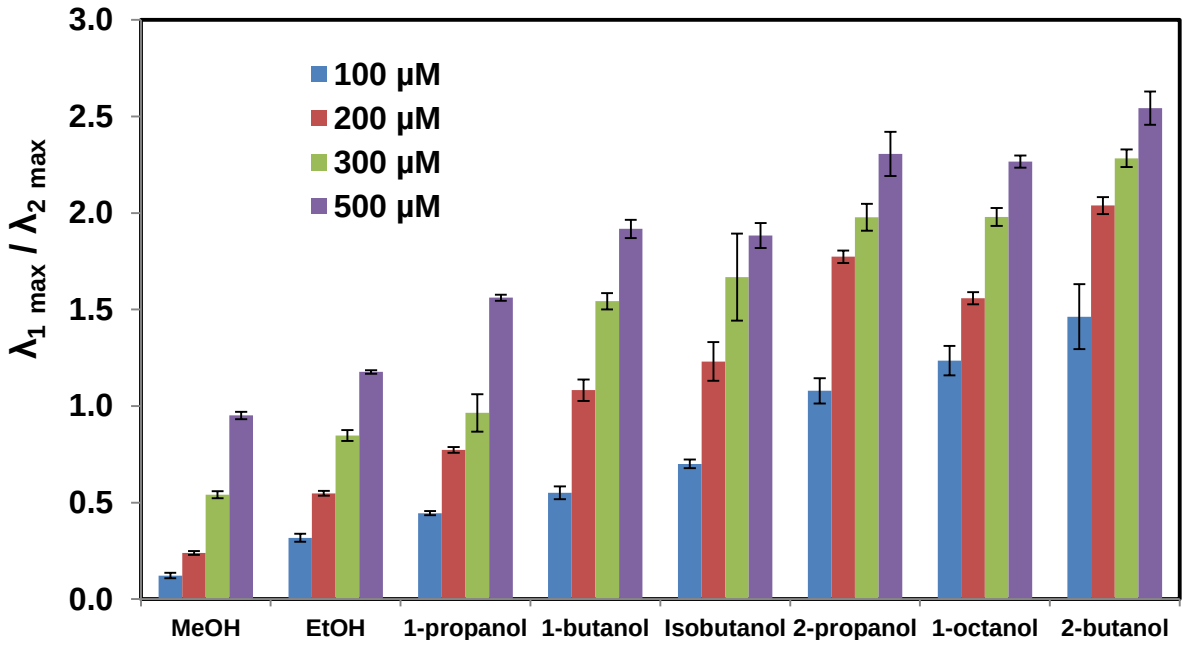

Figure 4.7. Absorption peak ratio ($^{\lambda_{1\,max}}/_{\lambda_{2\,max}}$) of various concentrations $[P_{66614}]_2[BTB]$ in eight different alcohols (Errors bars represent the standard deviations for seven replicate samples).

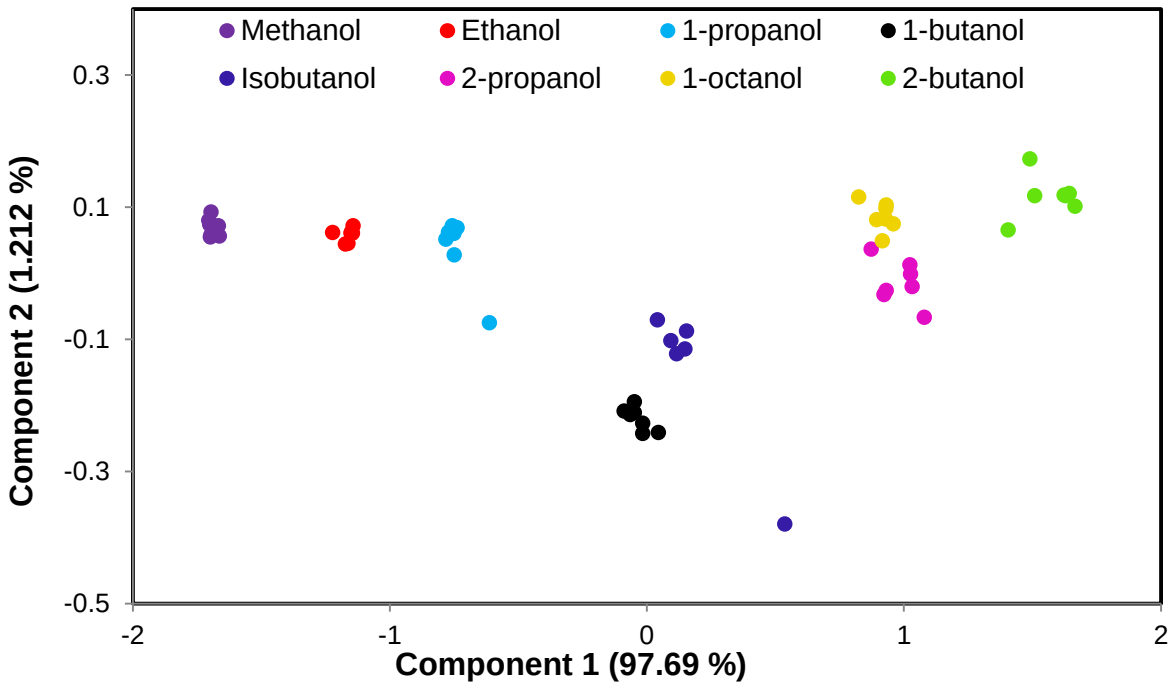

Figure 4.8. PCA score plot using the first two principal components based on the $^{\lambda_{1\,max}}/_{\lambda_{2\,max}}$ absorbance ratio of $[P_{66614}]_2[BTB]$ in eight different alcohols.

The virtual colorimetric sensor array approach outlined in this study has some notable advantages over traditional colorimetric sensor array approaches. Firstly, the use of multiple concentrations of a single sensor as multiple sensor elements instead of a number of chemically different sensor elements obviates the need for design and synthesis of a set of chemoresponsive dyes. In addition to requiring fewer dyes, this approach requires low amounts of the dyes, and therefore, fabrication of the sensor array is simple and inexpensive. In order to achieve high discriminatory power, traditional colorimetric sensor arrays typically require printing of sensor elements onto a solid matrix which is often expensive, complex, and time consuming. By use of our strategy, we have obtained very high discriminatory power through fabrication of a sensor array simply by dilution of $[P_{66614}]_2$[BTB] in analytical samples. Also, finding a suitable matrix is often problematic when fabricating typical optoelectronic sensor arrays.[35] However, our sensing strategy aims to avoid such limitations, which arise from immobilization of sensor elements on a matrix, by directly measuring the sensor color changes in analytical solvents. Based on the above discussions, we assert that our sensor array approach is quite simple, inexpensive, and easy-to-use as compared to traditional sensor arrays, and is therefore a very promising approach for chemical sensor applications.

When compared to traditional colorimetric sensor arrays, our sensor strategy requires a simple sample preparation step which involves dilution of $[P_{66614}]_2$[BTB] in an analytical solvent (different dilutions mimic individual sensor elements). Obviously, the precision of this dilution step is dependent on the pipetting instruments used, and thus can affect the discriminatory power of this sensor array.

4.3.3. Discrimination of Binary Mixtures of Ethanol and Methanol

After successful discrimination of these eight alcohols, our next goal was to discriminate alcohol mixtures by using our virtual sensor array. Discrimination of alcohol mixtures is far more challenging as compared to discrimination of pure alcohols, primarily due to the requirement of higher resolution. Additionally, the use of fingerprint peak patterns in the discrimination of analytes is tremendously important since two or more alcohol mixtures may provide the same peak ratio at different volume ratios. In order to perform even more stringent test of the sensor array, seven binary mixtures of methanol and ethanol (*i.e.*, ethanol 100%-methanol 0%, ethanol 98%-methanol 2%, ethanol 90%-methanol 10%, ethanol 50%-methanol 50%, ethanol 10%-methanol 90%, ethanol 2%-methanol 98%, and ethanol 0%-methanol 100%) were analyzed. We note that discrimination of ethanol-methanol mixtures is increasingly important primarily due to health concerns involved with these two solvents. Ethanol is used as the primary constituent in alcoholic beverages; however, methanol may be found as a toxic byproduct in alcoholic beverages, which results in severe illnesses or even death upon ingestion.[60] In this study, seven replicate experiments were performed for each ethanol-methanol mixture. In Figure 4.9, the PCA output data are plotted with respect to their first two principal components. In Figure 4.9, all seven mixtures are visually separated, and tightly grouped in the PCA score plot. In addition, the plot strongly suggests that two principal components should be used in developing the predictive model to distinguish among binary mixtures. These data were also subjected to LDA, and interestingly the cross-validation accuracy of identification was found to be 100%.

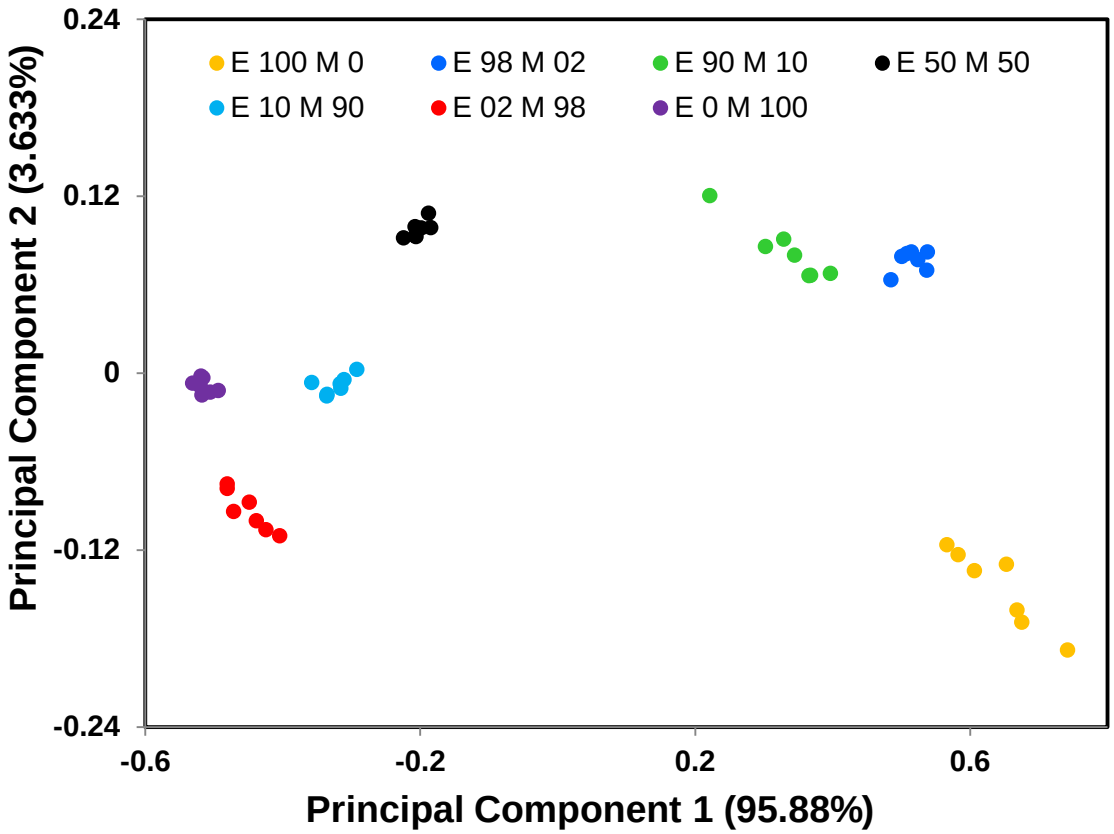

Figure 4.9. PCA score plot using the first two principal components based on the $^{630}/_{410}$ of $[P_{66614}]_2$[BTB] in seven different binary mixtures of ethanol and methanol (E 100 M 0 – ethanol 100%-methanol 0%; E 98 M 2 – ethanol 98%-methanol 2%; E 90 M 10 – ethanol 90%-methanol 10%; E 50 M 50 – ethanol 50%-methanol 50%; E10 M 90 – ethanol 10%-methanol 90%; E 2 M 98 – ethanol 2%-methanol 98%; and E 0 M 100 – ethanol 0%-methanol 100%)

4.4. Conclusion

In summary, we have introduced and demonstrated the concept of using a single IL for fabrication of a virtual sensor array for accurate discrimination of closely related organic solvents. A group of structurally and chemically similar alcohols and alcohol mixtures were chosen as representative analytes to test the performance of this sensor array. Interestingly, the IL, $[P_{66614}]_2$[BTB], used in this study shows a unique ratiometric absorption signal ($^{630}/_{410}$) in organic solvents in distinct contrast to that of the parent BTB compound. Furthermore, the

ratiometric signal observed due to the monoprotonated and deprotonated forms of BTB was found to undergo remarkable hyperchromic and hypochromic changes depending on the type of solvent, and concentration of the IL in the solvent. In addition, an excellent correlation between the $^{630}/_{410}$ absorption ratio and alcohol polarity was observed. The $^{630}/_{410}$ ratio was increased with decreasing polarity of alcohols and *vice versa*, inferring a polarity dependent equilibrium shift between HR^- and R^{2-} forms. It is observed that a single IL concentration itself is able to achieve discrimination among the majority of the analytes tested.

In order to further improve the resolving power of this system, the concept of a virtual sensor array was utilized. Specifically, four different concentrations of $[P_{66614}]_2$[BTB] were used as individual sensors during the fabrication of the sensor array. The $^{630}/_{410}$ ratios obtained from these four concentrations of IL in different analytes were evaluated using PCA and LDA. As a result, we were able to discriminate eight pure alcohols with 96.4% identification accuracy. In contrast, ethanol-methanol mixtures were identified with 100% accuracy. It is also important to mention that use of the fingerprint $^{630}/_{410}$ ratio patterns instead of single sensor response is very useful for discrimination of analyte mixtures. Finally, we believe that the IL, $[P_{66614}]_2$[BTB], reported in this manuscript should provide a new approach for facile fabrication of colorimetric sensors. Additionally, the novel sensor strategy outlined in this study should allow for rapid discrimination of closely related analytes with very high selectivity and accuracy.

4.5. References

(1) Lee, J.; Chang, H. T.; An, H.; Ahn, S.; Shim, J.; Kim, J.-M.: A protective layer approach to solvatochromic sensors. *Nature communications* **2013**, *4*, 2461.

(2) Zhang, Y.; Li, D.; Li, Y.; Yu, J.: Solvatochromic AIE luminogens as supersensitive water detectors in organic solvents and highly efficient cyanide chemosensors in water. *Chemical Science* **2014**, *5*, 2710-2716.

(3) Chang, C.-K.; Bastiaansen, C. W.; Broer, D. J.; Kuo, H.-L.: Discrimination of alcohol molecules using hydrogen-bridged cholesteric polymer networks. *Macromolecules* **2012**, *45*, 4550-4555.

(4) Ishihara, S.; Iyi, N.; Labuta, J.; Deguchi, K.; Ohki, S.; Tansho, M.; Shimizu, T.; Yamauchi, Y.; Sahoo, P.; Naito, M.; Abe, H.; Hill, J. P.; Ariga, K.: Naked-Eye Discrimination of Methanol from Ethanol Using Composite Film of Oxoporphyrinogen and Layered Double Hydroxide. *ACS Applied Materials & Interfaces* **2013**, *5*, 5927-5930.

(5) Schreiter, K.; Hofmann, K.; Seifert, A.; Oehlke, A.; Ladewig, K.; Rüffer, T.; Lang, H.; Spange, S.: Novel periphery-functionalized solvatochromic nitrostilbenes as precursors for class II hybrid materials. *Chemistry of Materials* **2010**, *22*, 2720-2729.

(6) Takagi, S.; Shimada, T.; Masui, D.; Tachibana, H.; Ishida, Y.; Tryk, D. A.; Inoue, H.: Unique Solvatochromism of a Membrane Composed of a Cationic Porphyrin− Clay Complex. *Langmuir* **2010**, *26*, 4639-4641.

(7) Bohne, C.; Ihmels, H.; Waidelich, M.; Yihwa, C.: N-acylureido functionality as acceptor substituent in solvatochromic fluorescence probes: Detection of carboxylic acids, alcohols, and fluoride ions. *Journal of the American Chemical Society* **2005**, *127*, 17158-17159.

(8) Benedetti, E.; Kocsis, L. S.; Brummond, K. M.: Synthesis and photophysical properties of a series of cyclopenta [b] naphthalene solvatochromic fluorophores. *Journal of the American Chemical Society* **2012**, *134*, 12418-12421.

(9) Kucherak, O. A.; Didier, P.; Mély, Y.; Klymchenko, A. S.: Fluorene analogues of Prodan with superior fluorescence brightness and solvatochromism. *The Journal of Physical Chemistry Letters* **2010**, *1*, 616-620.

(10) Giordano, L.; Shvadchak, V. V.; Fauerbach, J. A.; Jares-Erijman, E. A.; Jovin, T. M.: Highly solvatochromic 7-aryl-3-hydroxychromones. *The Journal of Physical Chemistry Letters* **2012**, *3*, 1011-1016.

(11) Fakhari, A.; Rokita, S. E.: A new solvatochromic fluorophore for exploring nonpolar environments created by biopolymers. *Chemical Communications* **2011**, *47*, 4222-4224.

(12) Achelle, S.; Barsella, A.; Baudequin, C.; Caro, B.; Robin-le Guen, F. o.: Synthesis and Photophysical Investigation of a Series of Push–Pull Arylvinyldiazine Chromophores. *The Journal of organic chemistry* **2012**, *77*, 4087-4096.

(13) Landis, R. F.; Yazdani, M.; Creran, B.; Yu, X.; Nandwana, V.; Cooke, G.; Rotello, V. M.: Solvatochromic probes for detecting hydrogen-bond-donating solvents. *Chemical Communications* **2014**, *50*, 4579-4581.

(14) Tso-Lun Lo, L.; Lai, S.-W.; Yiu, S.-M.; Ko, C.-C.: A new class of highly solvatochromic dicyano rhenate(i) diimine complexes - synthesis, photophysics and photocatalysis. *Chemical Communications* **2013**, *49*, 2311-2313.

(15) Cui, J.; Li, Y.; Guo, Z.; Zheng, H.: A porous metal-organic framework based on Zn6O2 clusters: chemical stability, gas adsorption properties and solvatochromic behavior. *Chemical Communications* **2013**, *49*, 555-557.

(16) Selvakumar, P. M.; Nadella, S.; Fröhlich, R.; Albrecht, M.; Subramanian, P.: A new class of solvatochromic material: geometrically unsaturated Ni (II) complexes. *Dyes and Pigments* **2012**, *95*, 563-571.

(17) Lu, Z.-Z.; Zhang, R.; Li, Y.-Z.; Guo, Z.-J.; Zheng, H.-G.: Solvatochromic behavior of a nanotubular metal− organic framework for sensing small molecules. *Journal of the American Chemical Society* **2011**, *133*, 4172-4174.

(18) Reichardt, C.: Solvatochromic dyes as solvent polarity indicators. *Chemical Reviews* **1994**, *94*, 2319-2358.

(19) Reichardt, C.; Welton, T.: *Solvents and solvent effects in organic chemistry*; John Wiley & Sons, 2011.

(20) Zhang, C.; Suslick, K. S.: A colorimetric sensor array for organics in water. *Journal of the American Chemical Society* **2005**, *127*, 11548-11549.

(21) Zhang, C.; Bailey, D. P.; Suslick, K. S.: Colorimetric sensor arrays for the analysis of beers: a feasibility study. *Journal of agricultural and food chemistry* **2006**, *54*, 4925-4931.

(22) Yoon, J.; Jung, Y. S.; Kim, J. M.: A Combinatorial Approach for Colorimetric Differentiation of Organic Solvents Based on Conjugated Polymer-Embedded Electrospun Fibers. *Advanced Functional Materials* **2009**, *19*, 209-214.

(23) Gardner, J. W.: Review of conventional electronic noses and their possible application to the detection of explosives. In *Electronic Noses & Sensors for the Detection of Explosives*; Springer, 2004; pp 1-28.

(24) Gouma, P.; Sberveglieri, G.; Dutta, R.; Gardner, J.; Hines, E.: Novel materials and applications of electronic noses and tongues. *MRS Bulletin-Materials Research Society* **2004**, *29*, 697-702.

(25) Askim, J. R.; Mahmoudi, M.; Suslick, K. S.: Optical sensor arrays for chemical sensing: the optoelectronic nose. *Chemical Society Reviews* **2013**, *42*, 8649-8682.

(26) Doleman, B. J.; Lonergan, M. C.; Severin, E. J.; Vaid, T. P.; Lewis, N. S.: Quantitative study of the resolving power of arrays of carbon black-polymer composites in various vapor-sensing tasks. *Analytical Chemistry* **1998**, *70*, 4177-4190.

(27) Frank, M. L.; Fulkerson, M. D.; Patton, B. R.; Dutta, P. K.: TiO< sub> 2</sub>-based sensor arrays modeled with nonlinear regression analysis for simultaneously determining CO and O< sub> 2</sub> concentrations at high temperatures. *Sensors and Actuators B: Chemical* **2002**, *87*, 471-479.

(28) De, M.; Rana, S.; Akpinar, H.; Miranda, O. R.; Arvizo, R. R.; Bunz, U. H.; Rotello, V. M.: Sensing of proteins in human serum using conjugates of nanoparticles and green fluorescent protein. *Nature chemistry* **2009**, *1*, 461-465.

(29) Basabe-Desmonts, L.; Reinhoudt, D. N.; Crego-Calama, M.: Design of fluorescent materials for chemical sensing. *Chemical Society Reviews* **2007**, *36*, 993-1017.

(30) Schauer, C. L.; Stitzel, S. E.; Walt, D. R.: Cross-reactive optical sensing arrays. *Chemistry Of Taste: Mechanisms, Behaviors, And Mimics* **2002**, *825*, 318-329.

(31) Mohr, G. J.; Citterio, D.; Spichiger-Keller, U. E.: Development of chromogenic reactands for optical sensing of alcohols. *Sensors and Actuators B: Chemical* **1998**, *49*, 226-234.

(32) Ragauskas, A. J.; Williams, C. K.; Davison, B. H.; Britovsek, G.; Cairney, J.; Eckert, C. A.; Frederick, W. J.; Hallett, J. P.; Leak, D. J.; Liotta, C. L.: The path forward for biofuels and biomaterials. *science* **2006**, *311*, 484-489.

(33) Salvi, B. L.; Panwar, N. L.: Biodiesel resources and production technologies – A review. *Renewable and Sustainable Energy Reviews* **2012**, *16*, 3680-3689.

(34) Katritzky, A. R.; Singh, S.; Kirichenko, K.; Smiglak, M.; Holbrey, J. D.; Reichert, W. M.; Spear, S. K.; Rogers, R. D.: In search of ionic liquids incorporating azolate anions. *Chemistry-A European Journal* **2006**, *12*, 4630-4641.

(35) Galpothdeniya, W. I. S.; McCarter, K. S.; De Rooy, S. L.; Regmi, B. P.; Das, S.; Hasan, F.; Tagge, A.; Warner, I. M.: Ionic liquid-based optoelectronic sensor arrays for chemical detection. *RSC Advances* **2014**, *4*, 7225-7234.

(36) Galpothdeniya, W. I. S.; Das, S.; De Rooy, S. L.; Regmi, B. P.; Hamdan, S.; Warner, I. M.: Fluorescein-based ionic liquid sensor for label-free detection of serum albumins. *Rsc Advances* **2014**, *4*, 17533-17540.

(37) Yung, K. Y.; Schadock-Hewitt, A. J.; Hunter, N. P.; Bright, F. V.; Baker, G. A.: 'Liquid litmus': chemosensory pH-responsive photonic ionic liquids. *Chemical Communications* **2011**, *47*, 4775-4777.

(38) Jia, F.; Shan, C.; Li, F.; Niu, L.: Carbon nanotube/gold nanoparticles/polyethylenimine-functionalized ionic liquid thin film composites for glucose biosensing. *Biosensors and Bioelectronics* **2008**, *24*, 945-950.

(39) Jin, X.; Yu, L.; Garcia, D.; Ren, R. X.; Zeng, X.: Ionic liquid high-temperature gas sensor array. *Analytical chemistry* **2006**, *78*, 6980-6989.

(40) Toniolo, R.; Pizzariello, A.; Dossi, N.; Lorenzon, S.; Abollino, O.; Bontempelli, G.: Room temperature ionic liquids as useful overlayers for estimating food quality from their odor analysis by quartz crystal microbalance measurements. *Analytical chemistry* **2013**, *85*, 7241-7247.

(41) Shu, Y.; Liu, M.; Chen, S.; Chen, X.; Wang, J.: New insight into molecular interactions of imidazolium ionic liquids with bovine serum albumin. *The Journal of Physical Chemistry B* **2011**, *115*, 12306-12314.

(42) Yu, L.; Garcia, D.; Ren, R.; Zeng, X.: Ionic liquid high temperature gas sensors. *Chemical communications* **2005**, 2277-2279.

(43) Zhang, Q.; Zhang, S.; Liu, S.; Ma, X.; Lu, L.; Deng, Y.: Ionic liquid-modified dyes and their sensing performance toward acids in aqueous and non-aqueous solutions. *Analyst* **2011**, *136*, 1302-1304.

(44) Regmi, B. P.; Speller, N. C.; Anderson, M. J.; Brutus, J. O.; Merid, Y.; Das, S.; El-Zahab, B.; Hayes, D. J.; Murray, K. K.; Warner, I. M.: Molecular weight sensing properties of ionic liquid-polymer composite films: theory and experiment. *Journal of Materials Chemistry C* **2014**, *2*, 4867-4878.

(45) Safavi, A.; Maleki, N.; Bagheri, M.: Modification of chemical performance of dopants in xerogel films with entrapped ionic liquid. *Journal of Materials Chemistry* **2007**, *17*, 1674-1681.

(46) Gorbenko, G. P.: Bromothymol blue as a probe for structural changes of model membranes induced by hemoglobin. *Biochimica et Biophysica Acta (BBA)-Biomembranes* **1998**, *1370*, 107-118.

(47) Casula, R.; Crisponi, G.; Cristiani, F.; Nurchi, V.; Casu, M.; Lai, A.: Characterization of the ionization and spectral properties of sulfonephthalein indicators. Correlation with substituent effects and structural features. *Talanta* **1993**, *40*, 1781-1788.

(48) Mai, J.; Sommer, G. J.; Hatch, A. V.: Microfluidic Digital Isoelectric Fractionation for Rapid Multidimensional Glycoprotein Analysis. *Analytical chemistry* **2012**, *84*, 3538-3545.

(49) Verhaeghe, E.; Buisson, D.; Zekri, E.; Leblanc, C.; Potin, P.; Ambroise, Y.: A colorimetric assay for steady-state analyses of iodo-and bromoperoxidase activities. *Analytical biochemistry* **2008**, *379*, 60-65.

(50) Del Sesto, R. E.; McCleskey, T. M.; Burrell, A. K.; Baker, G. A.; Thompson, J. D.; Scott, B. L.; Wilkes, J. S.; Williams, P.: Structure and magnetic behavior of transition metal based ionic liquids. *Chemical Communications* **2008**, 447-449.

(51) Doubla, A.; Bouba Bello, L.; Fotso, M.; Brisset, J. L.: Plasmachemical decolourisation of Bromothymol Blue by gliding electric discharge at atmospheric pressure. *Dyes and Pigments* **2008**, *77*, 118-124.

(52) Ooyama, Y.; Sumomogi, M.; Nagano, T.; Kushimoto, K.; Komaguchi, K.; Imae, I.; Harima, Y.: Detection of water in organic solvents by photo-induced electron transfer method. *Organic and Biomolecular Chemistry* **2011**, *9*, 1314-1316.

(53) Kruk, M.; Ngo, T. H.; Savva, V.; Starukhin, A.; Dehaen, W.; Maes, W.: Solvent-dependent deprotonation of meso-pyrimidinylcorroles: Absorption and fluorescence studies. *The Journal of Physical Chemistry A* **2012**, *116*, 10704-10711.

(54) Prukała, D.; Prukała, W.; Khmelinskii, I.; Karolczak, J.; Sikorski, M.: Influence of water on photophysical properties of N-bromobenzyl-or nitrobenzyl derivatives of substituted 4-hydroxystilbazolium hemicyanines. *Photochemical & Photobiological Sciences* **2011**, *10*, 1670-1679.

(55) Ariza-Avidad, M.; Salinas-Castillo, A.; Cuéllar, M. P.; Agudo-Acemel, M.; Pegalajar, M. C.; Capitán-Vallvey, L. F.: Printed Disposable Colorimetric Array for Metal Ion Discrimination. *Analytical Chemistry* **2014**, *86*, 8634-8641.

(56) Carey, J. R.; Suslick, K. S.; Hulkower, K. I.; Imlay, J. A.; Imlay, K. R. C.; Ingison, C. K.; Ponder, J. B.; Sen, A.; Wittrig, A. E.: Rapid Identification of Bacteria with a Disposable Colorimetric Sensing Array. *Journal of the American Chemical Society* **2011**, *133*, 7571-7576.

(57) LaGasse, M. K.; Rankin, J. M.; Askim, J. R.; Suslick, K. S.: Colorimetric sensor arrays: Interplay of geometry, substrate and immobilization. *Sensors and Actuators B: Chemical* **2014**, *197*, 116-122.

(58) Feng, L.; Musto, C. J.; Kemling, J. W.; Lim, S. H.; Suslick, K. S.: A colorimetric sensor array for identification of toxic gases below permissible exposure limits. *Chemical Communications* **2010**, *46*, 2037-2039.

(59) Feng, L.; Musto, C. J.; Kemling, J. W.; Lim, S. H.; Zhong, W.; Suslick, K. S.: Colorimetric Sensor Array for Determination and Identification of Toxic Industrial Chemicals. *Analytical Chemistry* **2010**, *82*, 9433-9440.

(60) Jammalamadaka, D.; Raissi, S.: Ethylene glycol, methanol and isopropyl alcohol intoxication. *The American journal of the medical sciences* **2010**, *339*, 276-281.

CHAPTER 5: TUNABLE GUMBOS-BASED SENSOR ARRAY FOR LABEL-FREE DETECTION AND DISCRIMINATION OF PROTEINS[§]

5.1. Introduction

Accurate detection of absolute and relative concentrations of proteins is critical to understanding various biological processes and disease states. Therefore, monitoring the concentration of certain proteins in serum and urine is an important tool for prevention and early detection of various medical conditions.[1-4] Currently, multiple approaches have been employed for protein detection and quantification. In the absence of traditional analytical techniques such as mass spectrometry[5-7], which usually require expensive instrumentation, immunoassays are often employed as a technique of choice.[8-11] Due to strong specific interactions between the antibody and a given protein, small quantities of proteins can be detected by use of this approach. However, a given immunoassay allows specific detection of a single protein. Additionally, the use of immunoassays requires expensive instrumentation and reagents, and is often quite labor intensive and time consuming.

Alternatively, there has been a recent upsurge of interest towards development of label-free fluorescence probes for protein sensing. In this regard, various organic, organometallic, and metal-organic materials have been investigated for determination of protein sensing properties.[12-20] Conventional fluorometric probes rely on emission spectral changes in intensity and/or wavelength upon interactions with proteins. However, despite considerable success in protein sensing, the ubiquitous use of such probes has been hindered due to multiple limitations such as synthesis involving multiple complex covalent-modification reactions with low product yields.

[§] This Chapter: Tunable GUMBOS-Based Sensor Array for Label-Free Detection and Discrimination of Proteins by Galpothdeniya, W. I. S; Frank R. Fronczek,; Mingyan Cong,; Nimisha Bhattarai,; Siraj, N.; Warner, I. M.: is curenty under review in *Analytical Chemistry*, **2015**

Moreover, these materials frequently display partial selectivity towards proteins, which limits accurate quantification of protein levels in mixtures.

In order to exploit the partial selectivity of label-free probes, which arises from nonspecific interactions towards a group of analytes, the concept of sensor arrays is employed. Typically, sensor arrays are fabricated by assembling a group of cross-reactive colorimetric sensor elements, which are designed to generate fingerprint response patterns for each analyte.[21,22] Essentially, the sensor array concept has been inspired by smell and taste recognition in the mammalian olfactory and gustatory processes, and therefore, these devices are often termed electronic noses and tongues.[23,24] To date, various array-based sensing strategies, which utilize different sensor frameworks, have been employed for protein sensing.[25-31] These systems are highly regarded as very effective for detection and identification of proteins, and often exhibit enhanced resolution and accuracy.[32] Regardless of these considerable advantages, most of these techniques have defined limitations that inhibit widespread application. For example, these approaches have high limits of detection. Furthermore, fabrication of sensor arrays can be complex, expensive, and time consuming as a result of requiring a large number of tailor-made protein probes that depend on the number of analytes.[30] More importantly, even the most efficient sensor array techniques will not perform if the concentrations of analytes are unknown or variable, primarily as a result of poor correlation between senor-response pattern and protein or protein mixture concentrations.[30]

In this manuscript, we demonstrate the concept of using a ***g***roup of ***u***niform ***m***aterials ***b***ased on ***o***rganic ***s***alts (GUMBOS) for accurate discrimination of proteins and protein mixtures. The GUMBOS employed in this manuscript consist of a common organic cation, i.e. 6-(p-toluidino)-2-naphthalenesulfonate (TNS), and various phosphonium-based counter-ions. These

TNS-based sensor materials are easy to synthesize with high yields, and physicochemical properties which can be easily tuned via changes in the counter-ion. The four sensors utilized in our sensor strategy, were observed to exhibit differential fluorescence responses with respect to differences in proteins and protein concentrations. Interestingly, these differential sensor responses are found to be unique to particular proteins and protein mixtures at various concentration levels. In order to accurately identify analytes, the resulting fingerprint sensor-response patterns are analyzed using principal component analysis (PCA) and linear discriminant analysis (LDA). In PCA, different proteins provide distinct PCA clusters. More importantly, PCA clusters generated from various concentrations of the same protein are found to follow a clear trend. Therefore, use of this approach for discrimination of proteins regardless of concentration is also examined. It is further demonstrated that our sensor array is capable of discriminating between protein mixtures at various concentrations. Overall, this sensor array concept allows for facile, inexpensive, sensitive, and label-free discrimination of proteins.

5.2. Materials and Methods

5.2.1. Materials

Sodium 6-(p-toluidino)-2-naphthalenesulfonate ([Na][TNS]), trihexyl(tetradecyl)phosphonium chloride ([P_{66614}][Cl]), tetrabutylphosphonium bromide ([P_{4444}][Br]), tetraphenylphosphonium chloride ([TPP][Cl]), (4-nitrophenyl)triphenylphosphonium bromide ([4NB][Br]), Benzyltriphenylphosphonium chloride ([BTP][Cl]), anhydrous ethanol (200 proof, 99.5%), anhydrous methylene chloride (DCM), and all proteins were purchased from Sigma-Aldrich, and used as received. Triply deionized water (18.2 MΩ cm) from an Elga model PURELAB ultra water-filtration system was used for preparation of sodium phosphate buffer (pH 7.4/10 mM).

5.2.2. Synthesis and Characterization of Functional GUMBOS

GUMBOS were synthesized using a modified ion exchange procedure reported in literature.[33,34] Briefly, a phosphonium salt (PR_4)[X]; R- hydrocarbon substituent, X- halide) was dissolved in DCM and added onto solid [Na][TNS] at a molar ratio of 1:1.1. Afterwards, a few drops of triply deionized water were added to the reaction mixture in order to collect the resulting byproduct (NaX), and then stirred for 24 h. Afterwards, the DCM layer was separated from the water layer and filtered in order to remove excess [Na][TNS]. Next, the filtrate was washed repeatedly with water in order to remove NaX byproduct. The product was recrystallized using a DCM/water solvent mixture. The final product [PR_4][TNS] was dried by removal of solvents *in vacuo*. Finally, the resultant GUMBOS were characterized by use of electron spray ionization mass spectrometry (ESI-MS) (Figure C1), and single-crystal X-ray crystallography. The ionic compounds [TPP][TNS], [P_{4444}][TNS], and [BTP][TNS] were found to be crystalline. Crystal data and details of the structural refinement for [TPP][TNS], [P_{4444}][TNS], and [BTP][TNS] are provided in the Table C1 in the Appendix C.

5.2.3. Single-Crystal X-ray Crystallographic Studies

Diffraction data were collected at low temperature on a Bruker Kappa Apex-II DUO diffractometer with Cu Kα (λ = 1.54184 Å) or MoKα radiation (λ = 0.71073 Å). Refinement was by full-matrix least squares using SHELXL[35,36], with H atoms in idealized positions except for those on N, for which coordinates were refined. [BTP][TNS] was the DCM solvate, and disordered water solvent in [TPP][TNS] was removed using SQUEEZE.[35,36] Crystal data: [P_{4444}][TNS], [$C_{16}H_{36}P$][$C_{17}H_{14}NO_3S$], monoclinic $P2_1/c$, a=10.3977(4), b=18.2132(7), c=17.4211(6) Å, β=102.071(3)°, Z=4, T=90K, θ_{max}=59.0° (Cu), R=0.070 for 2612 data with

I>2σ(I) (of 4636 unique), 359 parameters, CCDC 1058986; [BTP][TNS], $[C_{25}H_{22}P][C_{17}H_{14}NO_3S]$. CH_2Cl_2, triclinic P1, a=10.0089(4), b=10.4658(4), c=10.8995(4) Å, α=61.537(2), β=78.686(2), γ=66.103(2)°, Z=1, T=90K, θ_{max}=35.0° (Mo), R=0.041 for 11156 data with I>2σ(I) (of 12497 unique), 465 parameters, CCDC 1058985; [TPP][TNS], $[C_{24}H_{20}P][C_{17}H_{14}NO_3S]$. $0.7H_2O$, monoclinic $P2_1/c$, a=14.3436(10), b=13.8575(9), c=18.0804(12) Å, β=112.786(2)°, Z=4, T=90K, θ_{max}=68.8° (Cu), R=0.049 for 5188 data with I>2σ(I) (of 5810 unique), 428 parameters, CCDC 1058984.

5.2.4. Preparation of Protein Solutions

In this study, all protein samples were prepared in 10 mM sodium phosphate buffer (pH = 7.4). Initially, stock solutions of 5 μM proteins were prepared, and then diluted in buffer to obtain concentrations ranging from 10 to 200 nM.

5.2.5. Preparation of TNS-Based Sensor-Protein Solution

Preparation of TNS-based sensor-protein solutions was performed using a reprecipitation method previously employed by our group.[17] Briefly, 50 μL of 0.5 mM ethanolic TNS-based sensor solution was rapidly introduced into a 5 mL protein solution and ultra-sonicated for 5 min. Then, the sensor-protein mixture was allowed to equilibrate for 10 min. Finally, the solution was characterized spectroscopically using uv-vis and fluorescence spectrophotometry.

5.2.6. Absorption and Fluorescence Studies

A Shimadzu UV-3101PC spectrophotometer was used to acquire absorbance spectra. A Spex Fluorolog-3 spectrofluorimeter (model FL3- 22TAU3; Jobin Yvon, Edison, NJ) was used to perform fluorescence studies. A 1.0 cm path length quartz cuvette (Starna Cells) was used in

both absorbance and fluorescence data acquisition. Absorption spectra were collected against an identical cell filled with pH 7.4 phosphate buffer as the blank. Fluorescence studies were performed by adapting a synchronous scan protocol with right angle geometry.[37] A 5.0 mL buffer solution mixed with 50 µL of 0.5 mM ethanolic, TNS-based sensor solution was used as blank in fluorescence studies.

5.2.7. Absolute Quantum Yield Measurements

Absolute quantum yield measurements for all TNS-based GUMBOS were measured using an integrated sphere. A 1.0 cm path length quartz cuvette (Starna Cells) was used for data acquisition. The TNS-based GUMBOS were prepared at concentrations equivalent to 10 µM in ethanol to obtain quantum yield (φ_{fl}) in ethanol. In order to obtain φ_{fl} in water, 100 µL of 0.5 mM ethanolic TNS-based sensor solution was rapidly introduced into a 5 mL pH 7.4 buffer solution and ultra-sonicated for 5 min prior to measurements.

5.2.8. Octanol-Water Partition Coefficient ($K_{o/w}$)

The $K_{o/w}$ values were determined by use of absorbance measurements obtained from a Shimadzu UV-3101PC spectrophotometer. All absorbance measurements were performed using a 1.0 cm path length quartz cuvette (Starna Cells). Briefly, an equal amount of octanol and water were mixed and left standing overnight until the solubility of the water in octanol is equilibrated. The two phases were then separated into two different containers. Each compound was dissolved in 10 mL of the water saturated octanol to prepare a 1.0 mM stock solution. The 1.0 mM stock solution was then used to prepare 4 dilutions that were used to form a calibration curve based on the absorbance readings and a best-fit line was plotted. One concentration from the calibration curve was then chosen and mixed with an equal volume of the water mentioned in the separation

step above. This solution was then allowed to stir for 24 hours. Following the 24 hours, the octanol layer was then extracted and the absorbance was measured. The equation for the line of best-fit from the calibration curves was then used to determine the concentration of compounds within the octanol and water layers for all compounds. The equation $K_{(o/w)} = [octanol\ layer]\ /[water\ layer]$ was then used to calculate the octanol water partition coefficient.

5.2.9. Development of Predictive Models

In this study, predictive models were developed in order to accurately identify analytes used in each experiment. Fluorescence sensor-response patterns generated by use of the four TNS-based sensors (four TNS-GUMBOS × number of analytes × five replicates) were employed to develop the statistical models in each experiment. First, the dimensionality of the predictor space was reduced using PCA. In most experiments, the first two principal components in PCA accounted for more than 99% variance (except when the input data were normalized). Therefore, only the values of these two components were used to develop predictive models using LDA. Second, the predictive accuracy of each statistical model was assessed separately using cross-validation.

5.3. Results and Discussion

5.3.1. TNS-Based Sensors

The fluorescent probe, 6-(p-toluidino)-2-naphthalenesulfonate (TNS), has been extensively used for a wide range of applications, primarily due to its unique photophysical properties. TNS is considered a fluorescent probe which responds to hydrophobic environments. This is because TNS is non-fluorescent in water, but strongly fluorescent in organic solvents and when bound to hydrophobic surfaces such as some regions of proteins.[38] Therefore, TNS is ideal

for sensory applications which involve detection of hydrophobic regions. It has been previously reported that TNS can bind to proteins via hydrophobic, as well as ionic interactions.[39] In this study, we employ a TNS-based sensor array for accurate discrimination of proteins. Due to partial selectivity of TNS towards proteins, discrimination of proteins using TNS alone is a challenge. Hence, we have synthesized a group of chemically different sensors based on TNS (GUMBOS) with partial selectivities towards proteins. In this sensor design, an array of TNS-based sensors generates a fingerprint signal which can be used to detect and discriminate proteins, as well as protein concentrations.

Fabrication of TNS-based sensors was accomplished through ionic modification of [Na][TNS]. As compared to traditional covalent modification reactions, which usually require complex synthetic procedures with low product yields, ionic modification is extremely simple, usually a one-step ion exchange reaction resulting in very high product yield. Furthermore, physicochemical properties of ionic materials such as [Na][TNS] can be easily tuned by changing the counter cation. In this study, the ionic modification product yields for all five sensors, i.e., $[P_{66614}][TNS]$, $[P_{4444}][TNS]$, [4NB][TNS], [BTP][TNS], and [TPP][TNS], were found to be greater than 98% (Table 5.1). The chemical structures of these TNS-based GUMBOS are provided in Scheme 5.1. It is important to note that the chemical properties of these compounds such as hydrophobicity, aromaticity, and hydrogen-bonding ability were tuned with variations in the counter-ion.

In order to classify these TNS-based ion pairs, their melting points were studied. Examination of melting points for the five TNS-based organic salts reveals that $[P_{66614}][TNS]$ can also be categorized as a frozen ionic liquid (FIL) since its melting point is under 100 °C.[40]

Table 5.1 Molecular weight (MW), yield (%), melting point (°C), log $K_{o/w}$, and appearances of TNS-based GUMBOS

GUMBOS	MW	Yields (%)	Melting point (°C)	log $K_{o/w}$	Appearance
$[P_{66614}][TNS]$	796.22	98	78	1.41	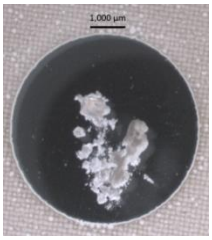
[4NB][TNS]	710.77	99	152	1.09	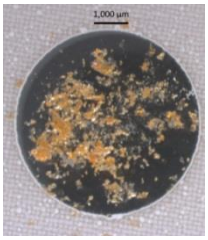
$[P_{4444}][TNS]$	571.79	98	162	1.04	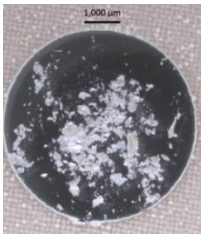
[BTP][TNS]	665.78	98	182	1.15	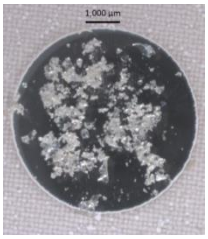
[TPP][TNS]	651.75	99	223	0.78	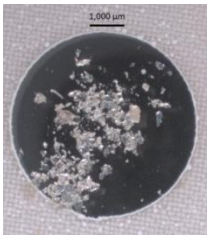

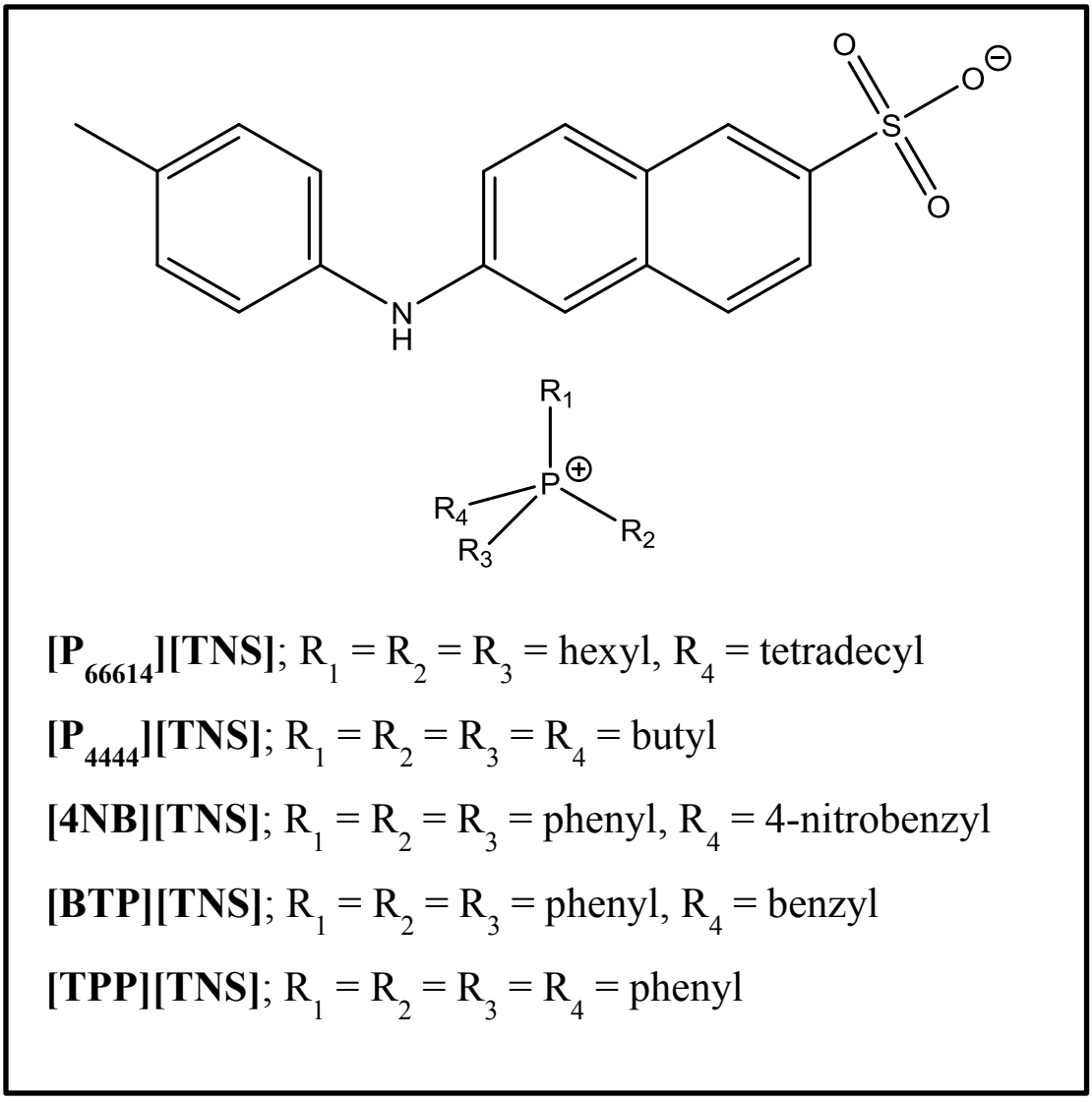

Scheme 5.1. Chemical structures of TNS-based compounds synthesized in this study

However, the other four organic salts, $[P_{4444}][TNS]$, [4NB][TNS], [BTP][TNS], and [TPP][TNS], do not fit into the classical definition for ILs, and are therefore, classified as GUMBOS. GUMBOS are defined as solid phase organic ionic materials with melting points between 25 °C and 250 °C.[41] In addition, the FIL, $[P_{66614}][TNS]$, can also be included under GUMBOS.

In contrast to traditional ionic compounds, ILs and GUMBOS have relatively lower melting points. The low melting point of these compounds can be attributed to the 'frustrated molecular packing' of the associated ions.[42] The ions found in ILs and GUMBOS are typically bulky and asymmetric, and therefore, amorphous materials. TNS-based GUMBOS studied in this manuscript are listed, in Table 5.1, in order of increasing melting points. In Table 5.1, $[P_{66614}][TNS]$ has the lowest melting point primarily due to the presence of the bulky, asymmetric P_{66614} cation, which is also regarded as a 'universal liquifier' within the IL community.[43] Among the GUMBOS materials employed in this study, $[P_{4444}][TNS]$, [BTP][TNS], and [TPP][TNS] were found to be crystalline. Hence, these compounds exhibited higher melting points, which may be attributed to improved stacking compatibility of their counter-ions. The molecular structures for $[P_{4444}][TNS]$, [BTP][TNS], and [TPP][TNS] obtained from single-crystal X-ray diffraction are given in Figure 5.1.

A list of selected bond distances and angles for $[P_{4444}][TNS]$, [BTP][TNS], and [TPP][TNS] generated from single-crystal X-ray diffraction studies is provided in Table C2 in the Appendix C. It is important to note that there are no notable changes in the bond distances of TNS in the presence of different cations. However, certain bond angles of the TNS moiety differ significantly, and may have a direct effect on the chemistry of these sensors, which may be important to sensor array performance.

As mentioned previously, chemical properties of organic salts such as hydrophobicity can be modified significantly by small changes in the counter-ion. In order to demonstrate this phenomenon, the relative hydrophobicities of all compounds were estimated by use of 1-octanol/water partition coefficients ($K_{o/w}$).

Figure 5.1. The solid state structures for (A) $[P_{4444}][TNS]$, (B) [BTP][TNS], and (C) [TPP][TNS] obtained from single-crystal X-ray diffraction. Solvent molecules were removed for clarity. For comparison purposes, TNS moiety was given the same numbering pattern in all three structures (continues through pages 151-153)

A

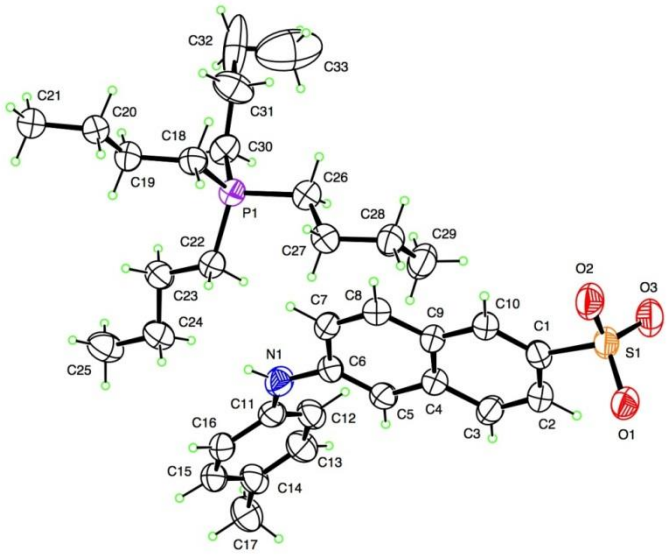
C32
C33
C31
C21
C20
C18
C30
C19
C26
P1
C28
C29
C27
C22
C23
C24
C25
O2
O3
C7
C8
C9
C10
C1
S1
N1
C6
C11
C12
C5
C4
C3
C2
O1
C16
C13
C15
C14
C17

B

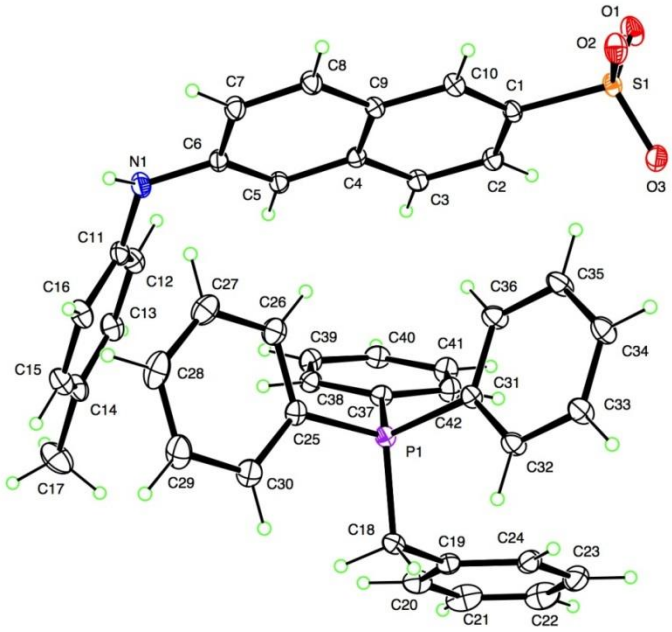
O1
O2
S1
C7
C8
C9
C10
C1
C6
N1
C5
C4
C3
C2
O3
C11
C12
C27
C26
C36
C35
C16
C13
C39
C40
C41
C34
C15
C28
C38
C31
C14
C37
C42
C33
C25
P1
C32
C17
C29
C30
C18
C19
C24
C23
C20
C21
C22

C

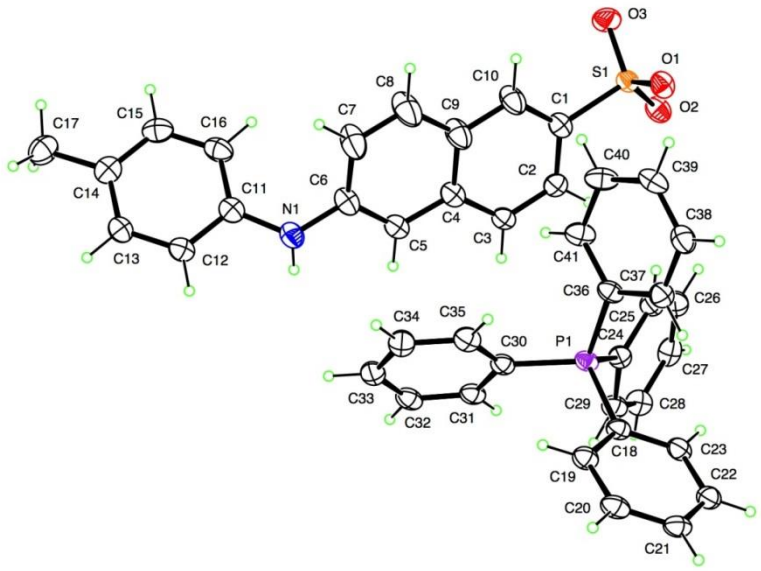

Hydrophobicity of a compound is assumed to be directly proportional to its $K_{o/w}$. The logarithm of 1-octanol/water partition coefficients (log $K_{o/w}$) for each compound is listed in Table 5.1. As inferred from the log $K_{o/w}$ values, relative hydrophobicities of TNS GUMBOS decrease in the order of [P66614][TNS] >> [BTP][TNS] > [4NB][TNS] > [P4444][TNS], > [TPP][TNS].

5.3.2. Spectral Properties of TNS-based GUMBOS

Absorption and emission spectra for all five TNS-based GUMBOS were measured at concentrations of 10 µM in ethanol. All five compounds showed multiple absorption bands with similar peak shifts and intensities. It is important to note that all absorption peaks observed for TNS GUMBOS are also characteristics of TNS. The longest wavelength absorption band, with absorption maximum at ~355 nm, corresponds to the $\pi - \pi^*$ transition of TNS.[44] The emission that corresponds to $\pi - \pi^*$ absorption band is extremely sensitive to polarity of its environment,

and is often targeted in sensory applications. The molar absorptivity coefficients for these GUMBOS at 355 nm ($\boldsymbol{\varepsilon_{355}}$) are listed in Table 5.2. The fluorescence emission spectra for these TNS compounds were recorded at an excitation wavelength of 355 nm. The corresponding emission spectra were recorded an excitation maximum at ~425 nm.

Table 5.2 Absorption maximum for π – π* transition (λ_{abs}), molar extinction coefficient at 355 nm (ε_{355}), emission maximum (λ_{em}), and quantum yield (φ_{fl}) of TNS-based GUMBOS

GUMBOS	**Solvent**	$\boldsymbol{\lambda_{abs}}$ **(nm)**	$\boldsymbol{\varepsilon_{355}/10^4}$ **(M^{-1} cm^{-1})**	$\boldsymbol{\lambda_{em}}$ **(nm)**	% $\boldsymbol{\varphi_{fl}}$
$[P_{66614}][TNS]$	Ethanol	356	6.3	427	5
[4NB][TNS]	Ethanol	352	5.6	425	11
$[P_{4444}][TNS]$	Ethanol	352	6.1	425	17
[BTP][TNS]	Ethanol	354	5.7	427	11
[TPP][TNS]	Ethanol	353	5.9	425	12

The normalized absorption and fluorescence emission spectra (λ_{ex}- 355 nm) of 10 μM [4NB][TPP] in ethanol are given in Figure 5.2. For comparison purposes, the normalized absorption and emission spectra for all five compounds are provided in the SI (Figure C2). Furthermore, absolute quantum yields for all TNS-based GUMBOS along with absorption and emission maxima are listed in Table 5.2. As seen in Table 5.2, absolute quantum yields of these organic salts depend on the counter-ion associated with TNS. In ethanol, the absolute quantum yield of each compound in ascending order is $[P_{66614}][TNS]$ < [BTP][TNS] ≈ [4NB][TNS] < [TPP][TNS] < $[P_{4444}][TNS]$. Similar to the parent compound, four of the TNS compounds (except $[P_{66614}][TNS]$) are weakly fluorescent in pH 7.4 buffer. The weak fluorescence signal of these compounds in buffer may be attributed to the presence of small amounts of ethanol, which

was added during the introduction of TNS-based GUMBOS to aqueous solution (see materials and method section for more details). As compared to those four GUMBOS, $[P_{66614}][TNS]$ is highly fluorescent in buffer. Furthermore, material properties of $[P_{66614}][TNS]$ appeared to be significantly different from the other TNS GUMBOS. Therefore, material properties of $[P_{66614}][TNS]$ will be studied further in a future manuscript.

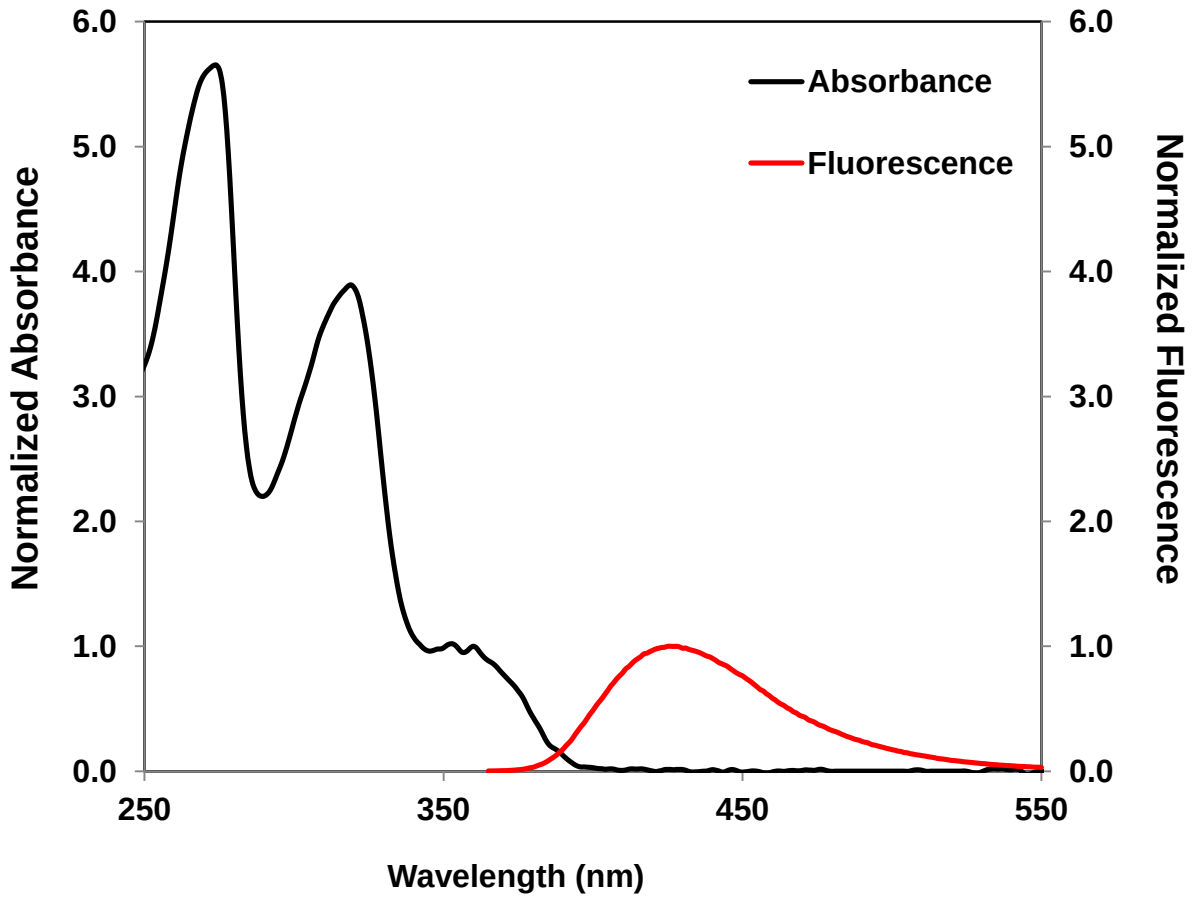

Figure 5.2. Normalized absorption and fluorescence emission spectra (λ_{ex}- 355 nm) of 10 µM [4NB][TPP] in ethanol. Absorption spectrum has been normalized to 1.0 at maximum of the longest wavelength absorbance band, and emission spectrum has been normalized to 1.0 at its maximum. A stoke shift of 66 nm was observed

5.3.3. Detection and Discrimination of Proteins using TNS-Based GUMBOS

Four of the five TNS-based salts, i.e. [P_{4444}][TNS], [4NB][TNS], [BTP][TNS], and [TPP][TNS], were selected as sensors for proteins. These four TNS-based sensors display similar spectral properties, and hence, simplify the sensor array approach and data analyses. Sensing of proteins using TNS-based GUMBOS was done using nine different proteins. Human serum is primarily composed of approximately 20 different serum proteins that typically constitute approximately 99% by mass.[45] In this study, we have selected five of the most abundant serum proteins, i.e., human serum albumin (HSA), α-antitrypsin, fibrinogen, immunoglobulin G (IgG) and transferrin, and four non-serum proteins, i.e., β-lactoglobulin (β-lac), ribonuclease a (RNase A), α- chymotrypsin (α-CTP), and lysozyme.

A comparison of the relative emission intensity (λ_{ex} – 355 nm) of 5 µM TNS-based GUMBOS in the presence of these proteins is given in Figure 5.3. The overall concentration of all protein samples was held constant at 100 nM. As mentioned earlier, the parent compound, TNS, is selective towards hydrophobic regions of proteins. Therefore, an increase in emission of TNS-based GUMBOS was expected in the presence of proteins with hydrophobic regions. In the presence of several proteins, the emission intensity of the GUMBOS increased significantly. Specifically, in the presence of HSA, α-antitrypsin, and β-lac all four TNS GUMBOS displayed a partially selective emission response. Furthermore, HSA produced a more than 19-fold enhancement in fluorescence for all four compounds. In contrast, α-antitrypsin and β-lac produced more than 5.5-fold enhancement in seven out of eight sensor responses. Further examination of these fluorescence signal changes in the presence of proteins also revealed different sensor signal patterns for each of the three proteins. In the presence of HSA, the highest fluorescence enhancement was observed with [4NB][TNS], whereas [TPP][TNS] produced the

lowest fluorescence enhancement. When comparing the relative sensor response for HSA, in the presence of α-antitrypsin or β-lac, [P_{4444}][TNS] produced the highest fluorescence intensity. In contrast, [4NB][TNS] exhibited the lowest fluorescence signal enhancement. However, the two proteins, α-antitrypsin and β-lac, deviate significantly with respect to the intensity of each sensor signal, and the relative signal intensity of [TPP][TNS] and [BTP][TNS]. From the viewpoint of discrimination, the existence of discrete sensor-response patterns for different analytes is extremely important for accurate discrimination.

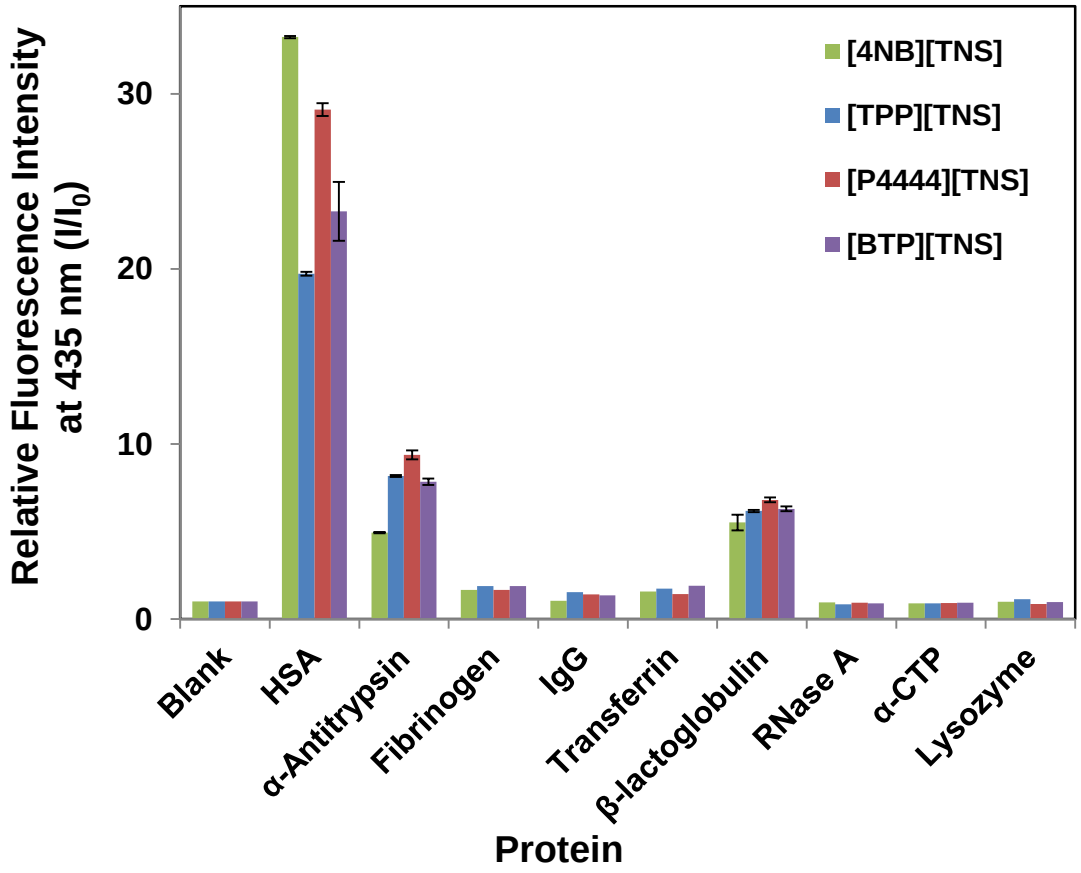

Figure 5.3. Relative fluorescence emission intensity (λ_{ex} – 355 nm) of 5 μM TNS-based GUMBOS at 435 nm in presence of different serum and non-serum proteins. Protein concentrations were fixed at 100 nM in pH 7.4 buffer. Error bars represent standard deviations of five replicate samples

In order to study the sensor response changes with respect to protein concentration, relative emission intensities of TNS-based GUMBOS at different concentrations of HSA (10 – 100 nM), α-antitrypsin (10 – 500 nM), and β-lac (20 – 500 nM) were measured (Figure 5.4). All four sensors exhibited an increase in emission signal with increasing concentrations of the three proteins. Furthermore, discrete sensor-response patterns, which are unique to each protein and their concentrations, were observed. For HSA, the intensity of the sensor response from lowest to highest increases as [TPP][TNS] < [P_{4444}][TNS] < [BTP][TNS] < [4NB][TNS] for almost all concentrations. For α-antitrypsin, emission intensities of the sensors typically varied in the order of [4NB][TPP] < [BTP][TNS] ≈ [TPP][TNS] < [P_{4444}][TNS]. However, in the presence of lower concentrations of β-lac, the four sensors responses do not exhibit large variations. At higher concentrations, [P_{4444}][TNS] response appears to be significantly higher as compared to the emission intensities of the other three GUMBOS.

In this study, the sensor-response pattern generated by the four TNS-based GUMBOS for each analyte was treated as a sensor-array response. The relative fluorescence intensities obtained from TNS-GUMBOS with various concentrations of HSA, α-antitrypsin, and β-lac were used to develop predictive models for accurate identification at each concentration. Our first experiment involved 21 analytes (HSA – six different concentrations, α-antitrypsin – eight different concentrations, and β-lac – seven different concentrations). For each analyte, five replicate samples were analyzed, producing a total training set of 105 observations/sensor-array responses. First, principal component analysis (PCA) was performed on the 105 observations. In PCA, four principal components were generated, and the first two components accounted for more than 99% of the variance. Therefore, the first two principal components were used to develop predictive models using linear discriminant analysis (LDA). The PCA plot, second

principal component *versus* first principal component, which corresponds to the analysis of various concentrations of HSA, α-antitrypsin and β-lac is given in Figure 5.5.

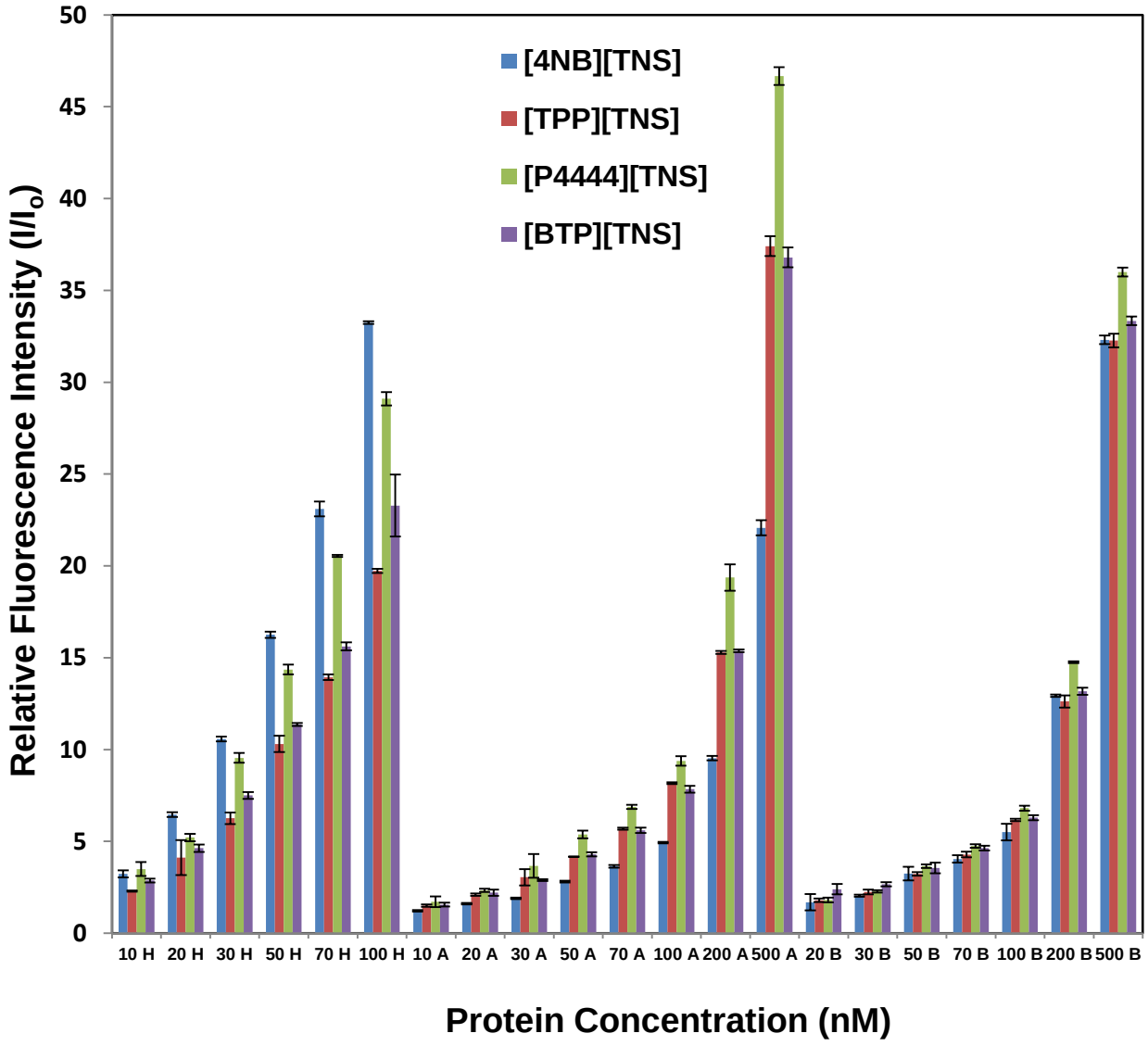

Figure 5.4. Relative emission intensity (λ_{ex} – 355 nm) of TNS-based GUMBOS at 435 nm in presence of different concentrations of HSA (H), α-antitrypsin (A) and β-lac (B). Error bars represent the standard deviations of five replicate samples

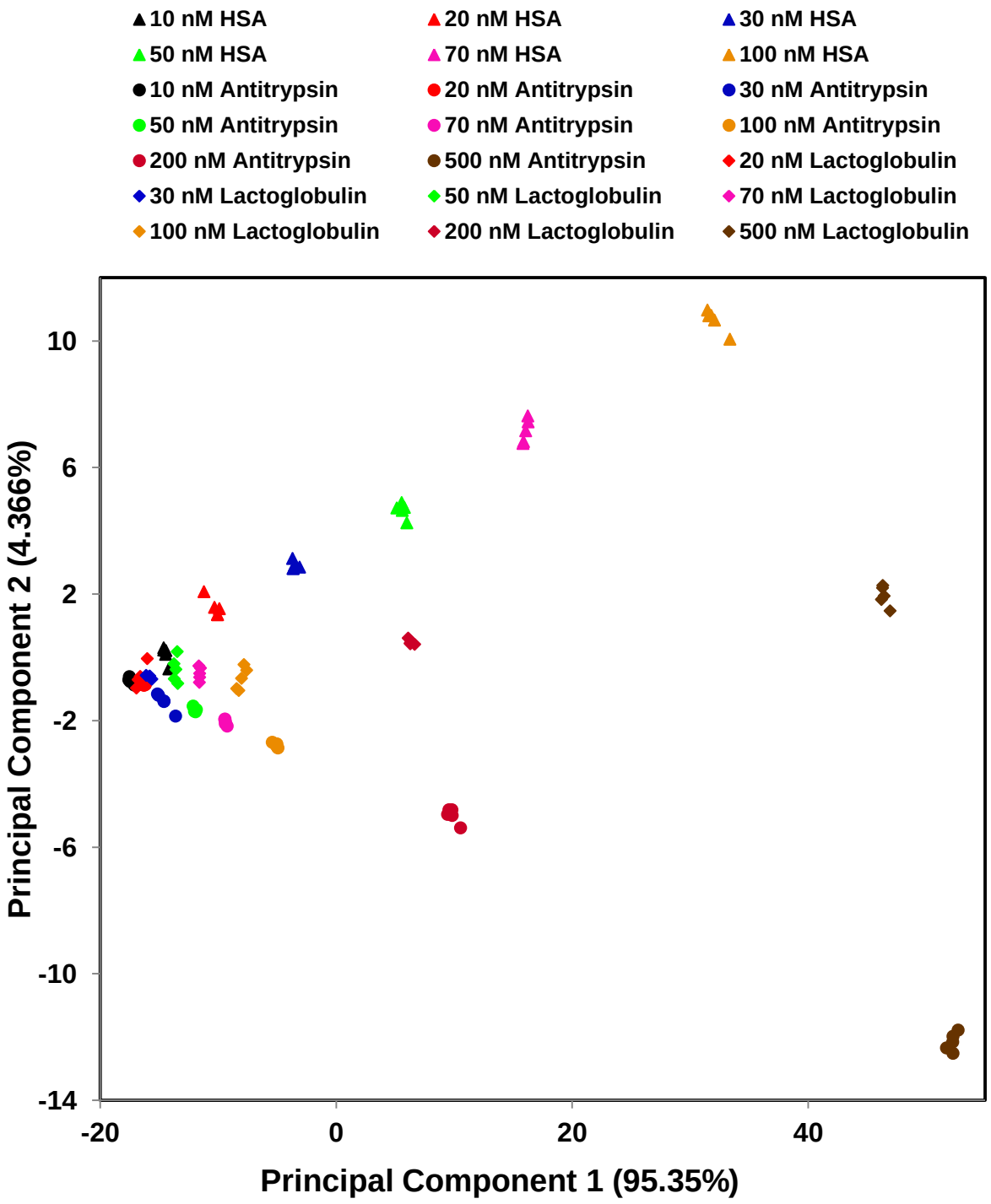

Figure 5.5. PCA score plot using the first two principal components based on the sensor-response patterns obtained from TNS-based sensors in 21 protein concentrations. Protein concentrations are listed in the legend

Each protein concentration in Figure 5.5 was found to form a tight cluster with its replicate measurements. In addition, there is a notable separation between each cluster especially at higher concentrations. Examination of Figure 5.5 also revealed two other interesting features. First, the PCA clusters that are responsible for different concentrations of the same protein are arranged in a linear trend. In addition, the concentration of protein gradually increased when going from left to right along the first principal component. Second, visual separation of PCA clusters of the three proteins increases at higher concentrations. Therefore, accurate discrimination of these three proteins at higher concentrations is relatively simple. The predictive accuracy of the resulting model was calculated using LDA, and the cross-validation accuracy for discrimination of various concentrations of HSA, α-antitrypsin, and β-lac was found to be 100%.

As mentioned earlier, we have selected five of the most abundant proteins in human serum to test our sensor array performance. However, TNS-based GUMBOS were not sensitive to three of those five proteins, and were highly sensitive toward the other two. After successful discrimination of various concentration levels for these two proteins, HSA and α-antitrypsin, our next goal was to assess the sensor array performance towards discrimination of these proteins regardless of their concentration. Most sensor arrays, immunosensors, as well as other protein sensing methods, have the ability to discriminate proteins at certain concentration levels. In general, those sensors provide random sensor-response patterns without correlation to protein concentration. Therefore, if the concentrations of proteins are unknown, the discrimination capabilities of those techniques are practically limited or insufficient.[30] In our study, we saw an excellent correlation between sensor-response pattern and protein concentration.

In order to prove that our sensor array can discriminate proteins regardless of protein concentration, two approaches were employed. In the first approach, new PCA and LDA were

performed using the same spectral data for HSA (10 – 100 nM) and α-antitrypsin (10 – 500 nM). However, for the new PCA and LDA analyses, the concentration of protein for each sensor response was not defined. Only the protein identity was defined. The experiment involved 70 observations (six HSA concentrations × five replicates + eight α-antitrypsin concentrations × five replicates); and PCA was performed first. Again, the first two principal components accounted for more than 99% of the variance, and those two principal components were used to develop predictive models. The PCA plot for discrimination of HSA and α-antitrypsin is provided in Figure 5.6. Obviously, there are two distinct clusters for these two proteins. The PCA data points generated from various concentrations of these two proteins follow two different patterns. LDA was performed to calculate the prediction accuracy, and the cross-validation accuracy for discrimination of the two proteins regardless of concentration was found to be 91.7 %. In this analysis, five of the 30 HSA measurements were misclassified as α-antitrypsin. Examination of those misclassified data points revealed that those five points were generated from the sensor array responses, which correspond to 10 nM HSA.

For comparison, a separate set of PCA and LDA was performed on the same 70 observations. In this study, the protein concentration that corresponds to each data point was defined during the analysis. The resulting PCA plot is given in Figure C3a in the Appendix C, and the PCA data points are identical to the previous version of the PCA plot. Therefore, the second version of the PCA plot can be used as a map to identify the protein concentration for each PCA data point. In both PCA plots (Figures 5.6, and C3a), the protein concentrations increase, when going from left to right along the first principal component. Furthermore, separation between the data points of the two proteins gradually increases with concentration, suggesting that discrimination of HSA and α-antitrypsin becomes easier at higher concentrations.

However, it is important to note that, the predictive accuracy of our statistical model can be improved by defining the protein concentration of each data point during the analysis. Thus, this helps to improve the accuracy of the predictive model, especially when protein concentrations are very low. During the second analysis, the cross-validation accuracy for LDA was improved from 91.7 to 100%.

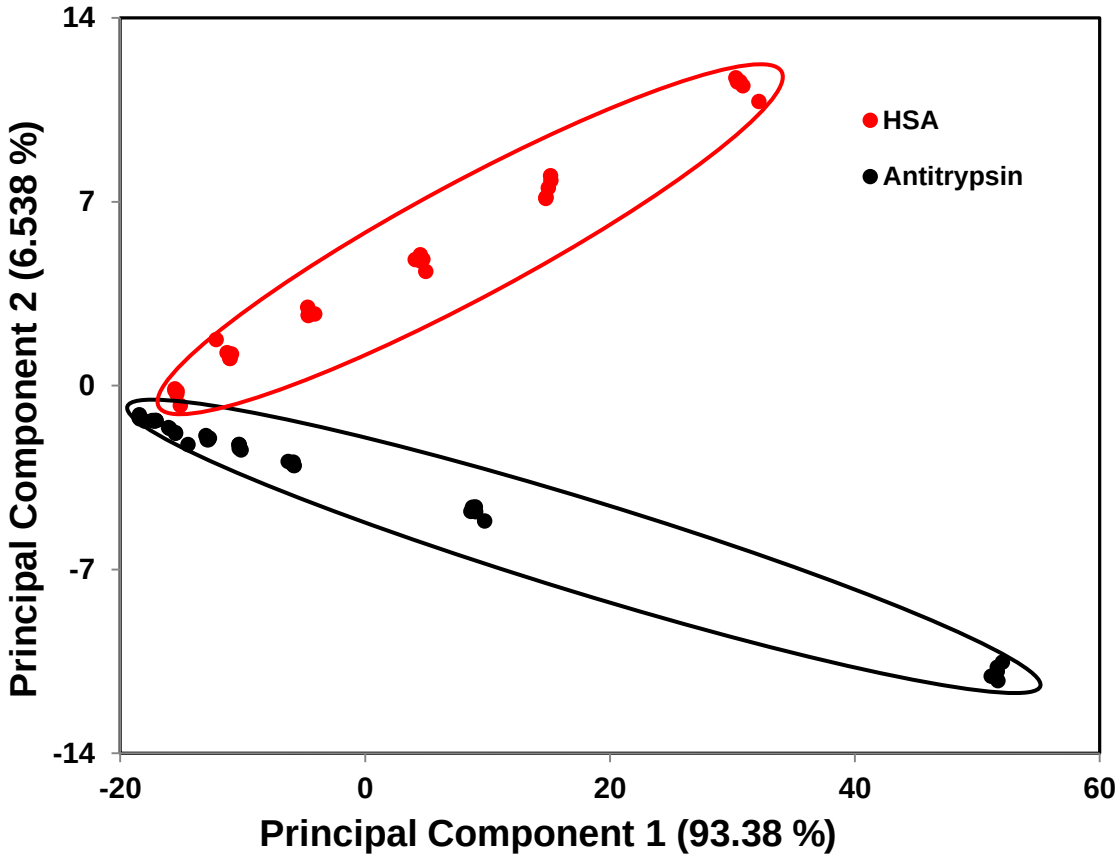

Figure 5.6. PCA score plot using the first two principal components based on the sensor-response patterns obtained from TNS-based sensors. In this experiment, HSA (red) and α-antitrypsin (black) concentrations were not defined during PCA

In the second approach, the sensor-response pattern for each analyte, i.e. emission from four sensors, was normalized for the sensor which displayed the highest fluorescence enhancement. Hence, the normalized emission intensity for each sensor ranges from 0 to 1,

where 1 is the normalized emission intensity of the sensor which displayed the highest fluorescence enhancement. Due to normalization, increase in sensor response with respect to protein concentration was insignificant, and only the sensor-response pattern was utilized for discrimination.

First, the 70 normalized observations were subjected to PCA. Three principal components accounted for approximately 99% variance, and those three principal components were used in LDA. The PCA plot constructed using three principal components for discrimination of HSA and α-antitrypsin irrespective of concentration is provided in Figure 5.7. Clearly, there are two different clusters for HSA and α-antitrypsin, and both of those clusters are visually well separated. Furthermore, the cross-validation accuracy for discrimination of the two proteins regardless of concentration was found to be 100%. For comparison purposes, PCA clusters were mapped using a second PCA plot as given in Figure C3b. In addition, a PCA plot with 95% confidence ellipses for the two proteins is given in Figure C3c. Examination of Figures 5.7, and C3b indicates that there is no correlation between PCA clusters and protein concentration. However, there is excellent separation between the clusters of each protein even at low concentrations. In conclusion, both approaches confirms that our sensor strategy is extremely capable of discriminating proteins regardless of concentration, and compared to the first approach, normalization of sensor-response patterns clearly improves the accuracy of discrimination.

We have successfully demonstrated that our sensor array strategy can be used to discriminate proteins not only at a given concentration, but also across a wide range of concentrations. Our next challenge was to apply our sensor strategy for discrimination of protein mixtures. Discrimination of protein mixtures is far more demanding because real samples

typically consist of complex protein mixtures. In this study, we employ TNS-based sensors which are partially selective for proteins. Therefore, our sensors should aid in reducing the complexity of the sample matrix, as well as allow discrimination of multiple analytes at the same time. As an example, HSA and α-antitrypsin are often found in the same sample matrices at significant concentration levels, and therefore, discrimination of such mixtures at different concentrations is extremely important.

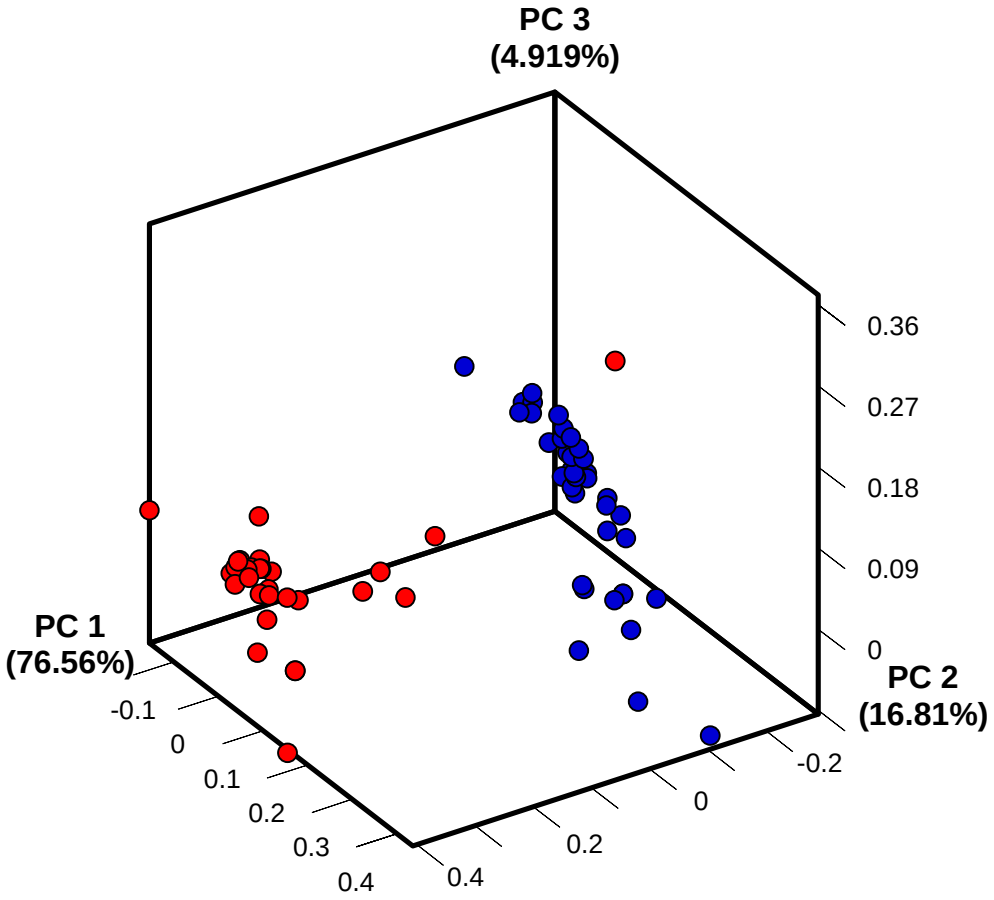

Figure 5.7. PCA score plot using three principal components based on the normalized sensor-response patterns obtained from TNS-based sensors; PC – principal component. In this experiment, HSA (red) and α-antitrypsin (blue) concentrations were not defined during PCA

Herein, a total of five mixtures of HSA and α-antitrypsin at various concentrations were analyzed, i.e., 10 nM HSA – 100 nM α-antitrypsin, 30 nM HSA – 70 nM α-antitrypsin, 50 nM HSA – 50 nM α-antitrypsin, 70 nM HSA – 30 nM α-antitrypsin, and 100 nM HSA – 10 nM α-antitrypsin. The sensor-response patterns (four TNS-based sensors × five protein mixtures × five replicates) obtained from these mixtures were compared with the response patterns obtained from the pure proteins. Hence, the 95 training sets (five protein mixtures × five replicates + six HSA concentrations × five replicates + eight α-antitrypsin concentrations × five replicates) were subjected to PCA and LDA. Output data from PCA of the 19 analytes are plotted with respect to the first two principal components (Figure 5.8). In this analysis, two principal components accounted for more than 99% of variance, and therefore the values of those two principal components were used to calculate the accuracy of analysis using LDA. By using LDA, the array was able to discriminate these proteins and protein mixtures at various concentrations with 100% accuracy. Therefore, we have successfully used these TNS-based sensor arrays for discrimination of protein mixtures.

Interestingly, examination of the PCA plot in Figure 5.8 reveals that there is excellent correlation between PCA clustering patterns and protein/protein mixture concentrations. When the ratio of [HSA]/[α-antitrypsin] for a protein mixture is high, the PCA cluster of the mixture is arranged close to pure HSA clusters. Similarly, if the ratio of [HSA]/[α-antitrypsin] for a protein mixture is low, the PCA cluster corresponding to that mixture will be arranged close to pure α-antitrypsin clusters. Furthermore, the PCA cluster from different mixtures gradually moves from α-antitrypsin towards HSA with increasing [HSA]/[α-antitrypsin].

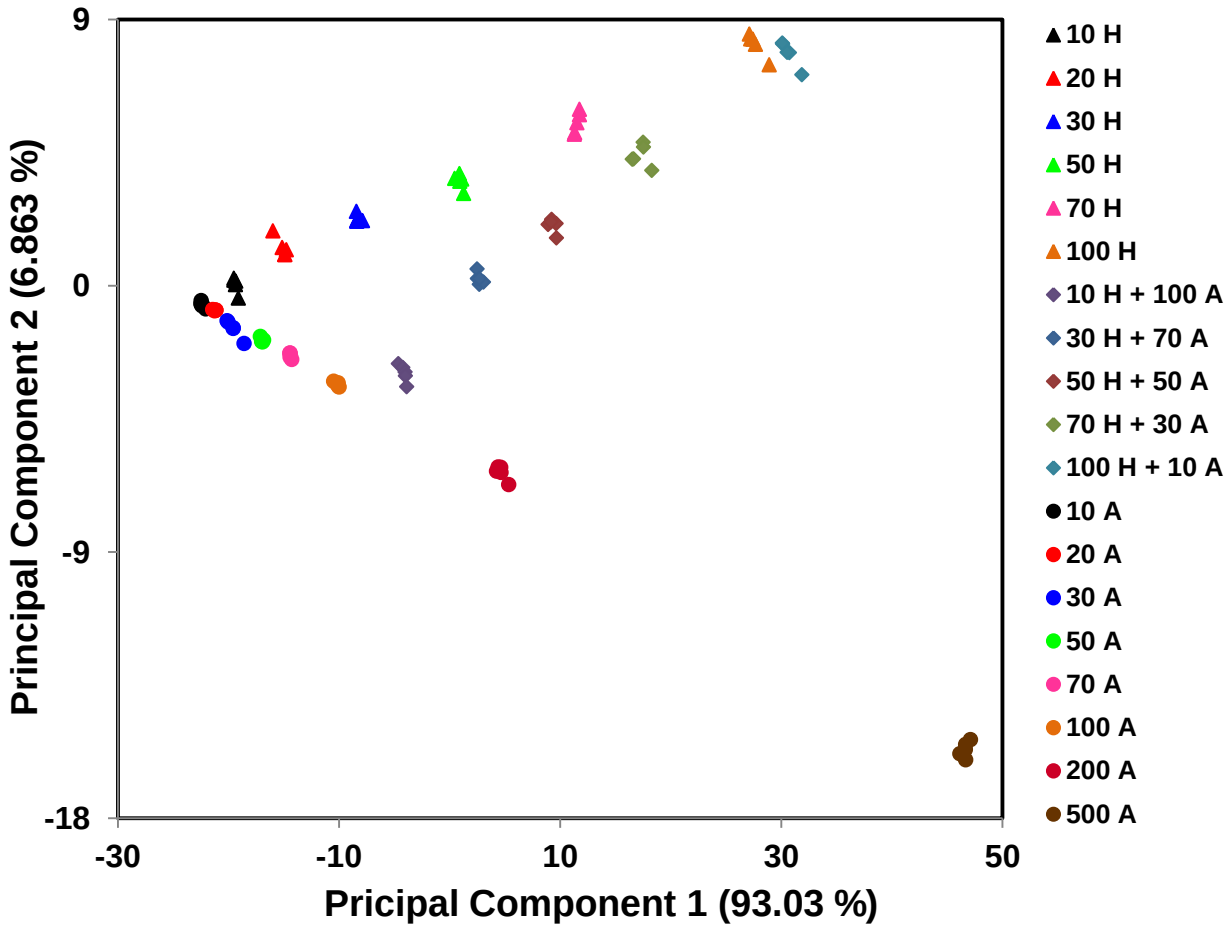

Figure 5.8. PCA score plot using the first two principal components based on the sensor-response patterns obtained from TNS-based sensors. Protein and protein mixture concentrations are listed in the legend. H – HSA; A – α-antitrypsin

Additionally, these correlations suggest that, by employing a large set of training sets which cover a wide range of relative protein concentrations, a predictive model can be generated to discriminate protein mixtures regardless of individual component concentrations. Moreover, it is important to note that even the most efficient sensor array systems, reported to date, have failed to generate a correlation between PCA clustering patterns and protein mixture concentrations.[30] Therefore, from an analytical perspective, this finding shows great promise in further advancing the field of protein sensing.

Finally, in an attempt to study trends in individual sensor responses with respect to HSA and α-antitrypsin concentrations, the relative emission intensity *versus* protein concentration was plotted for all four sensors (Figure 5.9a-d). As calculated from the plots, the four sensor responses for both HSA and α-antitrypsin concentrations were found to be linear with r^2 values of more than 0.99. Hence, the detection limit for HSA and α-antitrypsin was calculated using the equation $3\sigma/m_{sl}$, where σ is the standard deviation of three replicate blank samples, and m_{sl} is the slope of the calibration plot. For HSA, the calibration plot for [4NB][TNS] yielded the lowest detection limit, which was estimated to be ~ 650 pM. The detection limit for α-antitrypsin was estimated to be ~ 1 nM using the calibration plot for $[P_{4444}][TNS]$.

5.4. Conclusion

In this study, we have demonstrated the concept of using a partially selective fluorescent probe, i.e. TNS, for accurate discrimination of proteins and protein mixtures. A set of four TNS-based sensors, fabricated via ionic modification of TNS to produce GUMBOS, was employed in this array-based sensing strategy. These sensors exhibited differential sensor-response patterns depending on the proteins and their concentration levels. These fingerprint fluorescence-response patterns were statistically analyzed using PCA and LDA in order to accurately identify each analyte. First, PCA responses generated from different proteins clustered separately. Second, PCA responses that are responsible for different concentrations of the same protein are clustered according to concentrations. Furthermore, these clusters were arranged such that the concentration of each protein gradually increases when going from left to right along the first principal component. Moreover, we have demonstrated that this sensor approach can discriminate proteins regardless of concentration. In addition, this sensor strategy has the potential to discriminate protein mixtures at various concentrations.

Figure 5.9. Plot of relative fluorescence emission intensity *versus* the concentration of HSA (red), or α-antitrypsin (black) for (A) [4NB][TNS], (B) [P_{4444}][TNS], (C) [BTP][TNS], and (D) [TPP][TNS]. Error bars represent the standard deviations of five replicate measurements (Continues through pages 169-171)

A

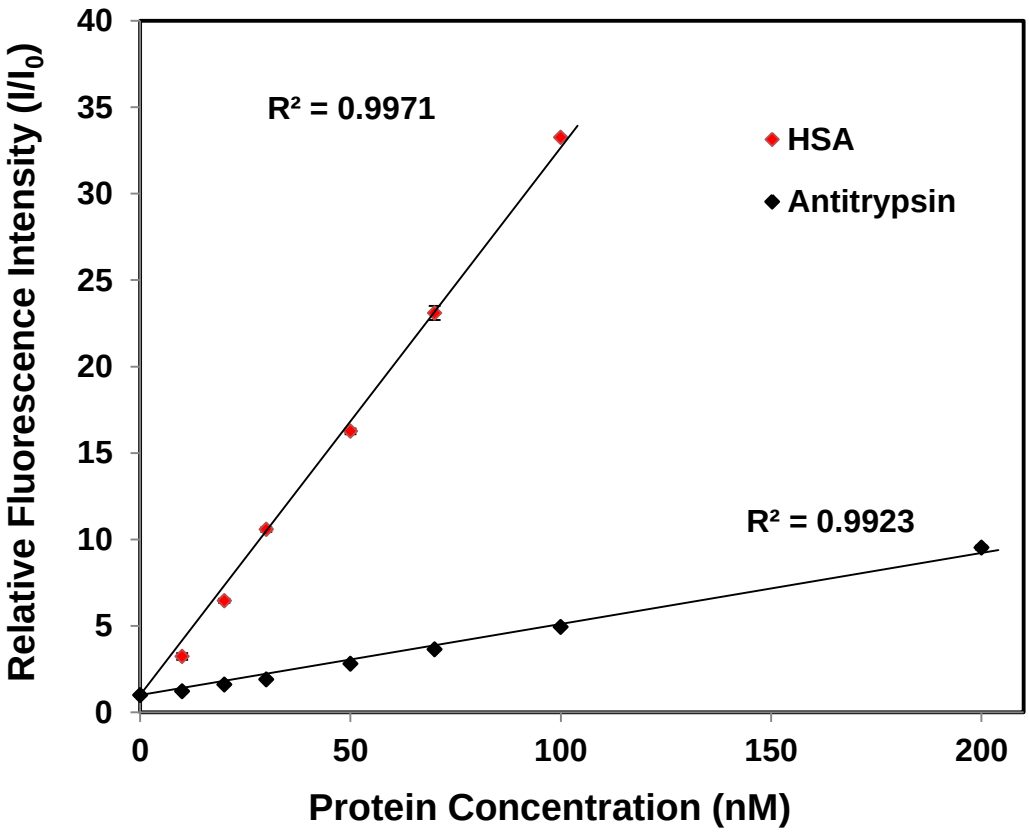
Relative Fluorescence Intensity (I/I0)
Protein Concentration (nM)
R² = 0.9971
R² = 0.9923
HSA
Antitrypsin
0
5
10
15
20
25
30
35
40
0
50
100
150
200

B

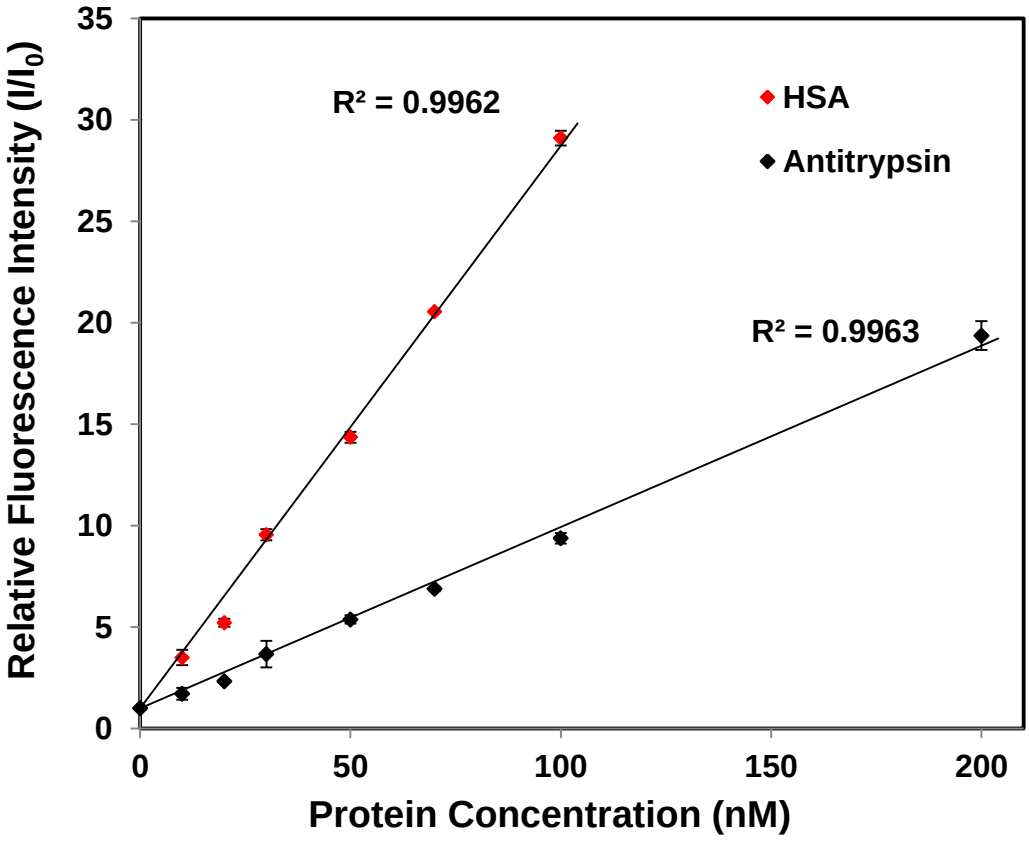
Relative Fluorescence Intensity (I/I0)
Protein Concentration (nM)
R² = 0.9962
R² = 0.9963
HSA
Antitrypsin
0
5
10
15
20
25
30
35
0
50
100
150
200

C

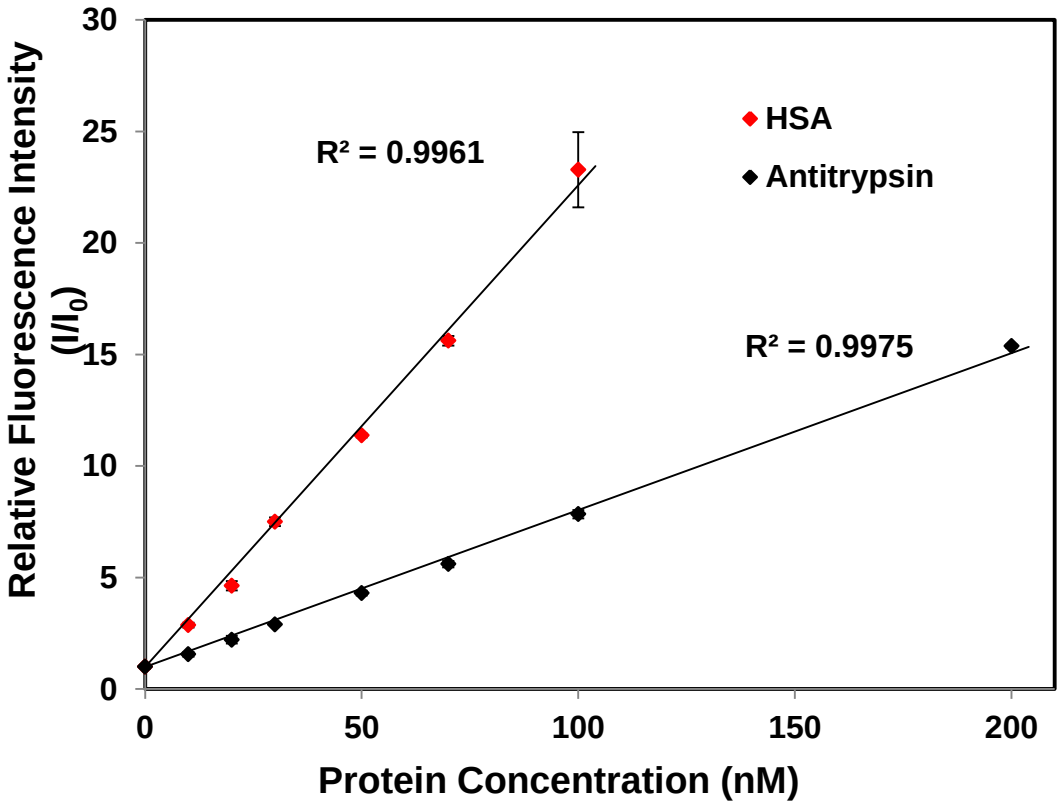
Relative Fluorescence Intensity (I/I0)
Protein Concentration (nM)
HSA
Antitrypsin
R² = 0.9961
R² = 0.9975
0
5
10
15
20
25
30
0
50
100
150
200

D

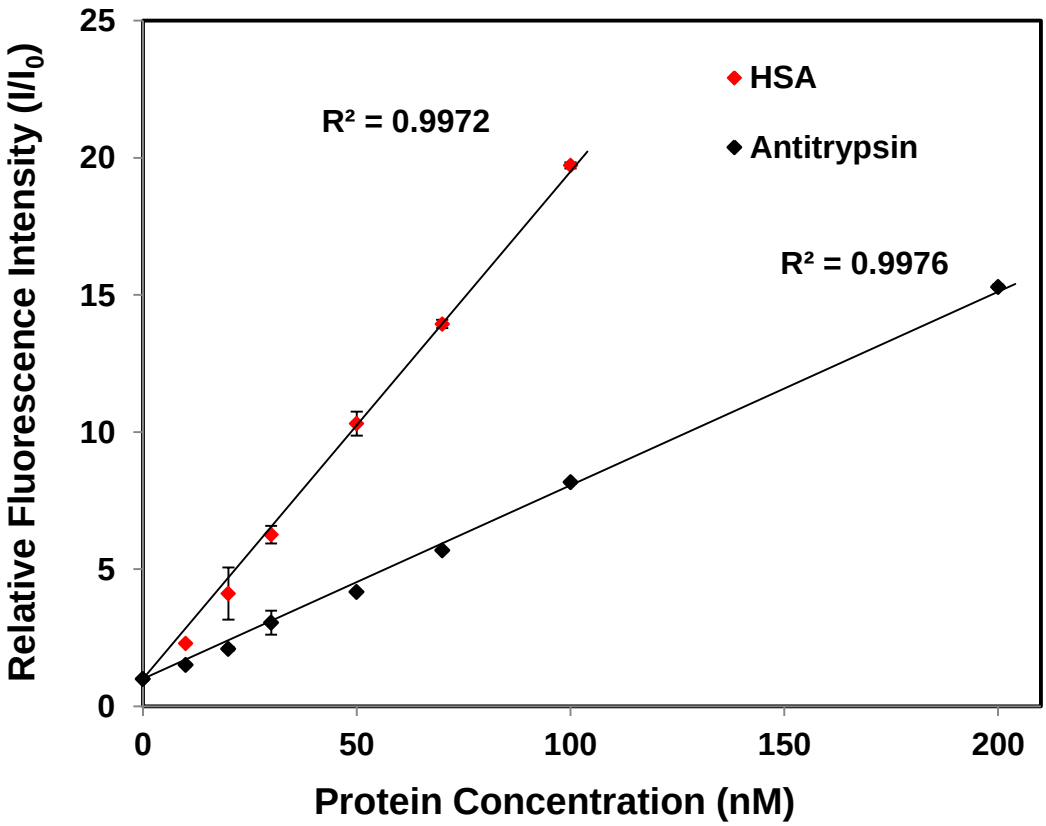
Relative Fluorescence Intensity (I/I0)
Protein Concentration (nM)
HSA
Antitrypsin
R² = 0.9972
R² = 0.9976
0
5
10
15
20
25
0
50
100
150
200

Furthermore, these clusters were arranged such that the concentration of each protein gradually increases when going from left to right along the first principal component. Moreover, we have demonstrated that this sensor approach can discriminate proteins regardless of concentration. In addition, this sensor strategy has the potential to discriminate protein mixtures at various concentrations. Due to excellent correlation between PCA clustering and protein and protein mixture concentrations, this new sensor concept is very promising for discrimination of proteins and protein mixtures with very high selectivity and accuracy.

5.5. References

(1) Kragh-Hansen, U.: Molecular and practical aspects of the enzymatic properties of human serum albumin and of albumin–ligand complexes. *Biochimica et Biophysica Acta (BBA)-General Subjects* **2013**, *1830*, 5535-5544.

(2) Bernardi, M.; Maggioli, C.; Zaccherini, G.: Human albumin in the management of complications of liver cirrhosis. *Critical Care* **2012**, *16*, 211-217.

(3) Kramer, H.; Molitch, M. E.: Screening for kidney disease in adults with diabetes. *Diabetes Care* **2005**, *28*, 1813-1816.

(4) Levey, A. S.; Coresh, J.: Chronic kidney disease. *The Lancet* **2012**, *379*, 165-180.

(5) Gillette, M. A.; Carr, S. A.: Quantitative analysis of peptides and proteins in biomedicine by targeted mass spectrometry. *Nature methods* **2013**, *10*, 28-34.

(6) Li, J.; Zhang, Z.; Rosenzweig, J.; Wang, Y. Y.; Chan, D. W.: Proteomics and bioinformatics approaches for identification of serum biomarkers to detect breast cancer. *Clinical chemistry* **2002**, *48*, 1296-1304.

(7) Baggerly, K. A.; Morris, J. S.; Coombes, K. R.: Reproducibility of SELDI-TOF protein patterns in serum: comparing datasets from different experiments. *Bioinformatics* **2004**, *20*, 777-785.

(8) Shamsi, M. H.; Choi, K.; Ng, A. H.; Wheeler, A. R.: A digital microfluidic electrochemical immunoassay. *Lab on a Chip* **2014**, *14*, 547-554.

(9) Yang, Z.; Zhu, J.; Dai, H.; Li, J.; Shen, J.; Jiao, X.; Hu, X.; Ju, H.: Graphene oxide based ultrasensitive flow-through chemiluminescent immunoassay for sub-picogram level detection of chicken interferon-γ. *Biosensors and Bioelectronics* **2014**, *51*, 356-361.

(10) Lai, G.; Zhang, H.; Tamanna, T.; Yu, A.: Ultrasensitive immunoassay based on electrochemical measurement of enzymatically produced polyaniline. *Analytical chemistry* **2014**, *86*, 1789-1793.

(11) Ren, K.; Wu, J.; Zhang, Y.; Yan, F.; Ju, H.: Proximity hybridization regulated DNA biogate for sensitive electrochemical immunoassay. *Analytical chemistry* **2014**, *86*, 7494-7499.

(12) Chung, C. Y.-S.; Yam, V. W.-W.: Induced Self-Assembly and Forster Resonance Energy Transfer Studies of Alkynylplatinum (II) Terpyridine Complex through Interaction with Water-Soluble Poly (Phenylene Ethynylene Sulfonate) and the Proof-of-Principle Demonstration of This Two-Component Ensemble for Selective Label-Free Detection of Human Serum Albumin. *Journal of the American Chemical Society* **2011**, *133*, 18775-18784.

(13) Tong, H.; Hong, Y.; Dong, Y.; Häussler, M.; Li, Z.; Lam, J. W.; Dong, Y.; Sung, H. H.-Y.; Williams, I. D.; Tang, B. Z.: Protein detection and quantitation by tetraphenylethene-based fluorescent probes with aggregation-induced emission characteristics. *The Journal of Physical Chemistry B* **2007**, *111*, 11817-11823.

(14) Kar, C.; Ojha, B.; Das, G.: A novel amphiphilic thiosemicarbazone derivative for binding and selective sensing of human serum albumin. *Luminescence* **2013**, *28*, 339-344.

(15) Comby, S.; Gunnlaugsson, T.: Luminescent lanthanide-functionalized gold nanoparticles: exploiting the interaction with bovine serum albumin for potential sensing applications. *ACS nano* **2011**, *5*, 7184-7197.

(16) Lacerda, S. H. D. P.; Park, J. J.; Meuse, C.; Pristinski, D.; Becker, M. L.; Karim, A.; Douglas, J. F.: Interaction of gold nanoparticles with common human blood proteins. *ACS nano* **2009**, *4*, 365-379.

(17) Galpothdeniya, W. I. S.; Das, S.; De Rooy, S. L.; Regmi, B. P.; Hamdan, S.; Warner, I. M.: Fluorescein-based ionic liquid sensor for label-free detection of serum albumins. *Rsc Advances* **2014**, *4*, 17533-17540.

(18) Chen, X.-W.; Liu, J.-W.; Wang, J.-H.: A highly fluorescent hydrophilic ionic liquid as a potential probe for the sensing of biomacromolecules. *The Journal of Physical Chemistry B* **2011**, *115*, 1524-1530.

(19) Shu, Y.; Liu, M.; Chen, S.; Chen, X.; Wang, J.: New insight into molecular interactions of imidazolium ionic liquids with bovine serum albumin. *The Journal of Physical Chemistry B* **2011**, *115*, 12306-12314.

(20) Lu, H.; Xu, B.; Dong, Y.; Chen, F.; Li, Y.; Li, Z.; He, J.; Li, H.; Tian, W.: Novel fluorescent pH sensors and a biological probe based on anthracene derivatives with aggregation-induced emission characteristics. *Langmuir* **2010**, *26*, 6838-6844.

(21) Palacios, M. A.; Nishiyabu, R.; Marquez, M.; Anzenbacher, P.: Supramolecular chemistry approach to the design of a high-resolution sensor array for multianion detection in water. *Journal of the American Chemical Society* **2007**, *129*, 7538-7544.

(22) Askim, J. R.; Mahmoudi, M.; Suslick, K. S.: Optical sensor arrays for chemical sensing: the optoelectronic nose. *Chemical Society Reviews* **2013**, *42*, 8649-8682.

(23) Gouma, P.; Sberveglieri, G.: Novel materials and applications of electronic noses and tongues. *MRS bulletin* **2004**, *29*, 697-702.

(24) Galpothdeniya, W. I. S.; McCarter, K. S.; De Rooy, S. L.; Regmi, B. P.; Das, S.; Hasan, F.; Tagge, A.; Warner, I. M.: Ionic liquid-based optoelectronic sensor arrays for chemical detection. *RSC Advances* **2014**, *4*, 7225-7234.

(25) Wright, A. T.; Anslyn, E. V.: Differential receptor arrays and assays for solution-based molecular recognition. *Chemical Society Reviews* **2006**, *35*, 14-28.

(26) Wright, A. T.; Edwards, N. Y.; Anslyn, E. V.; McDevitt, J. T.: The discriminatory power of differential receptor arrays is improved by prescreening—a demonstration in the analysis of tachykinins and similar peptides. *Angewandte Chemie International Edition* **2007**, *46*, 8212-8215.

(27) Zhou, H.; Baldini, L.; Hong, J.; Wilson, A. J.; Hamilton, A. D.: Pattern recognition of proteins based on an array of functionalized porphyrins. *Journal of the American Chemical Society* **2006**, *128*, 2421-2425.

(28) Miranda, O. R.; You, C.-C.; Phillips, R.; Kim, I.-B.; Ghosh, P. S.; Bunz, U. H.; Rotello, V. M.: Array-based sensing of proteins using conjugated polymers. *Journal of the American Chemical Society* **2007**, *129*, 9856-9857.

(29) You, C.-C.; Miranda, O. R.; Gider, B.; Ghosh, P. S.; Kim, I.-B.; Erdogan, B.; Krovi, S. A.; Bunz, U. H.; Rotello, V. M.: Detection and identification of proteins using nanoparticle–fluorescent polymer 'chemical nose'sensors. *Nature Nanotechnology* **2007**, *2*, 318-323.

(30) De, M.; Rana, S.; Akpinar, H.; Miranda, O. R.; Arvizo, R. R.; Bunz, U. H.; Rotello, V. M.: Sensing of proteins in human serum using conjugates of nanoparticles and green fluorescent protein. *Nature chemistry* **2009**, *1*, 461-465.

(31) Bunz, U. H. F.; Kumpf, J.; Freudenberg, J.: Distyrylbenzene-aldehydes: identification of proteins in water. *Analyst* **2015**.

(32) Galpothdeniya, W. I.; Regmi, B. P.; McCarter, K. S.; de Rooy, S. L.; Siraj, N.; Warner, I. M.: Virtual Colorimetric Sensor Array: Single Ionic Liquid for Solvent Discrimination. *Analytical Chemistry* **2015**.

(33) de Rooy, S. L.; Das, S.; Li, M.; El-Zahab, B.; Jordan, A.; Lodes, R.; Weber, A.; Chandler, L.; Baker, G. A.; Warner, I. M.: Ionically Self-Assembled, Multi-Luminophore One-Dimensional Micro-and Nanoscale Aggregates of Thiacarbocyanine GUMBOS. *The Journal of Physical Chemistry C* **2012**, *116*, 8251-8260.

(34) Wright, A.; Li, M.; Ravula, S.; Cadigan, M.; El-Zahab, B.; Das, S.; Baker, G.; Warner, I.: Soft-and hard-templated organic salt nanoparticles with the Midas touch: gold-shelled nanoGUMBOS. *Journal of Materials Chemistry C* **2014**, *2*, 8996-9003.

(35) Sheldrick, G. M.: A short history of SHELX. *Acta Crystallographica Section A: Foundations of Crystallography* **2007**, *64*, 112-122.

(36) Spek, A. L.: Structure validation in chemical crystallography. *Acta Crystallographica Section D: Biological Crystallography* **2009**, *65*, 148-155.

(37) Das, S.; de Rooy, S. L.; Jordan, A. N.; Chandler, L.; Negulescu, I. I.; El-Zahab, B.; Warner, I. M.: Tunable Size and Spectral Properties of Fluorescent NanoGUMBOS in Modified Sodium Deoxycholate Hydrogels. *Langmuir* **2012**, *28*, 757-765.

(38) McClure, W. O.; Edelman, G. M.: Fluorescent Probes for Conformational States of Proteins. I. Mechanism of Fluorescence of 2-p-Toluidinylnaphthalene-6-sulfonate, a Hydrophobic Probe. *Biochemistry* **1966**, *5*, 1908-1919.

(39) Haque, N.; Prabhu, N.: Insights into protein–TNS (2-< i> p</i>-toluidinylnaphthalene-6-sulfonate) interaction using molecular dynamics simulation. *Journal of Molecular Structure* **2014**, *1068*, 261-269.

(40) Hallett, J. P.; Welton, T.: Room-temperature ionic liquids: solvents for synthesis and catalysis. 2. *Chemical Reviews* **2011**, *111*, 3508-3576.

(41) Warner, I. M.; El-Zahab, B.; Siraj, N.: Perspectives on Moving Ionic Liquid Chemistry into the Solid Phase. *Analytical chemistry* **2014**, *86*, 7184-7191.

(42) Del Pópolo, M. G.; Voth, G. A.: On the structure and dynamics of ionic liquids. *The Journal of Physical Chemistry B* **2004**, *108*, 1744-1752.

(43) Yung, K. Y.; Schadock-Hewitt, A. J.; Hunter, N. P.; Bright, F. V.; Baker, G. A.: 'Liquid litmus': chemosensory pH-responsive photonic ionic liquids. *Chemical Communications* **2011**, *47*, 4775-4777.

(44) Edelman, G. M.; McClure, W. O.: Fluorescent probes and the conformation of proteins. *Accounts of Chemical Research* **1968**, *1*, 65-70.

(45) Anderson, N. L.; Anderson, N. G.: The human plasma proteome history, character, and diagnostic prospects. *Molecular & cellular proteomics* **2002**, *1*, 845-867.

CHAPTER 6: CONCLUSIONS AND FUTURE WORK

6.1. Conclusions

The research work presented in this dissertation is primarily focused on the development of novel sensors and sensor array strategies. These sensor approaches are demonstrated to be extremely useful for facile and inexpensive detection and discrimination of analytes. Two classes of materials were investigated for development of sensors and sensor arrays: ionic liquids (ILs) and a ***g***roup of ***u***niform ***m***aterials ***b***ased on ***o***rganic ***s***alts (GUMBOS). Physiochemical properties of these materials are easily tuned by altering either the cation or the anion through ionic modification. As compared to traditional covalent modification reactions, ionic modifications are extremely simple, one-step, high product yield, and often produce a single byproduct which can be separated by water washing. The ILs and GUMBOS, which are used in this dissertation, are designed to display two different functionalities from the respective cations and anions. As an example, the 12 ILs discussed in Chapter 2 display hydrophobic properties primarily because of the cation, whereas the anions are mostly responsible for the sensing properties.

In Chapter 2, a series of 12 ILs were used to fabricate sensor arrays using different matrices in order to discriminate analytes in both aqueous and vapor phases. In addition, fabrication of an IL-based wearable sensor array was demonstrated using cotton threads as matrix. Fabrication of an IL-based sensor for highly selective and sensitive detection of serum albumins is discussed in Chapter 3. In Chapter 4, a group of closely related alcohols and alcohol mixtures were discriminated by use of a virtual sensor array based on a single IL. Finally, the concept of using GUMBOS for discrimination of proteins and protein mixtures were investigated in Chapter 5. Overall, the sensors and sensor arrays approaches, which are based on ILs and

GUMBOS, are discovered to be very promising for detection and discrimination of a wide range of analytes both in both gas and liquid phase.

6.2. Future Work

Fundamental studies based on colorimetric IL sensor arrays have been completed and were recently published in *RSC Advances* and *Analytical Chemistry* (Chapters 2 and 4). The second part of these studies involves development of more facile and inexpensive IL sensor arrays that are capable of detecting and identifying a wide variety of analytes with higher degree of sensitivity and selectivity. In this regard, new types of ILs should be tested, in addition to pH indicator dye-based ILs, which can exhibit non-specific color-changes in the presence of different chemical species such as volatile-organic compounds (VOCs). The incorporation of ILs with different functionalities improves the dimensionality of sensor arrays, which is extremely important in discrimination of closely related analytes or complex analyte mixtures. It is also important to employ new techniques for printing these sensor arrays on different matrices in order to improve their applicability, sensitivity, and selectivity.

In addition, I have introduced and demonstrated a new approach to fabricate wearable sensor arrays using ILs (Chapter 2). This study is very promising, and overcomes a lot of limitations that are associated with the fabrication of traditional wearable sensor materials. The IL-based wearable sensor arrays are applicable in both aqueous- and gaseous-phase application. However, one of the limitations with these sensors is that they are not washable using detergents. Therefore, future studies are required to investigate new approaches that help to improve the washability of the proposed wearable sensor arrays.

The work related to sensing of proteins in aqueous solutions using ILs and GUMBOS are demonstrated in Chapters 3 and 5. These studies display true potential for developing rapid, facile and inexpensive sensors for the detection of proteins with higher sensitivity and selectivity. The next goal of these studies is to further investigate the interactions between proteins and ILs/GUMBOS, and subsequently apply these sensor materials to identify various proteins directly in biological samples, which is tremendously important for detection of disease states in human at early stages.

APPENDIX A: SUPPORTING INFORMATION FOR CHAPTER 2

Table A1. List of misclassifications by discriminant model based on three principal component, under cross-classification

Substance	Misclassified as Substance	Number of cases
pH1	pH7	1
pH4	pH1	1
pH4	pH7	2
pH10	pH7	1
pH13	pH7	2
CH_3COOH	CF_3COOH	1
HCl	CF_3COOH	2
HCOOH	CF_3COOH	3
Diethylamine	Triethylamine	1
DMF	Pyridine	1
Methylimidazole	CF_3COOH	1
Ammonia	Diethylamine	1
Pyridine	DMF	2
Triethylamine	Ammonia	1
Triethylamine	Diethylamine	1
Total Number of Misclassifications		21

Figure A1. Appearance of ILs (continues through pages 181-185)

$[P_{66614}]_2[PR]$

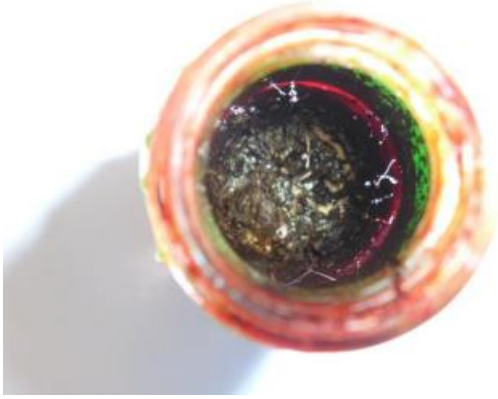

$[P_{66614}]_2[BY]$

$[P_{66614}]_2[BCG]$

$[P_{66614}]_2[mCP]$

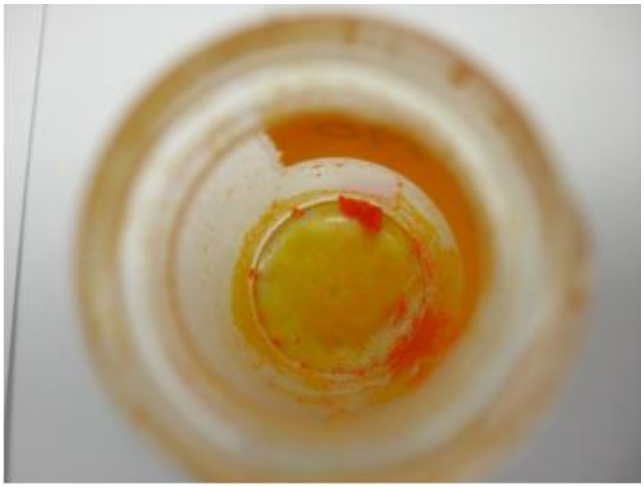

$[P_{66614}][MP]$

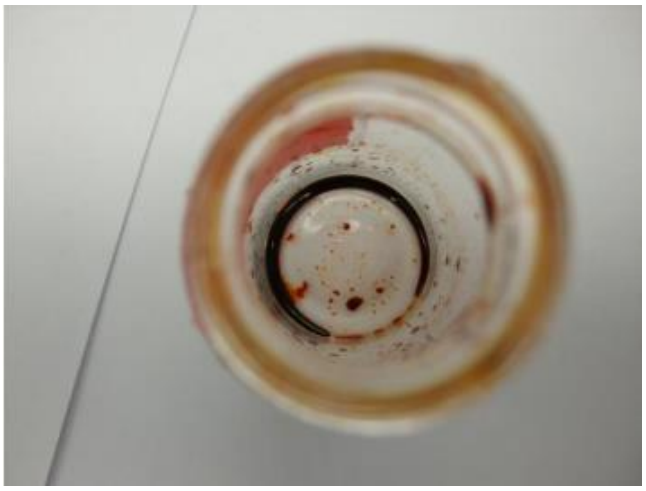

$[P_{66614}][MR]$

$[P_{66614}]_2[Xyl]$

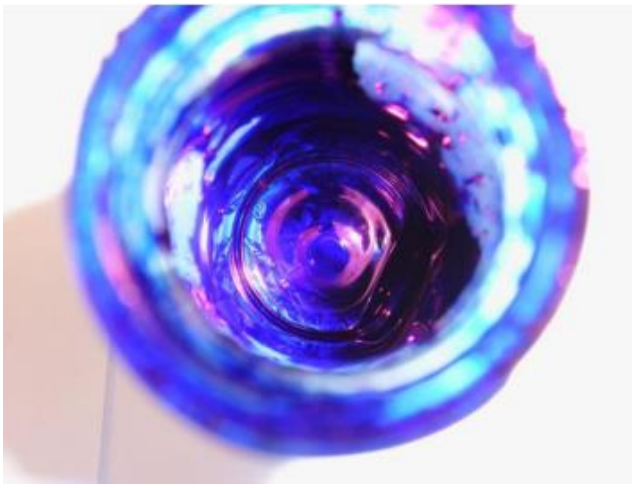

$[P_{66614}]_2[BPB]$

$[P_{66614}]_2[Thy]$

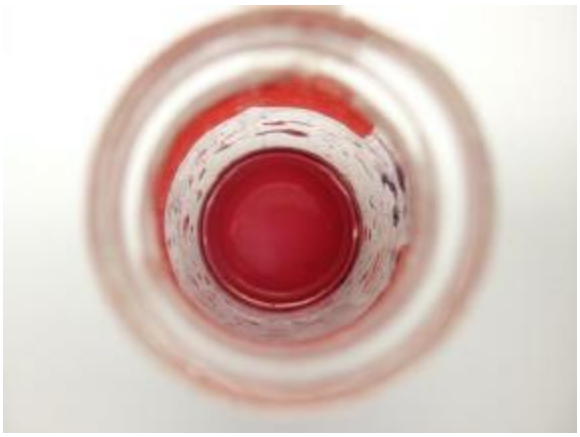

$[P_{66614}]_2[FFT]$

$[P_{66614}]_2[ClR]$

$[P_{66614}]_2[BTB]$

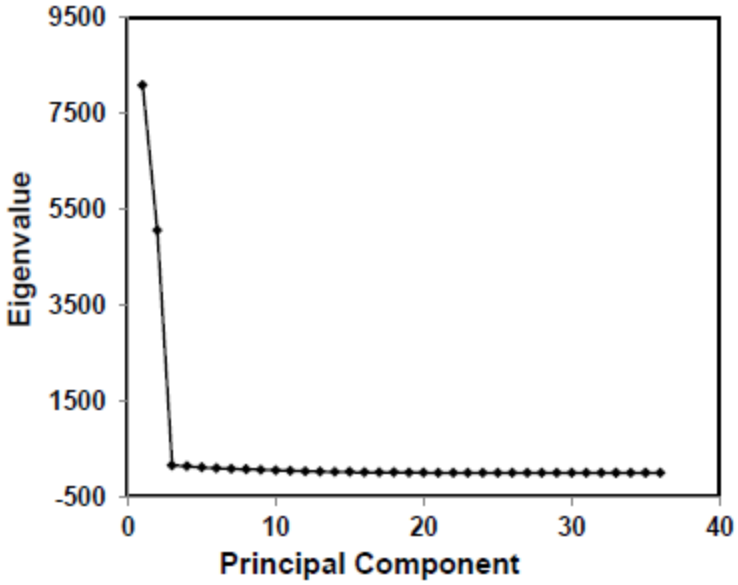

B

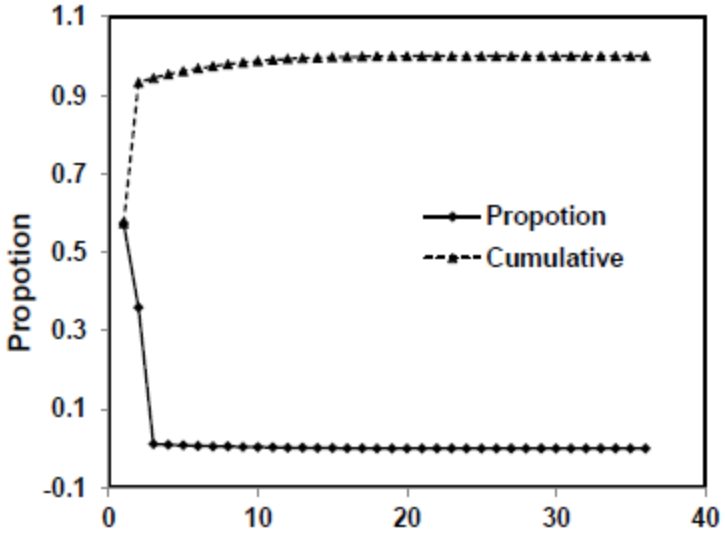

Figure A2. (A)Scree plot and (B) cumulative proportion of variability accounted for by the principal components obtained from the color change profile for the identification of cigarette smoke of Marlboro® red, Crowns® and Camel® by using filter paper based ionic liquid sensor arrays

APPENDIX B: SUPPORTING INFORMATION FOR CHAPTER 3

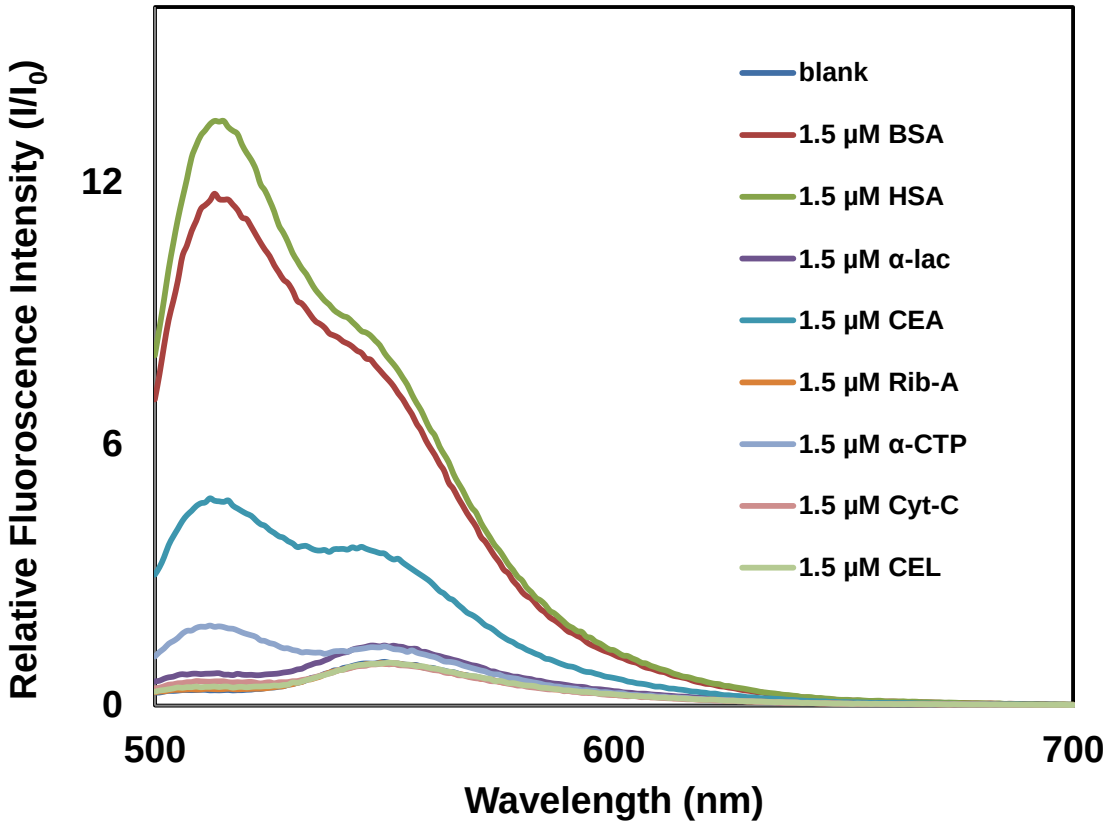

Figure B1. Fluorescence emission spectra (λ_{ex} – 490 nm) of 40 μM $[P_{66614}]_2[FL]$ nanodroplets in the presence of same concentration (1.5 μM) of different albumins and non-albumins

Figure B2. Fluorescence emission spectra (λ_{ex} = 490 nm) of 40 µM (A) Na_2FL, (B) $[TPP]_2[FL]$ and (C) $[4NB]_2[FL]$ with eight different proteins at the concentration of 1.5 µM (continues through 188-190)

A

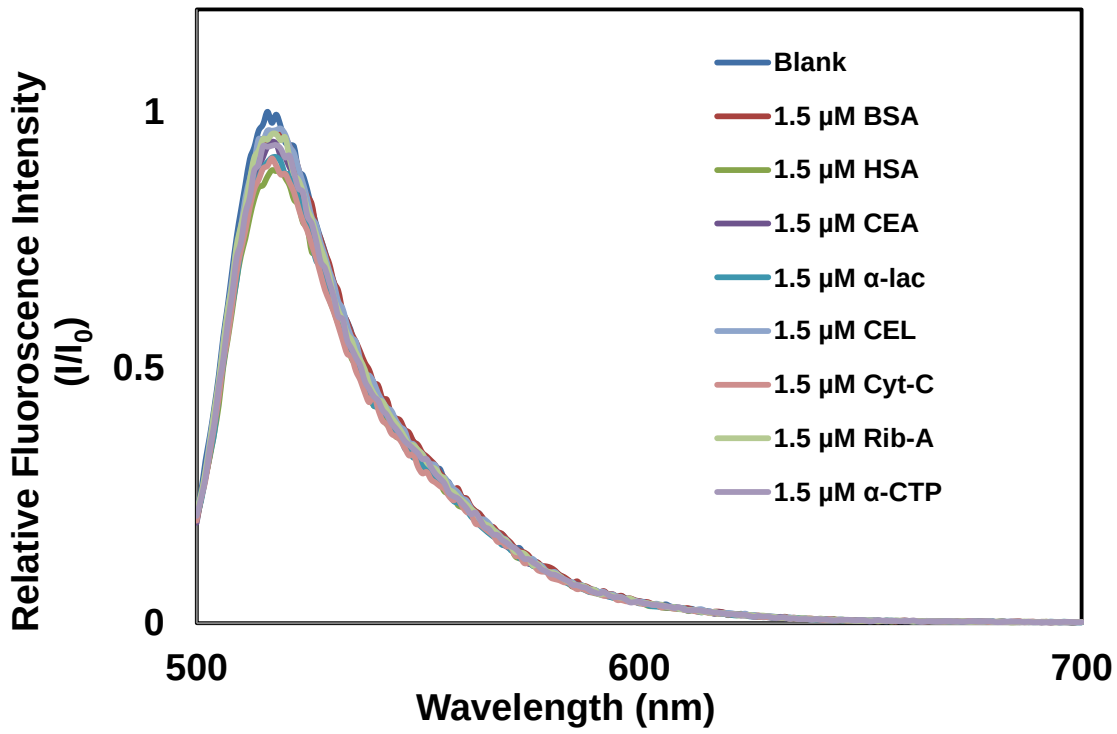
Relative Fluorescence Intensity (I/I0)
1
0.5
0
500
600
700
Wavelength (nm)
Blank
1.5 μM BSA
1.5 μM HSA
1.5 μM CEA
1.5 μM α-lac
1.5 μM CEL
1.5 μM Cyt-C
1.5 μM Rib-A
1.5 μM α-CTP

B

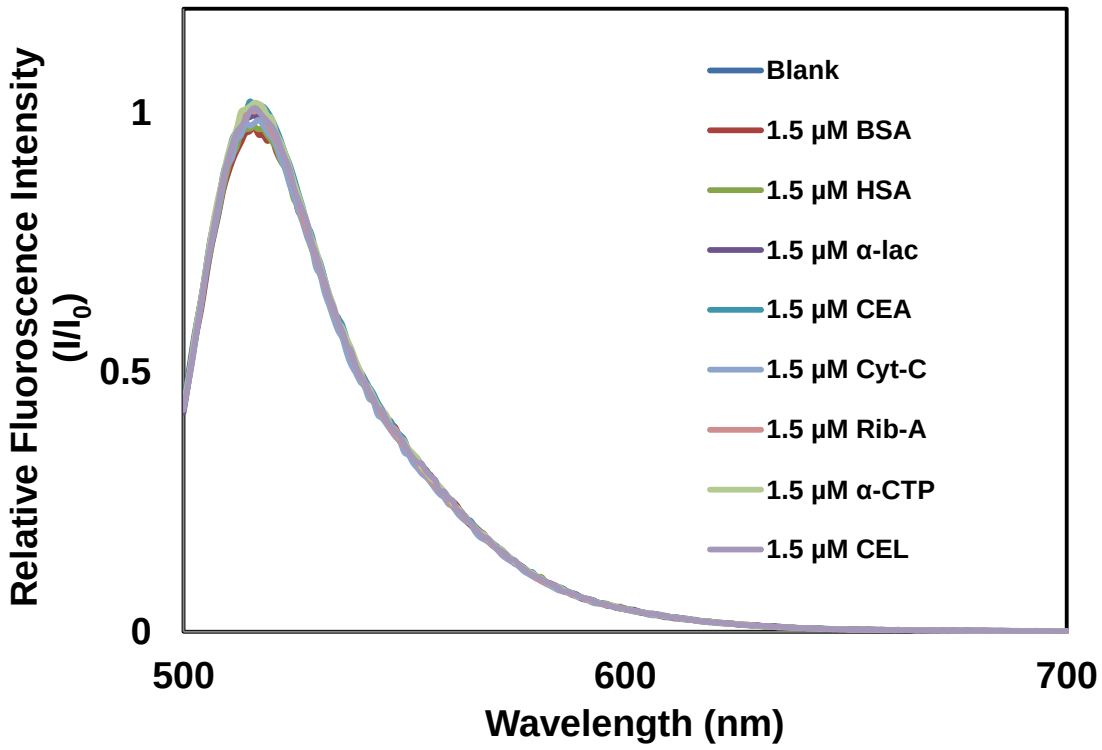
Relative Fluorescence Intensity (I/I0)
1
0.5
0
500
600
700
Wavelength (nm)
Blank
1.5 μM BSA
1.5 μM HSA
1.5 μM α-lac
1.5 μM CEA
1.5 μM Cyt-C
1.5 μM Rib-A
1.5 μM α-CTP
1.5 μM CEL

C

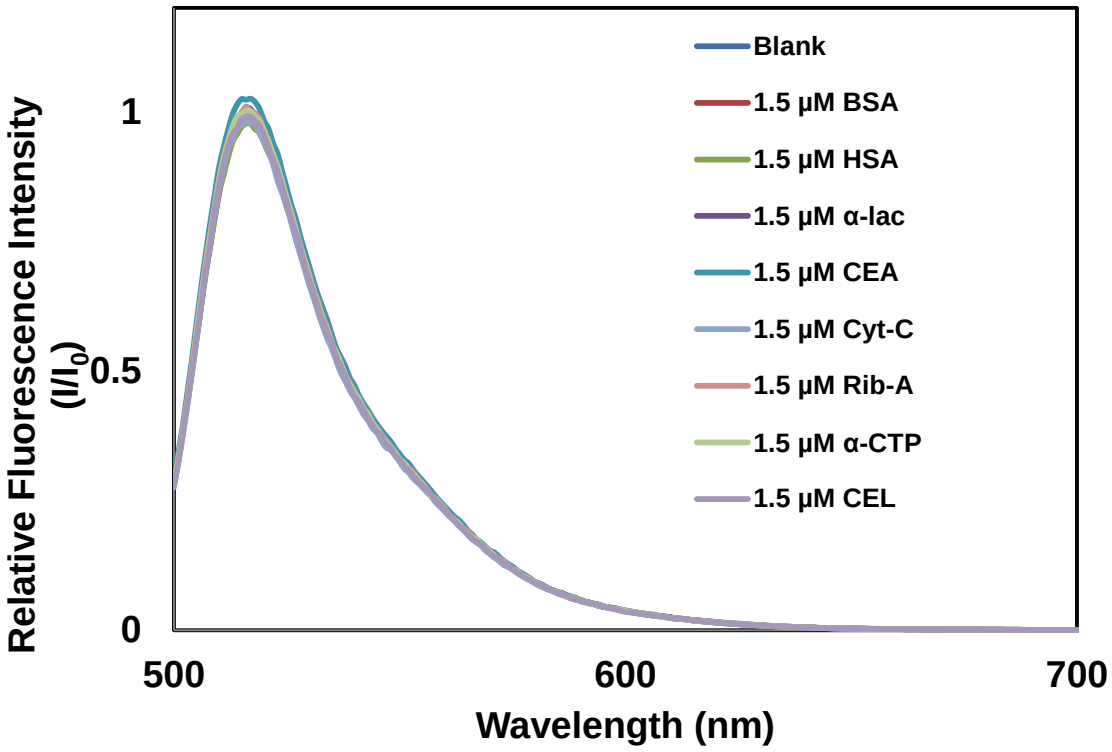
Relative Fluorescence Intensity (I/I0)
1
0.5
0
500
600
700
Wavelength (nm)
Blank
1.5 μM BSA
1.5 μM HSA
1.5 μM α-lac
1.5 μM CEA
1.5 μM Cyt-C
1.5 μM Rib-A
1.5 μM α-CTP
1.5 μM CEL

Figure B3. Fluorescence emission spectra (λ_{ex} = 490 nm) of (a) Eosin B, (b) Eosin Y, (c) Phloxine B (d) Erythrosin B and, (e) Rose Bengal nanoparticles dispersed in different concentrations of BSA (continues through pages 191-194)

A

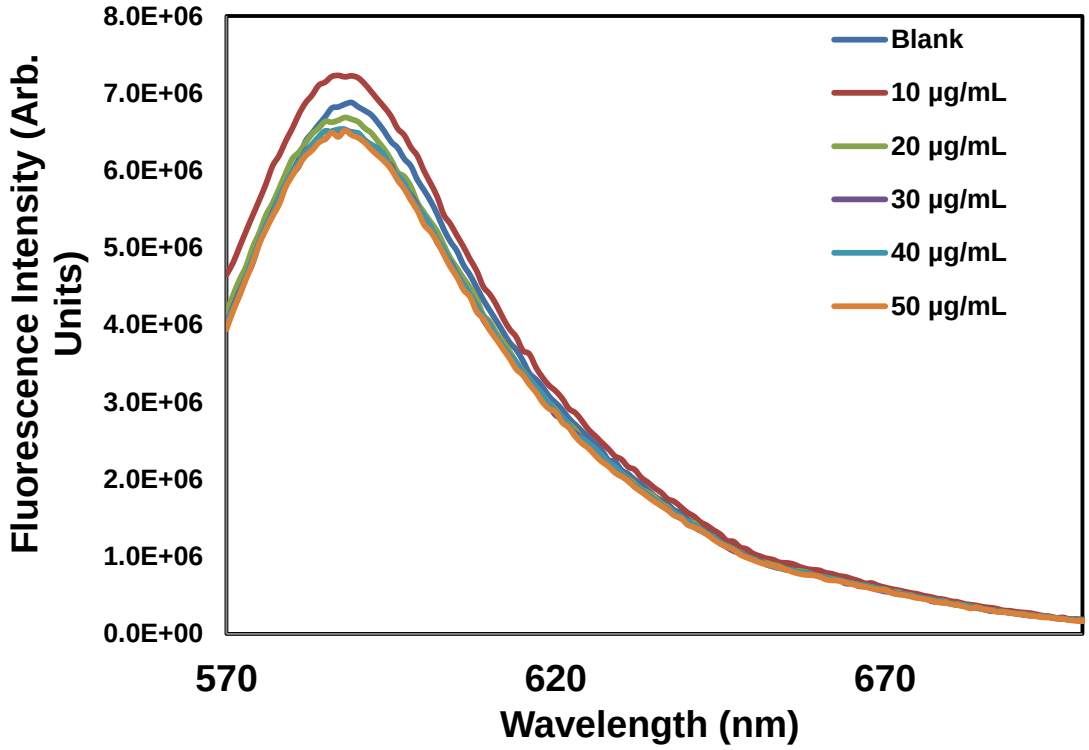
8.0E+06
7.0E+06
6.0E+06
5.0E+06
4.0E+06
3.0E+06
2.0E+06
1.0E+06
0.0E+00
Fluorescence Intensity (Arb. Units)
570
620
670
Wavelength (nm)
Blank
10 µg/mL
20 µg/mL
30 µg/mL
40 µg/mL
50 µg/mL

B

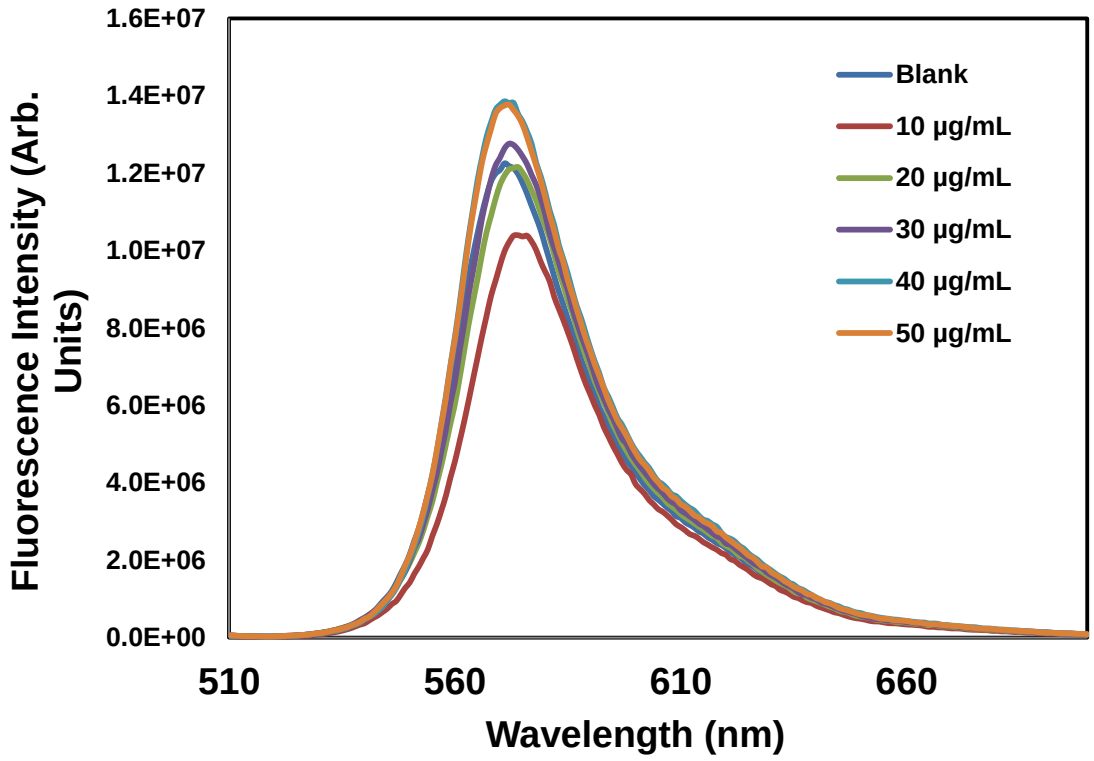
1.6E+07
1.4E+07
1.2E+07
1.0E+07
8.0E+06
6.0E+06
4.0E+06
2.0E+06
0.0E+00
Fluorescence Intensity (Arb. Units)
510
560
610
660
Wavelength (nm)
Blank
10 µg/mL
20 µg/mL
30 µg/mL
40 µg/mL
50 µg/mL

C

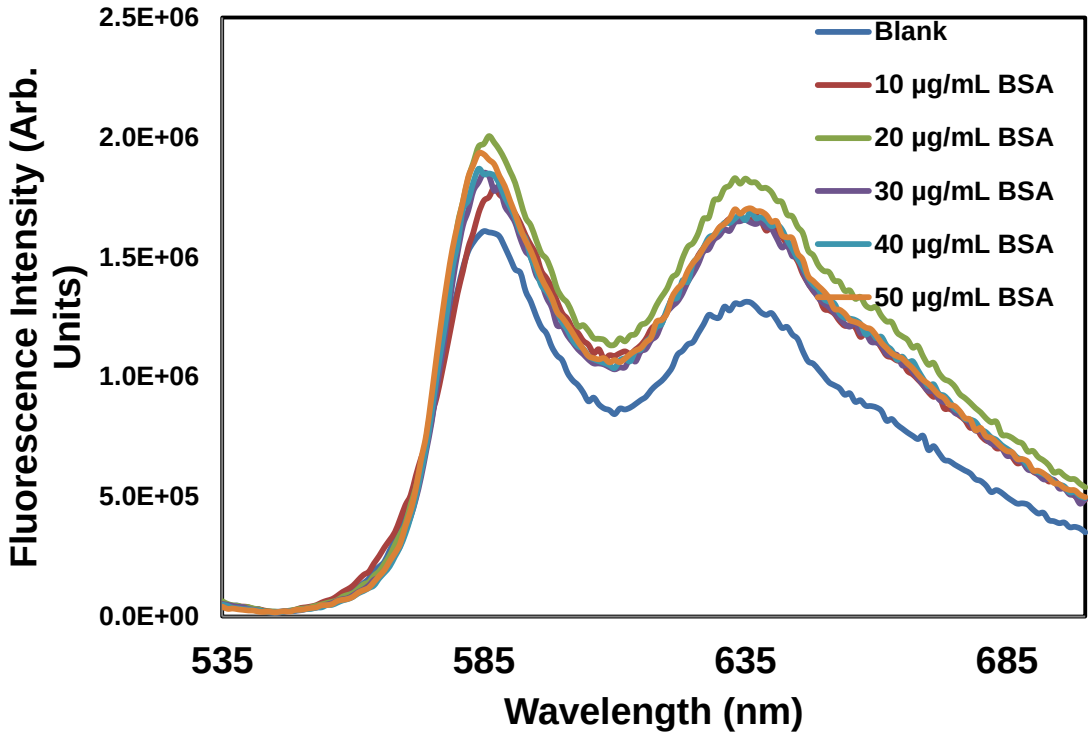
2.5E+06
2.0E+06
1.5E+06
1.0E+06
5.0E+05
0.0E+00
Fluorescence Intensity (Arb. Units)
535
585
635
685
Wavelength (nm)
Blank
10 µg/mL BSA
20 µg/mL BSA
30 µg/mL BSA
40 µg/mL BSA
50 µg/mL BSA

D

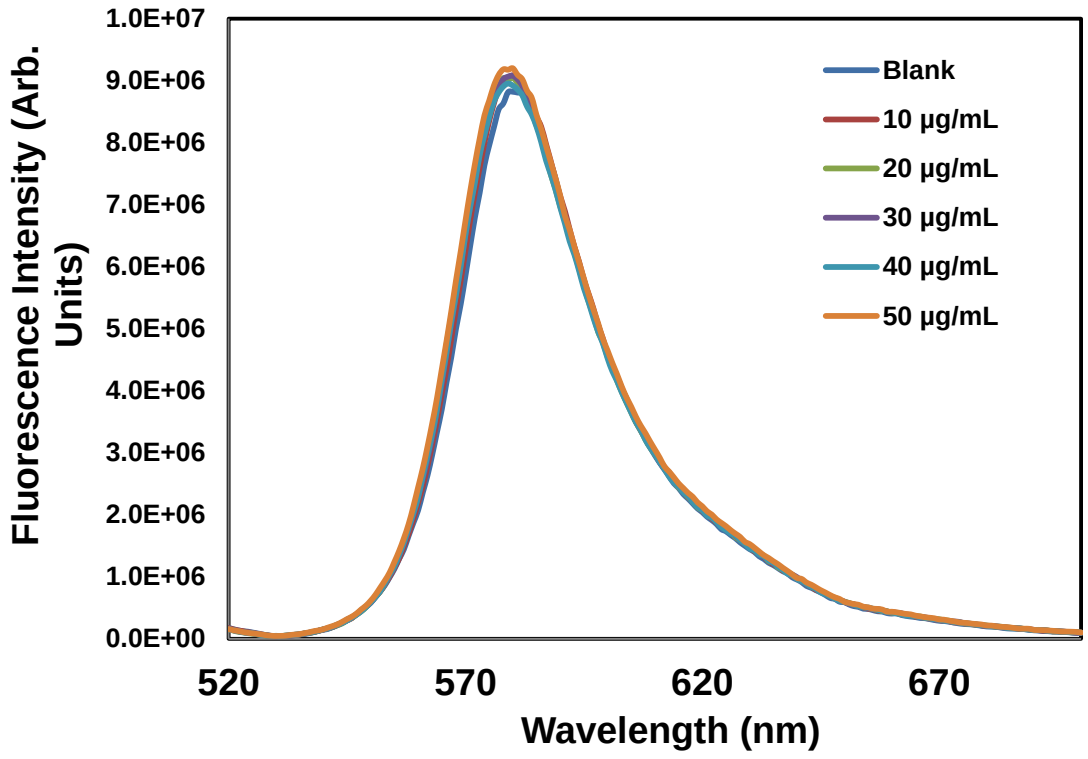
1.0E+07
9.0E+06
8.0E+06
7.0E+06
6.0E+06
5.0E+06
4.0E+06
3.0E+06
2.0E+06
1.0E+06
0.0E+00
Fluorescence Intensity (Arb. Units)
520
570
620
670
Wavelength (nm)
Blank
10 µg/mL
20 µg/mL
30 µg/mL
40 µg/mL
50 µg/mL

E

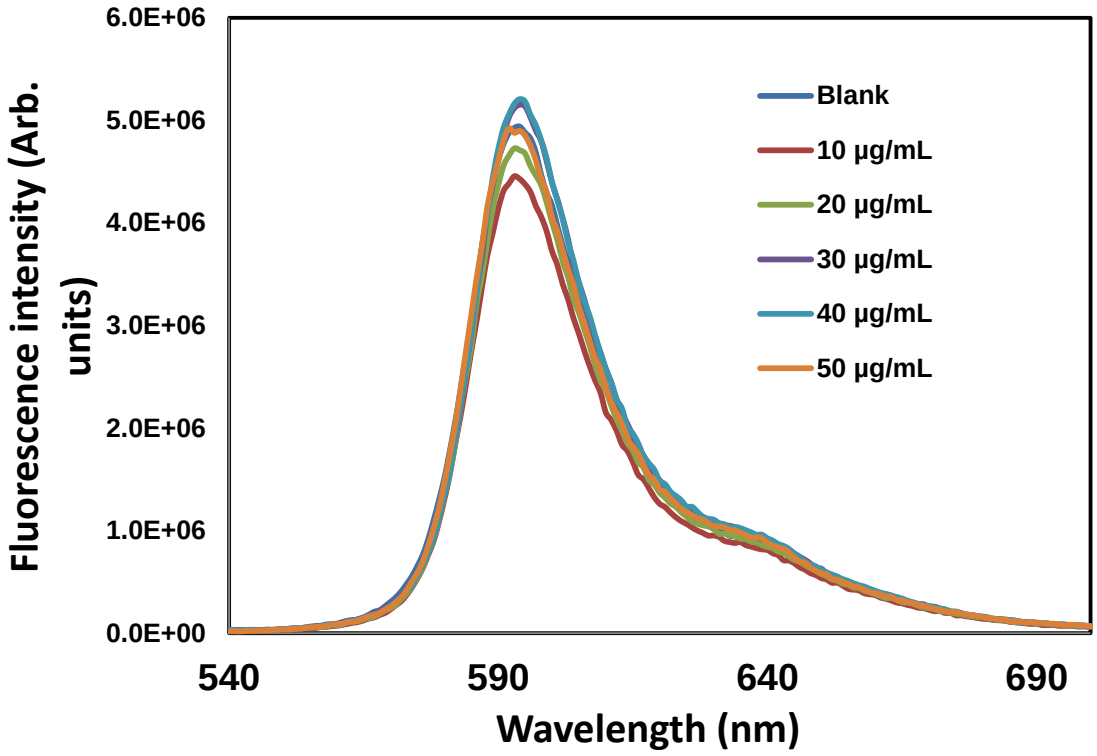
6.0E+06
5.0E+06
4.0E+06
3.0E+06
2.0E+06
1.0E+06
0.0E+00
Fluorescence intensity (Arb. units)
540
590
640
690
Wavelength (nm)
Blank
10 µg/mL
20 µg/mL
30 µg/mL
40 µg/mL
50 µg/mL

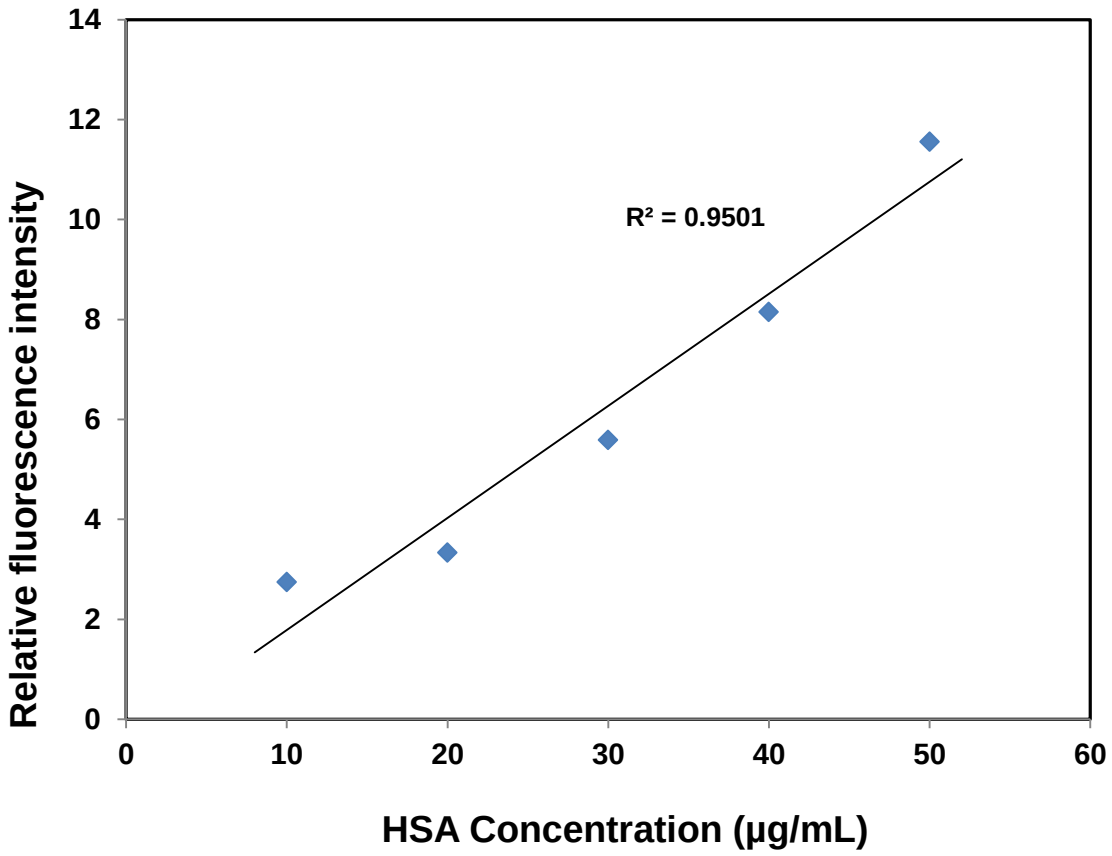

Figure B4. Relationship between relative fluorescence intensity at 512 nm and HSA concentration in human serum. Human serum samples were diluted for 1000 times before analysis. (concentration of $[P_{66614}]_2$[FL]- 24 µM)

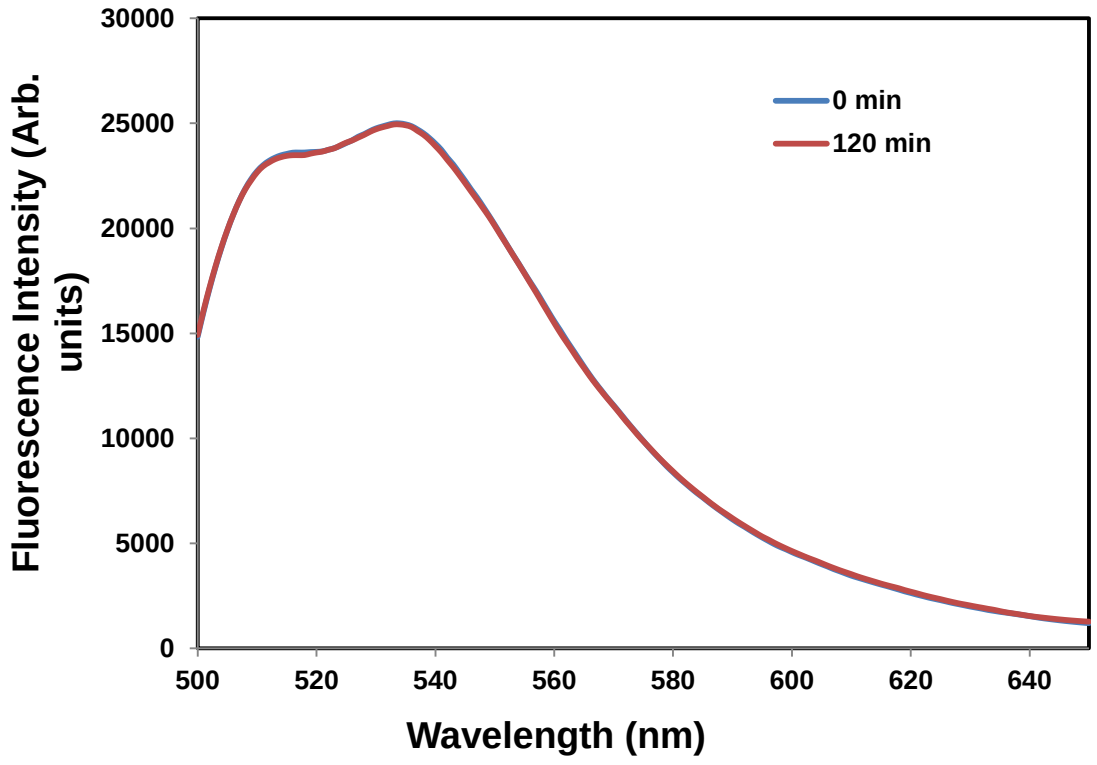

Figure B5. The fluorescence emission spectra (λ_{ex} – 490 nm) of 24 µM dispersions of $[P_{66614}]_2[FL]$ at 0 and 120 minutes

APPENDIX C: SUPPORTING INFORMATION FOR CHAPTER 5

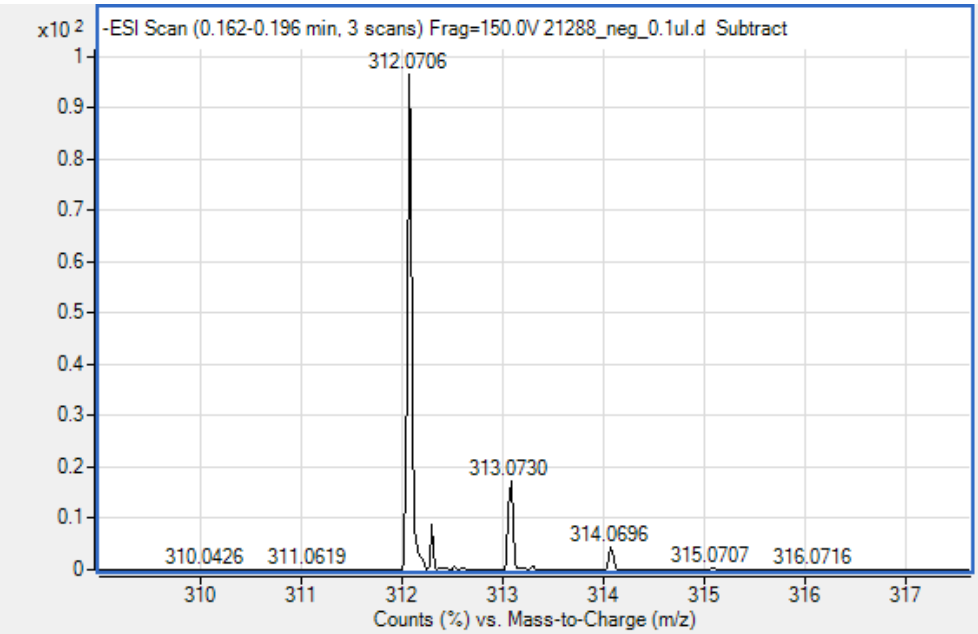

Figure C1-1A. Electrospray ionization mass spectrum in negative ion mode for TNS

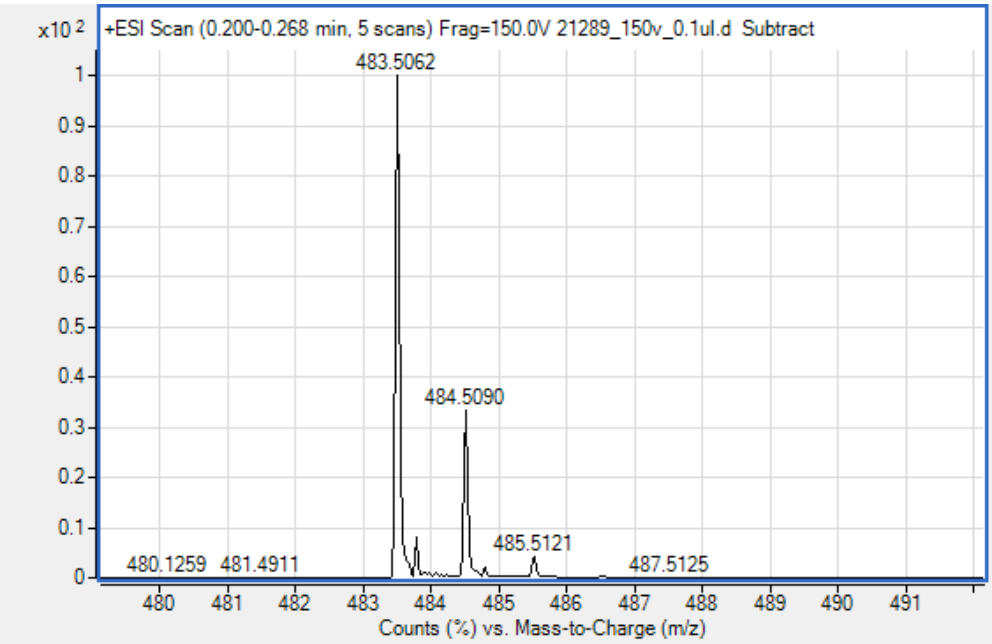

Figure C1-2A. Electrospray ionization mass spectrum in positive ion mode for $[P_{66614}][TNS]$

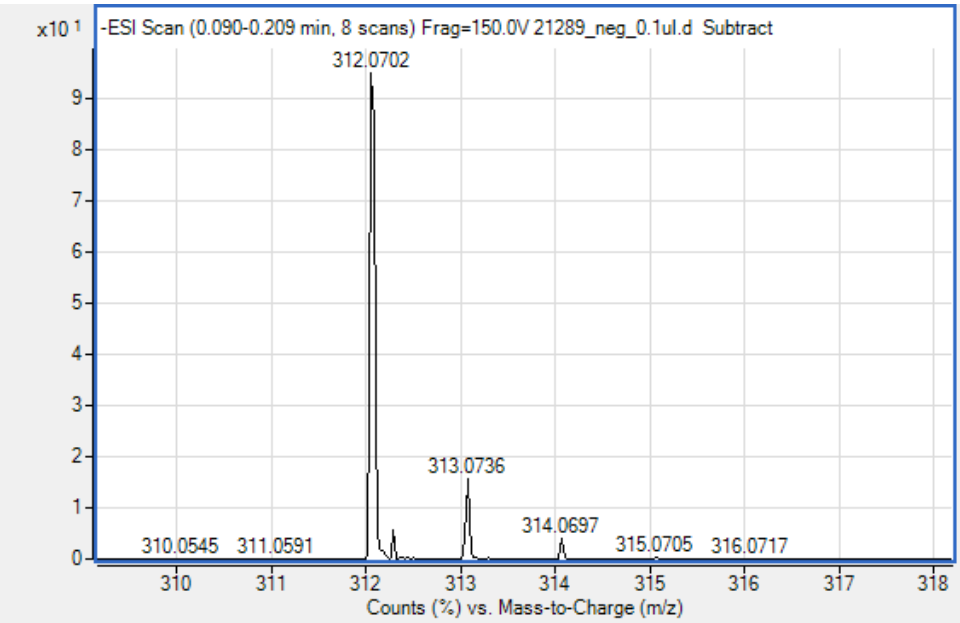

Figure C1-2B. Electrospray ionization mass spectrum in negative ion mode for $[P_{66614}][TNS]$

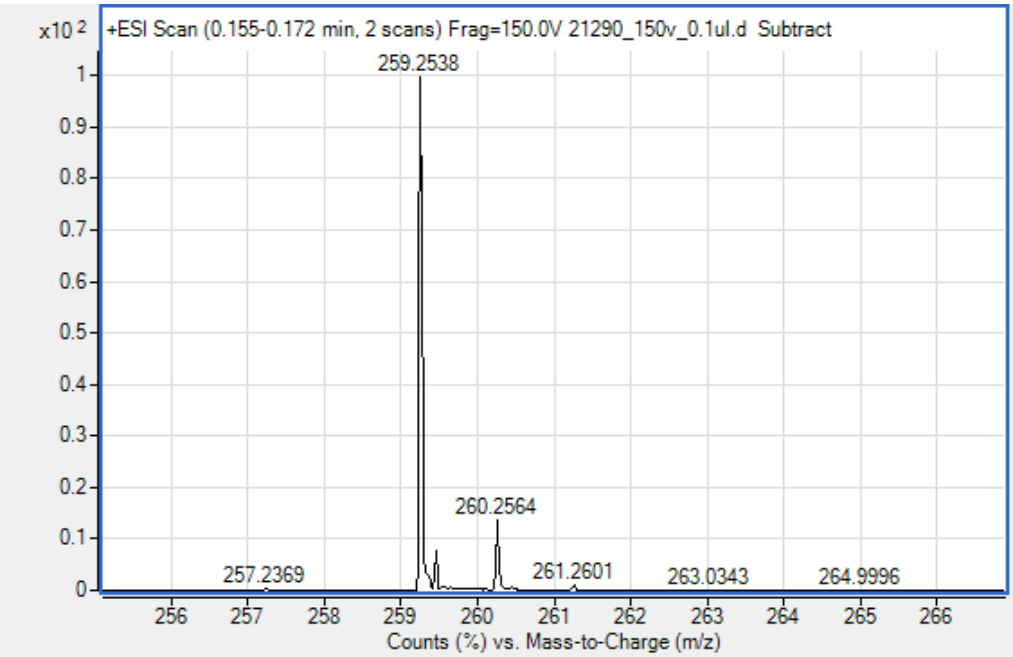

Figure C1-3A. Electrospray ionization mass spectrum in positive ion mode for $[P_{4444}][TNS]$

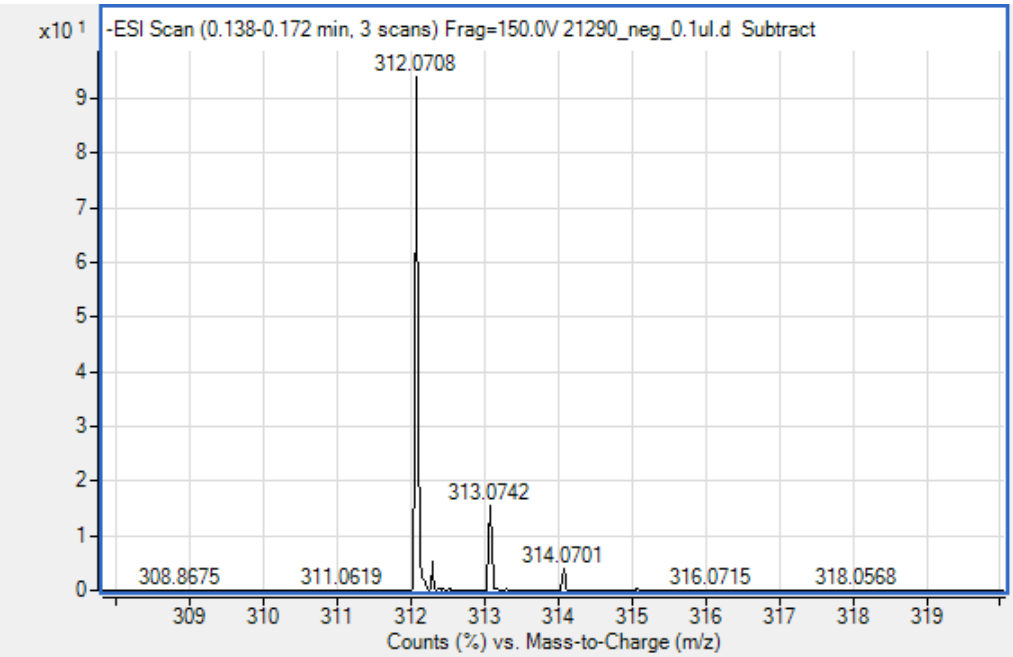

Figure C1-3B. Electrospray ionization mass spectrum in negative ion mode for $[P_{4444}][TNS]$

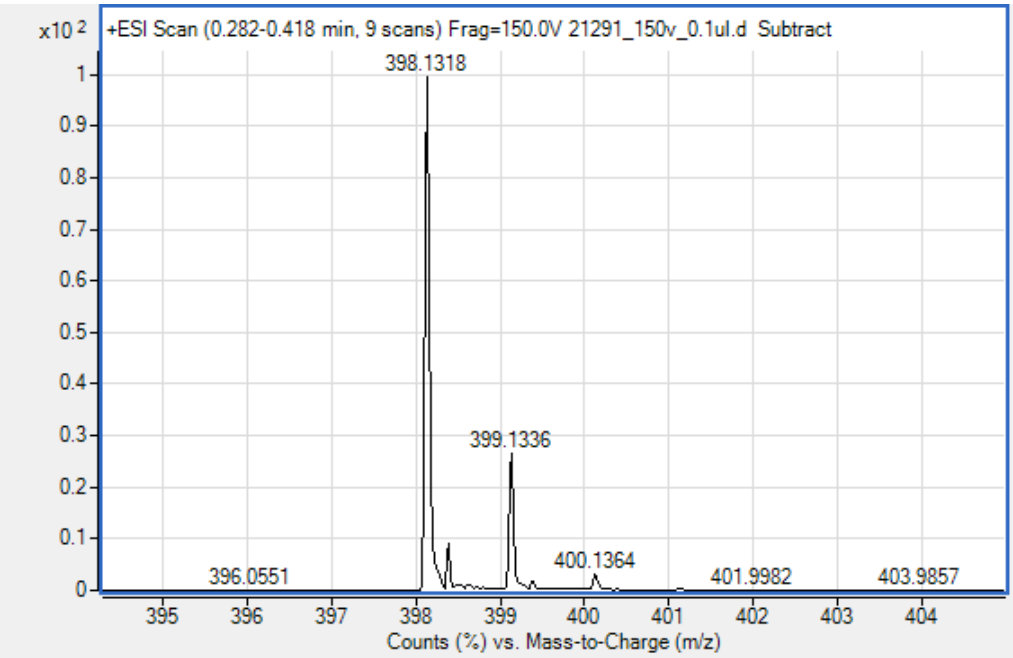

Figure C1-4A. Electrospray ionization mass spectrum in positive ion mode for [4NB][TNS]

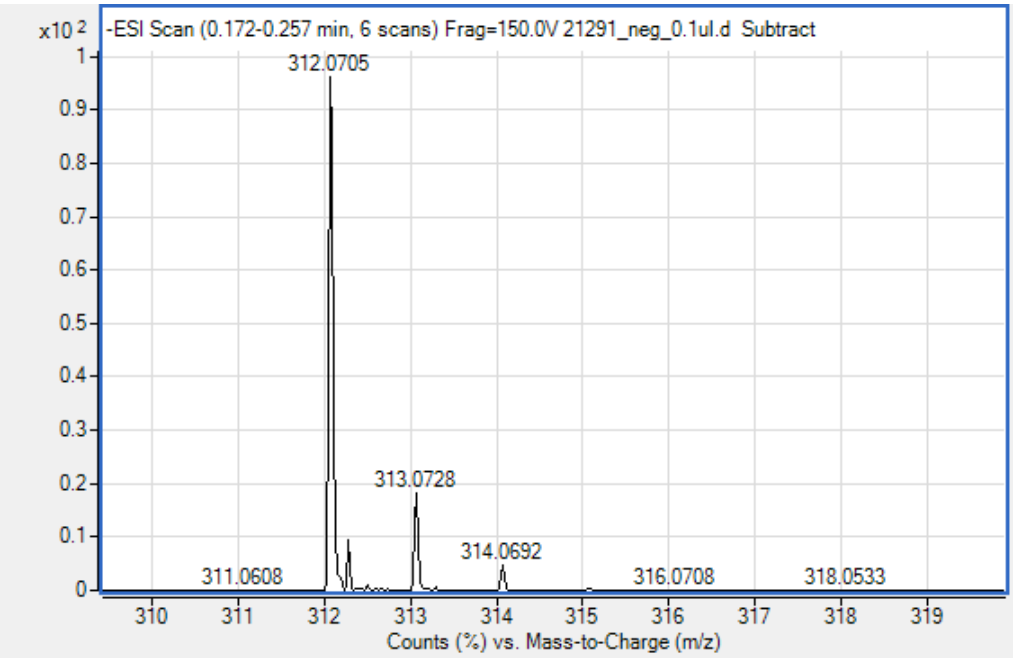

Figure C1-4B. Electrospray ionization mass spectrum in negative ion mode for [4NB][TNS]

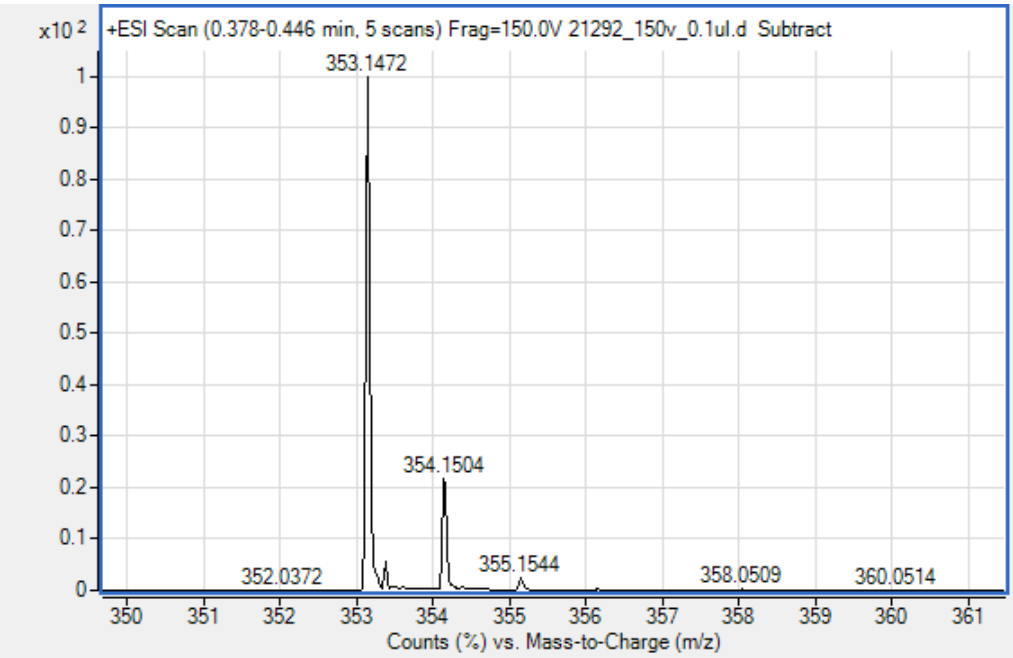

Figure C1-5A. Electrospray ionization mass spectrum in positive ion mode for [BTP][TNS]

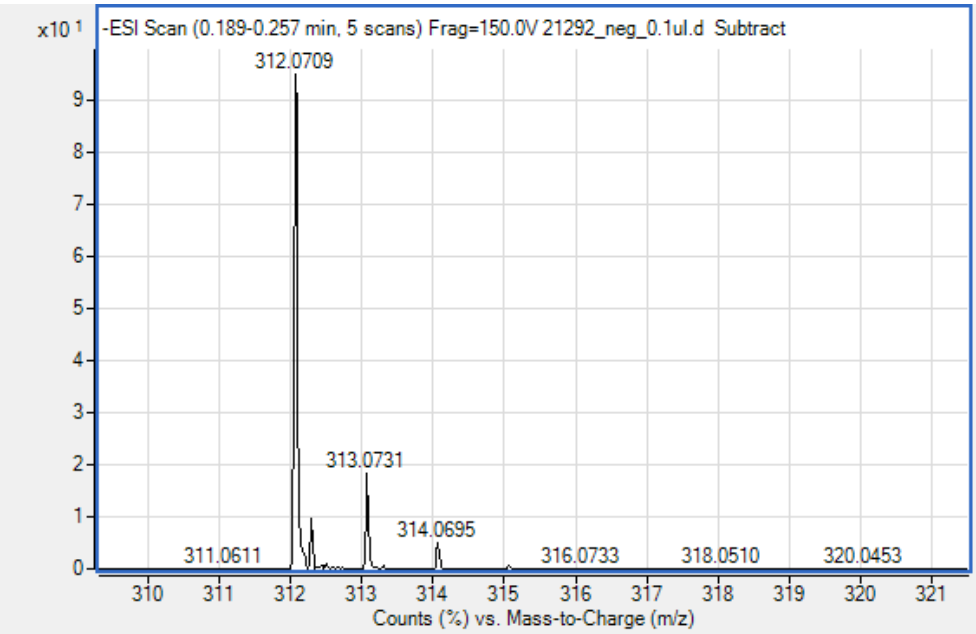

Figure C1-5B. Electrospray ionization mass spectrum in negative ion mode for [BTP][TNS]

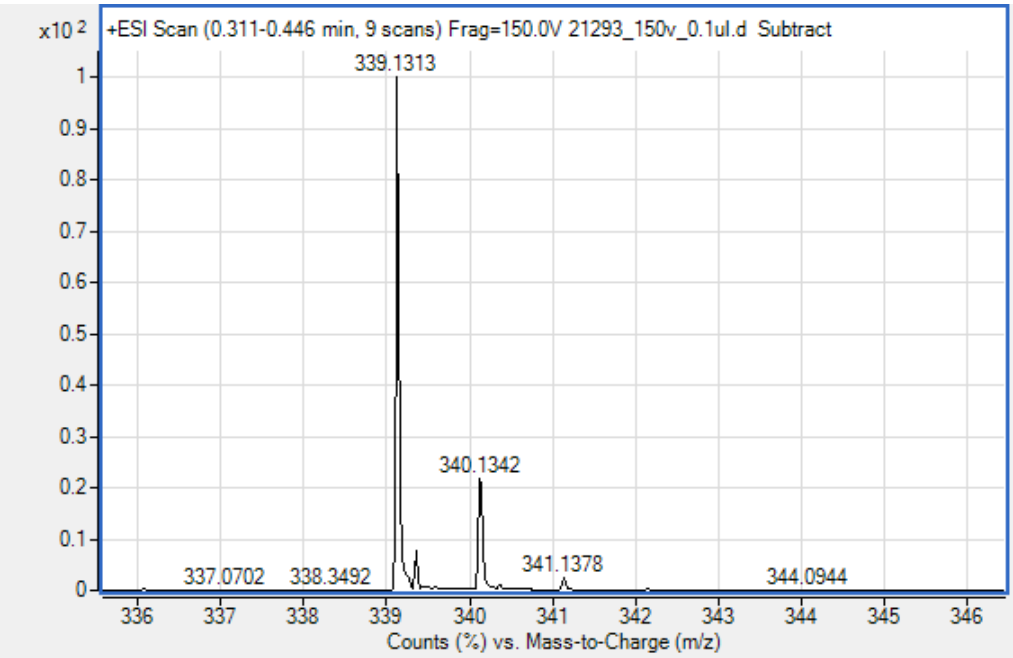

Figure C1-6A. Electrospray ionization mass spectrum in positive ion mode for [TPP][TNS]

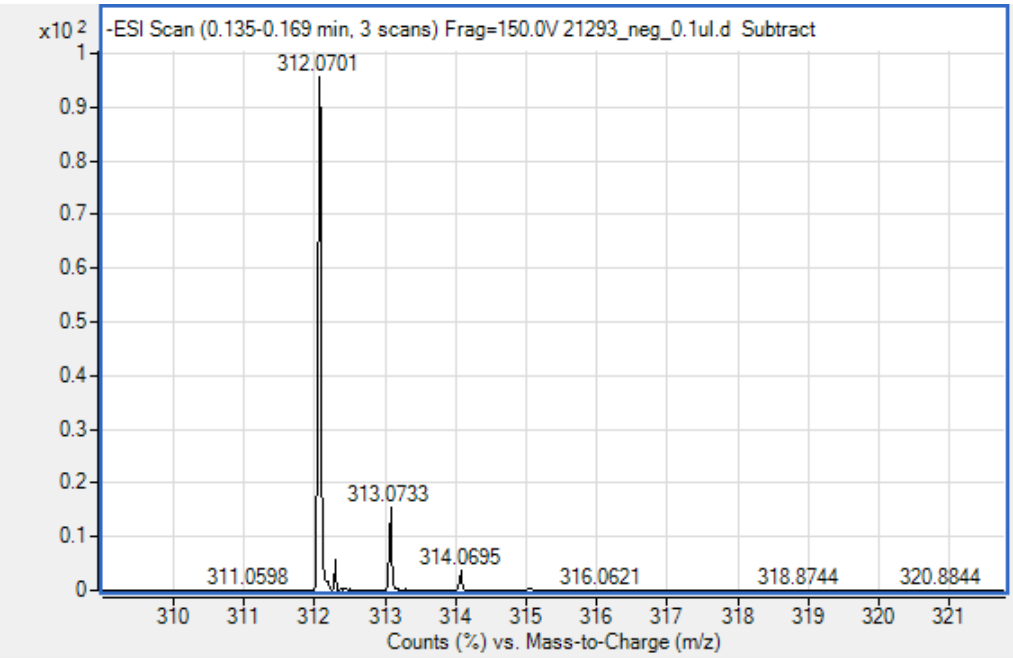

Figure C1-6B. Electrospray ionization mass spectrum in negative ion mode for [TPP][TNS]

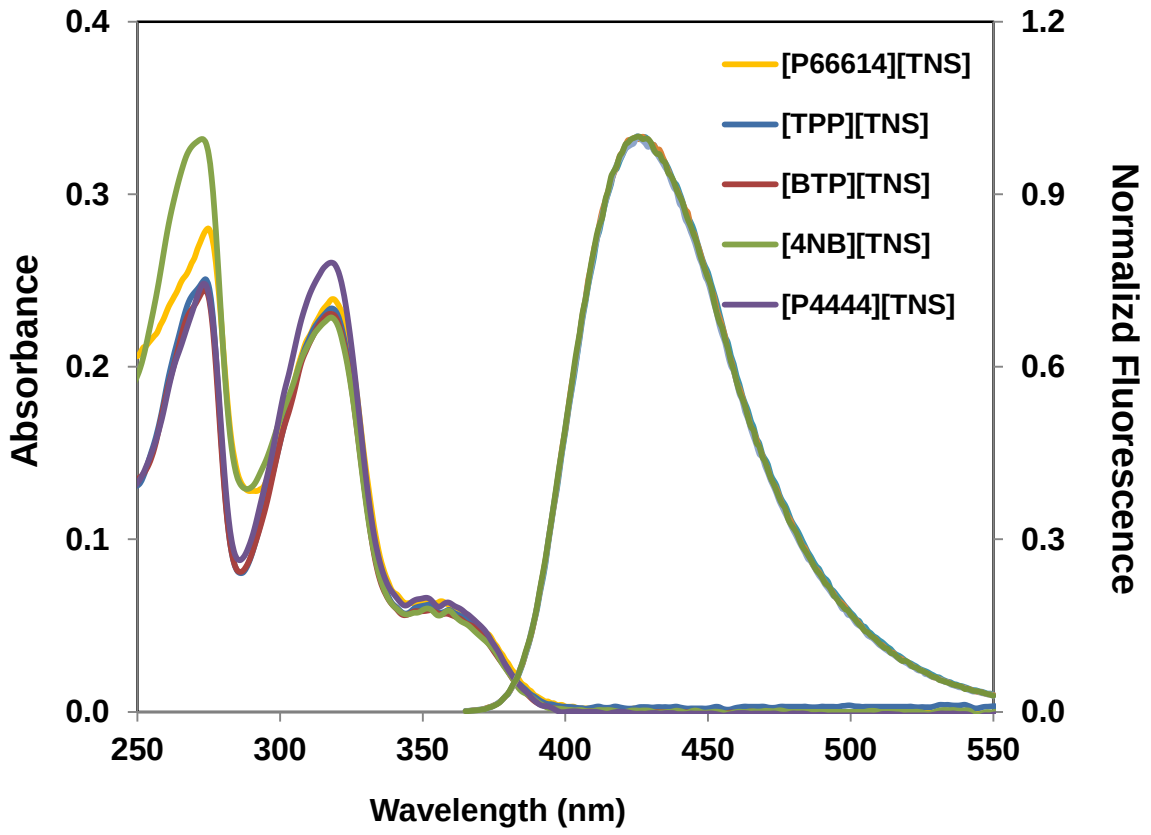

Figure C2. Absorption and fluorescence emission spectra (λ_{ex}- 355 nm) of 10 µM TNS GUMBOS in ethanol. Emission spectrum has been normalized to 1.0 at its maximum.

Table C1. Crystal Data and Structure Refinement for [TPP][TNS], [BTP][TNS] and [P_{4444}][TNS]

	[TPP][TNS]	[BTP][TNS]	[P_{4444}][TNS]
Empirical formula	$C_{24}H_{20}P.C_{17}H_{14}NO_3S.0.7(H_2O)$	$C_{25}H_{22}P.C_{17}H_{14}NO_3S.CH_2Cl_2$	$C_{16}H_{36}P.C_{17}H_{14}NO_3S$
M_r	664.33	750.67	571.77
Crystal system	Monoclinic	Triclinic	Monoclinic
Space group	$P2_1/c$	$P1$	$P2_1/c$
a (Å)	14.3436 (10) Å	10.0089 (4) Å	10.3977 (4) Å
b (Å)	13.8575 (9) Å	10.4658 (4) Å	18.2132 (7) Å
c (Å)	18.0804 (12) Å	10.8995 (4) Å	17.4211 (6) Å
α (deg)		61.537 (2)°	
β (deg)	112.786 (2)°	78.686 (2)°	102.071 (2) °
γ (deg)		66.103 (2)°	
V (Å^3)	3313.3 (4) Å^3	917.68 (6) Å^3	3226.2 (2) Å^3
T (K)	90 K	90 K	90 K
Z	4	1	4

Table C2. Selected Bond Distances (Å) and Angles (deg) for [TPP][TNS], [BTP][TNS] and [P_{4444}][TNS]

	[TPP][TNS]	[BTP][TNS]	[P_{4444}][TNS]
		Bond Distances	
S1—C1	1.778 (2)	1.7741 (16)	1.767 (5)
N1—C6	1.397 (3)	1.395 (2)	1.377 (6)
N1—C11	1.406 (3)	1.420 (2)	1.395 (7)
N1—H1N	0.84 (3)	0.89 (3)	0.868 (19)
C1—C10	1.361 (4)	1.373 (2)	1.369 (6)
C1—C2	1.412 (3)	1.421 (2)	1.403 (7)
C2—C3	1.370 (3)	1.376 (2)	1.364 (7)
C3—C4	1.415 (3)	1.423 (2)	1.434 (6)
C4—C5	1.419 (3)	1.419 (2)	1.412 (7)
C4—C9	1.425 (4)	1.427 (2)	1.412 (7)
C5—C6	1.380 (3)	1.382 (2)	1.377 (6)
C6—C7	1.422 (4)	1.432 (2)	1.417 (6)
C7—C8	1.358 (4)	1.367 (2)	1.357 (7)
C8—C9	1.421 (4)	1.425 (2)	1.409 (6)
C9—C10	1.409 (4)	1.413 (2)	1.410 (6)
C11—C12	1.397 (3)	1.392 (3)	1.384 (7)
C11—C16	1.395 (4)	1.399 (3)	1.403 (7)
C12—C13	1.391 (3)	1.398 (3)	1.386 (7)
C13—C14	1.395 (4)	1.388 (3)	1.381 (7)
C14—C15	1.390 (4)	1.396 (3)	1.392 (7)
C14—C17	1.504 (4)	1.511 (3)	1.511 (7)
C15—C16	1.392 (4)	1.395 (3)	1.367 (7)
		Bond Angles	
C6—N1—C11	125.6 (2)	123.35 (14)	128.6 (4)
C6—N1—H1N	113 (2)	115.7 (17)	112 (4)
C11—N1—H1N	112 (2)	110.1 (17)	119 (4)
C10—C1—C2	119.9 (2)	120.38 (14)	119.2 (5)
C10—C1—S1	118.79 (18)	119.69 (12)	122.1 (4)
C2—C1—S1	121.28 (18)	119.93 (12)	118.7 (4)
C3—C4—C5	122.9 (2)	122.09 (14)	121.6 (5)
C5—C6—N1	119.5 (2)	124.85 (15)	124.1 (5)
N1—C6—C7	121.3 (2)	116.30 (14)	116.9 (5)
C10—C9—C8	122.1 (2)	122.10 (14)	122.9 (5)
C16—C11—N1	124.4 (2)	118.42 (16)	119.1 (5)
C12—C11—N1	117.5 (2)	122.47 (16)	123.5 (5)

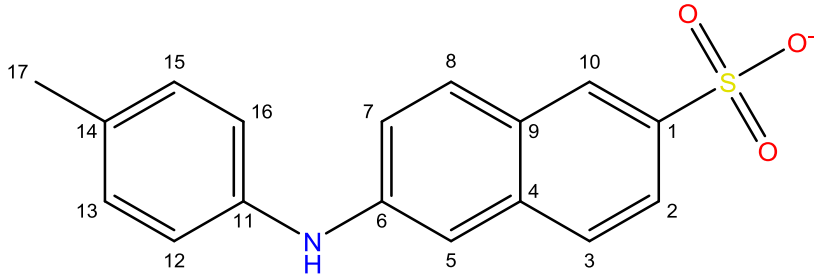

Figure C3. (A) PCA score plot using the first two principal components based on the sensor-response patterns obtained from TNS-based sensors. HSA and α-antitrypsin were labeled as given in the legend (B) PCA score plot using three principal components based on the normalized sensor-response patterns obtained from TNS-based sensors. Different proteins concentrations are given in the legend from top to bottom are 10 nM HSA, 20 nM HSA, 30 nM HSA, 50 nM HSA, 70 nM HSA, 100 nM HSA, 10 Antitrypsin, 20 Antitrypsin, 30 Antitrypsin, 50 Antitrypsin, 70 Antitrypsin, 100 Antitrypsin, 200 Antitrypsin, and 500 Antitrypsin. (C) PCA score plot using three principal components based on the normalized sensor-response patterns obtained from TNS-based sensors: Ellipsoids cover 95% of each cluster; HSA – blue ellipsoid, α-antitrypsin – red ellipsoid (continues through pages 205-208)

A

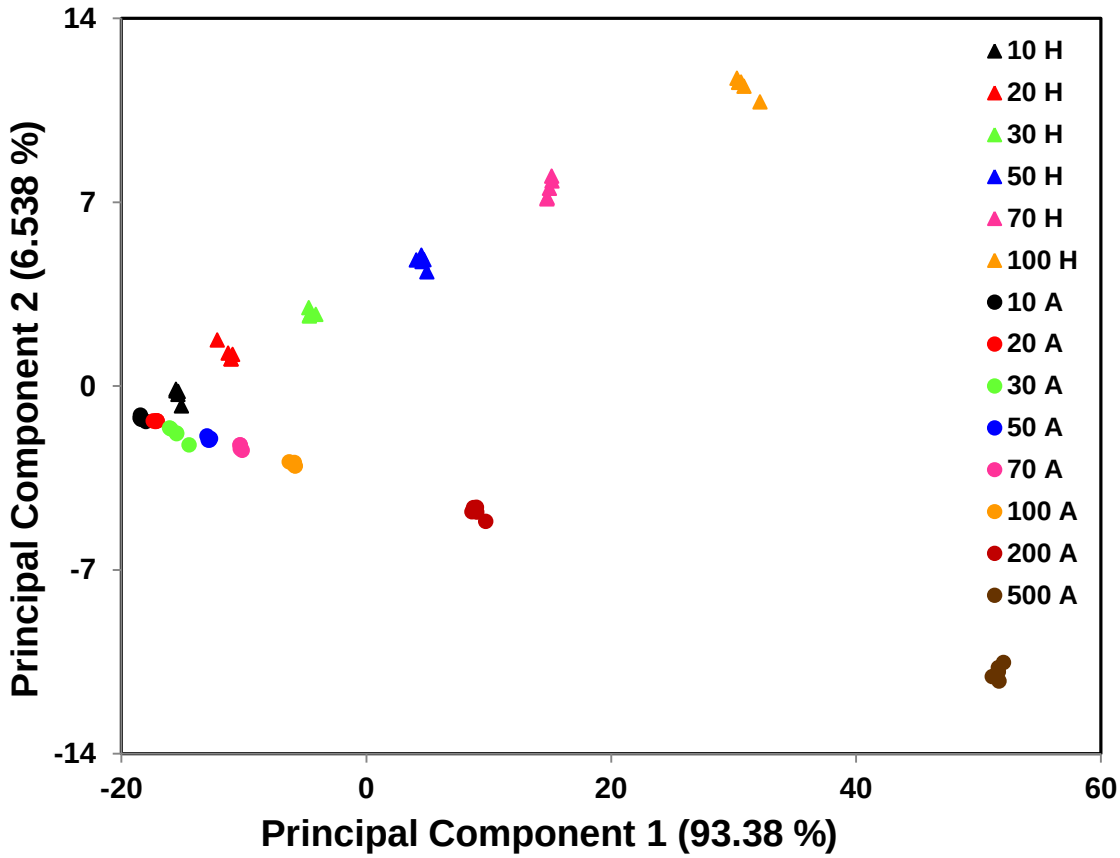
14
7
0
-7
-14
-20
0
20
40
60
Principal Component 2 (6.538 %)
Principal Component 1 (93.38 %)
10 H
20 H
30 H
50 H
70 H
100 H
10 A
20 A
30 A
50 A
70 A
100 A
200 A
500 A

B

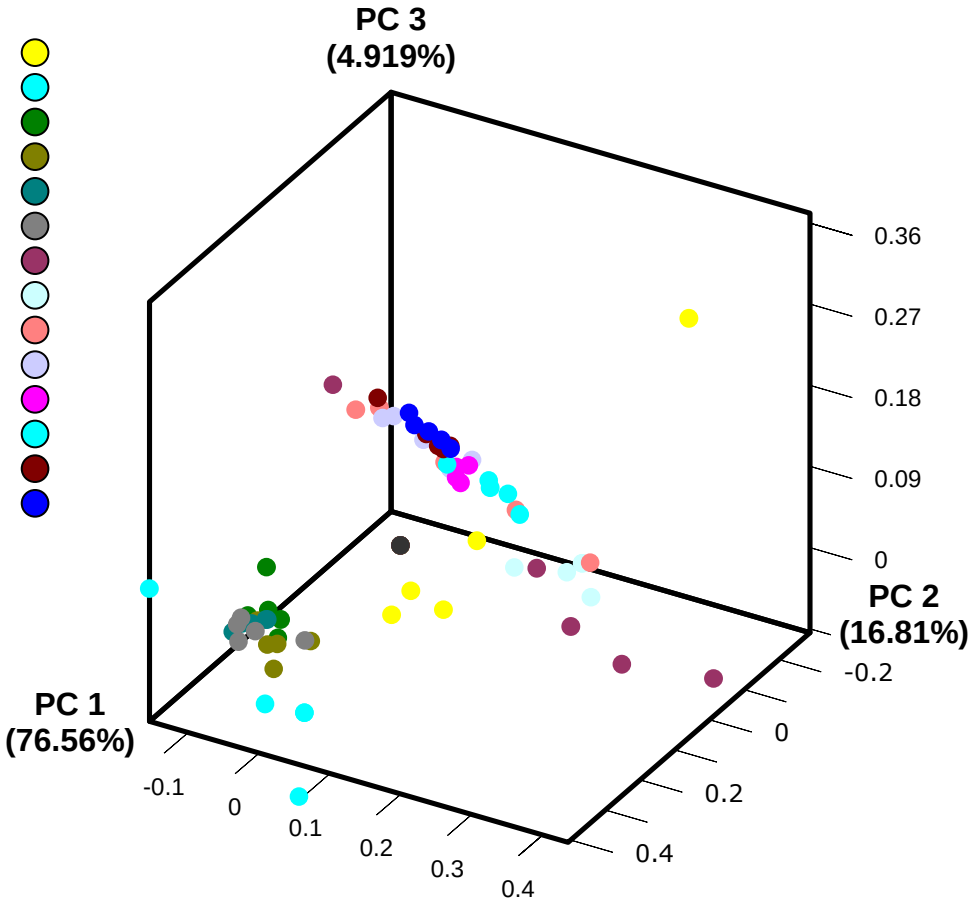
PC 3
(4.919%)
0.36
0.27
0.18
0.09
0
PC 2
(16.81%)
-0.2
0
0.2
0.4
PC 1
(76.56%)
-0.1
0
0.1
0.2
0.3
0.4

C

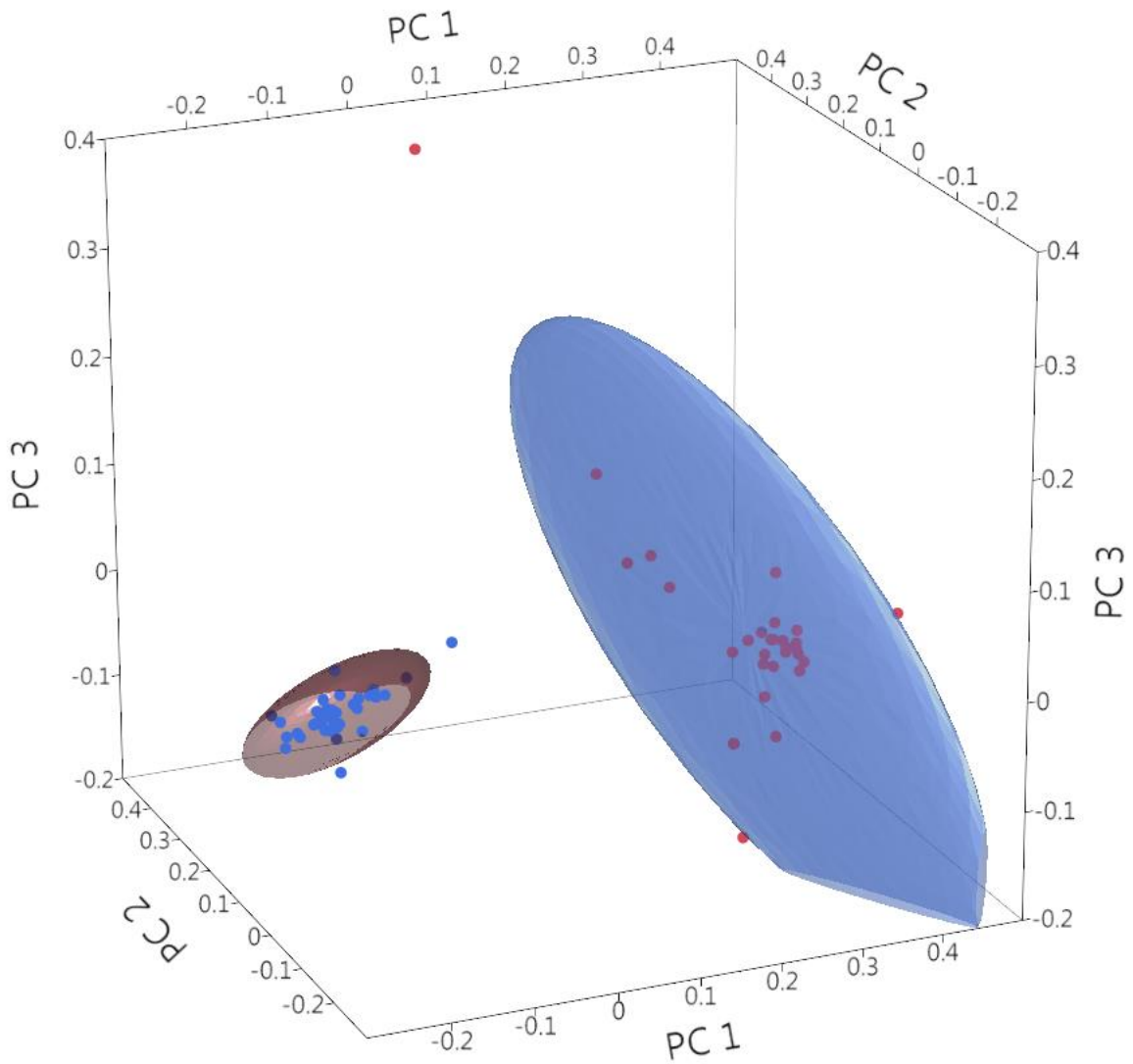

APPENDIX D: LETTERS OF PERMISSION

Site Search

About us | Membership & professional community | Campaigning & outreach | Journals & books | Resources & tools | News & events | Location & contacts

Thank you for your request.

For your records the following options have been submitted.

Name : Waduge Indika S. Galpothdeniya
Address : 432 Choppin Hall Baton Rouge LA 70803 USA
Tel : 225-578-3919
Fax : 225-578-3458
Email : wgalpo1@lsu.edu

I am preparing work for publication:

Article/Chapter title : Chapter2: Ionic liquid-based optoelectronic sensor arrays for chemical detection
Journal/Book Title : DESIGN AND APPLICATION OF TASK-SPECIFIC ORGANIC SALTS FOR CHEMICAL AND BIOCHEMICAL SENSING
Editor/Author(s) : Waduge Indika S. Galpothdeniya
Publisher : Doctoral Dissertation

I would very much appreciate your permission to use the following material:

Journal/Book Title : Ionic liquid-based optoelectronic sensor arrays for chemical detection
Editor/Author(s) : Waduge Indika S Galpothdeniya, Kevin S McCarter, Sergio L De Rooy, Bishnu P Regmi, Susmita Das, Farhana Hasan, Attres Tagge, Isiah M Warner
Volume Number : 4
Year of Publication : 2014
Description of Material : Journal Article
Page(s) : 7225-7234

Journal/Book Title : Fluorescein-based ionic liquid sensor for label-free detection of serum albumins
Editor/Author(s) : Waduge Indika S Galpothdeniya, Susmita Das, Sergio L De Rooy, Bishnu P Regmi, Suzana Hamdan, Isiah M Warner
Volume Number : 4
Year of Publication : 2014
Description of Material : Journal Article
Page(s) : 17533-17540

Additional Comments : Dear Sir/Madam, I am currently writing my doctoral dissertation and I hereby request permission to reproduce text, data and figures in my dissertation from the publications listed above. Sincerely, Waduge Indika S. Galpothdeniya

Title: Virtual Colorimetric Sensor Array: Single Ionic Liquid for Solvent Discrimination

Author: Waduge Indika S. Galpothdeniya, Bishnu P. Regmi, Kevin S. McCarter, et al

Publication: Analytical Chemistry

Publisher: American Chemical Society

Date: Apr 1, 2015

PERMISSION/LICENSE IS GRANTED FOR YOUR ORDER AT NO CHARGE

This type of permission/license, instead of the standard Terms & Conditions, is sent to you because no fee is being charged for your order. Please note the following:

- Permission is granted for your request in both print and electronic formats, and translations.
- If figures and/or tables were requested, they may be adapted or used in part.
- Please print this page for your records and send a copy of it to your publisher/graduate school.
- Appropriate credit for the requested material should be given as follows: "Reprinted (adapted) with permission from (COMPLETE REFERENCE CITATION). Copyright (YEAR) American Chemical Society." Insert appropriate information in place of the capitalized words.
- One-time permission is granted only for the use specified in your request. No additional uses are granted (such as derivative works or other editions). For any other uses, please submit a new request.

BACK CLOSE WINDOW

VITA

Waduge Indika S. Galpothdeniya was born in Colombo, Sri Lanka, to Ananda Galpothdeniya and Kanthi Hapuarachchi. Indika attended Karunarathna Buddhist Maha Vidyalaya, Subharathie Secondary School and Mahanama College (High School). Thereafter, he received his Bachelor of Science Degree in Chemistry in September 2009 from University of Colombo, Sri Lanka. From August 2009 to July 2010, he worked as a teaching assistant in the Chemistry Department of University of Colombo. In the fall of 2010, he attended the Chemistry Department of Louisiana State University as a graduate student and joined Professor Isiah M. Warner's research group in the spring of 2011 and continued his doctoral studies in analytical chemistry. During his PhD, Indika has received several honors, most notably 'RA Scholar Award' for outstanding research and teaching; presented by the Department of Chemistry, Louisiana State University, and NSF/NOBCChE Chairman's Award for outstanding research. Indika holds memberships from the American Chemical Society (ACS) and the National Organization for the Professional Advancement of Black Chemists and Chemical Engineers (NOBCChE). Presently, Indika has three first-author publications, one first-author manuscript (submitted for publication), and two co-author publications. Indika is a candidate to graduate with the degree of Doctor of Philosophy in Chemistry from Louisiana State University in August 2015. His publications and patent during his graduate career are listed below.

First-Author Publications

- **Waduge Indika S. Galpothdeniya**, Bishnu Regmi, Kevin S. McCarter, Sergio de Rooy, Noureen Siraj and Isiah M. Warner; "*Virtual Colorimetric Sensor Array: Single Ionic Liquid for Solvent Discrimination*" *Analytical Chemistry*, **2015**, *87*, 4464–4471.

- **Waduge Indika S. Galpothdeniya**, Kevin S. McCarter, Sergio L. De Rooy, Bishnu P. Regmi, Susmita Das, Farhana Hasan, Attres Tagge, and Isiah M. Warner; "Ionic Liquid-Based Optoelectronic Sensor Arrays for Chemical Detection", *RSC Advances*, **2014**, *4*, 7225–7234.

- **Waduge Indika S. Galpothdeniya**, Susmita Das, Sergio L. De Rooy, Bishnu P. Regmi, Suzana Hamdan, and Isiah M. Warner; "Fluorescein-Based Ionic Liquid Sensor for Serum Albumins", *RSC Advances*, **2014**, *4*, 17533–17540.

- **Waduge Indika S. Galpothdeniya**, Frank R. Fronczek , Mingyan Cong, Nimisha Bhattarai, Noureen Siraj, and Isiah M. Warner; "Tunable, GUMBOS-Based Sensor Array for Label-Free Detection and Discrimination of Proteins" Manuscript resubmitted to *Analytical Chemistry* after addressing the reviewers' comments.

Co-Author Publications

- Bishnu P. Regmi, **Waduge Indika S. Galpothdeniya**, Noureen Siraj, Marc H. Webb, Nicholas Speller and Isiah M. Warner, "Phthalocyanine- and porphyrin-based GUMBOS for rapid and sensitive detection of organic vapors" *Sensors and Actuators B: Chemical* **2015**, *209*, 172-179.

- Hashim, Alghafly, Noureen Siraj, Susmita Das, Bishnu P. Regmi, Paul Magut, **Waduge Indika S. Galpothdeniya**, Kermit K. Murray; Isiah M. Warner, "GUMBOS matrices of variable hydrophobicity for matrix-assisted laser desorption/ionization mass spectrometry" *Rapid Communications in Mass Spectrometry*, **2014**, *28*, 2307–2314.

Patent

- Noureen Siraj, Tony Eugene Karam, Louis H. Haber, Isiah M. Warner, **Waduge Indika S. Galpothdeniya,** Hashim Al Ghafly; "Compositions Including a Ruthenium Molecular Dye-Based GUMBOS, Methods of Making Compositions, Methods of Use of Compositions, and Devices Using the Compositions"; Serial No.: 62/102,754; Filing Date: January 13, 2015; LSU No.: 1428; TH Docket No.: 222220-8020